# THE ORIGIN AND PETROGENESIS OF THE ULTRAMAFIC ENCLAVES AT UNKI MINE, SELUKWE SUBCHAMBER, GREAT DYKE, ZIMBABWE

Sinikiwe Ncube

A dissertation submitted to the Faculty of Science, University of Witwatersrand in the fulfillment of the requirements for the degree of Master of Science

Johannesburg

August, 2013

# Declaration

I declare that this dissertation is my own, unaided work. It is being submitted for the Degree of Master of Science at the University of Witwatersrand, Johannesburg. It has not been submitted before for any degree or examination at any other University.

……  ……

30th day of August 2013 in Johannesburg

# Abstract

The unique Selukwe Subchamber of the Great Dyke is bounded by the Shurugwi greenstone belt (SGB) on the west side for approximately 25 km and granitoids on the east side, as compared to other subchambers of the Great Dyke that are bounded on both sides by granitoids. It is also the narrowest section of the entire Great Dyke. The extensive xenolith suite is found on the western flank and the central zone of the subchamber. This study focuses on the PAR 11 borehole and the surface xenoliths in the Selukwe Subchamber (SSC). The PAR 11 core was drilled into an anomalous sequence of ultramafic rocks situated in the Mafic Succession of the SSC.

There are basically two rock types in the PAR 11 borehole: peridotites and pyroxenites. Comparison of the major and trace element geochemistry of the PAR 11 body with the MR 92 data of Coghill (1994) for the SSC reveals that they are similar but less evolved. The mineral assemblages and proportions of phases in the PAR 11 borehole samples are indicative of essentially the same composition as that which formed the layered sequence of the Great Dyke. Therefore, on the basis of the rock types and chemical compositions, the PAR 11 body and the Great Dyke cumulates appear to be petrologically and chemically similar and had the same petrogenesis.

There are three rock types in the xenolith suite that have been observed in the mafic succession of the Unki area: peridotites, pyroxenites and gabbros. Major and trace elements show a wide range of compositions that have $CaO/Al_2O_3 \sim 1$, which are dissimilar to both PAR 11 and MR 92 borehole data. REE patterns show depletion of LREE, with flat HREEs indicating a different magma to that which gave rise to the Great Dyke. Such flat patterns are typical of a primitive mantle source similar to that of komatiite magma. Stowe, (1974) describes dunite and chromite in the SGB and does not describe pyroxenites and gabbros. Therefore, it is not clear in the first instance that the xenoliths were derived from the SGB. It also does not necessarily mean that these rock types did not occur in the SGB and, if they did, maybe they were derived from an intrusion within the SGB that is at depth and never been seen

before. The xenoliths do not have mineral compositions that are similar to the Great Dyke and therefore precludes them as having been derived from the Great Dyke Marginal Facies, a possible source of such rocks. Therefore, it is concluded from this study that they were inherited from another source which also does not appear to be the SGB because there is no report of such rock types (other than peridotite) in the SGB. They are also not mantle derived.

The metasedimentary rocks that occur as xenoliths are banded iron formation and quartzites and are all clearly derived from the different formations of the SGB. The quartzites are from the Mont d'Or Formation and Wanderer Formation. The BIFs are from the Upper Greenstone and Wanderer Formation. The Shurugwi Greenstones were stripped off from the western flank whereas the Archean granitoids to the eastern flank of the Great Dyke remained.

The conclusion from this study is that the Shurugwi greenstones and Archean granitoids of the Selukwe area were intruded by the large volume of new magma that was the parental magma to the Great Dyke. The hot parental magma carried up with it xenoliths from outside the Great Dyke and large blocks from within the Great Dyke to the uppermost rocks of the level of the P1 pyroxenite layer and mafic unit.

# Dedication

This thesis is dedicated to my mother Patricia N. Ncube and my children Shane and Sisanda Gondo.

# Acknowledgements

This study arose after a brief discussion with Prof. A.H. Wilson who has done great work on the Great Dyke of Zimbabwe and other layered intrusions worldwide. I would like to thank my supervisor who collected the surface samples in the early 1990s and kept them up to this day that I may do work on them. The PAR 11 borehole samples were made available by Collins Mwathahwa from Anglo Platinum Zimbabwe. I would like to thank the geological team of Unki Mine, Caston Musa, Fredrick Hlasi, Omberai Mandingaisa and Melusi Hlambelo for assisting me the times I spent at the mine during the field work and core logging. The analysis was done under the supervision of my supervisor at the Bernard Price Building, School of Geosciences, University of Witwatersrand, and Johannesburg. I would like to thank Janine Robertson who did the XRF analyses, Marlin Patchappa who carried out the ICP-MS, Musa Cebekhulu for preparing the thin and polished sections for me. All the sample preparation and analyses cost was taken care of by Prof. Allan Wilson. I would also like to thank Quartus Snyman on behalf of Anglo Platinum, South Africa for providing the financial support. I would like to thank my colleagues Irvin R. Matsheka, S'lindile S. Wela, Todani Funyufunyu, Musa Manzi, Trishya Owen-Smith, Grant Bybee. I would like to thank my officemate Masibulele Zintwana for being really helpful whenever possible. I would also like to thank my friends Nokuthula Dladla, for the love and support during the write of my thesis. At various stages of this study I have benefited for Prof. Lew Ashwell, Prof. Grant R Cawthorn and other staff and students of the School of Geosciences, University of Witwatersrand, and Johannesburg. Lastly I would like thank my mom Patricia N. Ncube, my children Shane and Sisanda to whom this project is dedicated.

# Table of Contents

# List of Figures

# List of Tables

# CHAPTER 1: INTRODUCTION

## 1.1 General Geology of the Great Dyke

The Great Dyke of Zimbabwe is a major intrusion of mafic/ultramafic layered rock that cuts across the dominantly Archean rocks of the Zimbabwe Craton (Fig.1.1)(Wilson *et al.*, 2000a). The Great Dyke, aligned approximately NNE, is 550 km in length and 4 to 11km wide (Worst 1958, 1960). The Great Dyke is composed of two main magma chambers; the North and South Chambers, which are further subdivided to five subchambers (Podmore and Wilson, 1987). These chambers and subchambers are defined on the basis of structure, style and continuity of layering (Prendergast and Wilson, 1989). The North Chamber is made up of the Musengezi Subchamber to the extreme north, the Darwendale, and the Sebakwe Subchamber in the south comprising the southern compartment of this chamber. The South Chamber comprises the Selukwe and the southern Wedza subchamber (Wilson *et al.*, 2000b).

Parallel to the Great Dyke are a number of satellite dykes that run for almost its entire length. The Umvimeela Dykes to the west and East Dyke to the east. The satellite dykes are at a distance of about 3-25km from the intrusion and consist mainly of the quartz gabbro. The satellite dykes are associated with a major fracture pattern that resulted in a Craton wide tectonic control which gave rise to the form and alignment of the major Great Dyke intrusion (Wilson, 1996; 2001).

The stratigraphy of the Great Dyke is similar in all magma chambers. It has a lower Ultramafic Sequence overlain by an upper Mafic Sequence. The latter are preserved as remnants along the length of the Great Dyke (Wilson, 1992). The Ultramafic Sequence is divided into two successions, the lower Dunite Succession and the upper Pyroxenite Succession, each containing well developed cyclic units.

The Dunite Succession is composed of dunite, harzburgite separated by chromite layers. The Pyroxenite Succession is also made of cyclic units of repeated occurrences of basal chromite, dunite, harzburgite and olivine pyroxenite which grade into pure pyroxenite. The Pyroxenite Succession in the North and South chambers has a marked difference. The North has six cyclic units approximately 100m thick while the South chamber has 16 units approximately 80m thick (Prendergast and Wilson, 1989).

The Marginal Border Group succession has been observed in most Subchambers (Wilson, 1982). This succession of layers is usually close to or at the margin of the Great Dyke. The Marginal Border Group is found lying at a higher angle to the main layered sequence almost parallel to the walls. The rock types of this unit are gabbros, norites and pyroxenites, some with strong crystal alignment perpendicular to the original walls of the magma chamber (Wilson and Prendergast, 2001).

The layers of the Great Dyke are synclinal in sectional shape. The layers dip inwardly with the dips increasing from the central axis towards the margins but increasing near the walls. The transverse section is thought to be trumpet-shaped with individual layers thinning away from the axis and join up the Border Group (Prendergast and Wilson, 1989). At depth the Great Dyke has a dyke feeder which is connected to magma chambers that are deep seated. It is hypothesized that the linear form of the Great Dyke developed as a series of isolated magma chamber become connected at higher stratigraphic levels during the filling (Podmore and Wilson, 1987).

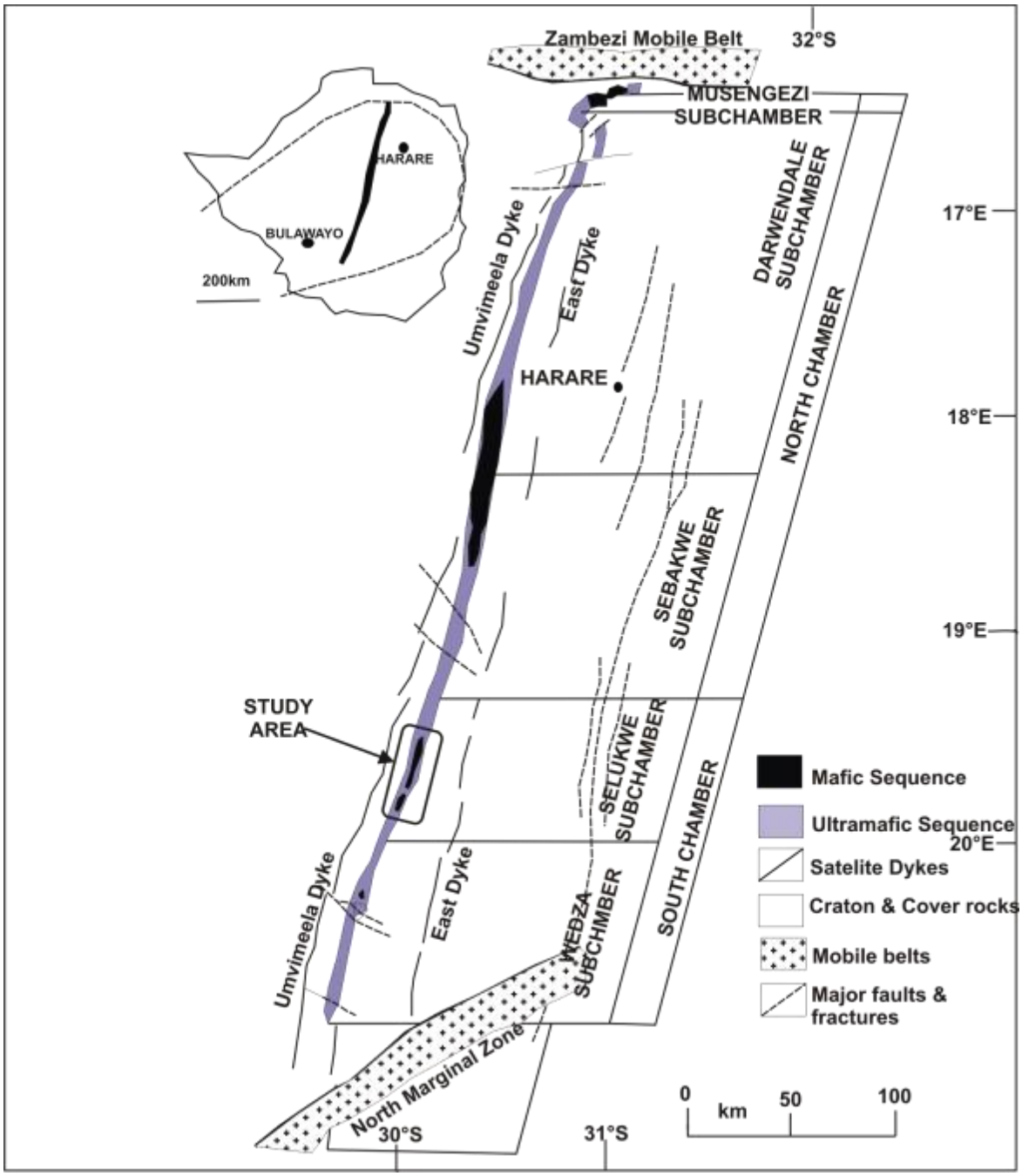


**Fig. 1.1.** The location of the Great Dyke within the Zimbabwe Craton. The Zambezi and Limpopo mobile belts which bound the Craton are indicated to the north and south. The chambers and subchambers are shown together with satellite dykes and major fracture patterns and faults. The detailed study area in the Selukwe Subchamber is shown (Wilson *et al.*, 2000a).

### 1.1.1 Geological Setting of the Great Dyke

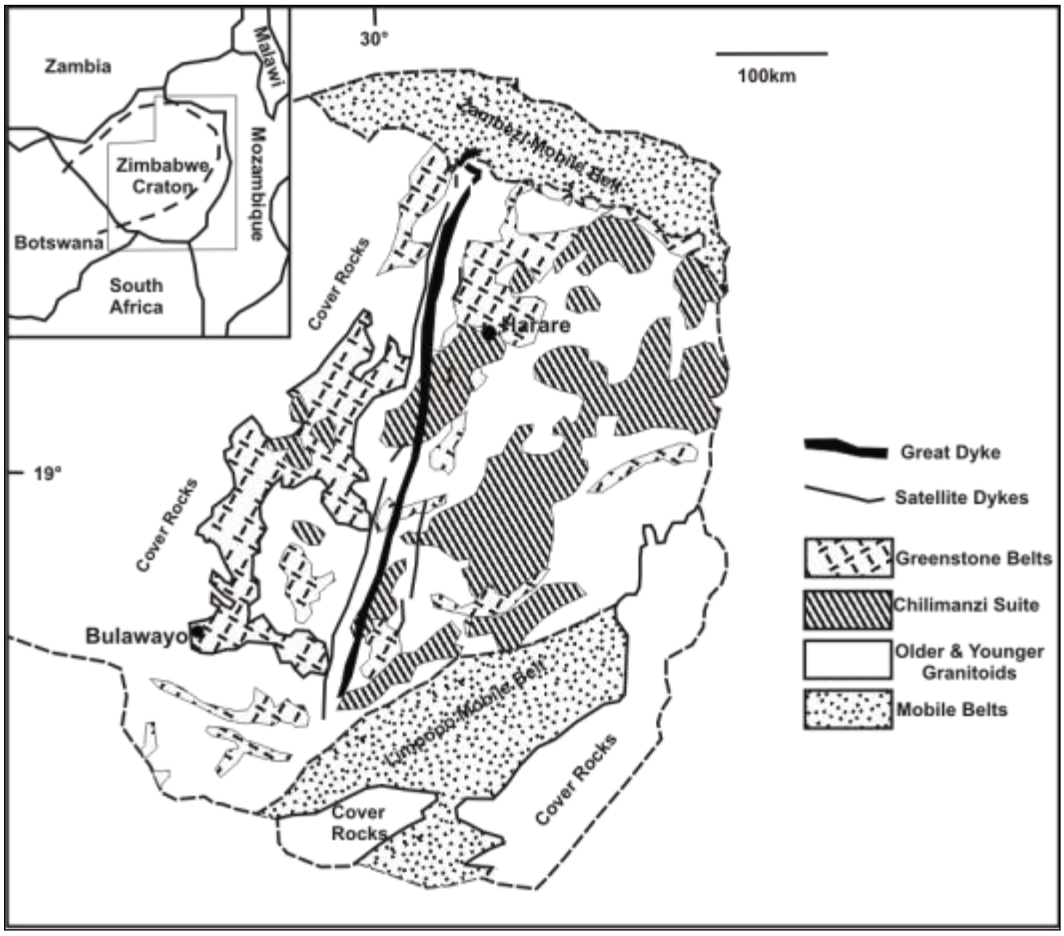


**Fig. 1.2.** Geological setting of the Great Dyke of Zimbabwe in relation to the Zimbabwe Archean Craton, the older and younger granitoid bodies, and the 2.6 Ga Chilimanzi granitoid suite (Mukasa *et al.*, 1998).

The Great Dyke intrudes the Basement Complex of the Zimbabwe Craton which consist of the primitive Archean granitoids (3.5 and 2.9 Ga) and gneisses of the associated greenstone belts (2.9 – 2.8 Ga), illustrated by Fig. 1.2 (Mukasa *et al.*, 1998). The Zimbabwean Craton is bounded by the Limpopo Mobile Belt to the south, the Mozambique Belt to the east and the Zambezi Mobile belt on the in the north. Proterozoic and Phanerozoic basin deposits cover the Archean rocks in the northern part of the Craton.

The granitoids cover two-thirds of the total area of the southern Zimbabwe and are related to the igneous cycle of the Bushveld complex (Worst, 1960). The Chilimanzi (2.6 Ga) granitoid suite mark the last major pre- Great Dyke granitic event (Mukasa *et al.*, 1998). Using the Rb-Sr method, age determinations yielded an age of 2.4Ga (Allsopp, 1965; Davies *et al.*, 1970) with the most precise being 2455±16Ma (Hamilton, 1977). Another study (Mukasa *et al.*, 1998) indicated an emplacement age of 2587±8Ma. Recently the Great Dyke has been dated together with the satellite dykes, the Umvimeela and East Dyke as 2574±2Ma (Wingate, 2000) using the SHRIMP U-Pb. A more recent study (Oberthür *et al.*, 2002) indicates an older and more reliable age of 2574±0.7 Ma using U-Pb, Rb-Sr and Sm-Nd method.

Fractures of several orientations in the Cratons are associated with the Great Dyke (Fig. 1.1). Some of these allowed for the emplacement of the Dyke itself, as well as, its associated satellite dyke. The whole structure has undergone tilting at the extreme north (Snake' Head) as a result of movement of the Zambezi Mobile belt during the Pan African deformation. This resulted in the severe faulting of the Great Dyke. The tectonic influence on the Great Dyke is not fully understood, however, a suggested model considered an abortive rift system. The Great Dyke and its satellites are believed to have been emplaced during a period of extension and development of a recent pure shear model better explains the fracturing that occurred.

## 1.2 General geology of the Selukwe Subchamber

The area of study is the located in the Selukwe Subchamber (Figure 1.1), which is one of the two subchambers found in the southern chamber of the Great Dyke. It is 90 km in length and is the northern compartment of the South Chamber. The Southern compartment is the Wedza Subchamber and is 85 km in length. The shape of the Selukwe Subchamber has been controlled by the proximity of the Shurugwi greenstone belt, which has also caused the Great Dyke to be deflected and constricted in places. The Selukwe Subchamber is described in detail in the next chapter; however, the broad structure of the belt is similar to that of the other subchambers

with an upper Mafic Sequence (280 m thick) overlying the thick succession of the Ultramafic Sequence which has been exposed thickness of 1600m (Wilson *et al.*, 2000a).

A number of major transverse, steeply dipping faults interrupts the overall continuity of the Selukwe subchamber and these, combined with the change in the shallow plunge direction, from north to south for the northern zone and in the opposite direction for the southern zone, result in then repetition of the lower gabbroic rocks on the longitudinal axis. This has important implications for the exposed strike length of the Platinum bearing Main Sulfide Zone (MSZ) (Wilson *et al.*, 2000a). The MSZ is located entirely within the pyroxenite close to the boundary of the Ultramafic – mafic sequence and consist of a zone of Base Metal Sulphides and a lower part of which is enriched in Platinum Group Elements (PGEs).

### 1.2.1 Some Unique Characteristics of the Selukwe Subchamber

The Selukwe Subchamber is unique in all the subchambers of the Great Dyke because of the following features;

a) in its central part it is the narrowest of all the subchambers at 3.5 km wide, and
b) it is bounded by both the Shurugwi greenstones for approximately 25 km and granitoids as compared to other subchambers that are bounded on both sides by granitoids.

As a result the contacts show different lithologies. The marginal rocks from the Border Group on the west side form a steep contact with the Shurugwi Greenstone Belt. The sequence is made up of fine grained feldpathic pyroxenite, including olivine-bearing websterite (Wilson *et al.*, 2000a). The east marginal rocks are in contact with the granitoids of the Zimbabwe Craton with a dip ~ 40º. These are characterized by abundant auto-intrusive granite dykes and pegmatoids resulting from melting of wall rocks and hydrous crystallization. Hybrid lithologies, such as pyroxene-bearing amphibolites, amphibole- bearing pegmatoids, amphibole gabbros

and magnetite diorites are common in the marginal zone as irregularly developed, steeply dipping, fine-grained layers (Wilson *et al.*, 2000a).

The layers in the west side have a tendency to be more irregular and complex than those on the east side and in place are discontinuous or comprise composite minor layers. Other features which characterize the lithologies on the west side include an abundance of nodular pyroxenite and harzburgite layers, crescumulates-type textures and the occurrence of xenoliths of various origins. Some layers are made up of pyroxenite fragments enclosed within a harzburgite matrix. The origin of the nodules are unknown but may have resulted from the fragmentation of partly consolidated layers followed by reaction or mechanical abrasion, before being incorporated into the new layer (Wilson *et al.*, 2000a).

There is a unique and extensive xenoliths suite in the central and western of the Selukwe Subchamber (described in detail in the next chapter) which is the main subject of this work. They have been divided into three types.

a) Ultramafic Rocks
b) Mafic and Ultramafic autoliths
c) Metasedimentary quartzite and Banded Iron Formation

These xenoliths represent a complex assemblage of fragments derived from the greenstones as well as possibly part of the Marginal Border Group (autoliths), which in other parts of the Great Dyke have been largely assimilated and digested as the magma chamber developed and the wall- rocks were heated. The fragments derived from the greenstones are serpentinites, chromitites and metasediments. The extensive suite of the fine-grained pyroxenites, olivine pyroxenite have no equivalent in the greenstone belt and may represent the earliest cumulates of the Great Dyke that formed on the walls of the magma chamber (Wilson *et al.*, 2000a). The main objective of the present work is to characterize the mafic and ultramafic xenoliths and to understand their origin. Xenoliths of the metasediments and banded iron formation were not studied.

## 1.3 Previous Geological Work

Zealley (1919) mapped and described a 37 km long section of the Selukwe Subchamber north of the Lundi River, which cuts across the Great Dyke approximately halfway along the length of the Selukwe Subchamber.

The occurrence of platinum mineralization in the P1 pyroxenite of the Selukwe Subchamber was first discussed by Mennell (1925). Tyndale- Biscoe (1949) published a report which included mapping and description of the geology of the Great Dyke Selukwe Subchamber between Lalapanzi and Shurugwi. Worst (1960) remapped and described the entire Selukwe Subchamber where he featured aspect of the xenoliths and described as inclusions in the Great Dyke. There were divided into three types; ultramafic, sedimentary and granite inclusions.

In 1987 and through the subsequent four years Prendergast and Wilson had visits on the xenolith suite and collected samples. Mr Murahwi of the Prospecting Ventures (Pty) Ltd provided a number of xenolith samples. A number of xenolith samples were also collected from an independent research which was carried out by Wilson and Coghill (1993). Thin sections where cut from the xenolith samples and some approximately 800 mineral analyses have been determined by electron microprobe. However, no document was produced from this data set. Coghill (1994) did her research on the aspects of the ultramafic rocks and platinum group mineralization of the Selukwe Subchamber and also featured an aspect on the xenolith suite. Her data being the most recent available record of the geology of the Selukwe Subchamber.

## 1.4 The Aims of this Study

This study focuses on the suite of ultramafic enclaves found on the Selukwe Subchamber located in the South Chamber of the Great Dyke of Zimbabwe. Many studies have been done on the entire length of the Great dyke, (Worst, 1960; Wilson, 1982; Prendergast, 1987; Wilson *et al.*, 2000b), with the main interest being the Platinum Group Element concentration and the stratigraphy of the Great Dyke.

Ultramafic fragments have been observed in the North Chamber (Ngezi mine) and Selukwe Subchamber (Unki mine) (Worst, 1960). They are highly abundant in the latter occurrence.

These enclaves are present in the form of xenoliths/autolith suites pose some difficulties in the ore body of the MSZ and in short and long term planning of Unki Mine. If they intersect the P1 pyroxenite layer where the where PGEs are found this can result in loss of grade in the mining operation. As a result the presence of xenoliths/autoliths has an impact on the mining operations of the platinum zone. Objectives of this dissertation are to;

- Present a detailed documentation of the various types of the mafic and ultramafic enclaves and their mineralogical variations.
- Present a detailed map showing the distribution of the enclaves.
- Investigate why these enclaves are located more in the western side of the Selukwe Subchamber.
- Investigate the origin and petrogenesis of the ultramafic enclaves.
- Establish the possible magma chamber processes that gave rise to them.

## 1.5 Methodology

The Selukwe Subchamber xenolith suite samples were collected in the 1990s by Prof. Allan Wilson for petrography and geochemical analyses. A total of more than 250 samples were collected between the periods of 1990 – 1994 for preliminary studies. Eighty six (86) samples representative of the xenolith suite were selected for the study. The PAR 11 borehole and other borehole were drilled by the South Mine Complex (Pvt) Limited for exploration and research.

The PAR 11 borehole is located northwest of the Unki mine shaft. A total of 152 samples were selected from the PAR 11 borehole for this study. The detailed lithological core logging of the PAR 11 was done at the Prospecting Ventures Ltd in

Harare, Zimbabwe where the core is currently kept. Other 10 samples will be take were be taken from boreholes with xenoliths in the surrounding area shown in the diagram. These boreholes are V58, PAR 28, MR 33, MR 102, MR125, MR 316, MR 327, MR 328, MR 330 and MR 331. The core logging of these other borehole samples of xenoliths was done at the Unki Mine, where the mining core is kept.

The petrographic work included a mineralogical study in terms of grain size, modal abundances and textural interpretation. Geochemical analysis for whole rock study was done using X-ray Fluorescence (XRF) spectrometry to determine major and trace element chemistry of each rock sample. Trace elements were determined using Inductive Coupled Plasma-Mass Spectrometry (ICP-MS). Microprobe analysis was also carried out for mineral chemistry on selected samples. The detailed methodology which includes sample preparation and analytical techniques together with the results are appended.

# CHAPTER 2: THE GEOLOGY OF THE SELUKWE SUBCHAMBER

## 2.1 Introduction

The Selukwe Subchamber is 90km in length and is the northern compartment of the South Chamber. The Southern part is the Wedza Subchamber, 85 km in length (Wilson *et al.,* 2000a). It comprises an (280m thick) upper Mafic Sequence overlying the Ultramafic Sequence which has an exposed thickness of 1600m (Wilson *et al.*, 2000b). The Selukwe Subchamber has a synclinal shape in transverse section, with the same lithological sequence being exposed on both sides of the longitudinal axis. The layers have an asymmetric pattern close to the walls is attributed to the physical shape of the chamber and the constricting shape nature of the wall rocks, which is the greenstone on the west flanks and granite on the east side (Wilson *et al.*, 2000b). The shape of the chamber has been controlled by the proximity of the greenstone belt, which also causes to be deflected and constricted in places (Wilson *et al.*, 2000a).

The same lithological sequence is exposed on both sides of the longitudinal axis because the Subchamber has a synclinal shape. The layering is asymmetrical in physical shape attributed by the constricting nature of the wall rocks, greenstones to the west and granites to the east side (Wilson *et al.*, 2000a; Wilson *et al.*, 2000b).

Similar in form to the other subchambers of the Great Dyke the layers, in the Selukwe Subchamber they are synclinal and dip inward toward the center of the subchamber. In the east side dips of (32-36º) are observed while in the west side steeper dips of (36-41º) are observed. The asymmetry of the layers is largely due to a result of the constricted walls of the two flanks (Wilson *et al.,* 2000a). Drilling through the Selukwe Subchamber shows that the topology of the mafic- ultramafic contact is highly regular and symmetrical (Fig 2.2 ) hence any asymmetry imposed on the lower part of the ultramafic sequence is not transmitted to the higher parts of the sequence (Wilson *et al.*, 2000a).

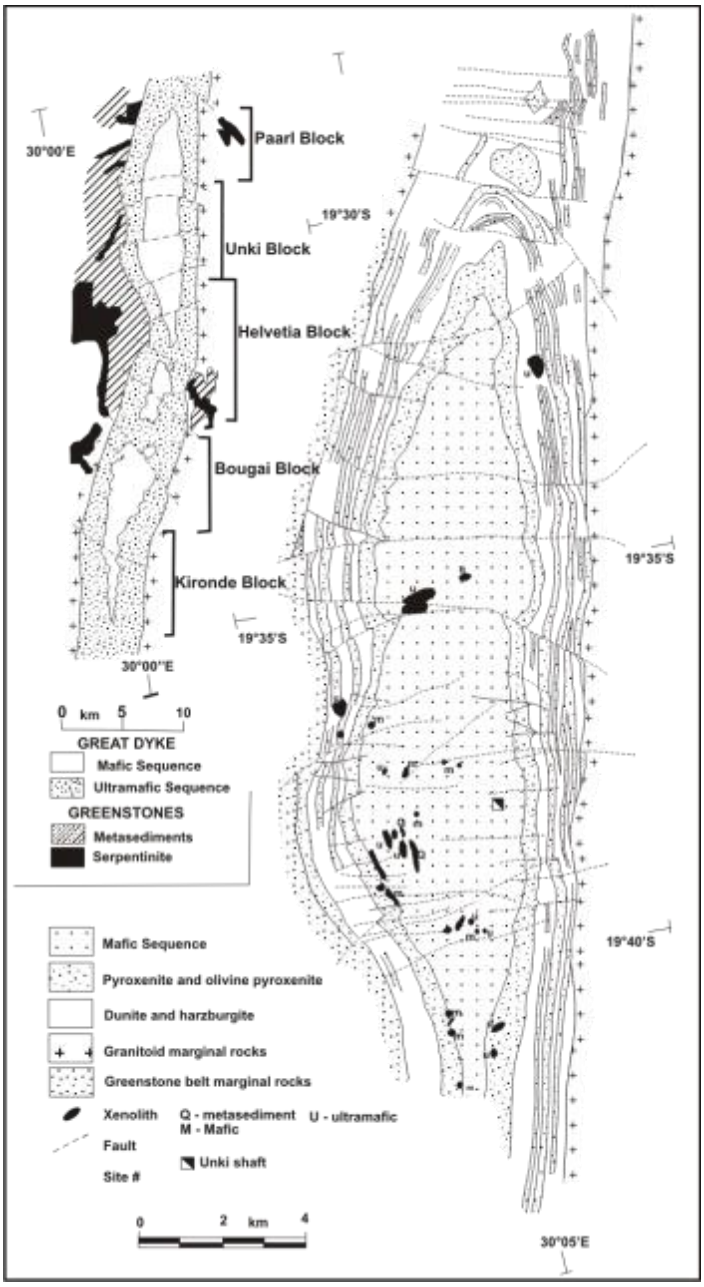


**Fig. 2.1.** The geology of the north-central zone of the Selukwe Subchamber. The simplified large- scale map shows the location of the Selukwe greenstone belt on the west contact of the subchamber. The various mining blocks are indicated. The map shown in greater detail is an outcrop and covers the Unki Block and parts of the Paarl and Helvetia Block. Also shown are fragments of xenolithic and autolithic suite (Wilson *et al.*, 2000a).

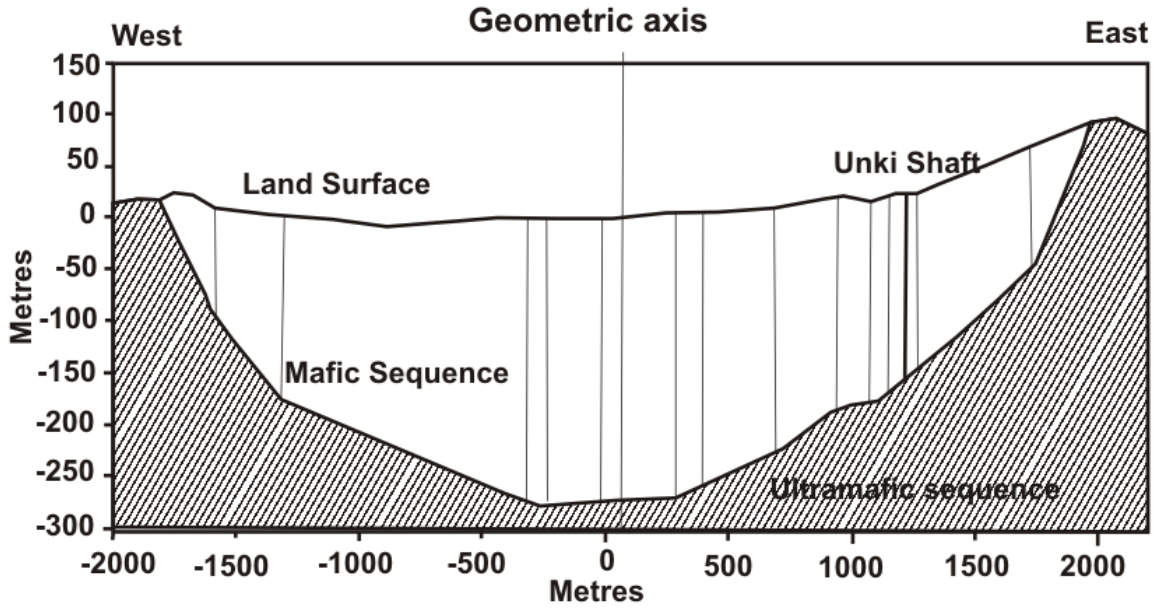


**Fig. 2.2.** Cross-section of the central zone of the Selukwe Subchamber showing the mafic-ultramafic contact as determined from drill core intersections (vertical lines). The position of the Unki prospect shaft is shown (Wilson *et al.*, 2000a).

There are several major transverse, steeply dipping faults interrupts the overall continuity of the Selukwe subchamber and these, combined with the change in the shallow plunge direction, from north to south for the northern zone and in the opposite direction for the southern zone, result in then repetition of the lower gabbroic rocks on the longitudinal axis. This has significant implications for the exposed strike length of the Platinum bearing Main Sulfide Zone (MSZ) (Wilson *et al.*, 2000a). The MSZ is located entirely within the pyroxenite close to the boundary of the Ultramafic –mafic sequence and consist of a zone of Base Metal Sulphides and a lower part of which is enriched in Platinum Group Elements (PGEs) (Wilson *et al.*, 2000b).

The various prospecting areas, which contain outcrops of the MSZ, are identified from the north to the south, as the Paarl, Unki, Heltavia, Bougai and Kironde areas (Fig. 2.1). The Unki area is has been extensively studied by as it holds the greatest (Wilson *et al.*, 2000a) economic potential for PGEs.

## 2.2 Stratigraphy and Rock Types of the Selukwe Subchamber

The ultramafic rocks outcrop in the exposed margins of the central gabbro and peripheral to it with a narrow websterite layer comprising to the topmost unit (Wilson *et al.*, 2000a). The underlying rock types include pyroxenites, olivine pyroxenites, harzburgite, serpentinized dunite and chromite layers of the lower cyclic unit. There is a marked degree of thinning of all units from the axis towards the margin. The uppermost lithology of the ultramafic sequence (Fig 2.3) is the P1 pyroxenite layer which comprises websterite in the upper 4-8 m, and this in turn overlies pyroxenite unit 220m in thickness. There is layering within the pyroxenite resulting from the cyclic variation of texture, modal composition and grain size (Wilson *et al.*, 2000b).

## 2.3 Country Rocks Contacts

The Selukwe Subchamber is different from the other four subchambers in that it is bounded by the Shurugwi greenstones and granites on the west and east respectively. The greenstones on the west form a steep contact with the Selukwe Border Group series. These include fine grained feldspathic pyroxenite and olivine bearing websterite. The granites on the east also form a steep contact of ~40° with the east marginal zone. Melting of the rocks resulted in abundant auto-intrusive granite dykes and pegmatoids. The contact is characterized by fine grained layers of pyroxenite bearing amphiboles, amphibole bearing pegmatoids, amphibole gabbros and magnetite diorites. These layers are in the eastern marginal zone are irregularly developed and steep (Wilson *et al.*, 2000a).

## 2.4 The Mafic Sequence

The Mafic Sequence is the thickest in the axis of the Selukwe Subchamber and thins towards the eastern and western margins owing to the synclinal nature of the Great Dyke layering. The mafic sequence of the Selukwe Subchamber is similar to the Lower Mafic Succession of the Darwendale Subchamber (Wilson, 1982).

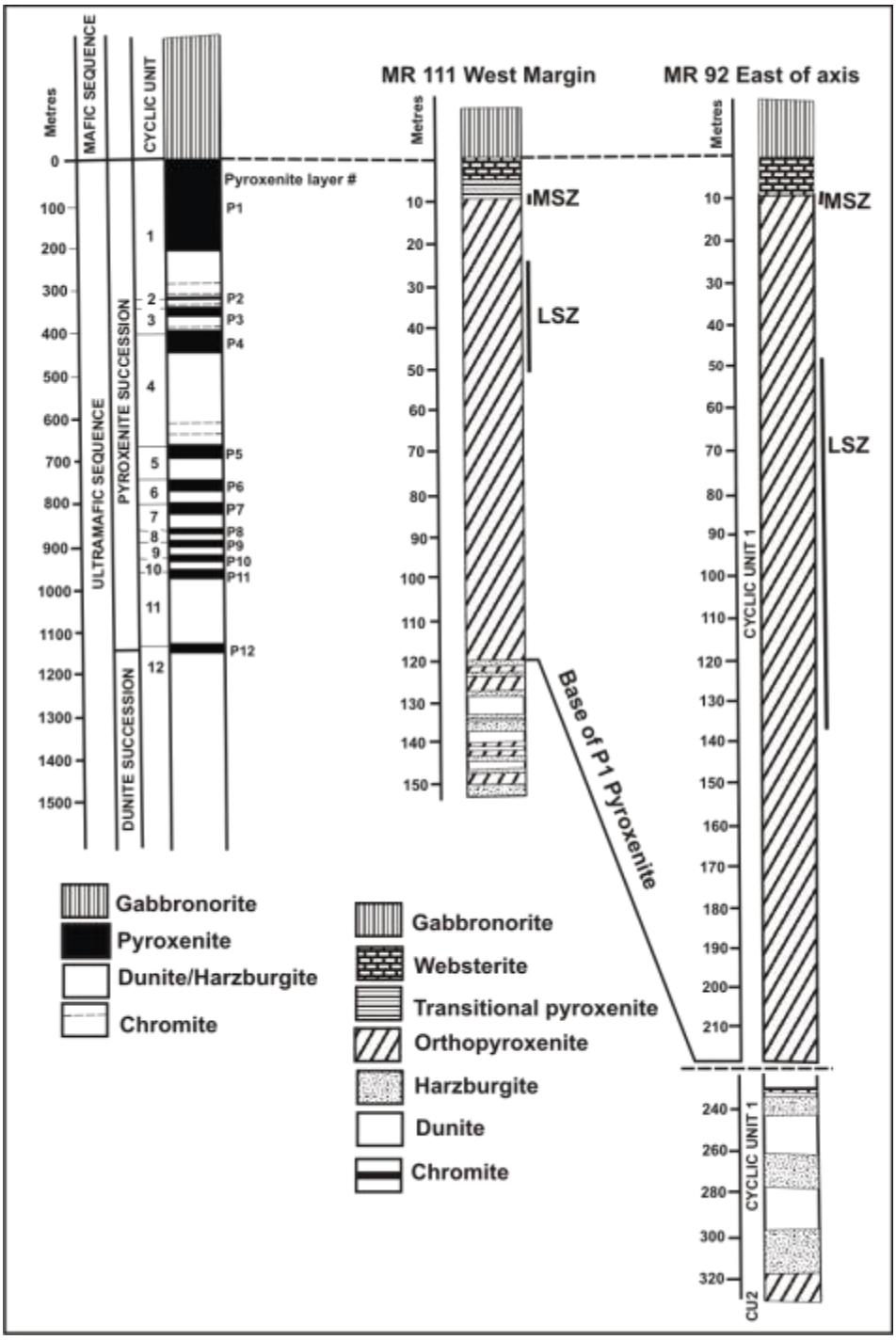


**Fig. 2.3.** Lithostratigraphic sections for the axial region in the Selukwe Subchamber derived from drilled core data. The section shown for MR 92 locality is 800 m east if the Unki area. MR 111 (correction has been made for a 17º is located on the west margin) (Wilson *et al.*, 2000b).

Orthopyroxene gradually changes from the equate cumulus grains at the base of the mafic sequence to large optically continuous phases at the present top of the sequence similar to the Darwendale Subchamber. The olivine gabbro is well developed in the Paarl Block and is characterized by optically continuous olivine and rare-green clinopyroxene which poikitically encloses plagioclase crystals (Wilson *et al.*, 2000b).

## 2.5 Mafic and Ultramafic contact

The contact between the gabbroic rocks and the P1 pyroxenite is locally andulating with some development of a mafic pegmatoid. An irregular and narrow chromite 2-5mm thick layer occurs at the interface of the websterite and the anorthositic gabbro. A similar chromite layer occurs in the Wedza Subchamber although it is absent in the North Chamber (Wilson *et al.*, 2000a).

## 2.6 P1 Pyroxenite layer

The P1 Pyroxenite is the uppermost unit of the lower ultramafic sequence. The uppermost 4-8mm layer is websterite with cumulus orthopyroxene and clinopyroxene enclosed in optically continuous plagioclase oikocrysts. The unit usually exhibits 10-50cm modal layering with significant grain-size variations. There are two main platinum group element (PGE) bearing sulphide zones; the Main Sulphide Zone (MSZ) is located close to the websterite- orthopyroxene boundary and the Lower Sulphide Zone (LSZ) in the same pyroxenite layer but some 35m below the MSZ (Wilson *et al.*, 2000a).

The pyroxenite is mainly medium grained, prismatic to tabular cumulus orthopyroxene with postcumulus plagioclase, clinopyroxene and late stage minerals quartz, k-feldspar, phlogopite, apatite, magnetite, rare rutile and zircon (Wilson *et al.*, 2000a; Wilson *et al.*, 2000b). The plagioclases are usually zoned and occur as oikocrysts of up to 10cm in diameter. The clinopyroxene similar to plagioclase occurs as oikocrysts but up to 20cm. Preferential weathering of the plagioclase grained

results in the nodular texture associated with the exposure of MSZ (Wilson *et al.*, 2000a) similar to that described by (Wilson, 1982) on the Darwendale Subchamber. The sulphides are (1) interstitial to the cumulus pyroxenes and closely associates with late stage minerals, (2) tend to concentrate around the margins of the plagioclase oikocrysts (Wilson, 1992).

The general patterns of metal and sulphide distribution in the MSZ gives rise to a well establish subdivision. The MSZ is made up of lower Platinum Group Element Subzone (PGEsz) generally 1.5-2.5m thick and an upper sulphide-rich Base Metal Subzone (BMsz). The base of the MSZ is where there is the visual appearance of sulphide in small amounts. The Hanging wall section is the unit stratigraphically overlying the PGEsz. The interval between the PGEsz and the top of the LSZ is called the Footwall section.

The contact between the websterite and the pyroxenite is not clearly defined in the western flank and normally grades to transition rock type as described in the Wedza Subchamber (Wilson and Prendergast, 2001).

## 2.7 Serpentinite Layer of Cyclic Unit 1

This layer is derived from the alteration of the dunites and harzburgites. These altered rocks are found at depths of 400m in drilled core. The contact in the west is discontinuous due to mass movement due to folding and faulting and soft sediment deformation at the steeply dipping margins. The rock types are variable and range from fine grained, almost pure, homogenous adcumulates, to much coarser grained feldspathic and phlogopite bearing variety. The contact of the serpentinite and the P1 Pyroxenite is marked by small scale layering also shows evidence of deformation and mass movement. Evidence in the west is the occurrence of boulder structures which resulted from in situ fragmentation and local milling of consolidated cumulates. Also nodular development is observed in the lower olivine-pyroxenite which separates the

P1 Pyroxenite from the underlying harzburgite (Wilson, 1996; Wilson *et al.*, 2000a; 2000b).

## 2.8 The Lower Ultramafic Succession

The layers below the Cyclic Unit 1 are dominated by dunite, olivine-pyroxenite grading to harzburgite. These layers are narrow, 40m thick as compared to the equivalent section in the Darwendale Subchamber which are 100m thick and lithologically homogenous (Wilson, 1996). On the west flank the pyroxenites are commonly very fine grained, contain chromite and become coarser-grained inward from the margins. The coarse pyroxenite has orthopyroxene grains from 5-15cm in length. The crystals are aligned parallel to the walls rocks and reflect growth in high thermal gradient. The pyroxenite ranges from adcumulates to orthocumulates and have 5-15% interstitial plagioclase as compared to the Darwendale Subchamber where interstitial phases are <5%. The association of pyroxenite, olivine-pyroxenite is less commonly defined as compared to the thick lithologically homogenous Darwendale Subchamber (Wilson, 1996; Wilson *et al.*, 2000a).

There is only a single unit of olivine-bearing pyroxenite in the Selukwe Subchamber. There is fine scale layering of olivine pyroxenite and harzburgite on a scale of 10-30cm and is also well developed in the lower part of the ultramafic sequence. A thick succession of dunite underlies the sequence of pyroxenites in the northern part of the subchamber but has not been intersected by drilled core. It is only exposed in the lowest part of the Selukwe stratigraphy.

## 2.9 Chromitites

Chromitite layers between the cyclic units are not observed in the western flank showing continuous layers are not well developed. Only one discontinuous layer, 1-10cm thick has been observed on the western side. It is located within the serpentinite and close to the P1 Pyroxenite. This is the only known occurrence of the chromite in

the Great Dyke at this stratigraphic location. Other fragments of chromitite are found in the harzburgite very close to the west margins and occur as pods, vertical stringers and discontinuous layers show evidence of slumping and folding (Wilson, 1996; Wilson *et al.,* 2000a). In the axial zone and east margin well developed chromite layers occur at the base of the Cyclic Unit 1. These occur as 30-80cm thick enclosed within harzburgites and dunite layers and in some places occur as series of narrow layers with combine thickness of 3m (Wilson *et al.,* 2000a).

## 2.10 The Border Group

The Border Group has been observed in most chambers of the Great Dyke, Darwendale, Wedza and Selukwe Subchamber (Wilson, 1982; 1996; Wilson *et al.*, 2000a; 2000b; Wilson, 2001) as a succession of layers close to or the margin of the magma chamber. The layers lie at a higher angle to the main layered sequence and almost parallel to the walls. The rock types are gabbros, norites, pyroxenites and have strong crystal alignment perpendicular to the original walls of the Great Dyke magma chamber (Wilson, 1996).

## 2.11 The Xenolith/Autolith Suite

The Selukwe Subchamber is characterized by xenoliths and possibly autolithic fragments (Wilson, 1996) which range from 1-2metres to several tens of metres in the west and central zone (Wilson *et al.*, 2000a). These are the main focus of this research project. The distribution of the xenoliths is in the subchamber is shown in MAP A, Appendix A. The xenoliths have been divided into three types; (1) Metasedimentary quartzite and banded iron formation, (2) Ultramafic rocks derived from the greenstones and (3) Possible mafic and ultramafic autolithic fragments.

The metasedimentary quartzite and banded iron formation fragments found in the western flank of the Selukwe Subchamber are clearly derived from the Wanderer Formation of the Shurugwi greenstone belt (Stowe, 1974; Stowe, 1968). They are

present in the upper part of the Mafic Sequence. The sizes of the xenoliths vary from small fragments, up to one metre in diameter, and large irregular blocks, up to 30 m in size. Pure quartz fragments occur, which are likely to have been derived from quartz vein rather than metasediments, are presents in the P1 pyroxenite at reaction on the margins of the quartz is apparent with pyroxene crystals radically developed by growth into the softened quartz (Wilson *et al.*, 2000a).

Ultramafic rocks derived from the greenstones include blocks of chromitites and serpentinite enclosed within pyroxenite or dunite are common in the ultramafic sequence on both the east and west sides. The blocks occur as irregular and rounded fragments 30cm to 30m in diameter with the largest fragment in the east side Chironde Chromite Claims and are of economic importance. The chromitites have clearly been derived from the surrounding greenstone belts as the spinel composition ($Mg/Mg+Fe^{2+}$) ranges from 0.51 to 0.62 with olivines with $Fo_{90-94}$ very low Ni content (<0.05% NiO), which indicates that the olivine is not primary igneous origin (Wilson *et al.*, 2000a).

Gabbros and pyroxenites have not been recognized in the SGB belt (Stowe, 1968) but these fragments are distributed within the gabbroic rocks and the upper Ultramafic Sequence. The rock types include olivine-pyroxenite, websterite, olivine gabbro and norite of evolved compositions. It has been postulated that these rocks could have been derived from an early formed Border Group of the Great Dyke magma chamber. The compositions are similar to those encountered where the Border group is preserved (Wilson, 1982; 1996; Wilson *et al.*, 2000a).

## 2.12 Summary and Discussion

The Selukwe Subchamber is part of the northern part of the Southern Chamber of the Great Dyke. It similar the other subchambers in that there is an Ultramafic Sequence overlain by the Mafic Sequence. There preservation of the xenolith suite and the Border Group rocks is not clear as in some places it has been totally destroyed by

active thermal and physical erosion (Wilson *et al.*, 2000a). The Selukwe Subchamber is unique in that several rocks of unknown origin have been preserved in the west. It is postulated that these autolithic fragments were preserved because of the rapid heat follow which did not allow them to melt back into the magma but were ripped off and preserved. The object of this study is to present a more detailed classification of the xenolithic/autolithic fragments. This study will enable an appreciation as to whether these fragments were derived from xenoliths of the Shurugwi Greenstone Belt or as autoliths of the Great Dyke Border Group or from elsewhere.

# CHAPTER 3: STRATIGRAPHY AND LITHOLOGIES OF THE PAR 11 BOREHOLE

## 3.1 Introduction

The 230.22m PAR 11 borehole is located in the Paarl block, (Fig 2.1) north-west of the Unki Shaft. The importance of this section is to show the stratigraphy of the PAR 11 borehole and the locations of where thin section samples were taken for petrographic studies discussed in the next chapter. A detailed log is also appended in Appendix C. The borehole is characterized by harzburgites and olivine-pyroxenite layers that occur within a regionally continuous P1 pyroxenite and gabbro and this therefore represents an anomalous occurrence. Although field exposures are poor in the area, gabbro surrounds this body and the question arises as to whether it is feeder-type structure or a xenolith of some type. The borehole was drilled to answer these questions as part of the exploration program by South Mine Complex (Pvt) Limited.

The stratigraphic log (Fig. 3.1) shows major layers developed within this body. It also shows the depths of where the thin sections described in the next chapter where taken from. A detailed stratigraphic log is appended in Appendix C. The uppermost layer is pyroxenite that grades to narrow layer of olivine-pyroxenite and then to dunite/harzburgite. The PAR 11 borehole is made up of three cyclic units of pyroxenites and peridotites with the lower most unit layer composed of dunite/harzburgite.

## 3.2 Characteristic Features of the Pyroxenite and Olivine-Pyroxenite

The pyroxenites contain 90-100% orthopyroxene and grade into olivine-pyroxenite which contains 10-40% olivine and 60-90% orthopyroxene with minor plagioclase and clinopyroxene. There are three distinct layers of pyroxenite and olivine-pyroxenite in the PAR 11 borehole;

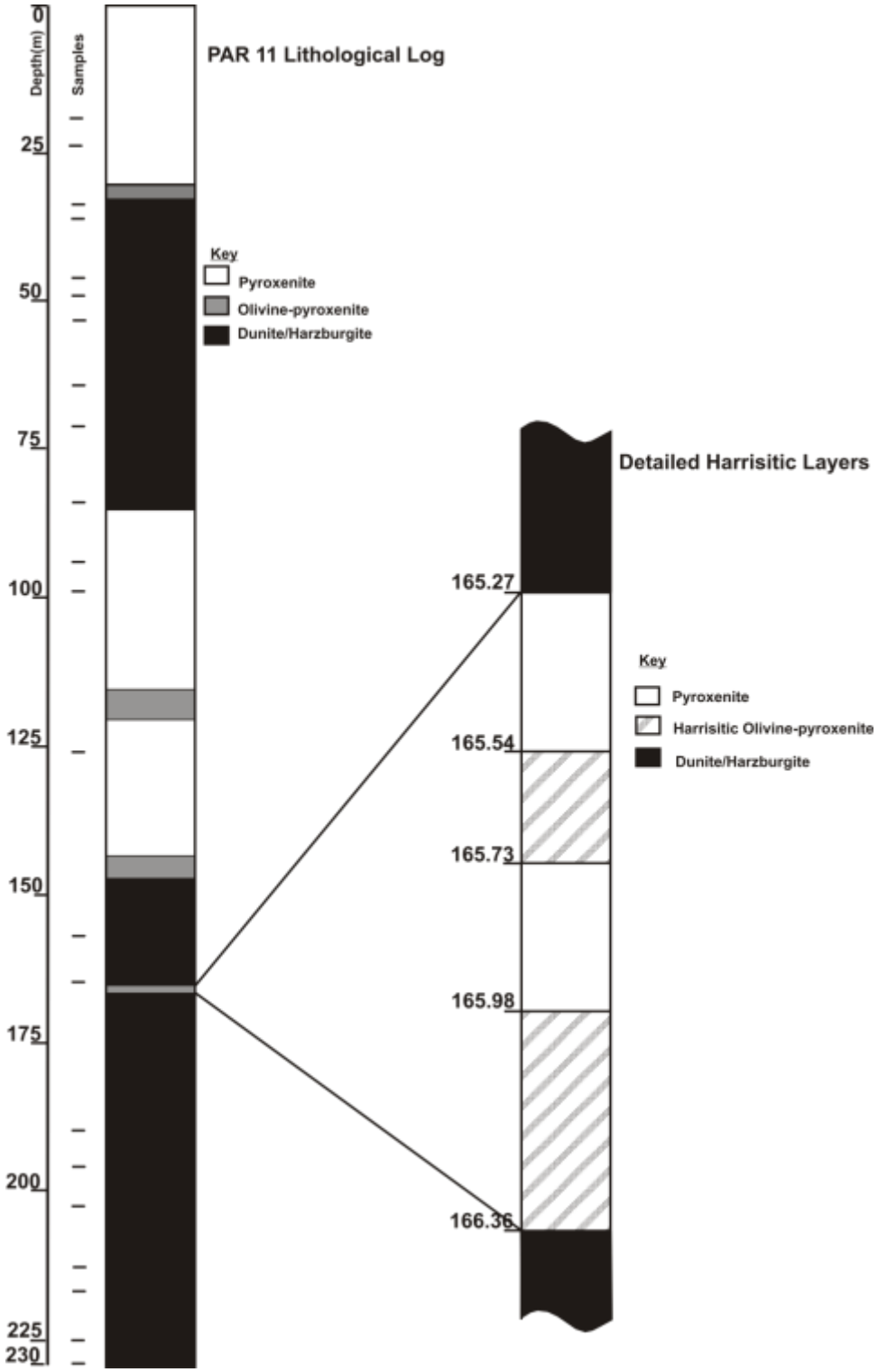


**Fig. 3.1.** Stratigraphy of the PAR 11 borehole. A total of 22 thin sections were cut for petrography and are indicated as thin black lines on the left side of the log.

i. 0 to 16m there is highly weathered coarse grained pyroxenite. At 16 to 30.26m (Fig. 3.2) is coarse grained pyroxenite which grades into olivine-pyroxenite between 30.26 to 30.46m.

ii. A medium grained pyroxenite layer at occurs at 85 to 87m with patches of olivine-pyroxenite. This layer grades to pyroxenite at 87- 116m which then grades into olivine-pyroxenite at 116 to 120m (Fig. 3.3). Thereafter pyroxenite occurs at 120 to 143m which grades into olivine-pyroxenite at 143 to 147m.

iii. Two narrow layers of coarse-grained of pyroxenite and olivine-pyroxenite occur between 165.27 to 166.36m (see insert in Fig. 3.1). From 165.27 to 165.54m is a coarse grained pyroxenite with plagioclase which is underlain by harristic olivine-pyroxenite layer from 165.54 to 165.73m (Fig 3.4). Thereafter is a layer of pyroxenite between 165.73 to 165.95m and olivine-pyroxenite at 165.95 to 166.36m.

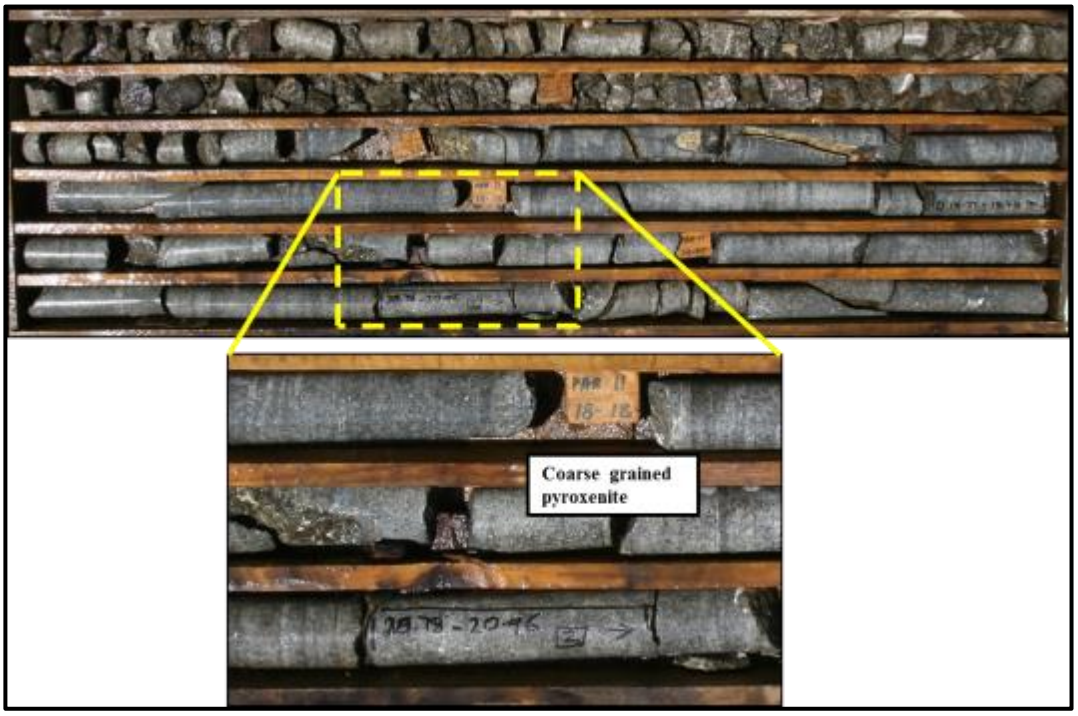


**Fig. 3.2.** Diamond drill core of the upper 16m weathered coarse grained pyroxenite of the PAR 11 borehole. More detailed insert shows micro-rhythmic layering (red arrows).

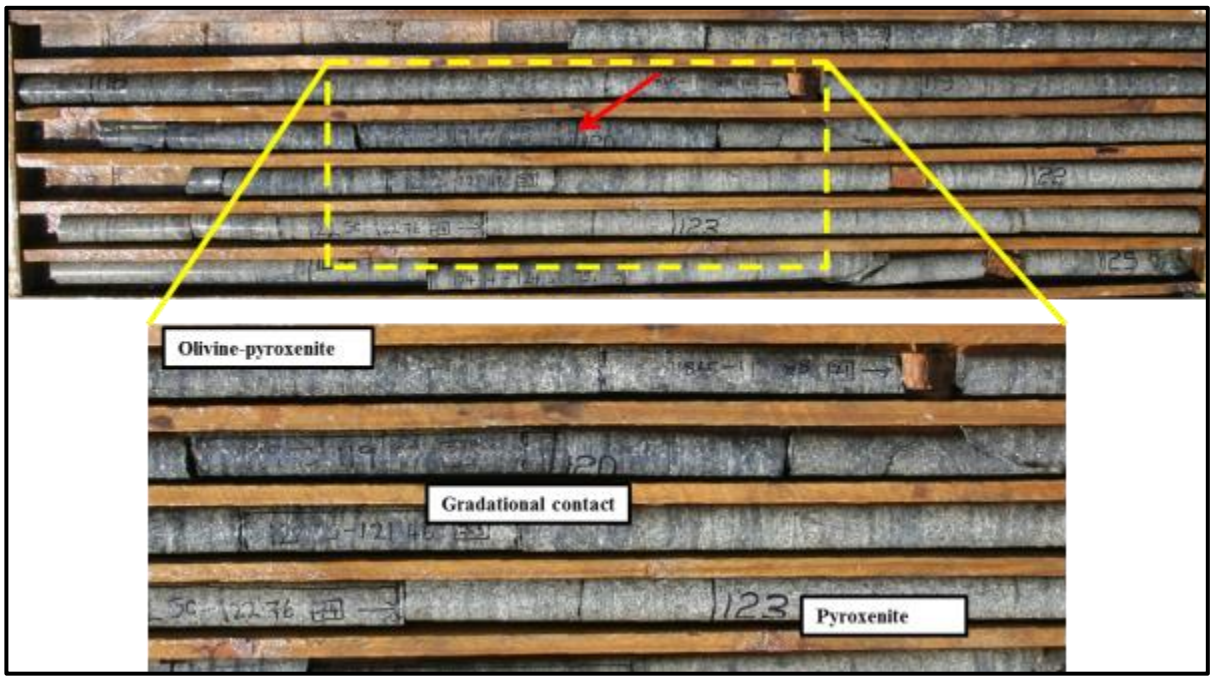


**Fig. 3.3.** The gradational contact between coarse grained olivine-pyroxenite with homogeneous pyroxenite at ~120m.


**Fig. 3.4**. Diamond drilled core from (A). 158.7 to 163.52m. (B) Typical coarse grained harzburgites. (C) Coarse feldspathic pyroxenite in contact with harristic-textured olivine-pyroxenite.

## 3.3 Characteristic Features of the Dunite and Harzburgite

The dunite and harzburgite layers (Fig. 3.1) generally have a granular coarse texture. The dunites have 90-100% olivine with minor plagioclase. The harzburgites have 40-90% olivine, 5-10% orthopyroxene and minor plagioclase. It is difficult to distinguish the dunite and the harzburgite on drilled core. There are three major layers of dunite/harzburgites occurring at depths of 30.49 to 85m, 147 to 165.27m and at 166.36 to 230.22m.

i. At a depth of 30.49-76.96m the dunite/harzburgite layer is coarse grained with narrow feldspathic zones (Fig. 3.5) at several locations. At 76.96 to 85m the harzburgite has minor layers olivine-pyroxenite of up to 10cm across (Fig. 3.6).
ii. At depths of 147 to 165.27 is coarse grained dunite/harzburgite with plagioclase.
iii. From 166 to the end of the borehole at 230.22m the dunite/harzburgite layers become coarser with large nodules of plagioclase (Fig. 3.4B).

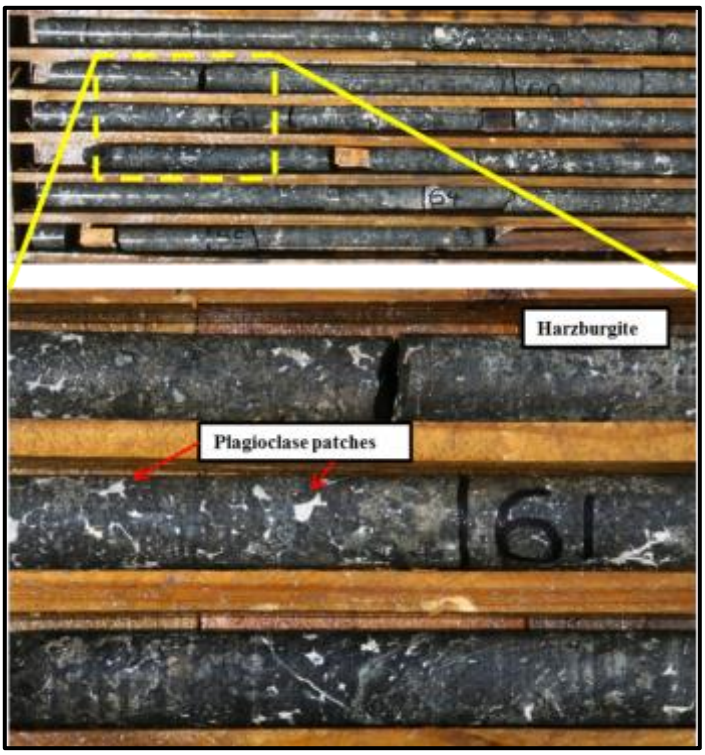


**Fig. 3.5.** Diamond drilled core of coarse-grained harzburgite with up to 2cm of patches of plagioclase at a depth of 61m.

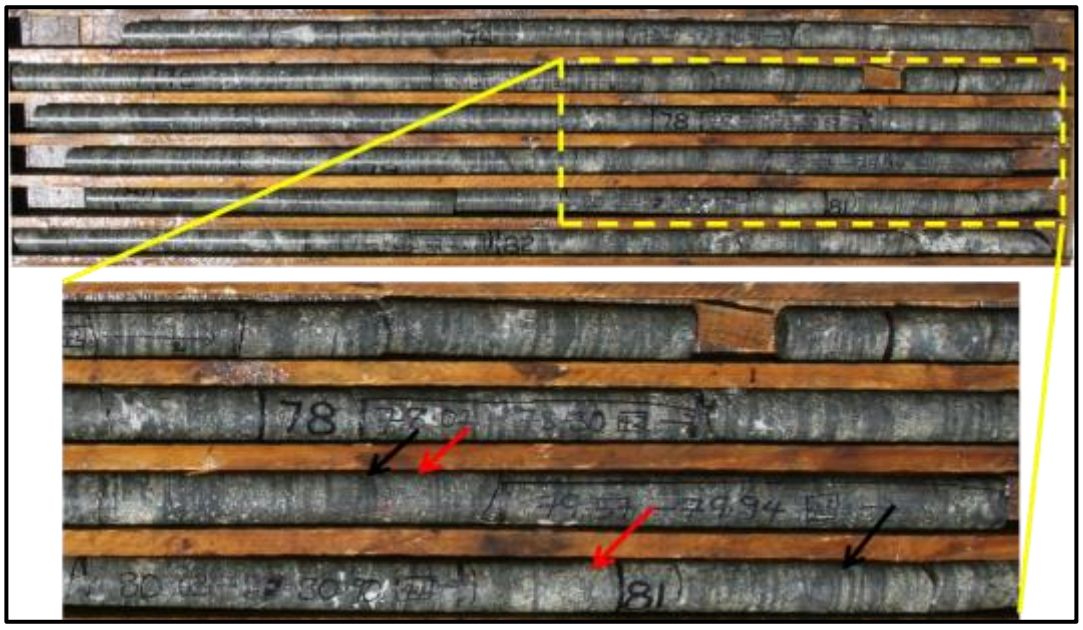


**Fig. 3.6.** Diamond drilled core of harzburgite (black arrows) dark greenish grey alternating with layers of olivine-pyroxenite (red arrows) light grey.

## 3.4 Summary and Discussion

The lithological log displays that the PAR 11 layers alternate between dunite, harzburgites, olivine-pyroxenite and pyroxenite. The uppermost layer is pyroxenite with the mafic succession completely absent even though it is located within rocks of the Mafic Succession. The pyroxenites occur as pure pyroxenite layers or layers with minor olivine pyroxenite layers. The olivine-pyroxenite occurs as pure olivine pyroxenite, gradational contact layers with pyroxenite layers or dunite/harzburgites. The dunite/harzburgite occurs as pure dunite/harzburgite or dunite/harzburgite with minor olivine pyroxenite layers. Typical of the Selukwe Subchamber the ultramafic layers, the PAR 11 borehole layers are narrow as compared to the equivalent thick section of the Darwendale Subchamber (Wilson, 1982; Wilson *et al.,* 2000a).

The PAR 11 borehole represents the only known occurrence in the Selukwe Subchamber of harzburgites and dunites within the P1 pyroxenite layer and gabbros. The body also is not a laterally continuous layer and therefore represents either a feeder dyke or a pipe like structure of a type not previously encountered in the Great Dyke. The harristic textures are found in the of the olivine-pyroxenite layer and have been observed in other layers of the Great Dyke (Wilson, 1982) in the Darwendale Subchamber. The harristic textures were from marginal occurrences of the Darwendale whereas the PAR 11 borehole occurrence is well within the Great Dyke intrusion. This leads us to the conclusion PAR 11 borehole was formed in marginal environment and was transported to its present location in the Mafic Succession.

# CHAPTER 4: PETROGRAPHY OF THE PAR 11 BOREHOLE AND THE UNKI XENOLITH SUITE

## 4.1 Introduction

A total of 22 samples were taken from the PAR 11 borehole for petrographic studies. The position of the depth of the samples is shown on the stratigraphic log in the previous chapter (Fig. 3.1). Other samples were selected from boreholes that intersected xenolith fragments VS8, PAR 28, MR33, MR102, MR125, MR 316, MR 327, MR 328, MR 330 and MR 331. The location of PAR 11 and the other boreholes are shown in the Map A, Appendix A. All thin sections studied are in Appendix D.

The PAR 11 borehole sequence has been classified into two groups, peridotites and pyroxenite. The surface xenolith suite samples were collected at various localities within the Selukwe Subchamber of the upper Ultramafic and Mafic successions. The positions of these samples are also shown in Map A, Appendix A. The Unki xenolith suite consists of ultramafic and mafic rocks have been classified into three groups, peridotites, pyroxenites and feldspathics.

## 4.2 Petrography of the PAR 11 Borehole Suite

### 4.2.1 Peridotite Group

The peridotites are mainly dunites and harzburgites. They dunites have cumulus olivine grains ranging from medium to coarse, 2-10mm with minor clinopyroxene, plagioclase, and spinel. The harzburgites have cumulus olivine and orthopyroxene with postcumulus plagioclase, clinopyroxene and spinel.

#### *4.2.1.1 Dunites*

The dunites are medium to coarse grained <2-10mm with more 90% olivine. The cumulus olivine crystals have well-developed grain boundaries meeting at triple point junctions with interstitial clinopyroxene. Spinel grains are found inside the olivine

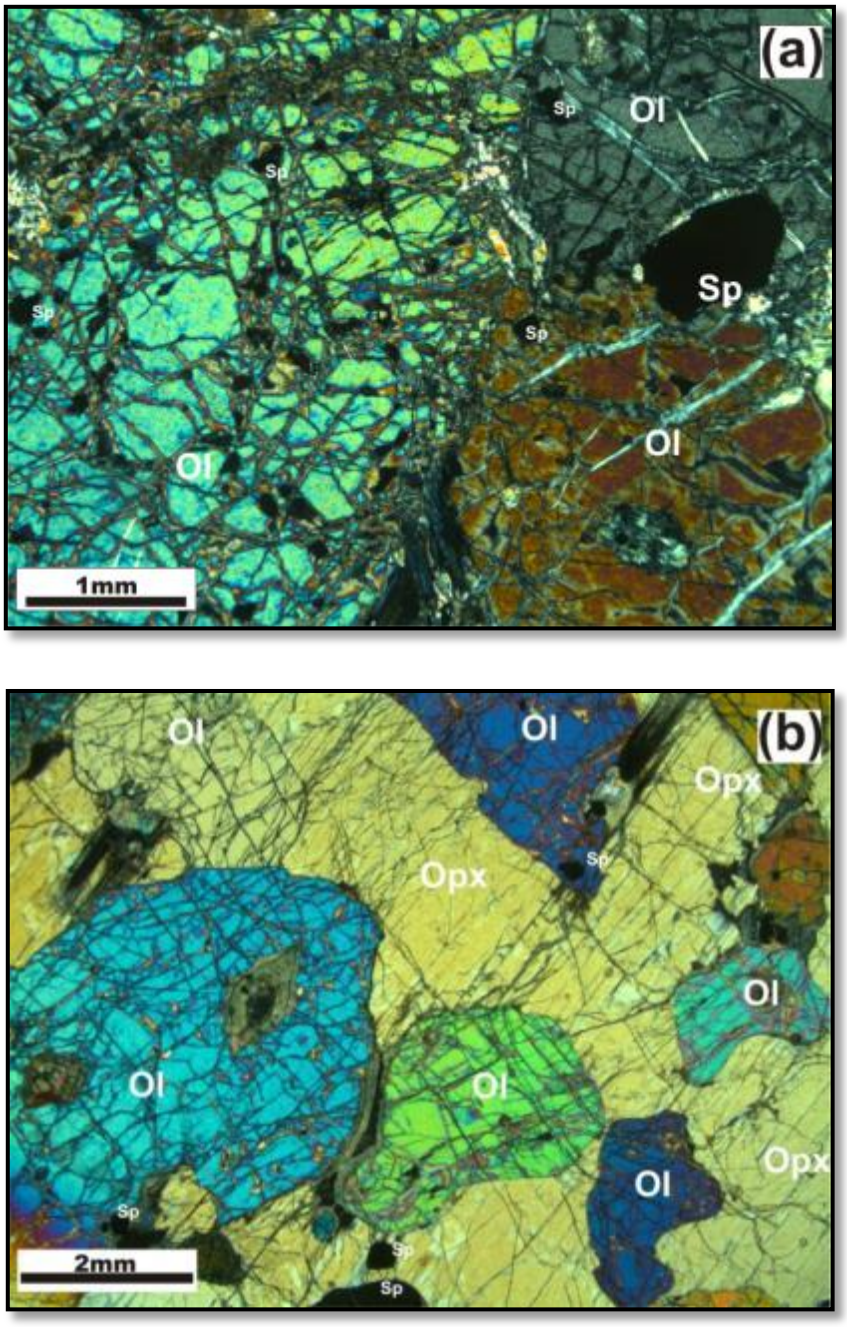


**Fig. 4.1.** (a) Photomicrograph of dunite with coarse crystals of olivine (Ol) enclosing fine crystals of spinel (Sp) in sample no. PAR 11-104 under XPL (b) Photomicrograph of harzburgite with large grains of olivine (Ol) enclosed in a large grain of orthopyroxene (Opx). There are fine grains of spinel (Sp) enclosed in the olivine in sample no. PAR 11-133 under XPL.

fractures and surrounding the grain edges shown in Sample No. PAR 11-104 in Fig. 4.1a taken at a depth of 164.88m.

#### *4.2.1.2 Harzburgites*

The harzburgite are medium to coarse grained with 10-40% orthopyroxene and 40-90% olivine. The harzburgites have optically continuous orthopyroxene with a first order yellow colour encloses smaller subrounded grains of olivine as displayed in sample no PAR 11-133 in Fig. 4.1b. The olivine grains also enclose grains of clinopyroxene and spinel grains. All the mineral grains are relatively fresh. This sample was taken from a depth of 203.48m.

### 4.2.2 Pyroxenite Group

The PAR 11 pyroxenite group is made up of pyroxenite and olivine pyroxenite. The pyroxenites have cumulus orthopyroxene grains ranging from 2-10mm with minor clinopyroxene, plagioclase and spinel. The olivine-pyroxenites have cumulus orthopyroxene and olivine with minor spinel and plagioclase. The grain shapes are generally equant and sometimes tabular. The grain boundaries are usually irregular. The mineral grains are show only slight internal strain.

#### *4.2.2.1 Pyroxenites*

The pyroxenites contain >90% tabular orthopyroxene with well-developed triple point junctions. The orthopyroxene grains are prismatic and polygonal with postcumulus 5-10% plagioclase and clinopyroxene. The pyroxenite sample PAR 11-53 is shown in Fig 4.2a taken at a depth of 93.58m displays are no kink bands or signs of deformation and the minerals are unzoned.

#### *4.2.2.2 Olivine-pyroxenites*

The olivine-pyroxenites have 10-40% olivine and 40-90% orthopyroxene. The optically continuous orthopyroxene encloses subrounded olivine grains in sample no. PAR 11-149 is shown Fig 4.2b. The olivine grains also enclose spinel in the fractures and pockets clinopyroxene. On the top left corner of the photomicrograph shows alteration of the orthopyroxene. This sample was taken at a depth of 225.48m.

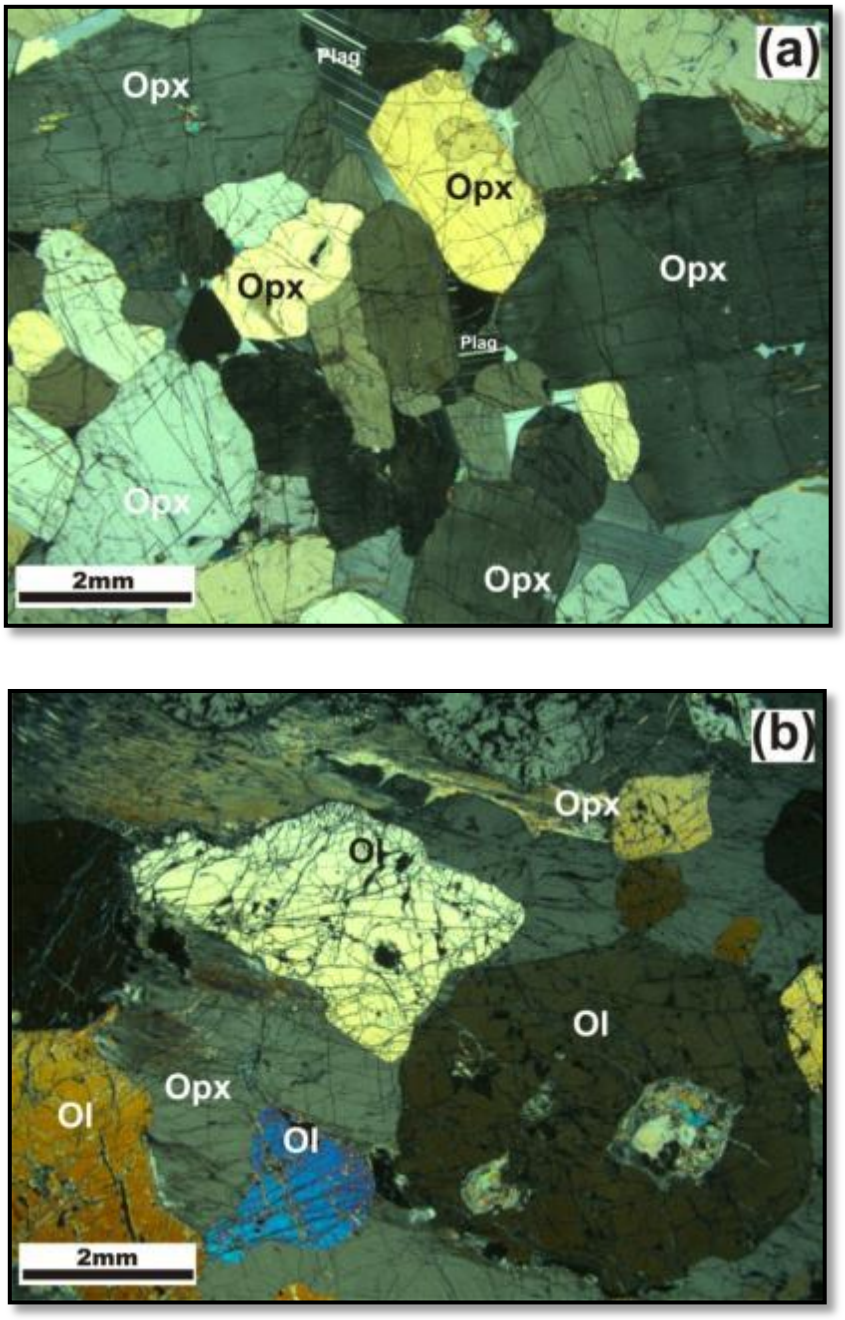


**Fig. 4.2.** (a) Photomicrograph of pyroxenite displaying tabular orthopyroxene (Opx) grains with well- developed triple junction points and postcumulus plagioclase (Plag) in sample no. PAR 11-53 under XPL. (b) Photomicrograph of olivine-pyroxenite with optically continuous orthopyroxene (Opx) enclosing and olivine (Ol) in sample no. PAR 11-149 under XPL. There are crystallized melt inclusions are within the olivine.

## 4.3 Petrography of the Unki Xenolith Suite

The Unki xenolith suite comprises ultramafic (feldspar free) and gabbroic rocks. These xenoliths contain minerals with no zoning and are generally mono-, bi- and tri-mineralic assemblages. They are classified into the peridotite group (dunites, harzburgites, and lherzolites), pyroxenite group (pyroxenites, olivine-pyroxenites, websterite, and olivine websterite) and the feldspathic group (gabbro, orthopyroxene gabbro, clinopyroxene norite). There are also olivine bearing gabbros and norites.

### 4.2.1 Peridotite Group

#### *4.2.1.1 Dunites*

Dunites consist originally of cumulus olivine (80- 90%) with minor chromite and postcumulus orthopyroxene and biotite (5-10%). The dunites from the xenolith suite are very fine grained (grain size <1mm) and most are completely altered to serpentinite. Fig. 4.3 shows a photomicrograph of a typical sample of serpentinized dunite. The original olivine grains are altered and seem to be elongated with some weak alignment.

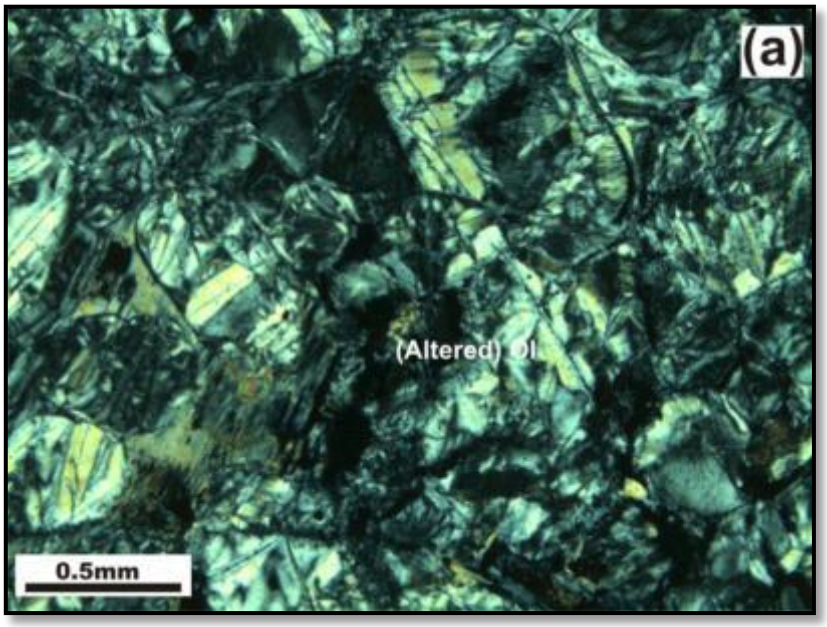


**Fig. 4.3.** Photomicrograph of serpentinized micro-dunite. The relict olivine (Ol) grains have now been altered in sample no. MR 33/2 under XPL.

#### *4.2.1.2 Harzburgites*

Harzburgites in the xenolith suite are composed of cumulus olivine (60-85%), orthopyroxene (10-35%) with minor clinopyroxene, plagioclase and biotite. A total of 21 samples of harzburgite xenolith samples were used in this study. They are fine to medium-grained and show an equigranular texture. In Fig. 4.4a, sample no. UNK 93-16 is a micro-harzburgite with polygonal grains of orthopyroxene in the top western corner and serpentinized olivine grains at the bottom of the slide. The serpentinized olivines are usually surrounded by original crystals of chromite.

A medium grained (0.5-1mm) harzburgite is shown in Fig. 4.4b. It has cumulus orthopyroxene and fresh olivine. There are two populations of olivine and orthopyroxene, the well-developed large grains and the very fine grains. The mineral grains in both samples have well-developed triple point junctions indicating complete equilibration of the phases.

#### *4.2.1.3 Lherzolites*

Lherzolites normally have a composition of olivine > orthopyroxene > clinopyroxene > spinel. They consist of 40-90%, olivine 5-40% orthopyroxene or clinopyroxene and ± 5% spinel. A total of 8 samples of lherzolite xenoliths were studied. The grain sizes vary from fine-grained to medium-grained. A very fine grained (<1mm) lherzolite is shown in Fig. 4.5a. The cumulus olivine, orthopyroxene, clinopyroxene grains all show well-developed triple junctions. The spinel lherzolite in Fig. 4.5b shows large anhedral oikocryts of orthopyroxene and olivine with clinopyroxene. All the mineral grains meet at triple point junction. There are spinel grains enclosed in and around the edges of the olivine grains.

### 4.3.2 Pyroxenite Group

There are two types of pyroxenites, the olivine-free (pyroxenite and websterite) and those with ~30% olivine, already serpentinized (olivine-pyroxenite and olivine websterite).

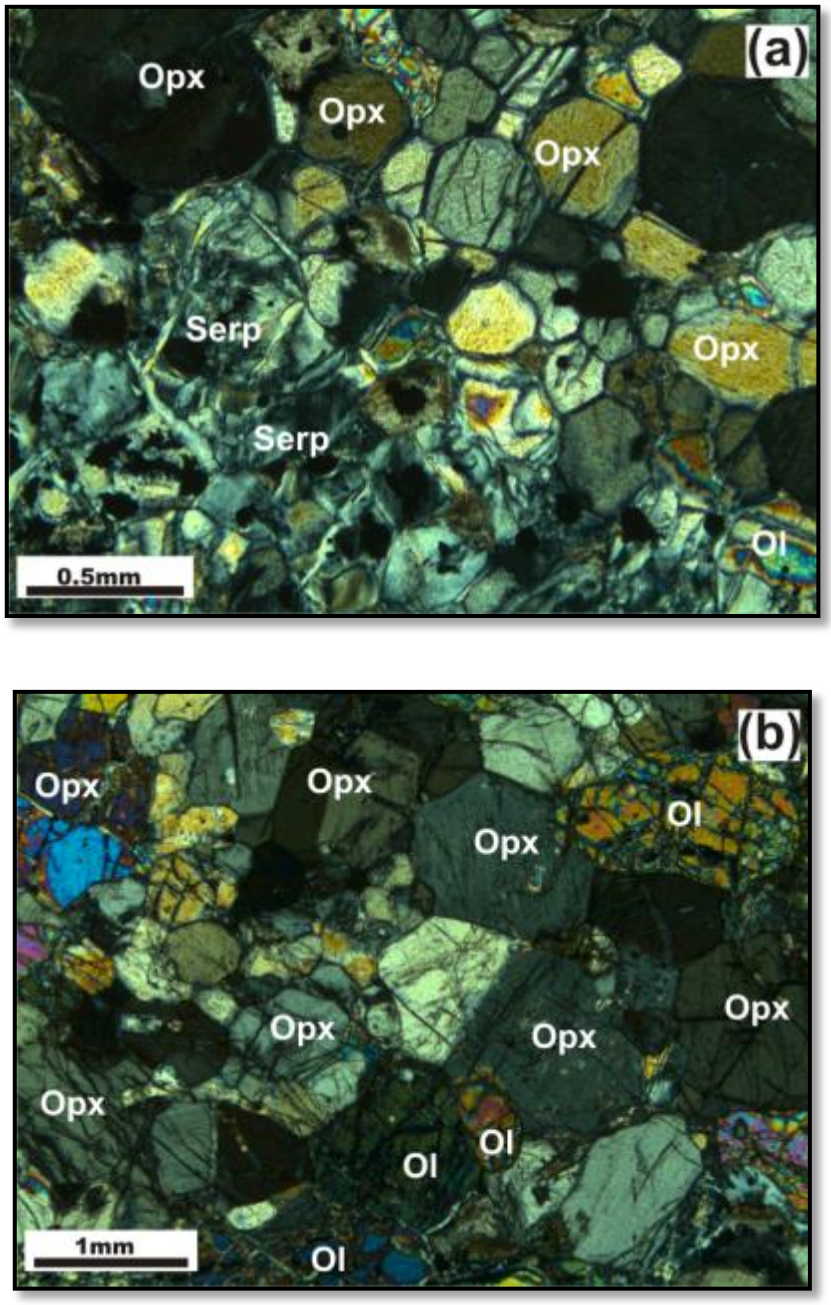


**Fig. 4.4.** Photomicrographs of harzburgites from the Selukwe xenolith suite. (a) Micro harzburgite with polygonal aggregates of orthopyroxene (Opx) and serpertinized (Serp) olivine grains and Olivine (Ol) in sample no. UNK 93-16 under XPL. (b) Medium grained harzburgite with polygonal aggregates of Opx and Ol central part of the thin section with minor spinel on the edges of the grains in sample no. UNK 93-26 under XPL.

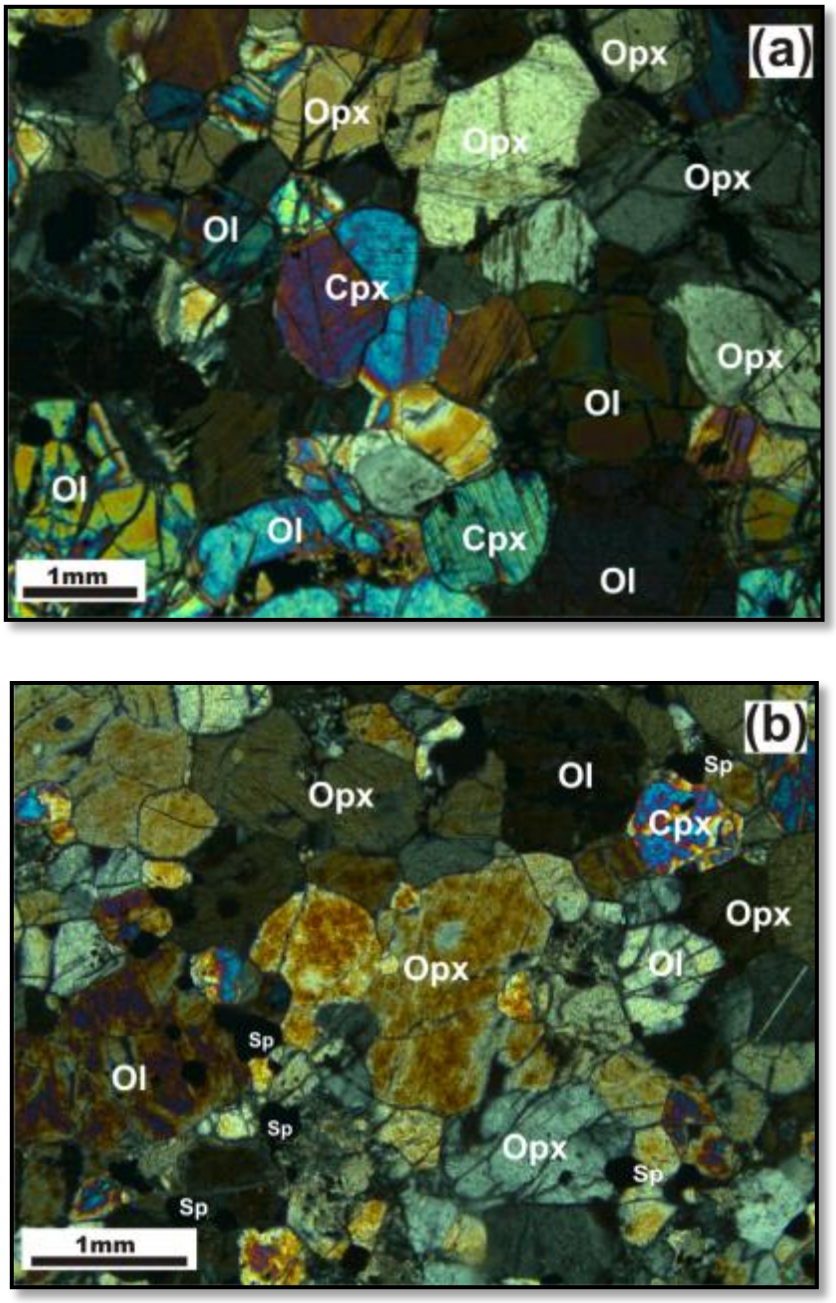


**Fig. 4.5.** Photomicrographs of (a) micro-lherzolite olivine (Ol), orthopyroxene (Opx) and clinopyroxene showing well-developed triple points junctions in sample no. UNK 93-46 under XPL. (b) Spinel lherzolite with orthopyroxene (Opx), clinopyroxene (Cpx) and small grains of spinel (Sp) enclosed by olivine (Ol) or on its edges in sample no. USM 10 under XPL.

#### *4.3.2.1 Pyroxenite*

Pyroxenite occurs in two forms: (1) very fine grained with equigranular and polygonal grains with crystal size less than 1 mm, and (2) the coarse grained/porphyritic textured with two populations of orthopyroxene, subhedral oikocrysts surrounded by fine grained matrix of polygonal crystals. A total of six pyroxenite xenolith samples of have been studied. The pyroxenites are mono-mineralic with < 90% orthopyroxene while some a bi or tri-mineral with interstitial (< 5%) plagioclase, clinopyroxene, olivine, spinel. A porphyritic pyroxenite in Fig 4.6, sample no. UNK 93-59 displays two populations of orthopyroxene, large grains of orthopyroxene are set in a fine-grained matrix of equigranular grains of orthopyroxene. The matrix consists of polygonal and tabular grains all with well-developed triple junction points.

#### *4.3.2.2 Olivine-pyroxenite*

The olivine-pyroxenites are commonly fined grained with 10- 40% of olivine and 40-90% orthopyroxene. A total of eight olivine-pyroxenite xenolith samples have been studied. A porphyritic texture is shown in Fig 4.7 with large phenocrysts of orthopyroxene in a fine grain matrix of olivine and orthopyroxene. In the matrix the orthopyroxene grains are equigranular and show a polygonal texture with well-developed triple point junctions. Fig 4.7(a) shows a wider field of view of the sample no. UNK 93-2A displaying the distribution of phenocrysts and matrix and Fig. 4.7(b) shows well developed triple point junctions of the phenocrysts. The matrix is made up fine grained orthopyroxene, clinopyroxene and minor spinel scattered at the edges of olivine grains.

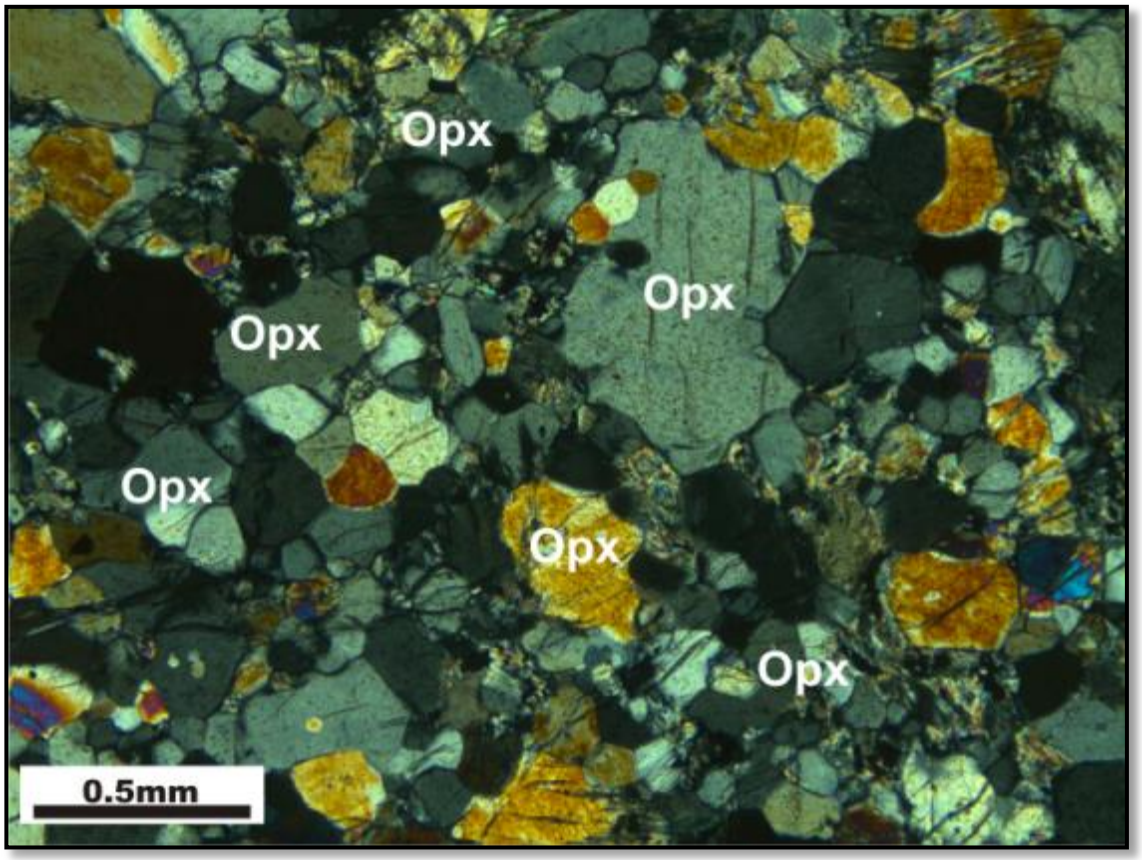


**Fig. 4.6.** Photomicrograph of a porphyritic pyroxenite showing cumulus orthopyroxene (Opx) grains and interstitial olivine (Ol) in sample no. UNK 93-59 under XPL.

***4.3.2.3 Websterites***

These have 95-100% of both cumulus orthopyroxene or clinopyroxene and minor plagioclase and olivine. The samples studied here have an equigranular texture with well-developed polygonal grains. Websterites have never been reported in the Shurugwi Greenstone Belt. There are three websterite in xenolith samples. Sample USM 74 is a granular fine grained websterite that contain 90-95%, of both orthopyroxene and clinopyroxene and <5% olivine.

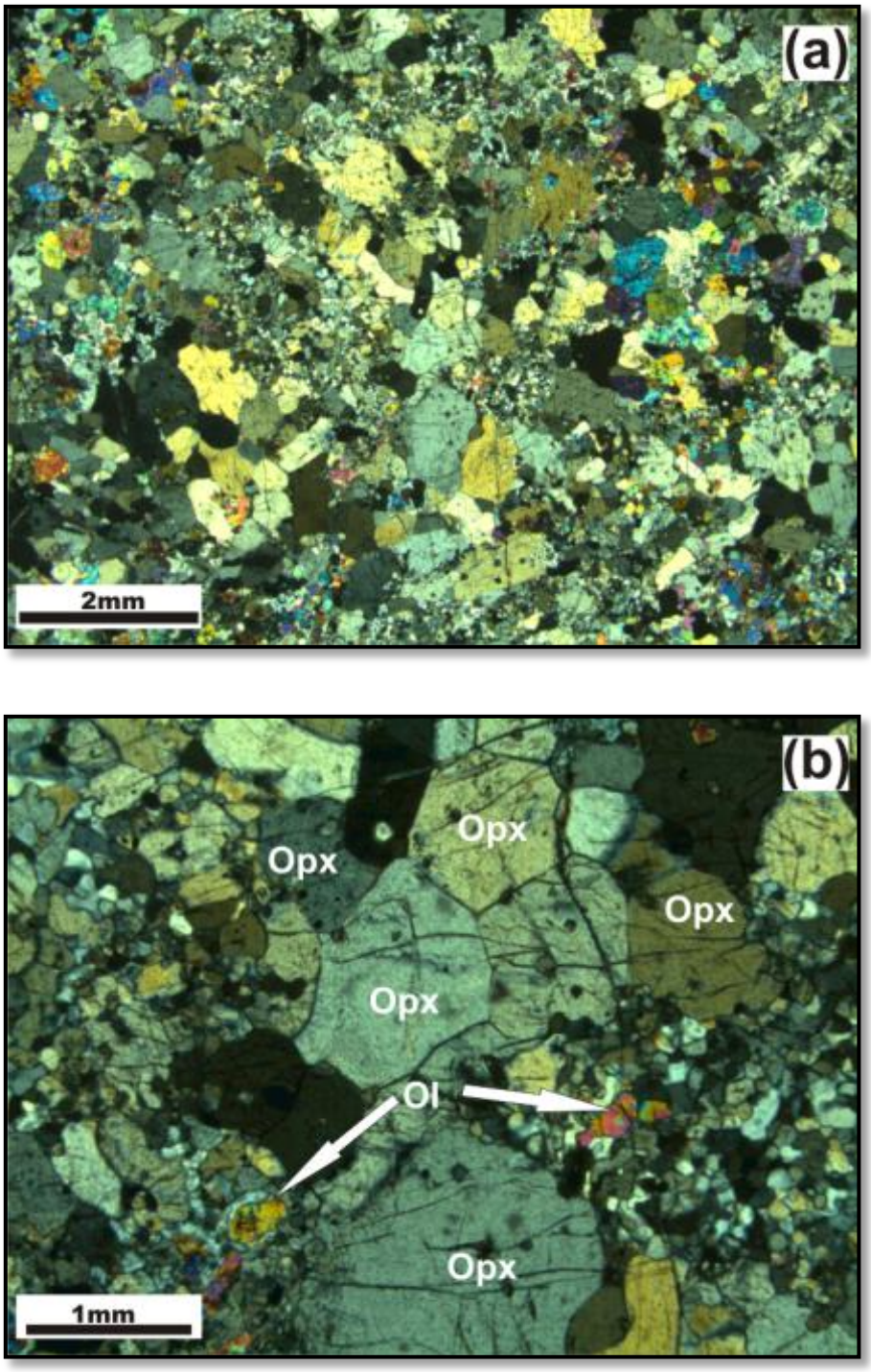


**Fig. 4.7.** Photomicrographs of an olivine-pyroxenite with olivine (Ol) and orthopyroxene (Opx), (a) shows a wider view the sample no. UNK 93/2A under XPL. (b) Large phenocrysts of Opx and a matrix of Ol and Opx forming a polygonal mosaic with triple point junctions in sample no. UNK 93/2A under XPL.

#### *4.3.2.4 Olivine Websterites*

These are mostly fine grained containing 90-95% of both orthopyroxene and clinopyroxene and > 5% olivine. The olivines are partially altered or completely altered to serpentine in these rocks. The orthopyroxene grains have a polygonal shape and some have rounded edges showing triple point junctions. Clinopyroxene occurs as large oikocrysts with exsolution lamellae of orthopyroxene. The olivine websterite has large oikocrysts of olivine that are partially serpentinized, with a fine matrix of polygonal grains of orthopyroxene, relatively fresh olivine and interstitial clinopyroxene. There are 5 surface samples of olivine websterite, sample no. USM 1, UNK 93-52, 53, 56, 69 and 3 from borehole samples MR 102/1, MR125/2, and MR125/3 that have been studied. Fig. 4.8 (a) shows a wide view of an olivine websterite sample no. MR125/3 and (b) shows more detail of the same sample. The olivine occurs as sub-rounded oikocrysts altered to serpentine with a matrix of fine of olivine, orthopyroxene and clinopyroxene. The matrix grains show polygonal aggregates with well-developed triple-point junctions.

An olivine websterite is shown in Fig. 4.9a of sample no. MR 102/1 with altered an anhedral olivine crystal in the middle of the photomicrograph. The other mineral grains are orthopyroxene and clinopyroxene with well-developed triple point junctions at the boundaries of small polygonal crystals. The clinopyroxene displays well developed exsolution lamellae. Fig. 4.9b shows another sample of olivine websterite sample no. UNK 93/69 that displays an equigranular texture. All the minerals olivine, orthopyroxene and clinopyroxene have well-developed polygonal grains. The olivine is completely altered and interlocks with the orthopyroxene and clinopyroxene. Very fine grains of spinel surround the olivine.

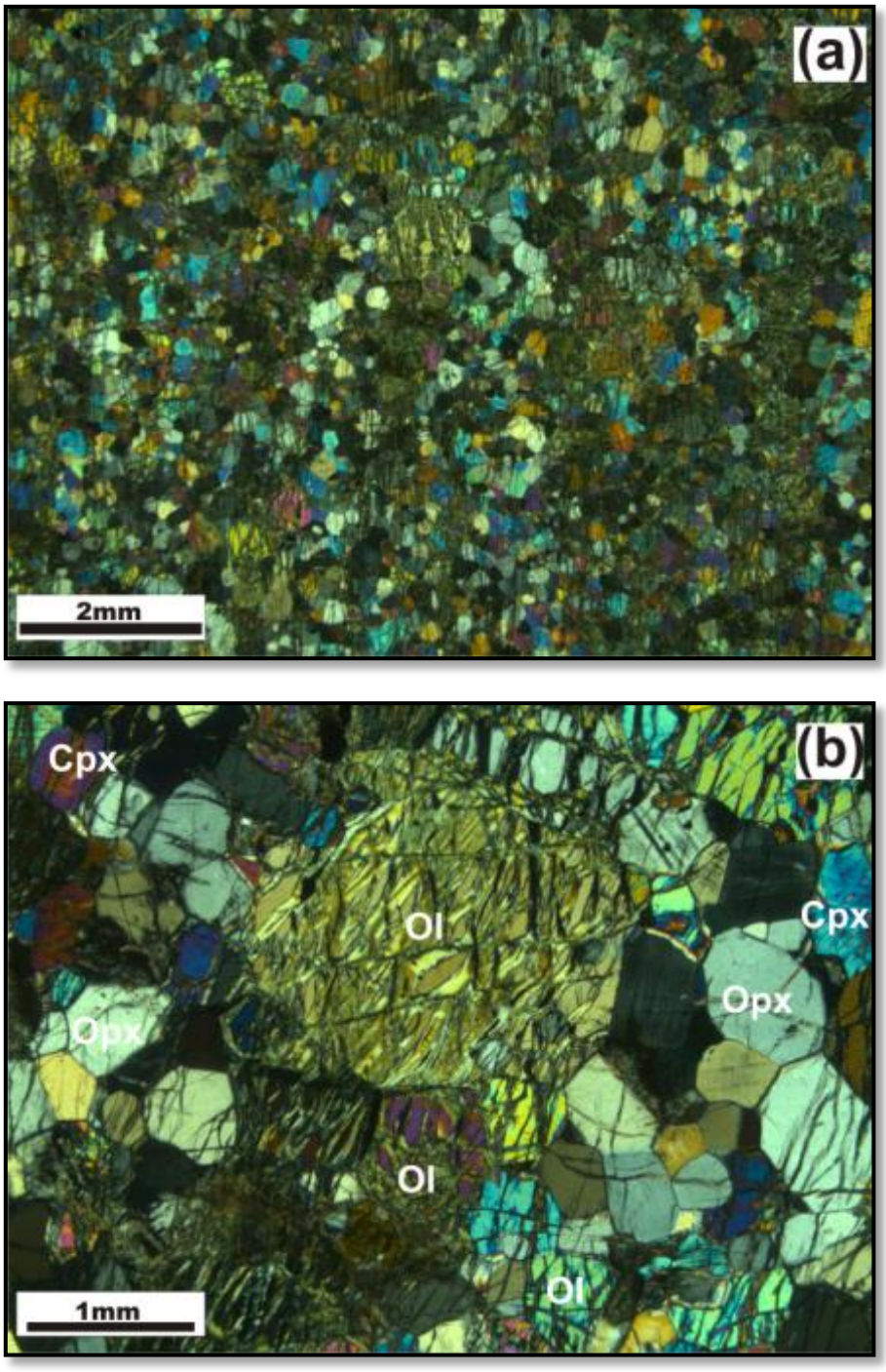


**Fig. 4.8.** Photomicrographs shows (a) fine grained olivine websterite displayed on a wider view under XPL and (b) a large oikocryst of an altered olivine (Ol) polygonal orthopyroxene (Opx) and clinopyroxene (Cpx) more detailed in sample no. MR125/3 under XPL.

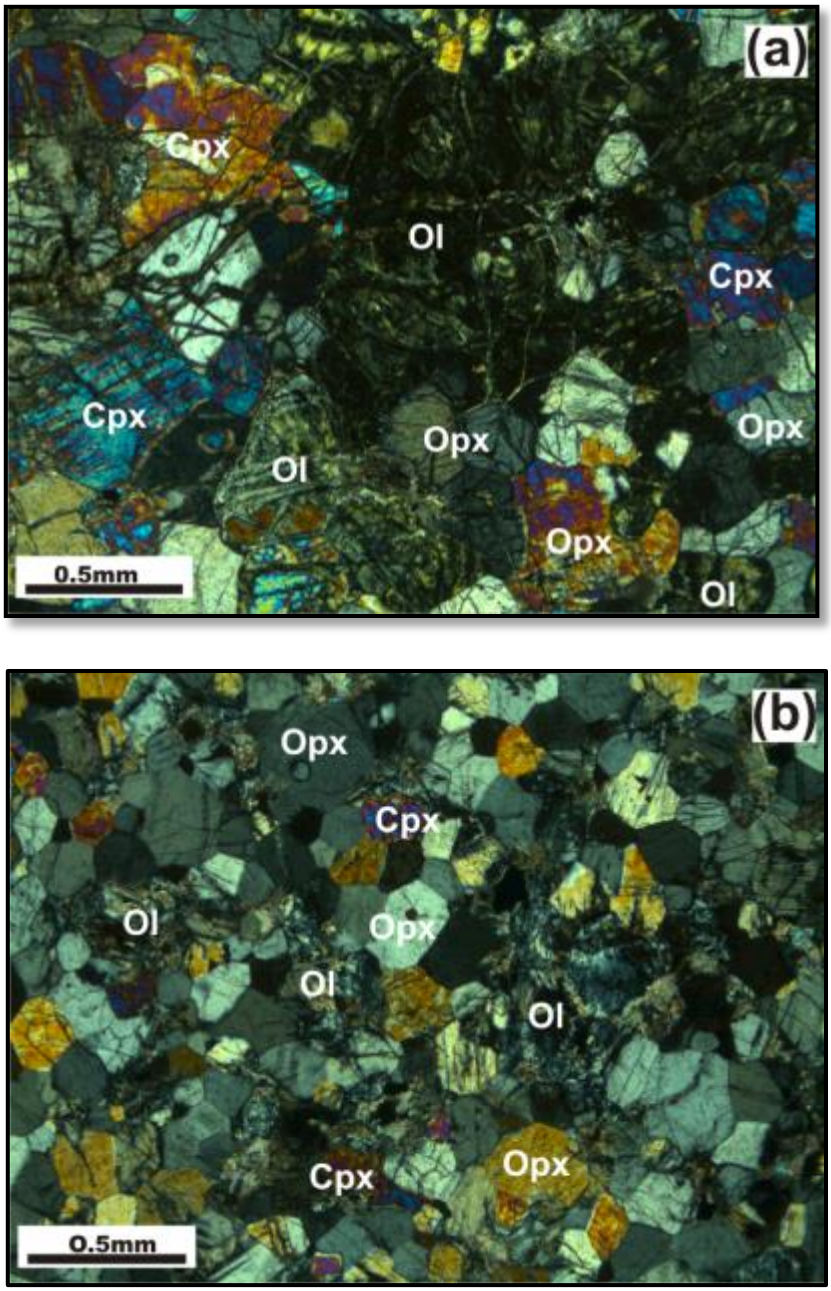


**Fig. 4.9.** Photomicrographs shows olivine websterites (a) The large olivine (Ol) oikocryst is almost completely serpentinized with anhedral clinopyroxene (Cpx) and orthopyroxene (Opx) all displaying triple point junctions in sample no. MR102/1 under XPL. (b) Polygonal aggregate fine grains of olivine, orthopyroxene and clinopyroxene. Some of the olivine grains are almost completely serpertinized while others are mainly unaltered in sample no. UNK 93/69 under XPL.

### 4.3.3 Feldspathic Group

Feldspathic xenoliths are made up of variable amounts of plagioclase and clinopyroxene with minor orthopyroxene or serpentinized olivine. The grain sizes range from fine < 1mm to medium grained (2-3mm) to distinctly coarse grained with olivine up to 6mm. The clinopyroxene occurs as oikocryts surrounded by cumulus plagioclase that lacks zoning. A total of 13 samples of feldspathic xenoliths were studied that include gabbro, norite, gabbronorite, magnetite gabbronorite pigeonite, olivine bearing gabbros and norites.

#### *4.3.3.1 Orthopyroxene gabbro/Clinopyroxene norite*

These comprise 60- 80% plagioclase with >20-40 % orthopyroxene or clinopyroxene. Minor minerals include interstitial biotite and olivine. A micro norite (Fig 4.10a) shows plagioclase some well-developed triple point junctions and large oikocryts of orthopyroxene with exsolution lamellae. There is also postcumulus clinopyroxene that has been altered far right. A micro-gabbro (Fig. 4.10b) displays large sub-rounded oikocrysts of clinopyroxene with 90° pyroxene cleavage. The cumulus plagioclase shows well-developed triple junction points.

A micro gabbronorite is shown in Fig. 4.11a displaying large oikocryts of pigeonite interlocking with clinopyroxene, orthopyroxene and plagioclase grains. All the minerals grains show well-developed triple junction points and the pyroxenes show some degree of alteration. A magnetite gabbronorite pigeonite is shown in Fig. 4.11b with fine to medium-sized grains of cumulus pigeonite, clinopyroxene, orthopyroxene and magnetite. The plagioclase show triple point junctions with the pyroxene grains. The magnetite varies in grain size from fine to medium grained.

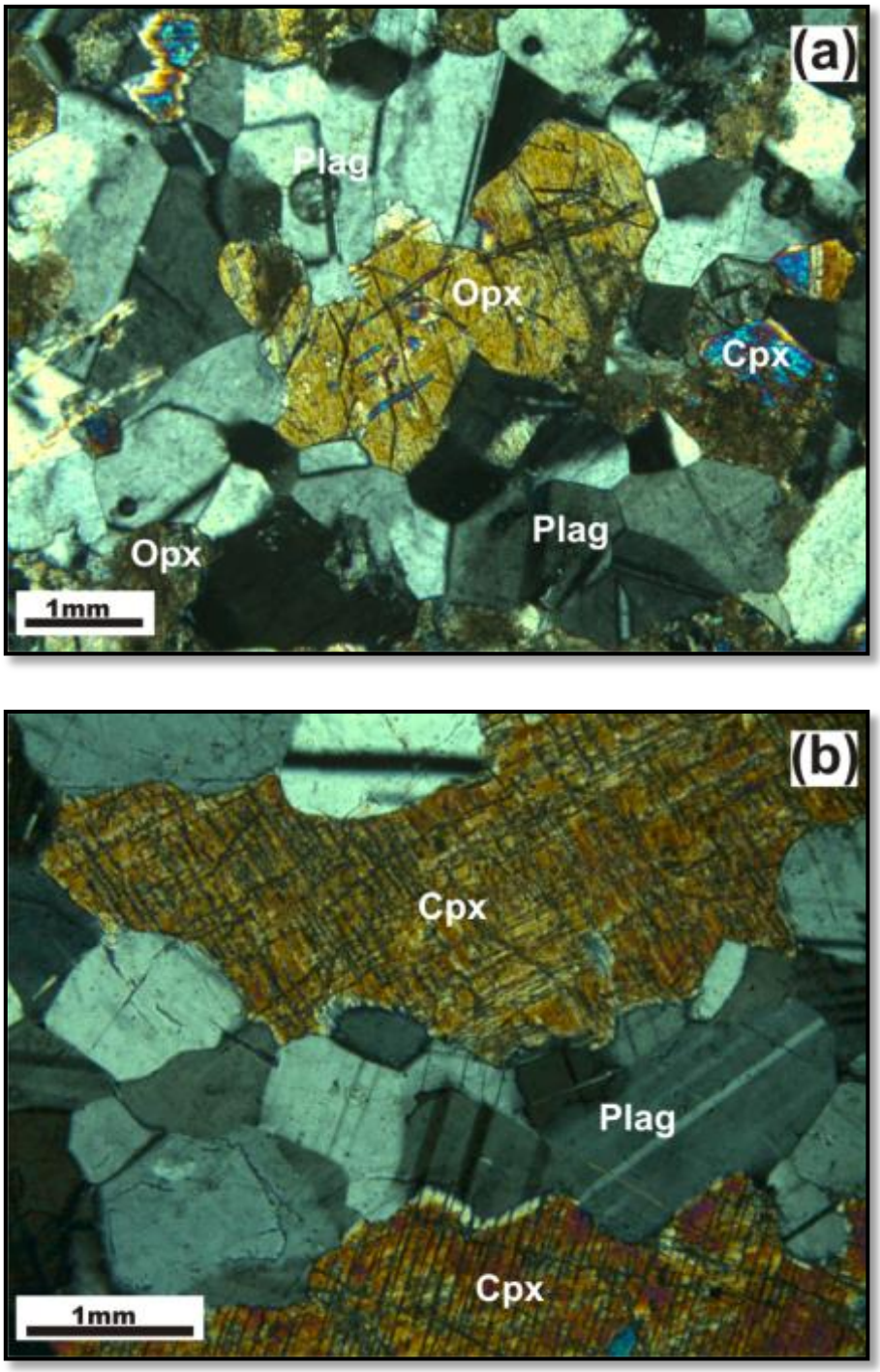


**Fig. 4.10.** Photomicrographs of (a) Micro norite with oikocrysts of orthopyroxene (Opx) with exsolution lamellae of clinopyroxene (Cpx) and plagioclase (Plag) in sample no. USM 1 under XPL (b) Micro gabbro with large oikocrysts of Cpx and cumulus plagioclase (Plag) in sample no. UNK 93-54 under XPL.

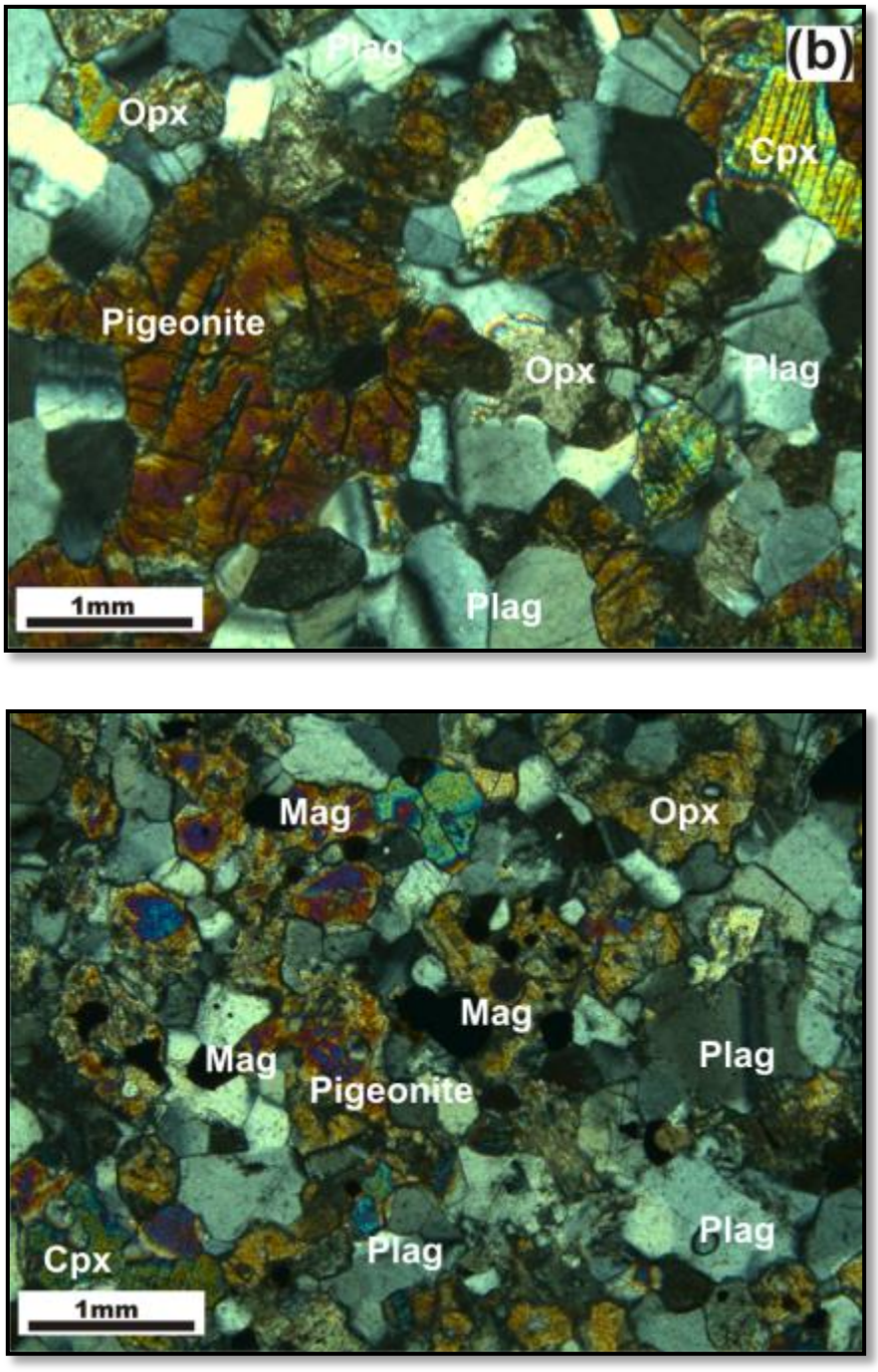


**Fig. 4.11.** Photomicrographs of (a) Micro-gabbronorite with pigeonite showing a large pigeonite grain (now inverted) interlocking with cumulus plagioclase and clinopyroxene in sample no. 10430 under XPL (b) magnetite gabbronorite with inverted pigeonite showing plagioclase (Plag) grains interlocking with orthopyroxene (Opx), and magnetite (Mag) in sample no. USM 3 under XPL.

#### *4.3.3.2 Olivine gabbro/norites*

Rocks of this group consist of cumulus plagioclase with > 5 % olivine, clinopyroxene/orthopyroxene and subordinate spinel. The olivine bearing gabbro/norite in Fig. 4.12a has more than 20-40% olivine and 60-80% plagioclase. A large poikilitic olivine grain encloses small grains of plagioclase in sample no USM 4. Smaller spinel grains can also be seen around the olivine grains. The plagioclase, olivine and clinopyroxene in the matrix display triple point junctions.

Another sample of xenolith olivine micro gabbro xenolith is shown in Fig 4.12b displaying very fine to medium grain-size with an equigranular texture. The plagioclase, olivine, and clinopyroxene meet at well-developed triple point junction. The olivine grains range from rounded to tabular crystals.

## 4.4 The Greenstone Belt Xenoliths

All the samples in this category are xenoliths that were clearly derived from outside the Great Dyke magma chamber. The have been reported as country rocks of Shurugwi Greenstone Belt (Wilson *et al.,* 2000a). The locations of the following samples are show in MAP A, with most been taken close to the margin of the Great Dyke. These samples include (1) quartzites sample no. USM 26, USM 29, USM 39, UNK 93/76. (2) Amygdaloidal basalt sample no. USM 76. (3) Banded iron formation sample no. USM 28 (4) amphibolite/tremolite schist sample no. USM 102.

A sample of quartzite UNK 93-76 is shown in Fig 4.13, which was collected close to the margin of the greenstone belt and the Great Dyke. It shows rounded quartz grains intergrown with clinopyroxene grain due to softening and reaction.

## 4.5 Mineral and Textural Relations

The PAR 11 borehole samples are defined in terms of their coarse texture. The following textural relationships were observed in all the rock types studied i.e. gabbro/norites. These show two populations of the same mineral in some of the

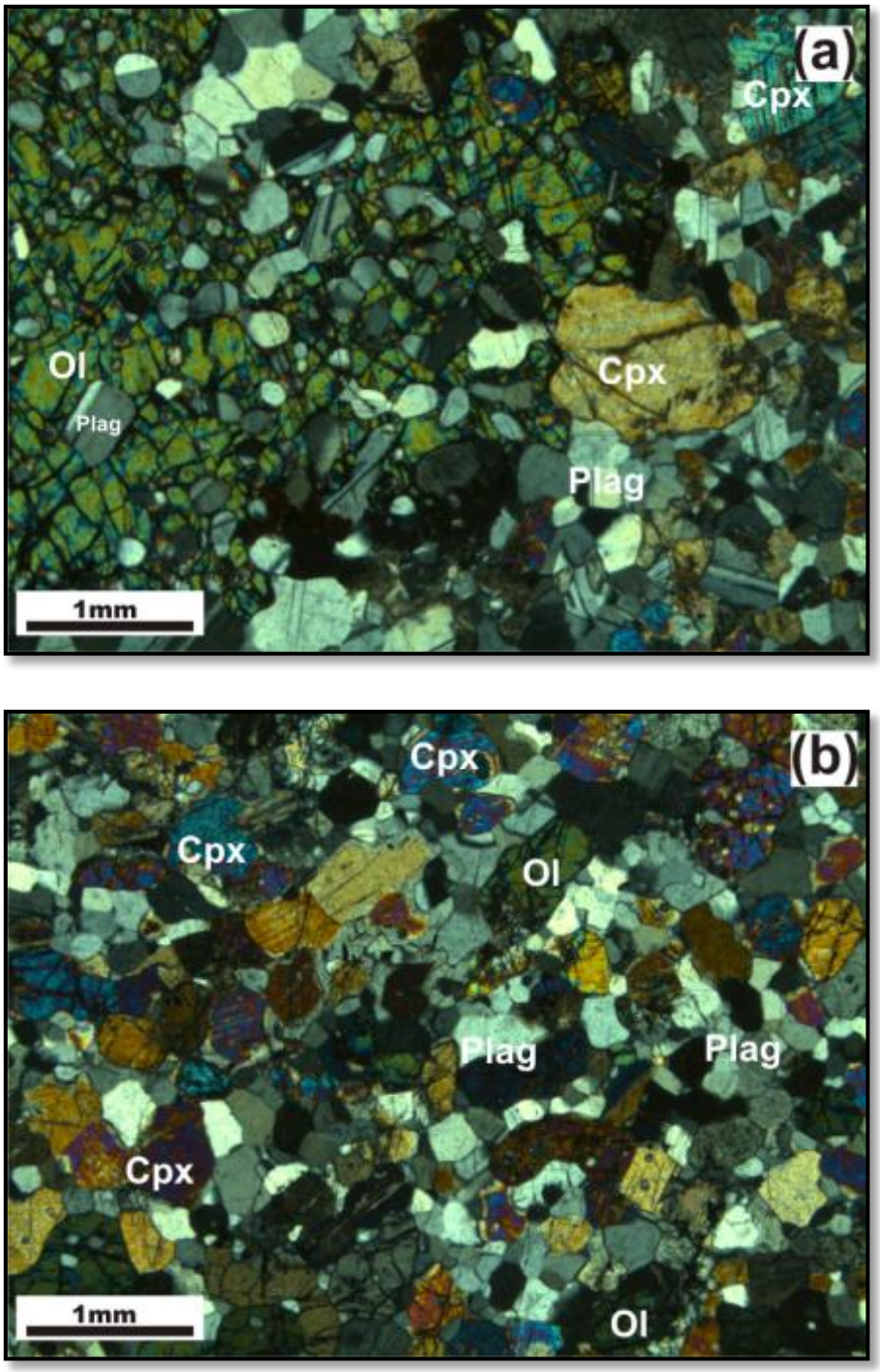


**Fig. 4.12.** Photomicrographs of (a) Micro-olivine gabbronorite with olivine (Ol), clinopyroxene (Cpx) and plagioclase (Plag). The large oikocryts of olivine encloses smaller grains of plagioclase in sample no. USM 4 under XPL (b) The micro olivine gabbro displays an equigranular texture in sample no. USM 66 under XPL.

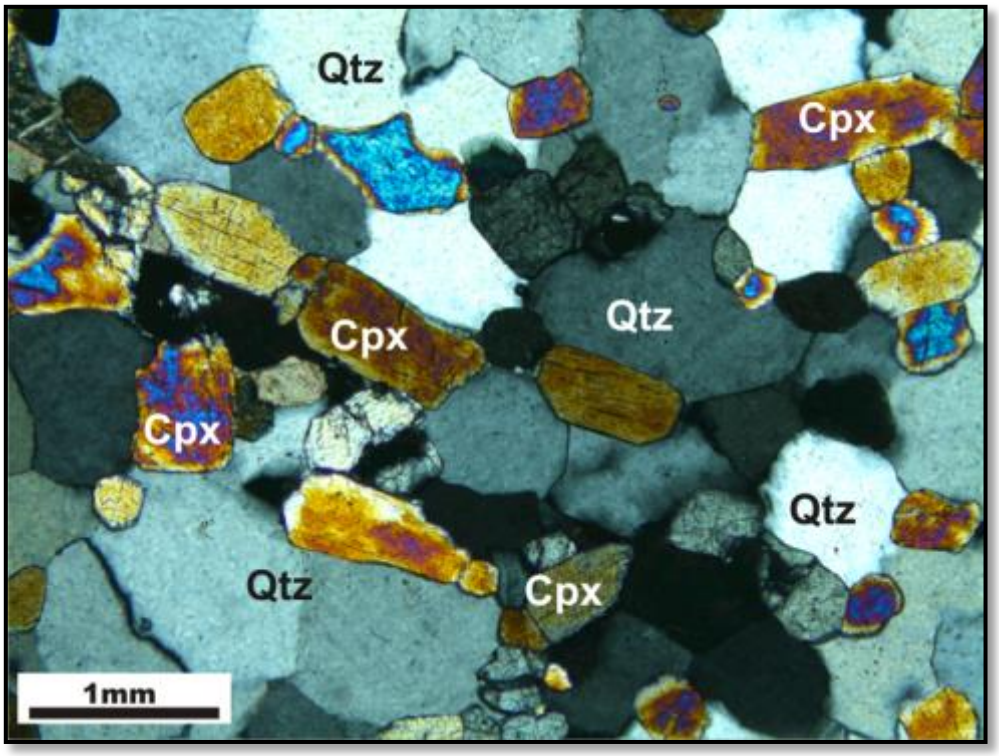


**Fig. 4.13.** Photomicrograph of metasedimentary quartzite with sub-rounded quartz (Qtz) grains with tabular clinopyroxene (Cpx) grains. The grains are aligned in particular direction in sample no. UNK 93-76 under XPL.

dunites, harzburgites, olivine-pyroxenite and pyroxenite. The cumulus phases (olivine and orthopyroxene) are coarse (2mm or more in diameter) while the postcumulus phases are much smaller plagioclase, clinopyroxene and spinel are generally <1mm. The grains are characterised by straight or smoothly curved boundaries shown in (Fig 4.1 and 4.2) with little elongation and mild evidence of strain such as undulose extinction. The plagioclase, clinopyroxene and spinel are found around the edges or enclosed inside the grains. No foliation or lineation was observed in any of the samples studied.

The Unki xenolith suite shows three types of textures, porphyritic, poikilitic and equigranular with increase in strain and deformation. The porphyritic textures are shown in pyroxenites, olivine-pyroxenite, olivine websterites and olivine bearing

samples, with phenocrysts (>2mm) set in a fine-grained matrix (<1mm). The feldspathic xenoliths are sometimes poikilitic with plagioclase always appearing rounded. The olivine bearing variety of gabbro/norites also displays a poikilitic texture in Fig 4.12a with olivine enclosing fine grains of rounded plagioclase grains. A rare dark green clinopyroxene is found in the xenolith suite generally occurs as large grains (oikocryts) with abundant exsolution lamellae. An equigranular or fine texture is also observed in most of the rocks and is result of long term annealing and recrystallization as they were carried up in during the Great Dyke magmatic event.

## 4.6 Summary and Discussion

The PAR 11 borehole series is ultramafic and ranges compositionally from dunite and harzburgite to olivine-pyroxenite and pyroxenite. The dunites are the dominate lithology followed by harzburgites with a few olivine-pyroxenites and pyroxenite. The rock types in the borehole are coarse grained. The rocks in the PAR 11 borehole are similar to those in the ultramafic succession of the Selukwe Subchamber of the Great Dyke, but are enclosed within gabbro of the layered sequence.

The Unki xenolith suite ranges from ultramafic to mafic xenoliths. The ultramafic rocks range from the dunites and harzburgites to lherzolite and websterites to olivine websterite and pyroxenite. The mafic rocks include gabbros, gabbronorites and olivine gabbronorites. Texturally they a mostly fine grained (equigranular texture) to coarse grained (porphyritic, poikilitic textures). It has also observed that in the mafic rocks, the clinopyroxene bearing plagioclase rocks are more common than the orthopyroxene bearing rocks. The clinopyroxene large oikocrysts have abundant exsolution lamellae as shown in Fig. 4.8 surrounded by cumulus phases.

It has been clearly observed from this study that most of the xenolith fragments in the Unki area do not have equivalents in the Shurugwi Greenstone Belt except for the peridotites (Stowe, 1968).

The clearly identified greenstone xenoliths are mainly metasedimentary quartzites and banded iron formations observed in some localities on the western margin of the Selukwe Subchamber but they are not the primary focus of this study. These are clearly derived from the Shurugwi Greenstone Belt (Stowe, 1968).

# CHAPTER 5: WHOLE ROCK CHEMISTRY OF THE PAR 11 BOREHOLE

## 5.1 Introduction

A total of 152 samples were collected from PAR 11 for geochemical analyses. Other borehole xenoliths used in the study include V58, PAR 28, MR 33, MR 102, MR 125, MR 316, MR 327, MR 328, MR 330 and MR 331. The locations of these boreholes and samples are shown in Map A, Appendix A. The analytical techniques and results are given in Appendix B and Appendix E, Table E1.1 and E1.2 respectively.

Samples from a reference borehole MR 92 will be used in comparison with PAR 11 in Chapter 7. The MR 92 borehole is located in the middle part of the Subchamber and mainly consists of P1 pyroxenite layer overlain by the mafic succession. If the PAR 11 pyroxenites are from the upper most P1 pyroxenite they will plot in the same chemical compositions as those in the MR 92 borehole. However if they are from the lower ultramafic sequence they will plot away from the MR 92 borehole composition, with higher MgO and Mg#.

Major element oxides analyzed were (wt %) $SiO_2$, $TiO_2$, $Al_2O_3$, total Fe as $Fe_2O_3$, MnO, MgO, CaO, $Na_2O$, $K_2O$, $P_2O_5$ and Loss on Ignition (LOI) using X-ray Fluorescence (XRF). Trace Elements (ppm) analyzed were Rb, Ba, Nb, Sr, Co, Cu, Zn, V, Cr, Sc, Zr, Pb and S. Rare earth elements (ppm) analyzed were La, Ce, Pr, Nd, Pm, Sm, Eu, Gd, Tb, Dy, Ho, Er, Tm, Yb, Lu using Inductive Coupled Plasma-Mass Spectrometry (ICP-MS. Sulphur (wt %) was determined on borehole samples from the PAR 11 borehole using a Lincoln Electric Co. CS244 infra-red sulphur analyser. The full details of methodology are found Appendix B.

## 5. 2 Major Element Variations

The major element oxides of the PAR 11 borehole where plotted on the total alkali-silica diagram for plutonic rocks in Fig 5.1. The rock compositions are sub-alkalic characterized by low total alkalis from 0 to 3 (wt %) with silica contents of 40-55 (wt%) In the diagram the ultramafic samples fall in the peridotite field while the samples logged as pyroxenites are in the gabbro diorite field. The pyroxenites do not contain cumulus plagioclase as reported in the petrography section in Chapter 4.

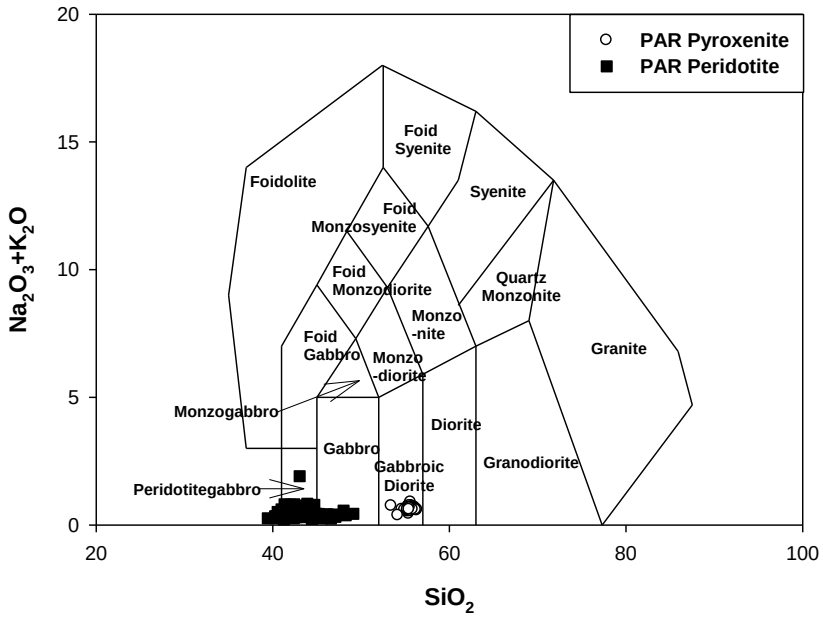


**Fig. 5.1.** Chemical classification and nomenclature of PAR 11 borehole samples using the total alkali versus silica (TAS) diagram after Le Maitre (1989) (Appendix E, Table E1.1 and E1.2).

Major element variations of the PAR 11 borehole are controlled by modal abundances of the constituent mineral in the rock. This is demonstrated by plotting major element oxides are against MgO (Fig. 5.2) as an index of fractionation. Stratigraphic major element oxides are displayed showing variation with depth (Fig. 5.3). Table 5.1 shows the averages and standard deviation of the major oxides in the pyroxenites and peridotites.

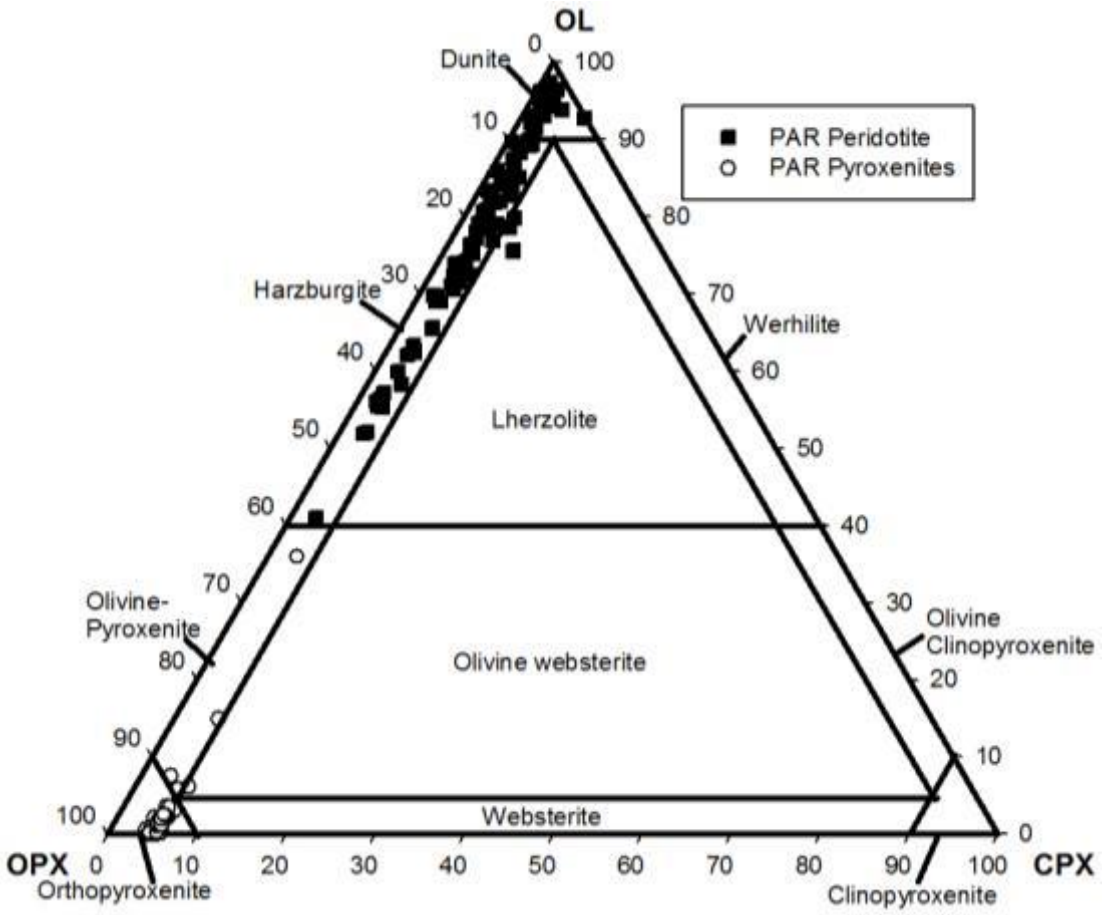


**Fig. 5.2.** Normative compositions of the PAR 11 borehole samples. Olivine – orthopyroxene – clinopyroxene classification after Streckeisen (1976) closed squares (■) represent peridotites and open cycles (○) represent pyroxenites (Appendix E, Table E1.1 and E1.2).

The PAR 11 borehole samples are classified after Streckeisen (1976) in Fig 5.2 using normative data from the geochemical analyses. The peridotite samples in the PAR 11 borehole are dunites and harzburgites. The dunites have up-to 90% normative olivine and are distinguished from harzburgite by higher MgO content 38.7- 43.06 (wt %). The harzburgite samples have 10 – 40% normative olivine and MgO values of 37.5-40.46 (wt %). The harzburgite can be distinguished from the dunites layers by their lower MgO value and lower NiO. The pyroxenite samples are pure pyroxenite and olivine-pyroxenite. The pyroxenite have MgO 27.96 – 30.51 (wt %) and plot away

from the olivine-pyroxenites. There are only four samples of olivine-pyroxenite PAR 11/46, 47, 149, 151. These have higher MgO of 34.56- 37.89 (wt %) because of the presence of olivine.

The major element variation diagrams show a negative correlation with MgO for $Na_2O$, $SiO_2$, $TiO_2$, and CaO in both populations as displayed in Fig. 5.3. There is positive correlation with MgO for $Fe_2O_3$ and weak negative correlation with $K_2O$. Broadly, two different trends can be distinguished within the peridotites and pyroxenite. These trends differ significantly in the gradients. The pyroxenites tend to have a steep gradient with a small concentration range while peridotites have a less steep gradient with a greater range.

Table 5.1 displays the averages and standard deviations of the PAR 11 pyroxenites and peridotites.

The Mg# was calculated as 100*MgO/40.32/[(100*MgO/40.32)+(100*FeO/71.85)]. The Mg# is plotted against MgO, to show the variation in values that range in contents is 0.86 to 0.88 in both peridotites and pyroxenites. The pyroxenites have a high Mg# with an average of 0.8735 and the peridotites have a lower Mg# of with an average of 0.87. The pyroxenites are statistically different from the peridotites even though they overlap in values. The range MgO% is 27.96 to 43.06 with peridotites having slightly higher values than the pyroxenites. The peridotites show a greater range and are clearly distinguished from the pyroxenites.

Stratigraphic variations of the major element oxides are shown in Fig. 5.4. The uppermost pyroxenite is weathered in the drill core to 18m. Sampling was therefore started at 18.34 m. There are four distinct layers of pyroxenites alternating with the peridotites with the upper-most layer being pyroxenite.

The range of $Al_2O_3$ is 1 to 4 wt% with pyroxenites having slightly higher values than the peridotites. The peridotites show a greater range than the pyroxenites. However,

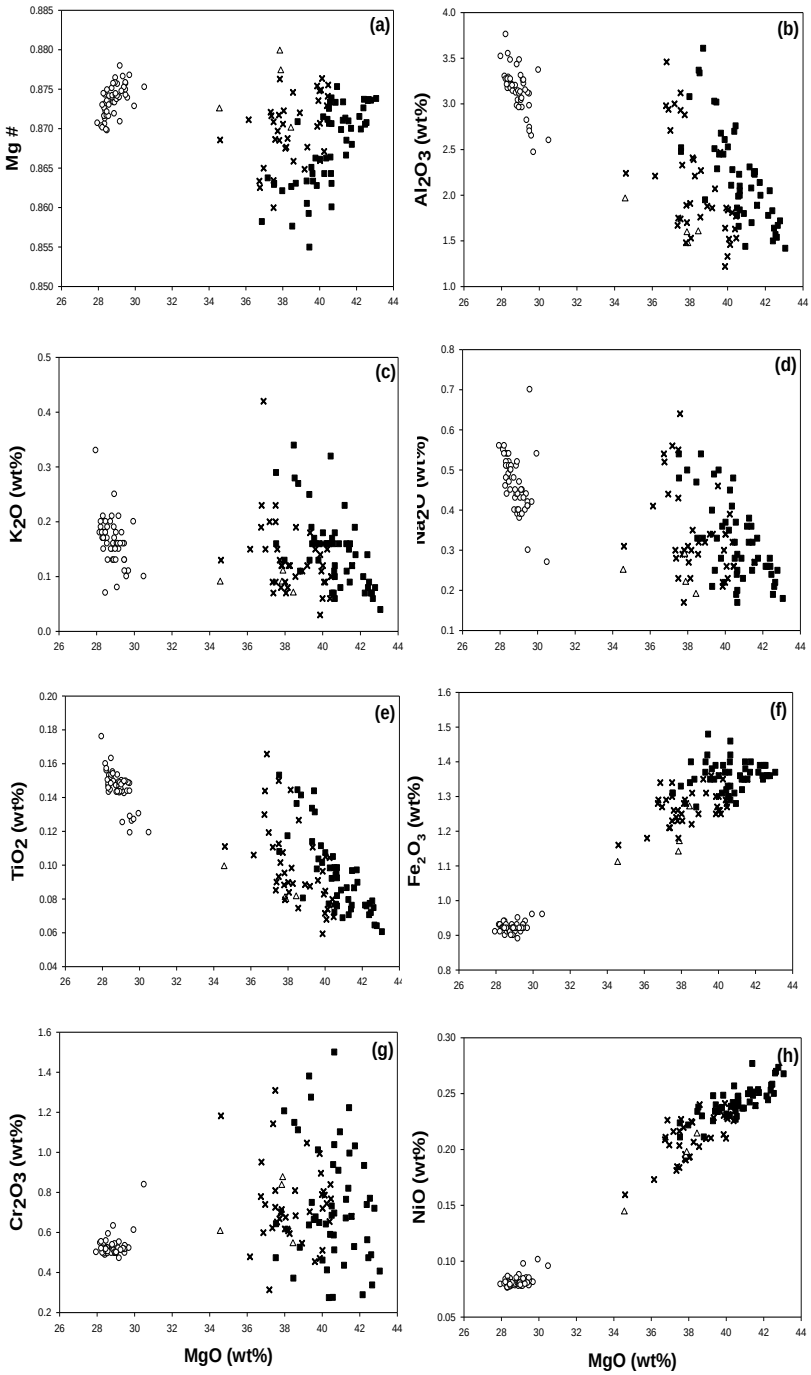


**Fig. 5.3.** Variation diagrams for major element oxides variation plotted against with MgO as an index of differentiation. Open cycles (○) represent pyroxenite, open triangles (Δ) represent olivine - pyroxenite, closed squares (■) represent dunites and **(x)** represent harzburgites.

**Table 5.1:** Whole rock major element oxides (wt%) averages and standard deviations for the pyroxenite and peridotites in the for the PAR 11 borehole by XRF analyses in Appendix E, Table E1.1.

| ROCK TYPE | No. of Samples | STATISTICS | $Al_2O_3$ | $Fe_2O_3$ | MgO | $Na_2O$ | $K_2O$ | $TiO_2$ | $Cr_2O_3$ | NiO | Mg# |
|---|---|---|---|---|---|---|---|---|---|---|---|
| PYROXENITES | 53 | AVERAGE | 3.13 | 0.93 | 28.95 | 0.46 | 0.16 | 0.15 | 0.53 | 0.08 | 0.87 |
| | | STAND. DEV. | 0.29 | 0.06 | 0.94 | 0.08 | 0.04 | 0.01 | 0.05 | 0.01 | 0.00 |
| PERIDOTITES | 93 | AVERAGE | 2.13 | 1.32 | 39.59 | 0.34 | 0.14 | 0.10 | 0.74 | 0.23 | 0.87 |
| | | STAND DEV | 0.54 | 0.07 | 1.76 | 0.16 | 0.07 | 0.024 | 0.26 | 0.02 | 0.01 |

**Table 5.2:** Whole rock trace element (ppm) averages and standard deviations for the pyroxenite and peridotites in the for the PAR 11 borehole by XRF analyses in Appendix E, Table E1.2.

| ROCK TYPE | No. of Samples | STATISTICS | Zr | Ba | Sr | Rb | Y | Cr | Sc | V | Zn | Co | Ni | Cu | S |
|---|---|---|---|---|---|---|---|---|---|---|---|---|---|---|---|
| PYROXENITES | 53 | AVERAGE | 11.2 | 49.5 | 26 | 6.9 | 2.5 | 3356.7 | 19.6 | 84.3 | 61.8 | 88.3 | 653.5 | 28.2 | 1583.9 |
| | | STAND. DEV. | 2.1 | 9.7 | 4.9 | 1.6 | 0.8 | 325.1 | 2.8 | 9.6 | 2.6 | 12.7 | 196.2 | 9.0 | 613.8 |
| PERIDOTITES | 93 | AVERAGE | 9.2 | 43.7 | 24.3 | 6.4 | 1.3 | 3705.0 | 9.7 | 48.6 | 74.4 | 155.6 | 1717 | 19.7 | 4377.4 |
| | | STAND DEV | 3.4 | 4.7 | 16.2 | 2.7 | 0.7 | 1288.9 | 2.6 | 11.0 | 4.1 | 11.0 | 163.5 | 12.3 | 797.5 |

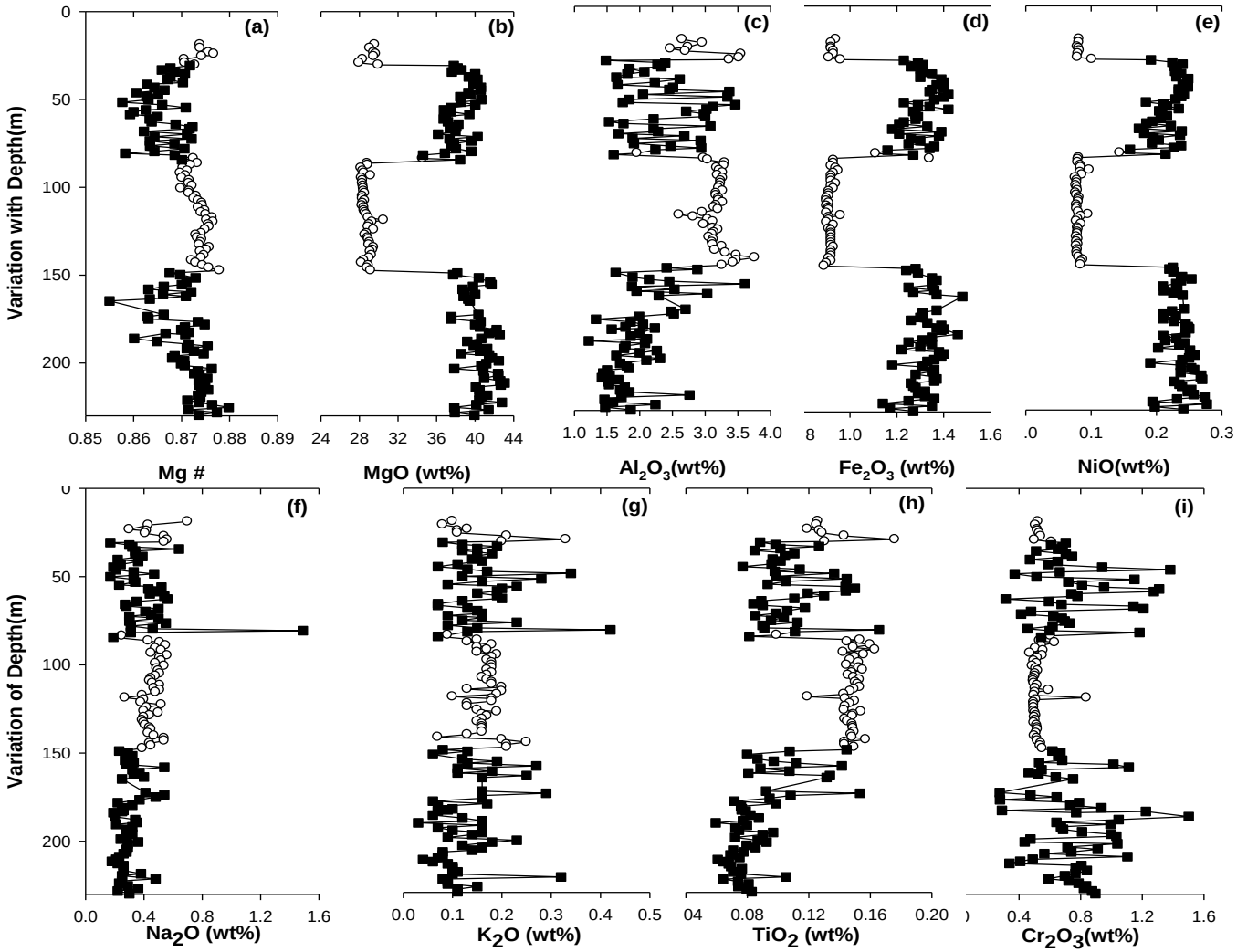


**Fig. 5.4.** Whole rock major element oxides variations with depth for the PAR 11 borehole. Open cycles (○) represent pyroxenite closed squares (■) represent peridotites.

in the lower peridotites there is a gradual increase in $Al_2O_3$ upwards increase towards the base of the pyroxenite. $Al_2O_3$ has an average of 3.13% which slightly overlaps with peridotites which have an average of 2.13%. The range in $Fe_2O_3$ contents is 0.3 to 1.5 wt% with peridotites having slightly higher values than the pyroxenites. However, the peridotites show a greater range than the pyroxenites. In the lower peridotites there is a gradual decrease in $Fe_2O_3$ upwards towards the base of the pyroxenite.

The range of NiO contents is 0.08 to 0.28 wt% with peridotites having slightly higher values than the pyroxenites. The peridotites show a greater range than the pyroxenites. The range $Na_2O$ in contents is 0.17 to 1.49wt% with pyroxenites having slightly higher values than the peridotites. However, the peridotites show a greater range than the pyroxenites. In the lower peridotites there is a gradual increase in $Na_2O$ upwards towards the base of the pyroxenite. The pyroxenites are statistically different from the peridotites even though they overlap in values.

The range $K_2O$ in contents is 0.07 to 0.42 wt% with pyroxenites having slightly higher values than the peridotites. However, the peridotites show a greater range than the pyroxenites. In the lower peridotites there is a gradual decrease in $K_2O$ upwards towards the base of the pyroxenite. The pyroxenites are statistically different from the peridotites even though they overlap in values. The range $TiO_2$ in contents is 0.06 to 0.18 wt% with pyroxenites having slightly higher values than the peridotites. However, the peridotites show a greater range than the pyroxenites. In the lower peridotites there is a gradual increase in $TiO_2$ upwards towards the base of the pyroxenite. The pyroxenites are statistically different from the peridotites even though they overlap in values.

The range $Cr_2O_3$ in contents is 0.27 to 1.38 wt% with peridotites having slightly higher values than the pyroxenites. However, the peridotites show a greater range than the pyroxenites. In the lower peridotites there is a gradual decrease in $Cr_2O_3$

upwards towards the base of the pyroxenite. The pyroxenites are statistically different from the peridotites even though they overlap in values.

## 5. 3 Trace Element Variations

The whole rock trace element concentration is controlled by the partition coefficient of the elements into the minerals present in the pyroxenite and peridotites of the PAR 11 borehole as well as the content of trapped liquid in the cumulates, particularly for the incompatible trace elements. Trace elements are presented in four groups in terms of behavior and these include (1) incompatible elements Zr, Ba, Sr, Rb, Y, $K_2O$, $TiO_2$ or (2) compatible elements Cr, V, Sc (3) chalcophile and transition elements , Co, Zn, Cu, Ni, S and (4) Rare Earth Elements (La to Lu). The trace element variations of the borehole down-hole are shown in Fig. 5.5. Table 5.2 displays the averages and standard deviations of the trace elements for the different rock groups.

### 5.3.1 Incompatible Elements

The range in Zr contents is 3 to 22 ppm with pyroxenites having slightly higher values than the peridotites. However, the peridotites show a greater range than the pyroxenites. In the lower peridotites there is a gradual increase in Zr upwards towards the base of the pyroxenite. The pyroxenites are statistically different from peridotites even though there is an overlap in values in Fig 5.5.

Ba and Sr are slightly compatible with plagioclase but are incompatible with olivine, orthopyroxene. The range in Ba contents is 12 to 75 ppm with an almost constant range in both peridotites and pyroxenites except one dunite sample PAR 11-23 which contains 152.8 ppm. The pyroxenites are statistically different from peridotites even though there is an overlap in values. Similar to Ba the range in Sr 5 to 45 ppm with an almost constant range in both peridotites and pyroxenites except one dunite sample PAR 11-23 with 461.5 ppm. The pyroxenites are statistically different from peridotites even though there is an overlap in values.

The range in Rb contents is 1 to 15 ppm with pyroxenites having slightly higher values than in the peridotites. However, the peridotites show a greater range than the pyroxenites. In the lower peridotites there is a gradual increase in Rb upwards towards the base of the pyroxenite. There is a statistical overlap in pyroxenites and the peridotites. The range in Y contents is 0.2 to 4 ppm with pyroxenites having slightly higher values than the peridotites. Both the peridotites and pyroxenites show a wide range of values and statistically overlap. The ranges in $K_2O$ and $TiO_2$ contents have been described in the major element section although they are trace elements in these rocks.

### 5.3.2 Chalcophile Elements

The chalcophile trace elements are Cu, Ni, Co, Zn and by definition form sulphides Ni, Co and Zn are compatible with both olivine and orthopyroxene. The range in Cu is 2 to 50 ppm with pyroxenites having slightly higher values than the peridotites. In the lower peridotites there is a gradual increase in Cu upwards towards the base of the pyroxenite. Both the peridotites and pyroxenites show a wide range of values and statistically overlap as shown in Fig. 5.5. Three cycles of variation are observed in the lower peridotites on the basis of Cu systematically increasing and decreasing indicating a varying control by sulphide. The range of S in contents is 1073 to 6895 ppm with greater ranges of S in the peridotites than in the pyroxenites. There is a gradual increase of S in the lower peridotites upwards to the base of the pyroxenites.

The range in Zn is 56 to 88 ppm with peridotites having slightly higher values than the pyroxenites. The peridotites also show a greater range than the pyroxenites. Zn shows a similar pattern like Cu with three cycles systematically increasing and decreasing towards the base of the pyroxenites. The range in Ni is 583 to 2083 ppm peridotites having higher values than the pyroxenites. The peridotites also show a greater range than the pyroxenites. In the lower peridotites there is a gradual increase in Ni upwards towards the base of the pyroxenite. Both the peridotites and pyroxenites show a wide range of values and statistically overlap. The Co range is 81

to 176 ppm with the peridotites having higher values than the pyroxenites. The peridotites also show a greater range than the pyroxenites and can be clearly distinguished from each other. In the lower peridotites there is a gradual decrease in Co upwards towards the base of the pyroxenite.

### 5.3.3 Compatible Elements

The compatible elements Cr, V and Sc stratigraphic variation diagrams are displayed in Fig. 5.6. Cr is compatible with olivine, the range in Cr is 1448.8 to 7128.5 ppm with peridotites having slightly higher values than the pyroxenites. However, the peridotites show a greater range than the pyroxenites. The pyroxenites are clearly distinguished from the peridotites. V is compatible with chromite and magnetite, the range in V is 27 to 97 ppm with pyroxenites having slightly higher values than the peridotites. However, the peridotites show a greater range than the pyroxenites. The pyroxenites can be clearly distinguished from peridotites by higher values. The range in Sc is 3.8 to 24.9 ppm with pyroxenites having slightly higher values than the peridotites. However, the peridotites show a greater range than the pyroxenites and tend to gradually increase towards the base of the pyroxenites.

The inter-element diagrams are shown in Fig. 5.7. The trace elements used in these diagrams were analyzed using XRF except Y which was analyzed using ICP-MS as Y requires low detection limits. Variation diagrams of incompatible elements Rb, Ba, and Y show positive correlations with Zr with pyroxenites statistically overlapping with peridotites. The $Al_2O_3$ and $TiO_2$ also display a positive correlation with Zr with separate populations of pyroxenites and peridotites. The transition elements variation diagram Ni vs S, show peridotites plotting away from pyroxenites. The peridotites display strong positive correlations while pyroxenites show no correlation. Cu vs S shows weak negative correlation with S in both separate populations of pyroxenites and peridotites. In the Cu vs Ni variation diagram the pyroxenites plot away with a strong positive linear trend while the peridotites show a scatter in Cu with increase in Ni.

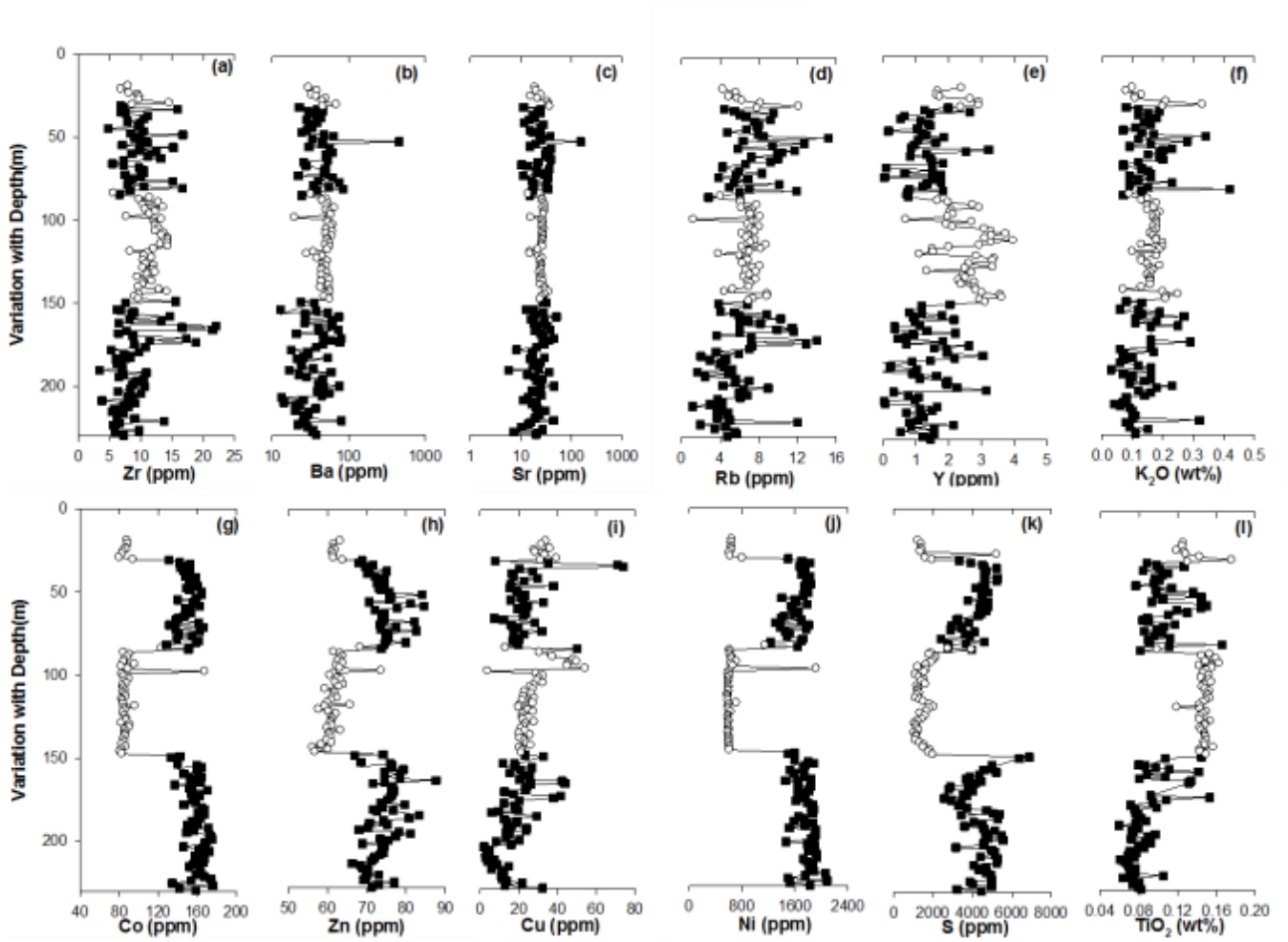


**Fig. 5.5.** Whole rock trace elements variations with depth (m) for the PAR 11 borehole. Open cycles (○) represent pyroxenite closed squares (■) represent peridotites.

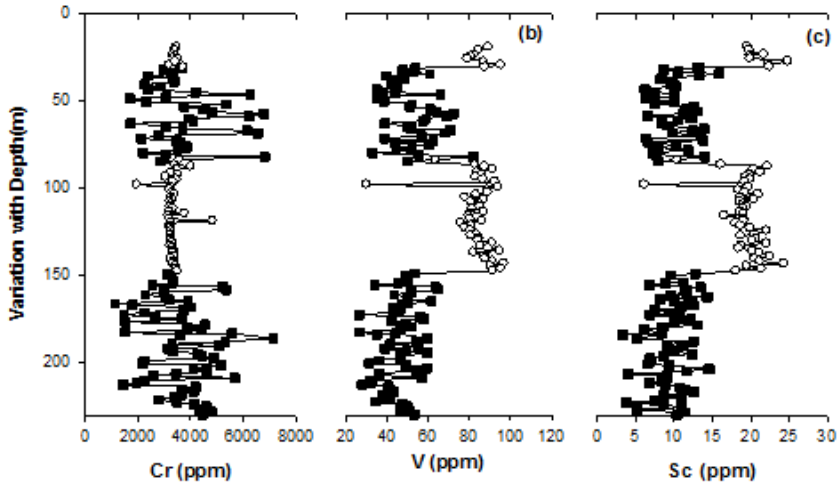


**Fig. 5.6.** Stratigraphic variations of the compatible elements Cr, V and Sc in the PAR 11 borehole samples. Open cycles (○) represent pyroxenite and closed squares (■) represent peridotites.

### 5.3.4 Rare Earth Elements

Stratigraphic variations of La, Sm, Yb and total REE are displayed in Fig. 5.8. Table 5.3 displays their averages and standard deviations. The diagrams of La, Sm, and Total REEs have essentially identical patterns downhole while Yb is slightly different. The range in La contents is 0.68 to 3.4 ppm with pyroxenites having slightly higher values than the peridotites. However, the peridotites show a greater range than the pyroxenites. In the lower peridotites there is a gradual increase in La upwards towards the base of the pyroxenite. The range in Sm contents is 0.15 to 0.67 ppm. The peridotites show a greater range than the pyroxenites. In the lower peridotites there is a gradual increase in Sm upwards towards the base of the pyroxenite while the pyroxenites show a gradual decrease upward.

The range in Yb contents is 0.10 to 0.26 ppm. The peridotites show a much greater range than the pyroxenites. In the lower peridotites there is a gradual increase in Yb upwards towards the base of the pyroxenite while the pyroxenites show a gradual decrease upward. The range in Total REE contents is 3.52 to 17.50 ppm the

peridotites show a greater range than the pyroxenites. In the lower peridotites there is a gradual increase in Total REE upwards towards the base of the pyroxenite.

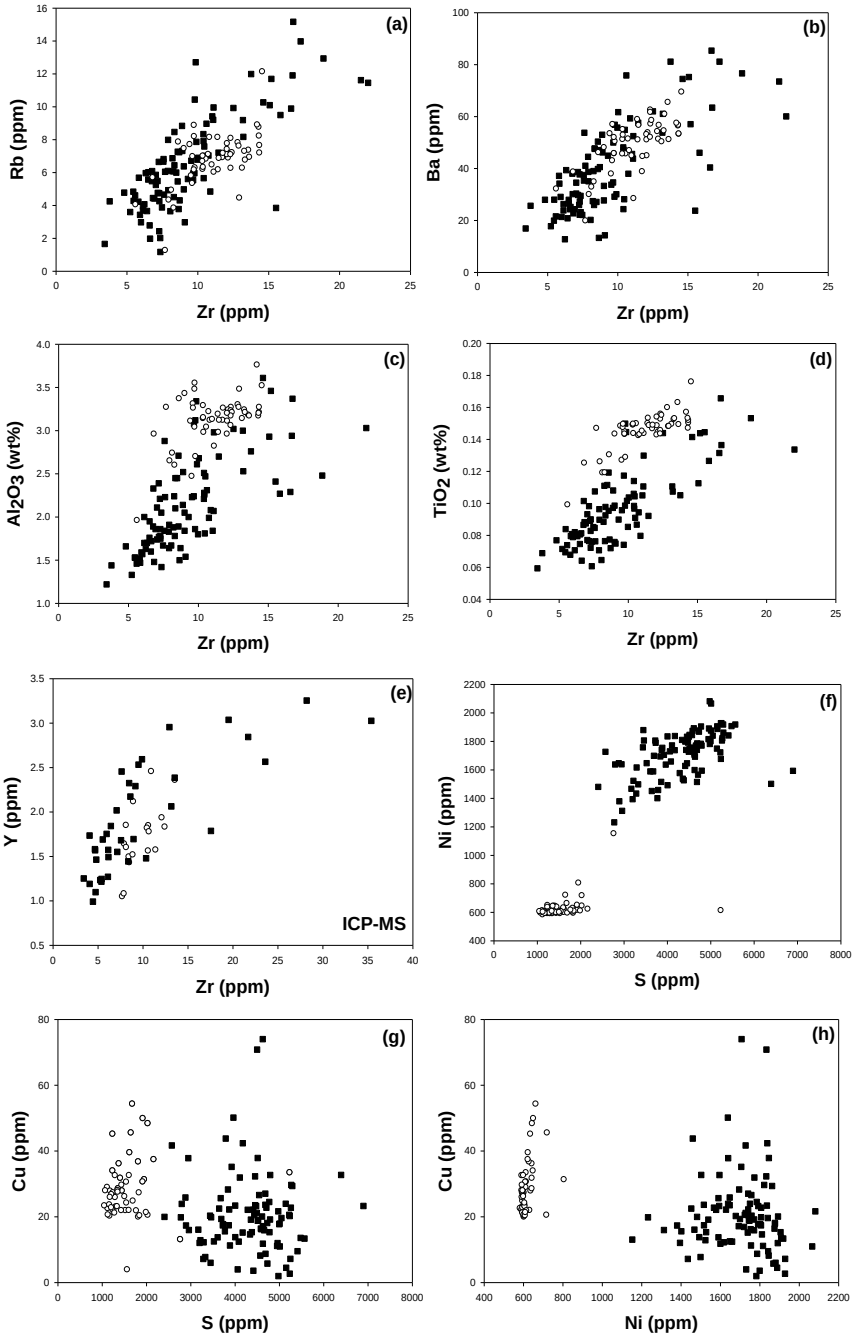


**Fig. 5.7.** Inter -element variation diagrams for trace elements (a) Rb vs Zr, (b) Ba vs Zr (c) $Al_2O_3$ vs Zr, (d) Zr vs $TiO_5$, (e) Zr vs Y, (f) Ni vs S, (g) Cu vs S, (h) Cu vs Ni. Open cycles (○) represent pyroxenite and closed squares (■) represent peridotites.

**Table 5.3:** Whole rock averages (ppm) and standard deviations for La, Sm, Yb and Total REEs for the PAR 11 borehole series by ICP-MS.

| ROCK TYPE | No. of Samples | STATISTICS | La | Sm | Yb | Total REE |
|---|---|---|---|---|---|---|
| PYROXENITES | 18 | AVERAGE | 1.40 | 0.28 | 0.17 | 7.17 |
| | | STAND DEV | 0.42 | 0.09 | 0.09 | 2.30 |
| PERIDOTITES | 40 | AVERAGE | 1.59 | 0.31 | 0.17 | 7.87 |
| | | STAND DEV | 0.63 | 0.13 | 0.05 | 3.27 |

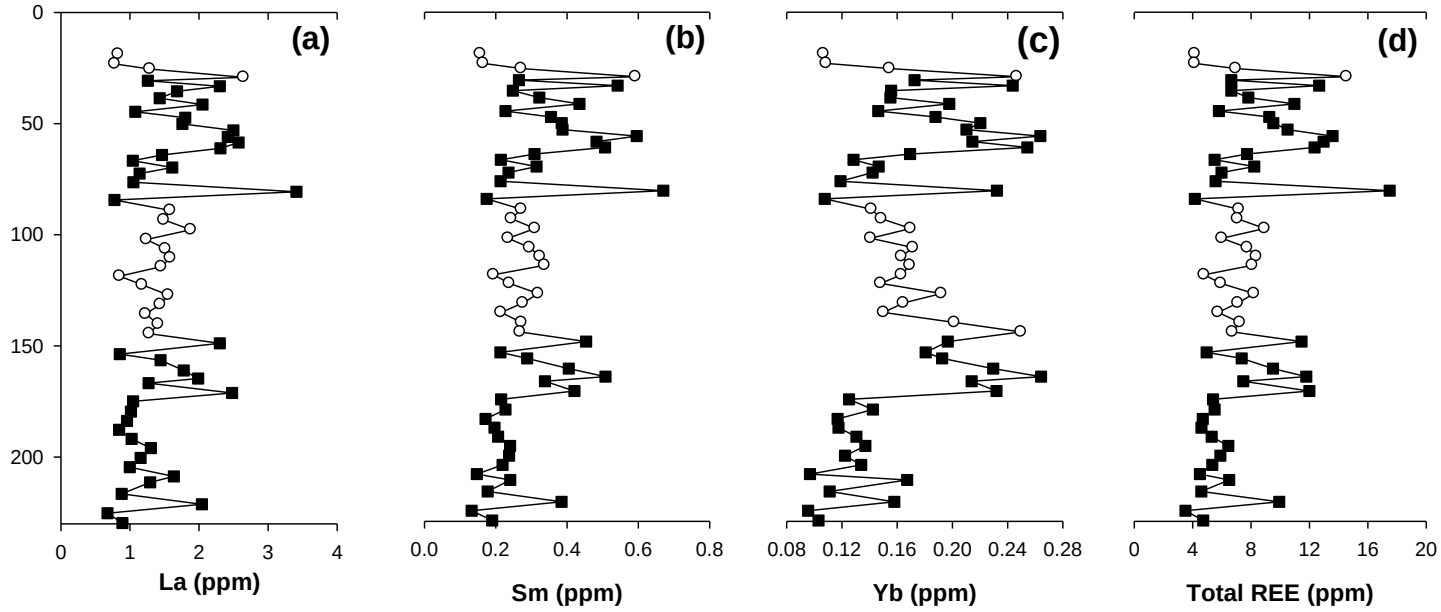


**Fig. 5.8.** Stratigraphic variation downhole of REE elements La, Sm, Yb and total (sum) REEs in the PAR 11 borehole. Open cycles (○) represent pyroxenite and closed squares (■) represent peridotites.

**Table 5.4:** Whole rock REE averages (ppm) and standard deviations for the PAR 11 borehole by ICP-MS. All values are Primitive Mantle normalized after Sun and McDonough (1995).

| ROCK TYPE | STATISTICS | La | Ce | Pr | Nd | Sm | Eu | Gd | Tb | Dy | Ho | Er | Tm | Yb | Lu |
|---|---|---|---|---|---|---|---|---|---|---|---|---|---|---|---|
| PYROXENITES | AVERAGE | 1.98 | 1.48 | 1.21 | 0.96 | 0.62 | 0.47 | 0.49 | 0.41 | 0.37 | 0.35 | 0.33 | 0.32 | 0.35 | 0.36 |
| 18 Samples | STAND DEV. | 0.60 | 0.51 | 0.45 | 0.36 | 0.21 | 0.11 | 0.14 | 0.11 | 0.09 | 0.09 | 0.08 | 0.07 | 0.08 | 0.09 |
| PERIDOTITES | AVERAGE | 2.17 | 1.64 | 1.30 | 1.05 | 0.70 | 0.51 | 0.55 | 0.47 | 0.42 | 0.38 | 0.36 | 0.35 | 0.35 | 0.36 |
| 40 Samples | STAND. DEV. | 0.90 | 0.72 | 0.58 | 0.47 | 0.30 | 0.20 | 0.22 | 0.18 | 0.16 | 0.14 | 0.12 | 0.11 | 0.10 | 0.10 |

**Table 5.5:** Whole rock trace element averages (ppm) and standard deviations for the PAR 11 borehole by ICP-MS. All values are Primitive Mantle normalized values after Sun and McDonough(1989)

| ROCK TYPE | STATISTICS | Cs | Rb | Ba | Th | U | Nb | K | La | Ce | Pb | Pr |
|---|---|---|---|---|---|---|---|---|---|---|---|---|
| PYROXENITES | AVERAGE | 14.37 | 9.29 | 2.70 | 6.21 | 8.16 | 0.95 | 5.67 | 1.98 | 1.48 | 25.84 | 1.21 |
| 18 Samples | STAND DEV. | 6.05 | 3.80 | 1.05 | 2.11 | 2.37 | 0.43 | 1.92 | 0.60 | 0.51 | 6.88 | 0.45 |
| PERIDOTITES | AVERAGE | 17.22 | 9.37 | 3.77 | 6.00 | 10.26 | 0.93 | 5.19 | 2.18 | 1.64 | 26.41 | 1.31 |
| 36 Samples | STAND DEV | 7.29 | 3.56 | 1.64 | 2.81 | 4.62 | 0.82 | 2.56 | 0.90 | 0.73 | 18.04 | 0.59 |

**Table 5.5:** Whole rock trace element averages (ppm) and standard deviations for the PAR 11 borehole by ICP-MS. All values are Primitive Mantle normalized values after McDonough (1989) continued.

| ROCK TYPE | STATISTICS | Sr | P | Nd | Zr | Sm | Eu | Ti | Dy | Y | Yb | Lu |
|---|---|---|---|---|---|---|---|---|---|---|---|---|
| PYROXENITES | AVERAGE | 1.23 | 1.46 | 0.96 | 0.98 | 0.62 | 0.47 | 0.68 | 0.37 | 0.08 | 0.35 | 0.36 |
| 18 Samples | STAND. DEV. | 0.31 | 0.50 | 0.36 | 0.52 | 0.21 | 0.11 | 0.07 | 0.09 | 0.02 | 0.08 | 0.09 |
| PERIDOTITES | AVERAGE | 1.05 | 1.24 | 1.05 | 0.98 | 0.70 | 0.50 | 0.47 | 0.41 | 0.09 | 0.34 | 0.35 |
| 36 Samples | STAND. DEV. | 0.42 | 0.80 | 0.48 | 0.93 | 0.31 | 0.20 | 0.11 | 0.16 | 0.04 | 0.11 | 0.10 |

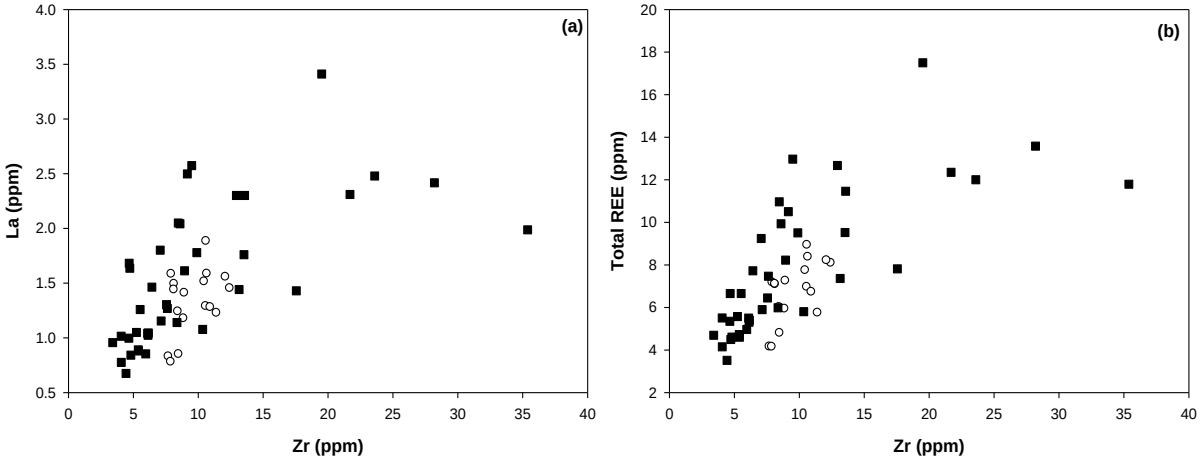


**Fig. 5.9.** Variation of LREEs, La (ppm) and Total REE (ppm) with incompatible element Zr (ppm) for the PAR 11 borehole. Open cycles (○) represents pyroxenites closed squares (■) represents peridotites.

The inter-element variation diagrams of La and Total REE with the incompatible element Zr in ppm are displayed in Fig. 5.9. A positive correlation is shown with overlapping of pyroxenites and peridotites.

The Rare Earth Elements (REEs) patterns of average samples of the peridotites and pyroxenite show similar patterns when normalized to Primitive Mantle after Sun and McDonough (1995). REEs averages and standard deviations of the peridotites and pyroxenites are displayed in Table 5.4. REEs ratios were used to measure the degree of fractionation of the PAR 11 borehole and were plotted on Table 5.6. The REE diagram shows Light Rare Earth Elements (LREE) displaying a slight enrichment (Fig 5.10). This is reflected in the LaN/YbN ratio (used to indicated the slope of the normalized trends). The Heavy Rare Earth Elements (HREE) are slightly depleted with an upward concave pattern and a negative Europium (Eu) anomaly.

Total REE values for the pyroxenites varies from 4.15 to 17.50ppm with average enriched REE (LaN/YbN = 3.5 to 4.71). The LREE is enriched in REE (LaN/GdN = 3.50 to 4.71) and HREE with limited fractionation (GdN/YbN = 0.97-1.69). Total

REE values for the peridotites varies from 3.52 to 13.581ppm with average enriched REE (LaN/YbN = 3.2 to 11.5). The LREE is enriched in REE (LaN/GdN = 2.78 to 8.34) and HREE with slight fractionation or rather flat (GdN/YbN = 1.07-2.25).

**Table 5.6:** The average (ppm) and standard deviation for REE ratios LaN/GdN, LaN/YbN and GdN/YbN for the PAR 11 borehole series by ICP-MS. All values are Primitive Mantle after Sun and McDonough (1995).

| ROCK TYPE | No. of Samples | STATISTICS | [La/Gd]N | [La/Yb]N | [Gd/Yb]N |
|---|---|---|---|---|---|
| PYROXENITES | 18 | AVERAGE | 4.01 | 5.75 | 1.43 |
| | | STAND DEV | 0.7 | 1.17 | 0.22 |
| PERIDOTITES | 40 | AVERAGE | 4.00 | 6.15 | 1.54 |
| | | STAND DEV | 0.9 | 1.58 | 0.23 |

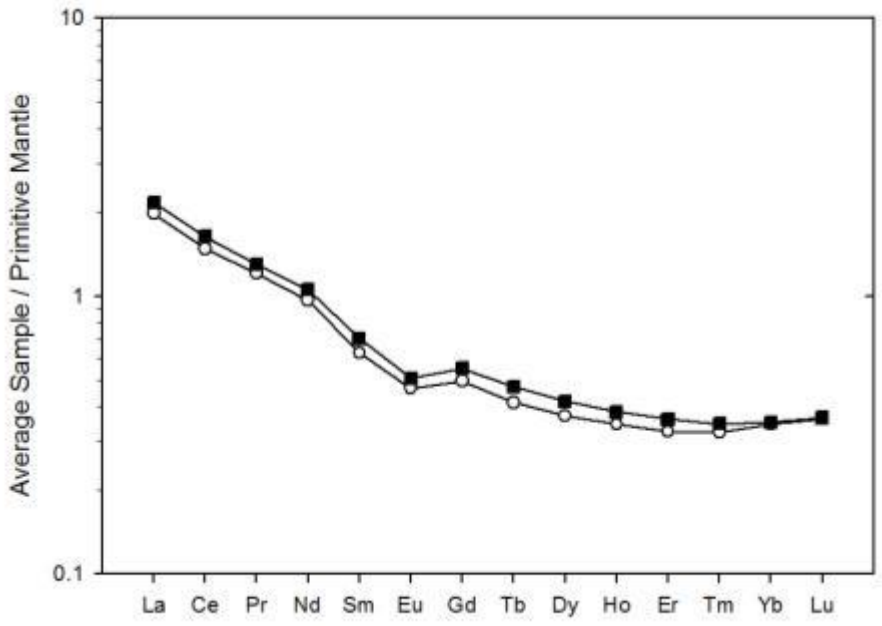


**Fig. 5.10.** The average sample REE patterns for the PAR 11 peridotites and pyroxenites normalized to Primitive Mantle after Sun and McDonough (1995). The diagram displays a negative Eu anomaly with strong enrichment of LREE and a gentle to flat HREE pattern. Open cycles (○) represent pyroxenite closed squares (■) represent peridotites.

### 5.3.5 Multi-element diagrams

The average sample primitive mantle normalized trace element plot after Sun and McDonough (1989) for the pyroxenite and peridotites in the PAR 11 borehole is presented in Fig. 5.11 (a). Trace element averages and standard deviations of the peridotites and pyroxenites are displayed in Table 5.5. Relative to primitive mantle (also in comparison with MORB) both rock types displays a LREE and incompatible element enrichment with positive anomalies in Cs, K, Pb, U and negative Nb anomaly. There is strong HREE fractionation with a slight negative Eu anomaly.

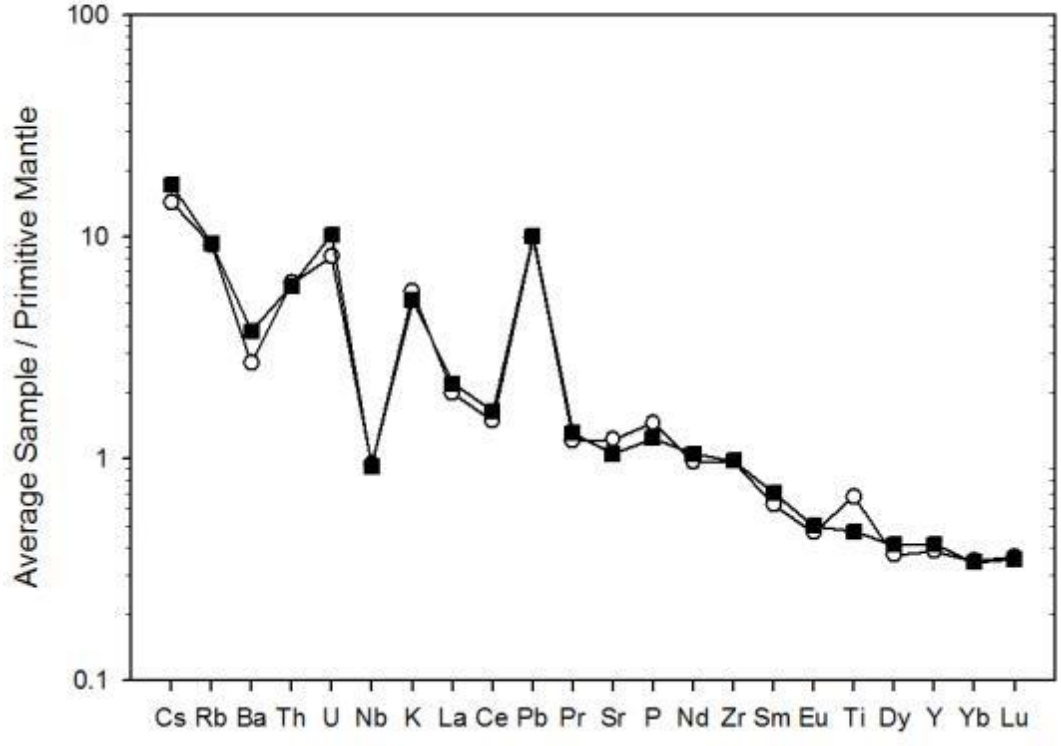


**Fig. 5.11.** Average trace element concentrations for the PAR 11 peridotites and pyroxenites normalized to primitive mantle and plotted from left to right in order of increasing compatibility in a small fraction of the melt. The normalizing values for Primitive Mantle are from Sun and McDonough (1989). Open cycles (○) represent pyroxenite closed squares (■) represent peridotites.

## 5. 4 Summary and Discussion

The geochemical characteristics of the PAR 11 borehole reveal the more homogenous compositions of the pyroxenites and the more variable ones of peridotites. The pyroxenites plot away from peridotites with lower MgO, high Mg# and variable contents of Ca, Al, Ti. The peridotites are characterized by the presence of chromite, have high MgO, high Mg#, and Ni because of the presence of olivine. The low amounts of Ca and low Al due to the small amounts of plagioclase and clinopyroxene. Ti is also lower in peridotites because it is incompatible with olivine. The pyroxenite and peridotites major element oxides contents are typical cumulate origin.

The incompatible trace elements are entirely dependent on the amount of trapped liquid. Variations with depth of Zr, Y, Rb, K and Ti show similar trends of gradual decreasing concentrations upward with higher ranges in pyroxenite than peridotites. Ba and Sr also show similar trends with also slightly higher values in pyroxenites. The MgO variation diagrams also show that incompatible trace elements are more in pyroxenites than peridotites, these ranges are due to differences in the amount of trapped liquid. The fact that there is no positive Eu anomaly means that plagioclase did not fractionate from the magma and crystallized from trapped liquid. That is further supported by the positive correlation between $Al_2O_3$ and Zr as shown in the inter-element variations of trace elements. The chalcophile and transition elements (Cr, Ni, Zn Co) increase with increase in MgO in agreement with fractionation of mafic minerals such as olivine and orthopyroxene. Trace element variations indicate that fractional crystallization was an important process.

The normalized REE patterns (Fig 5.10) of both pyroxenites and peridotites show LREE enrichment and a negative Eu anomaly and depletion in HREE. The negative Eu anomaly is mainly due to the removal of plagioclase by fractionation. To a lesser extent the presence of orthopyroxene and clinopyroxene may contribution to the negative Eu anomaly. The REE patterns between the pyroxenite samples and the

peridotites are so similar that it is clear that both rock types must have been derived from the same parent magma.

The REE pattern of the PAR 11 borehole is similar that described by (Wilson, 2012) has an upturn HREE. This reflects both the cumulate assemblage as well as the characteristics of the magma source.

The multi-element diagram displays enrichment in LREE with positive anomalies for Cs, Pb, K, U and a negative Nb anomaly. The negative Nb anomaly is characteristic of continental crust and may be an indicator of continental crust involvement in magma processes. There is also HREE depletion.

# CHAPTER 6: WHOLE ROCK GEOCHEMISTRY OF THE UNKI XENOLITH SUITE

## 6.1 Introduction

A total of 134 samples from the Selukwe Subchamber xenolith suite were collected for this study of which 86 were geochemically analysed. The locations of these borehole and samples are shown in the locality sites map in Appendix A.

## 6.2 Major Element Variations

The major element oxides geochemistry results of the USM, UNK and BC suites of xenolith samples are given in Appendix E, Table E2.1, E3.1 and E 4.1 respectively. The major element oxides of the Unki xenolith suite where plotted on the total alkali-silica diagram for plutonic rocks in Fig. 6.1. The mafic-ultramafic xenoliths are sub-alkali characterized by low alkalis from 0 to 4 (wt %) with silica contents of 40-55 (wt %) which are typical of ultramafic rocks. They are classified as peridotite, gabbro and gabbroic diorite according to LeMaitre (1984).

Using the Streckeisen (1976), the xenoliths can be classified on a modal basis on either Olivine – Clinopyroxene – Orthopyroxene (ol-cpx-opx), Plagioclase – Clinopyroxene – Orthopyroxene (plag-cpx-opx) and Plagioclase – Olivine – Pyroxene (Plag-Olivine-Pyroxene) diagrams shown in Fig 6.2 (a-c). The ol-cpx-opx is appropriate for the peridotite group (dunites, harzburgites, and lherzolites) and pyroxenite group (pyroxenites, olivine-pyroxenites, websterite, and olivine websterite). The plag-cpx-opx is appropriate to the gabbroic group (gabbro, orthopyroxene gabbro, clinopyroxene gabbro). The xenolith suite is also characterized by olivine bearing gabbros and norites that are shown in the Plag-Olivine-Pyroxene diagram.

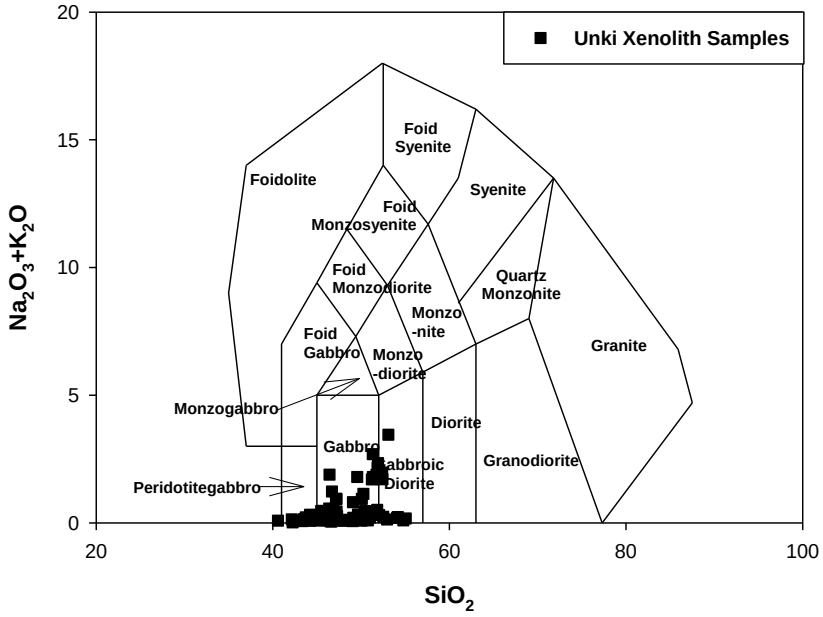


**Fig. 6.1.** Chemical classification and nomenclature of the Unki xenolith suite samples using the total alkali versus silica (TAS) diagram (after Le Maitre 1984). Closed squares (■) represent Unki xenolith sample (Table E2.1, E3.1 and E 4.1).

The Unki xenoliths are classified after Streckeisen (1976) on either the (a) ol-cpx-opx or (b) plag-cpx-opx diagram in Fig. 6.2 using normative data from the geochemical analyses. Diagram (a) is appropriate for the peridotite group (dunites, harzburgites, and lherzolites) and pyroxenite group (pyroxenites, olivine-pyroxenite, olivine websterite, websterite). Diagram (b-c) is appropriate for the gabbroic group (gabbro, gabbro/norites and olivine gabbro/norites).

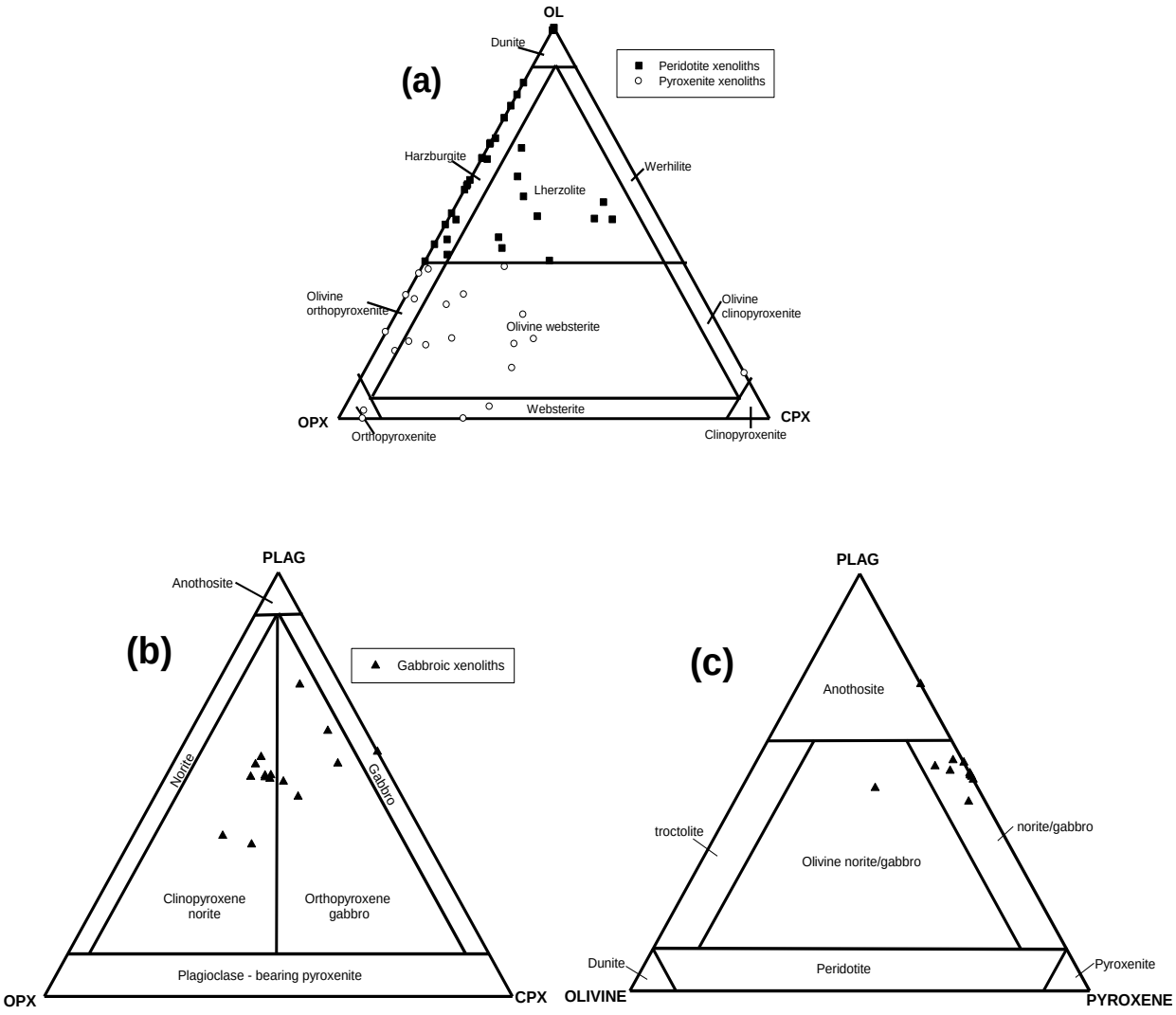


**Fig. 6.2**. Normative compositions of the Unki xenolith samples. (a) Olivine – Orthopyroxene – Clinopyroxene. (b) Plagioclase – Orthopyroxene – Clinopyroxene and (c) Plagioclase – Olivine – Pyroxene. Classification after Streckeisen (1976) closed squares (■) represent peridotites, open cycles (○) represent pyroxenites and closed triangles (▲) represent gabbros (Appendix E, Table E2.1, E3.1 and E 4.1).

Chemical variation diagrams of the Unki xenolith suite are shown in Fig. 6.3. Major element oxides are plotted against MgO, which is used as an index of fractionation and also reflects mineralogy. Trends of the major element variation are controlled by modal variations and compositions of the constituent minerals. There is considerable overlap between the peridotites, pyroxenites and gabbros in all major oxides as shown in the major element ratios are shown Table 6.1 and Fig. 6.3. However, the gabbros display more variability compared with the other rock types.

The range in MgO contents is 4.16 to 43.21 (wt%) with peridotites having slightly higher values than the pyroxenites and gabbros. The peridotites have a high average of 33.32% while pyroxenites the average is 25.94%. The gabbros plot separate from the ultramafics with a lower MgO, average of 10%.

The range in Mg# is 0.48 to 0.89 with the peridotites having higher values than pyroxenites and gabbros. There is a positive correlation in Mg# with MgO. The peridotites have a range of 0.79 to 0.90 similar to pyroxenites with a range of 0.79 to 0.89. The gabbros have a much greater range of 0.48 to 0.76.

The range in $SiO_2$ contents is 40.59 to 55.06 (wt%) and displays a negative correlation with MgO. The gabbros have slightly higher values than the pyroxenites and peridotites. The xenoliths all plot as a separate population with the highest values in the gabbros with lower values for the pyroxenites and peridotites.

The range in $Al_2O_3$ contents is 1.57 to 21.78 (wt%) and displays a negative correlation with the gabbros having markedly higher values than the pyroxenites and peridotites.

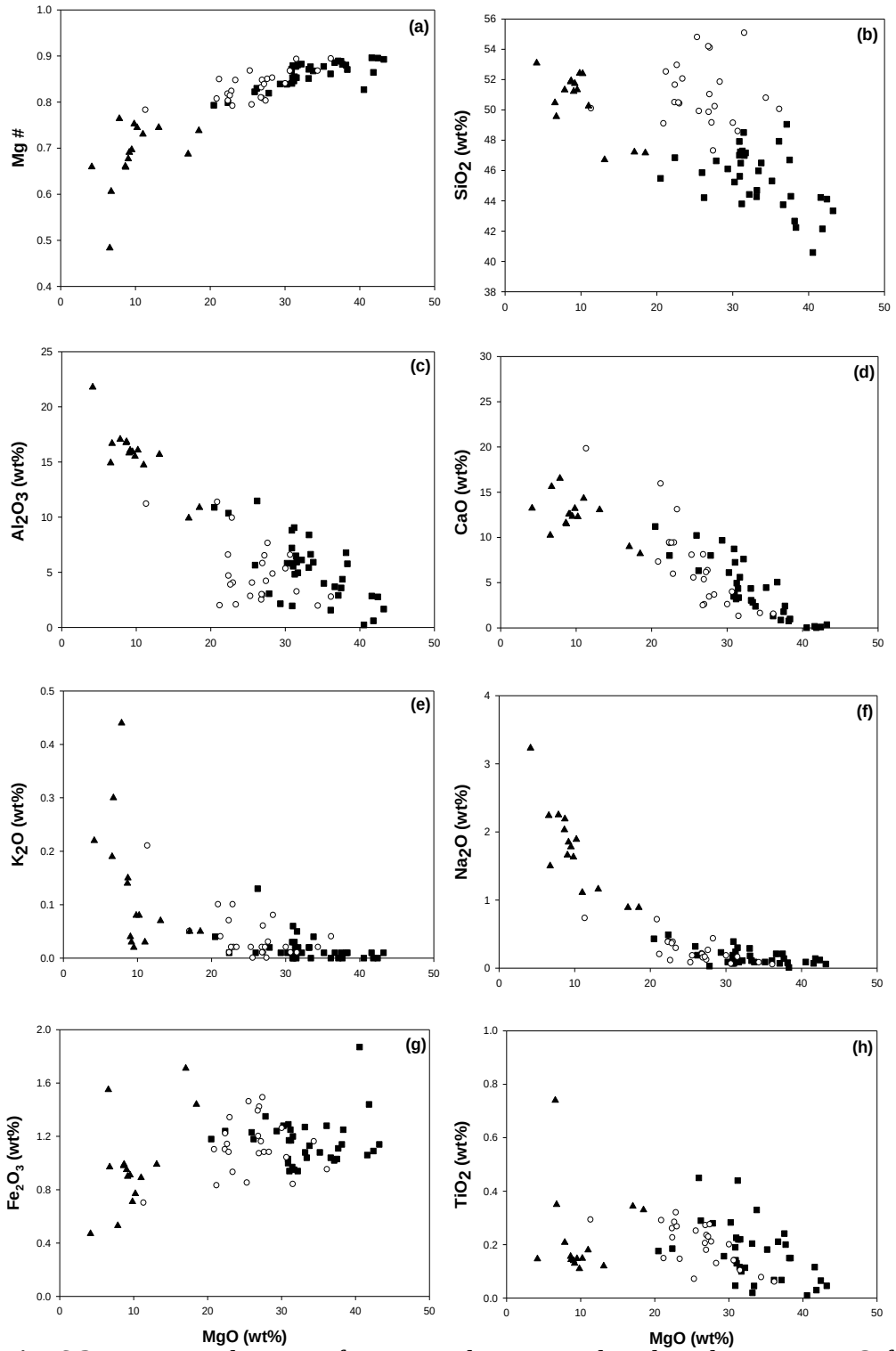


**Fig. 6.3.** Variation diagrams for major element oxides plotted against MgO for Unki xenolith suite samples. Closed squares (■) represent peridotites, open cycles (○) represent pyroxenites and closed triangles (▲) represent gabbros.

**Table 6.1.** Whole rock major element oxides (wt%) averages and standard deviations for the Unki xenolith samples by XRF analyses in Appendix E, Table E2.1, E3.1 and E 4.1 respectively.

| ROCK TYPE | STATISTICS | $SiO_2$ | $Al_2O_3$ | $Fe_2O_3$ | MgO | CaO | $Na_2O$ | $Cr_2O_3$ | NiO |
|---|---|---|---|---|---|---|---|---|---|
| PERIDOTITES | AVERAGE | 45.45 | 5.24 | 1.16 | 33.32 | 4.18 | 0.16 | 0.49 | 0.24 |
| 35 | STAND. DEV. | 1.95 | 2.82 | 1.17 | 5.39 | 3.16 | 0.11 | 0.12 | 0.07 |
| PYROXENITES | AVERAGE | 51.06 | 4.98 | 1.12 | 25.94 | 6.74 | 0.25 | 0.41 | 0.16 |
| 24 | STAND. DEV. | 2.03 | 2.77 | 0.20 | 5.04 | 4.65 | 0.18 | 0.11 | 0.06 |
| GABBROS | AVERAGE | 50.58 | 15.64 | 0.98 | 10.00 | 12.41 | 1.75 | 0.08 | 0.03 |
| 15 | STAND. DEV. | 2.04 | 2.68 | 0.35 | 3.77 | 2.21 | 0.62 | 0.07 | 0.02 |

The range in CaO contents is 0.02 to 19.80 (wt%) and displays a negative correlation with MgO. The gabbros have higher than the pyroxenites and peridotites. The gabbros have a high average of 12.41 (wt%) , the pyroxenites have a lower average of 6.74 while peridotites have the lowest average of 4.18 (wt%).

The range in $Fe_2O_3$ contents is 0.47 to 1.87 (wt%) and displays with a weak positive correlation with MgO. The peridotites have a slightly higher average of 1.16 (wt%), the pyroxenites have the average of 1.12 while gabbros have an average of 0.98 (wt%). The range in $Na_2O$ contents is 0.03 to 3.23 (wt %) and displays a negative correlation with MgO. The gabbros have higher values than the pyroxenites and peridotites. The gabbros have an average of 1.75 (wt%), the pyroxenites have an average of 0.25 while peridotites have an average of 0.16 (wt%).

The ratios of $K_2O$ and $TiO_2$ are shown in Table 6.2. The $K_2O$ range in contents is 0 to 0.44 (wt%). The gabbros have slightly higher values than the pyroxenites and peridotites. The gabbros have an average (wt%) of 0.13, the pyroxenites have an average of 0.04 (wt%) while peridotites have an average of 0.02 (wt%). The range in $TiO_2$ contents is 0.01 to 0.3 (wt%) with no significant trend with MgO. The gabbros have an average of 0.23 the pyroxenites have an average of 0.20 (wt%) while peridotites have an average of 0.23 (wt%).

Generally there is a weak negative correlation with MgO for $Na_2O$, $SiO_2$, $TiO_2$, CaO and weak or no significant correlation with $K_2O$ and $TiO_2$. Mg# and FeO display positive correlations.

## 6.3 Trace Element Variation

The whole rock trace elements of the Unki xenolith samples of USM, UNK and BC are given in Appendix E, in Table E2.2, E 2.3, E3.2, E3.3 and E4.2 respectively. The trace elements will be presented in three groups (1) incompatible components are Zr, Rb, Ba, Sr, Y, $TiO_2$, $K_2O$ (2) compatible elements Cr, V, Sc and (3) chalcophile or transition elements Co, Zn, Cu, and Ni. Trace elements were plotted against MgO and are displayed in Fig. 6.4 – 6.5. Inter-element variations of the Unki xenoliths are shown in Fig 6.6. Trace element ratios are displayed in Table 6.2. The trace elements used in these diagrams were analyzed using ICP-MS.

The range in Zr contents is 0.2 to 43.5 ppm with pyroxenites having the highest values. There is a diffuse trend with increasing Zr at lower MgO with pyroxenites having slightly higher values than the peridotites and gabbros. The pyroxenites have a greater range, with an average of 8.85 ppm while in peridotites have an average of 7.41 ppm. The gabbros also have low values with an average of 4.76 ppm. The range in Rb contents is 0.1 to 15.6 ppm with gabbro with the highest value and a greater range. There is also a diffuse trend between the Rb against MgO. The gabbros have an average of 2.11 ppm while in pyroxenites the average is 1.45 ppm and peridotites have an average of 0.66 ppm. The range in Ba contents is 0.3 to 108.3 ppm and displays a weak negative correlation with MgO. The gabbros have much higher values than the pyroxenites and peridotites. The gabbros have a wide range with an average of 34.19 ppm. The pyroxenites have values less than 40 ppm with an average is 10.69 ppm while peridotites the average is 6.05 ppm.

**Table 6.2.** Whole rock incompatible trace element (ppm) averages and standard deviations ratios for the Unki xenolith samples by ICP-MS.

| ROCK TYPE | STATISTICS | Zr | Rb | Sr | Y | $K_2O$ | $TiO_2$ |
|---|---|---|---|---|---|---|---|
| PERIDOTITES | AVERAGE | 8.80 | 1.35 | 21.66 | 3.66 | 0.01 | 0.15 |
| | STAND.DEV. | 13.80 | 1.00 | 19.34 | 3.15 | 0.02 | 0.10 |
| PYROXENITES | AVERAGE | 17.03 | 1.87 | 31.50 | 5.28 | 0.04 | 0.22 |
| | STAND.DEV. | 41.60 | 1.64 | 24.66 | 3.87 | 0.05 | 0.09 |
| GABBROS | AVERAGE | 7.21 | 3.64 | 149.91 | 5.59 | 0.13 | 0.23 |
| | STAND.DEV. | 9.08 | 5.35 | 68.69 | 3.66 | 0.12 | 0.16 |

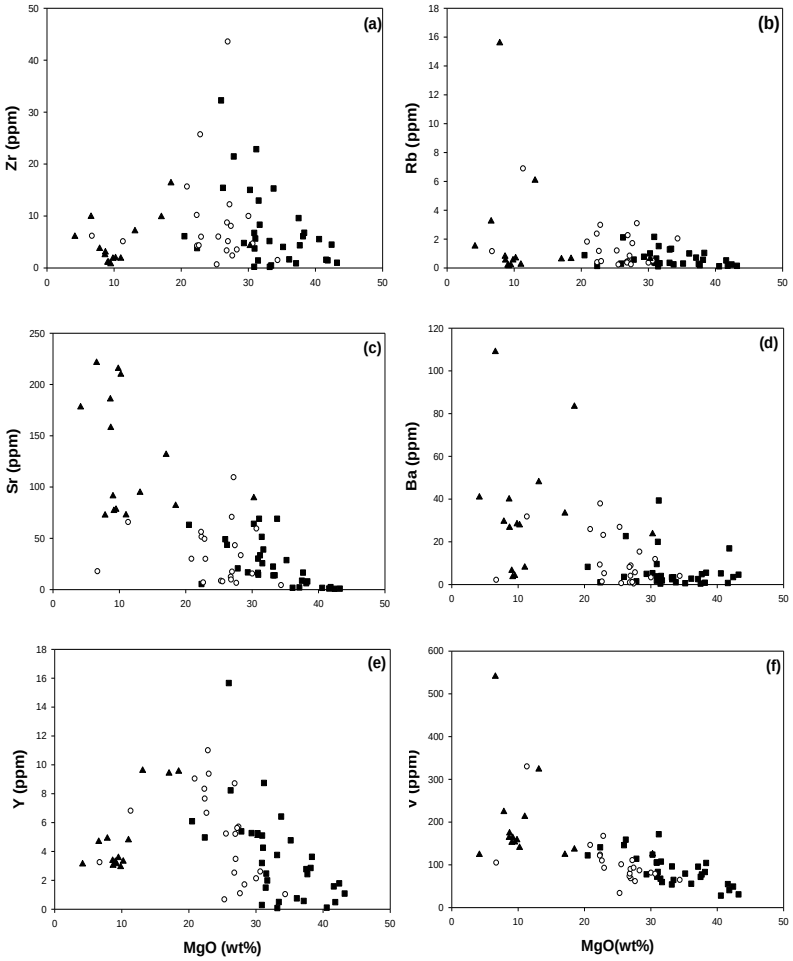


**Fig. 6.4.** Variation diagrams for trace elements plotted against MgO for the Unki xenolith samples. Closed squares (■) represent peridotites, open cycles (○) represent pyroxenites and closed triangles (▲) represent gabbros.

The range in Sr contents is 0.80 to 221.30 ppm and is negatively correlation with MgO. The gabbros have much higher values than the pyroxenite and peridotites. The gabbros also show a greater range with an average of 130.48 ppm. The pyroxenite shows a much lower average of 35.26 ppm while the peridotites have an average of 23.93 ppm. The range in Y contents is 0.10 to 15.70 ppm and displays a separate population of gabbros while peridotites and pyroxenites have a negative correlation with MgO. The gabbros have a low average of 4.92 ppm. The pyroxenites and peridotites show a negative correlation when plotted against MgO. The pyroxenites show a wider range with an average of 5.11 ppm while peridotites have an average of 3.61 ppm.

The range in V contents is 31 to 540.6 ppm with gabbros having slightly higher values than the pyroxenites and peridotites. There is a strong negative correlation when V is plotted with MgO. The gabbros have the highest values with an average of 194.37 ppm. The pyroxenites have an average of 104.84 ppm while the peridotites have an average of 87.80 ppm. The range in Cu contents is 0.90 to 149.40 ppm with gabbros having slightly higher values than the pyroxenites and peridotites. The Cu shows a weak negative trend with MgO with the gabbros with average 46.96 ppm. The pyroxenites have an average of 17.77 ppm while the peridotites have the lowest average of 11.82 ppm.

**Table 6.3:** Whole rock chalcophile and compatible trace element averages (ppm) and standard deviations ratios for the Unki xenolith samples by ICP-MS.

| ROCK TYPE | STATISTICS | Cu | Ni | Zn | Co | V | Cr | Sc |
|---|---|---|---|---|---|---|---|---|
| PERIDOTITES | AVERAGE | 8.80 | 1882.74 | 61.71 | 111.27 | 84.92 | 2864.50 | 18.93 |
| | STAND. DEV. | 8.70 | 365.74 | 20.36 | 8.50 | 28.46 | 675.87 | 5.90 |
| PYROXENITES | AVERAGE | 14.58 | 1284.02 | 76.53 | 102.20 | 118.29 | 2622.05 | 24.36 |
| | STAND. DEV. | 19.65 | 434.41 | 25.83 | 17.00 | 59.76 | 750.96 | 9.87 |
| GABBROS | AVERAGE | 48.16 | 203.05 | 52.49 | 57.92 | 156.68 | 439.36 | 38.29 |
| | STAND. DEV. | 50.47 | 162.32 | 24.55 | 21.59 | 34.43 | 379.42 | 11.24 |

The range in Zn contents is 21.40 to 134.90 ppm with no significant trend against MgO. The pyroxenites have the highest values with an average of 69.07 ppm while the peridotites have an average of 57.21 ppm. The gabbros have an average of 48 ppm. The range in Ni contents is 70 to 2896.40 ppm with peridotite having the highest values than the pyroxenites and gabbro. There is a positive correlation when Ni is plotted with MgO. The peridotites have an average of 1254 ppm while pyroxenites have an average of 1729.14. The gabbros have an average of 220.69. The range in Co contents is 22 to 149.30 ppm with peridotites having the highest values than the pyroxenites and gabbros. There is a positive correlation when Co is plotted with MgO. The peridotites have an average of 105.88 ppm while the pyroxenites have an average of 92.03 ppm. The gabbros have an average of 61.33 ppm.

The range in Cr contents is 170.1 to 4693 ppm and shows a positive correlation with MgO. The peridotites having the highest values followed pyroxenites and gabbros have the lowest. The peridotites also show a greater range with an average of 3115.81 ppm. The pyroxenites also have a high average of 2576.46 ppm. The gabbros have an average of 548.75 ppm which is generally high compared to most gabbros in layered intrusions but the lowest in the xenolith suite. The range in Sc contents is 2.50 to 56.60 ppm and shows a negative correlation with MgO. The highest values found in gabbros then pyroxenites then peridotites. The gabbros have an average of 37.15 ppm. The pyroxenites have an average of 20.58 ppm while the peridotites have an average of 16.79 ppm.

The inter-element diagrams of selected elements are shown in Fig 6.6. Variation diagrams of incompatible elements Rb, Ba, show weak positive correlations with Zr with peridotites, pyroxenites and gabbros all statistically overlapping. The $Al_2O_3$, Y $TiO_2$ and diagrams also shows a positive correlation with Zr and overlapping of all rock types. The Cu vs Ni variation diagram shows no significant trend.

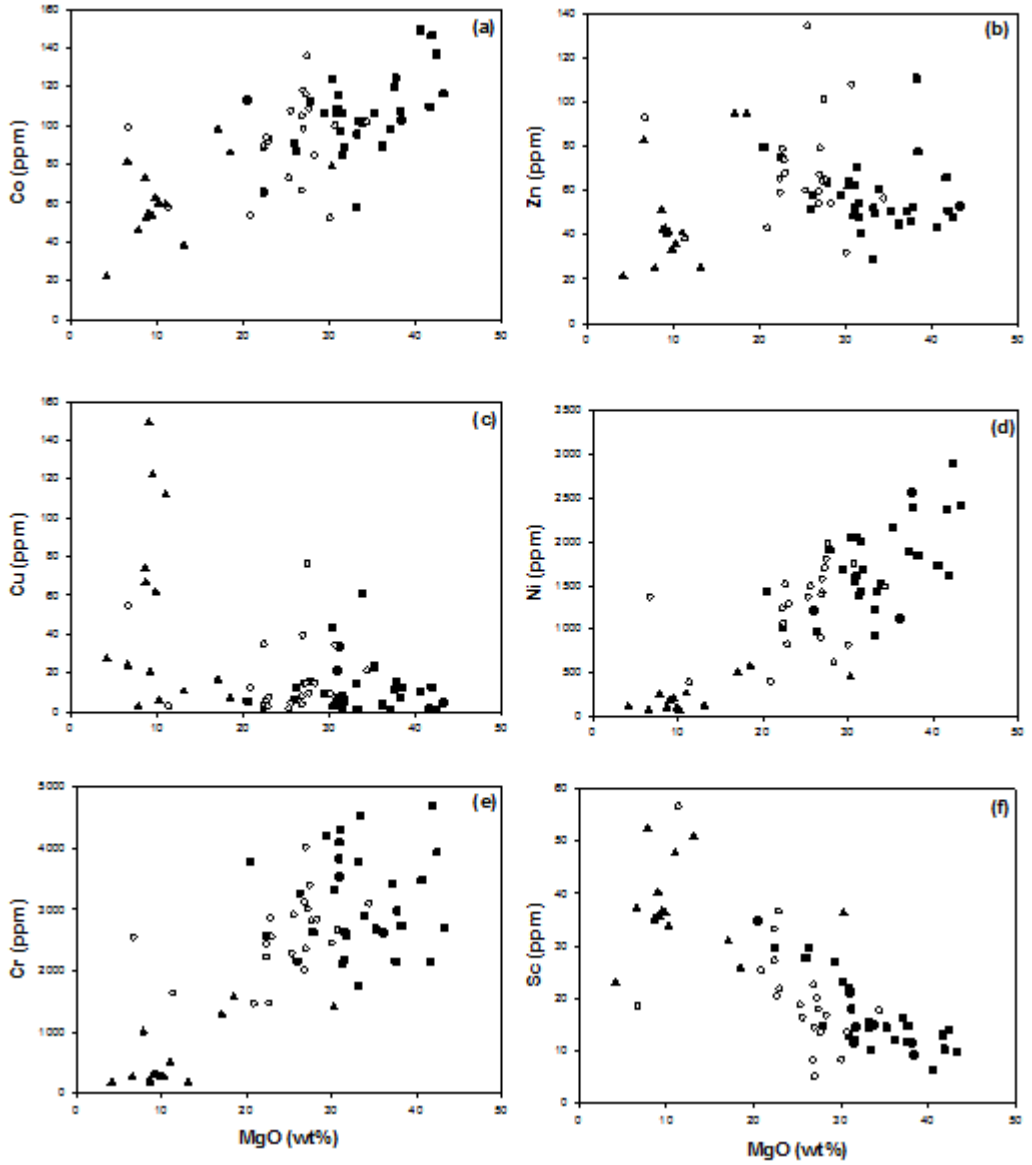


**Fig. 6.5.** Variation diagrams continued for trace elements plotted against MgO for the Unki xenolith samples. Closed squares (■) represent peridotites, open cycles (○) represent pyroxenites and closed triangles (▲) represent gabbros.

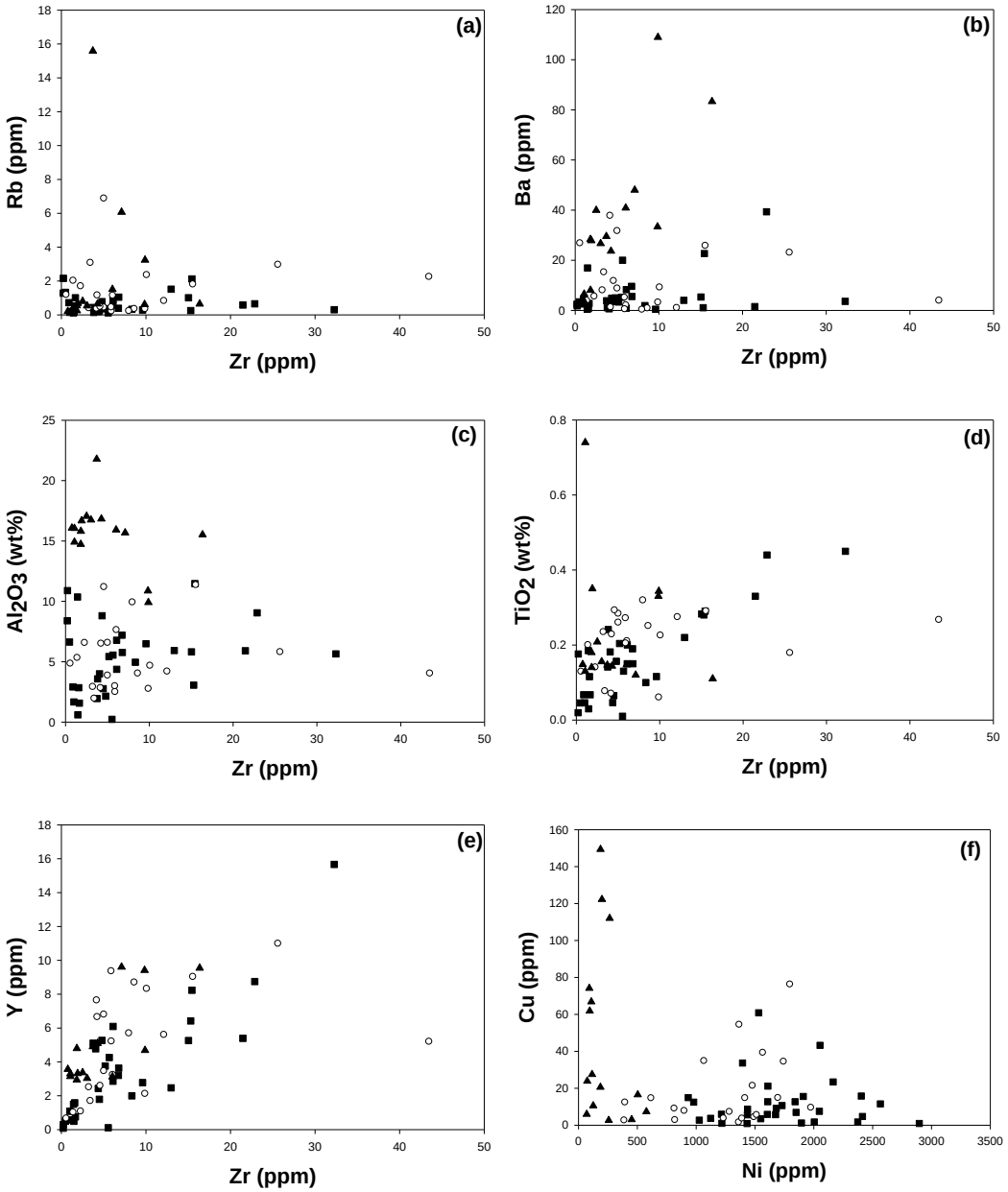


**Fig. 6.6.** Inter -element variation diagrams for trace elements in the Unki xenolith samples (a) Rb vs Zr, (b) Ba vs Zr (c) $Al_2O_3$ vs Zr, (d) $TiO_5$,vs Zr (e) Y vs Zr, (f) Cu vs Ni. Closed squares (■) represent peridotites, open cycles (○) represent pyroxenites and closed triangles (▲) represent gabbros.

## 6.4 Rare Earth Elements Variation

REEs averages and standard deviations of the three rock types are displayed in Table 6.4 with the normalised ratios shown in Table 6.5. The inter-element variation diagrams of La and Total REE with the incompatible element Zr in ppm are displayed in Fig. 6.7. A positive correlation is shown with overlapping of pyroxenites, peridotites and gabbros.

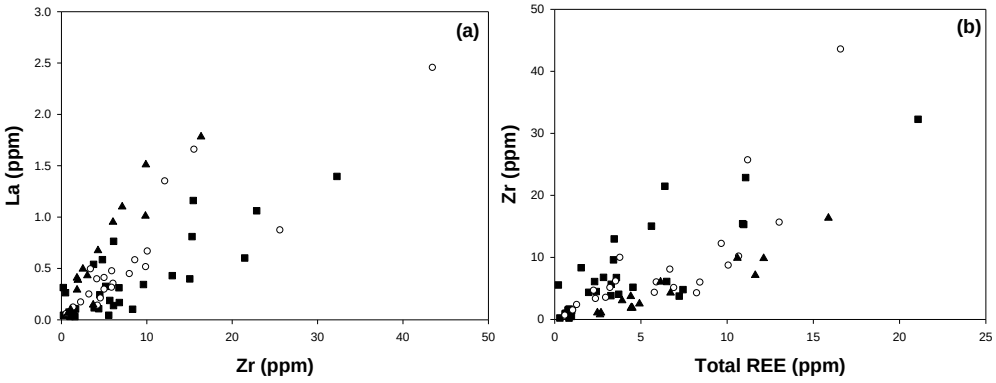


**Fig. 6.7.** Variations of (LREE) La (ppm) and Total REE (ppm) with incompatible element Zr (ppm) in the Unki xenolith suite Closed squares (■) represent peridotites, open cycles (○) represent pyroxenites and closed triangles (▲) represent gabbros.

The average sample REEs patterns of the peridotites, pyroxenites and gabbros normalized to primitive mantle are displayed in Fig.6.8. The REEs were normalized after Sun & McDonough (1995). The Total REE for the peridotites ranges from 0.37 to 40.923 ppm, which is the lowest in the three rock types. The peridotites are depleted in both LREE and HREE with a negative Eu anomaly. The LREEs are depleted with LaN/YbN range from 0.12 to 6.52 with an average ratio of 0.855. The LaN/GdN ranges from 0.31 to 40.32 with an average of 3.26. The HREEs have a flat depleted pattern with GdN/YbN range from 0.04 to 1.17 with an average of 0.52.

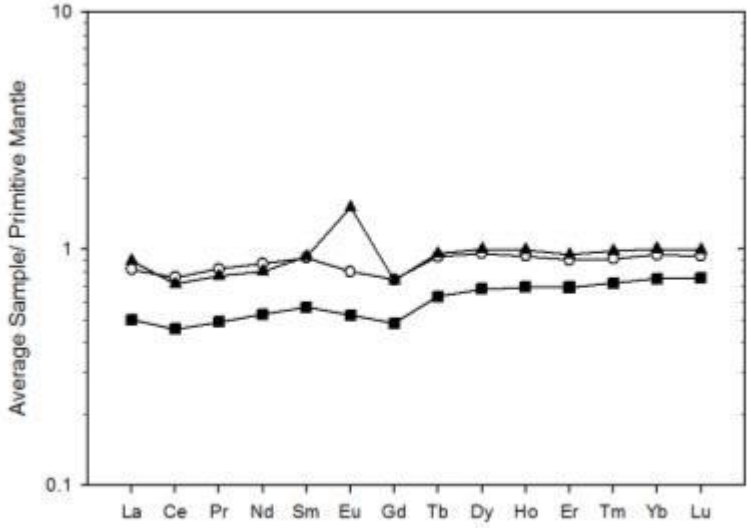


**Fig. 6.8.** The average sample primitive mantle-normalized REE patterns for the Unki xenolith suite for the peridotites, pyroxenites and gabbro samples. Normalising values to primitive mantle are from Sun and McDonough (1995). Closed squares (■) represent peridotites, open cycles (○) represent pyroxenites and closed triangles (▲) represent gabbros.

The Total REE range for the pyroxenites samples is 1.63 to 24.08 ppm. The pyroxenites are LREE depleted with a LaN/YbN range 0.16 to 4.89 and an average ratio of 0.97. The LaN/GdN range is 0.21 to 3.23 with an average 1.38. The HREEs are also slightly depleted and a negative Eu anomaly. GdN/YbN range is 0.28 to 1.76 with an average of 0.72.

The total REE range for the gabbro samples is 7.21 to 29.08 ppm and shows fractionation in a limited range. The gabbros are LREE depleted with a LaN/YbN range from 0.11 to 2.47 with an average ratio of 0.886. The LREE LaN/GdN range 0.24 to 2.47 with an average of 1.12. The HREEs are also slightly depleted and a positive Eu anomaly range 0.17 to 1.06 with an average 0.73.

**Table 6.4:** Whole rock REE averages (ppm) and standard deviations for the Unki xenolith samples by ICP-MS. All values are Primitive Mantle normalized after Sun and McDonough (1995).

| ROCK TYPE | STATISTICS | La | Ce | Pr | Nd | Sm | Eu | Gd |
|---|---|---|---|---|---|---|---|---|
| PERIDOTITES | AVERAGE | 0.50 | 0.46 | 0.49 | 0.53 | 0.56 | 0.52 | 0.48 |
| 31 | STAND. DEV | 0.50 | 0.53 | 0.62 | 0.67 | 0.70 | 0.54 | 0.55 |
| PYROXENITES | AVERAGE | 0.89 | 0.76 | 0.82 | 0.86 | 0.92 | 0.80 | 0.74 |
| 21 | STAND. DEV | 0.82 | 0.74 | 0.70 | 0.66 | 0.65 | 0.48 | 0.50 |
| GABBROS | AVERAGE | 0.89 | 0.71 | 0.77 | 0.80 | 0.93 | 1.49 | 0.73 |
| 15 | STAND. DEV | 0.76 | 0.61 | 0.6057 | 0.59 | 0.58 | 0.56 | 0.43 |

**Table 6.4:** Whole rock REE averages (ppm) and standard deviations for the Unki xenolith samples by ICP-MS continued.

| ROCK TYPE | STATISTICS | Tb | Dy | Ho | Er | Tm | Yb | Lu |
|---|---|---|---|---|---|---|---|---|
| PERIDOTITES | AVERAGE | 0.69 | 0.67 | 0.69 | 0.69 | 0.71 | 0.75 | 0.75 |
| 31 | STAND. DEV | 0.69 | 0.68 | 0.67 | 0.63 | 0.65 | 0.63 | 0.63 |
| PYROXENITES | AVERAGE | 0.93 | 0.95 | 0.93 | 0.90 | 0.91 | 0.94 | 0.93 |
| 21 | STAND. DEV | 0.63 | 0.62 | 0.59 | 0.53 | 0.55 | 0.52 | 0.51 |
| GABBROS | AVERAGE | 0.95 | 0.1 | 0.99 | 0.95 | 0.98 | 0.10 | 0.99 |
| 15 | STAND. DEV | 0.52 | 0.51 | 0.49 | 0.464 | 0.49 | 0.48 | 0.50 |

**Table 6.5:** The averages (ppm) and standard deviations for REE ratios; LaN/GdN, LaN/YbN and GdN/YbN for the Unki xenolith samples by ICP-MS. All values are Primitive Mantle after Sun and McDonough (1995).

| ROCK TYPE | STATISTICS | LaN/YbN | LaN/GdN | GdN/YbN |
|---|---|---|---|---|
| PERIDOTITE | AVERAGE | 0.85 | 3.26 | 0.59 |
| 31 | STAND. DEV. | 1.13 | 7.42 | 0.30 |
| PYROXENITE | AVERAGE | 0.97 | 1.38 | 0.72 |
| 25 | STAND. DEV. | 1.04 | 0.84 | 0.36 |
| GABBRO | AVERAGE | 0.89 | 1.12 | 0.73 |
| 15 | STAND. DEV. | 0.68 | 0.69 | 0.17 |

## 6.5 Multi-Element Diagrams

The average sample primitive mantle normalised trace element diagram after Sun and McDonough (1989) for the peridotite, pyroxenite and gabbro xenoliths are displayed in Fig. 6.9. Trace element averages and standard deviations of the three rock types are displayed in Table 6.6. Relative to primitive mantle (and also to in comparison with MORB) the three rock types show similar patterns with relative enrichment of LILs and LREE. They are further characterised by positive anomalies for Th, K, Pb, Sr and negative anomalies of Nb, Pr and Dy. Eu is positive in the gabbros and flat for peridotites and pyroxenite. The gabbros are more enriched in trace elements than pyroxenite and peridotites with the lowest.

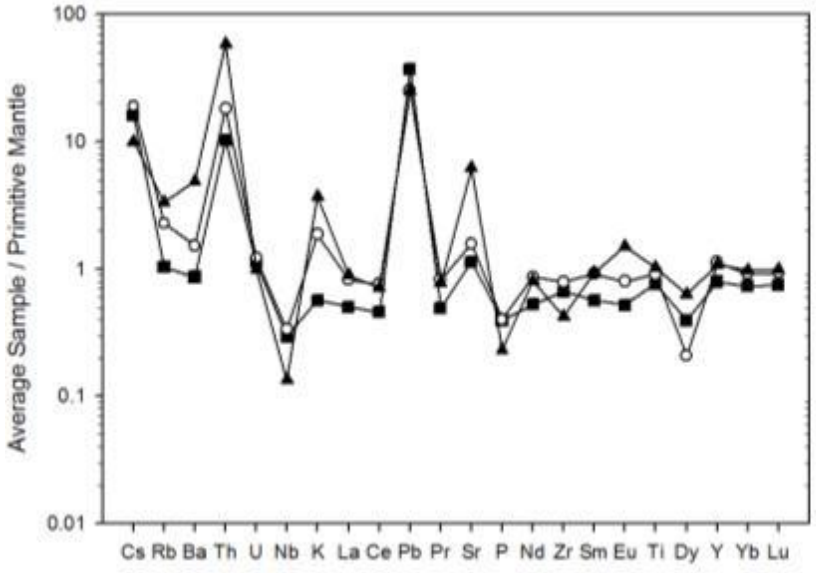


**Fig. 6.9.** The average sample primitive mantle-normalized multi-element patterns for the Unki xenolith suite peridotites, pyroxenites and gabbro samples. All values are Primitive Mantle normalising after Sun and McDonough (1989). Closed squares (■) represent peridotites, open cycles (○) represent pyroxenites and closed triangles (▲) represent gabbros.

**Table 6.6:** Whole rock trace element averages (ppm) and standard deviations for Unki xenolith samples by ICP-MS. All values are Primitive Mantle normalized values after McDonough (1989).

| ROCK TYPE | STATISTICS | Cs | Rb | Ba | Th | U | Nb | K | La | Ce | Pb | Pr |
|---|---|---|---|---|---|---|---|---|---|---|---|---|
| PERIDOTITE | AVERAGE | 16.20 | 1.03 | 0.87 | 10.30 | 0.11 | 0.29 | 0.57 | 0.50 | 0.46 | 37.06 | 0.49 |
| | STAND. | | | | | | | | | | | |
| 31 | DEV. | 21.76 | 0.87 | 1.18 | 14.06 | 0.15 | 0.38 | 0.86 | 0.50 | 0.53 | 54.15 | 0.62 |
| PYROXENITE | AVERAGE | 18.90 | 2.28 | 1.53 | 18.20 | 0.12 | 0.33 | 1.86 | 0.82 | 0.76 | 25.03 | 0.83 |
| | STAND. | | | | | | | | | | | |
| 21 | DEV. | 22.36 | 2.43 | 1.64 | 19.50 | 0.14 | 0.44 | 2.59 | 0.82 | 0.74 | 26.62 | 0.70 |
| GABBRO | AVERAGE | 9.96 | 3.32 | 4.90 | 58.23 | 0.01 | 0.13 | 3.69 | 0.89 | 0.71 | 24.79 | 0.77 |
| | STAND. | | | | | | | | | | | |
| 15 | DEV. | 16.03 | 6.37 | 4.16 | 49.49 | 0.11 | 0.15 | 3.88 | 0.76 | 0.61 | 21.83 | 0.61 |

**Table 6.6:** Whole rock trace element averages (ppm) and standard deviations for Unki xenolith samples by ICP-MS All values are Primitive Mantle normalized values after McDonough (1989) continued.

| ROCK TYPE | STATISTICS | Sr | P | Nd | Zr | Sm | Eu | Ti | Dy | Y | Yb | Lu |
|---|---|---|---|---|---|---|---|---|---|---|---|---|
| PERIDOTITE | AVERAGE | 1.13 | 0.39 | 0.53 | 0.66 | 0.57 | 0.52 | 0.76 | 0.40 | 0.79 | 0.73 | 0.75 |
| | STAND. | | | | | | | | | | | |
| 31 | DEV. | 1.04 | 0.36 | 0.67 | 0.68 | 0.70 | 0.54 | 0.54 | 0.72 | 0.72 | 0.61 | 0.62 |
| PYROXENITE | AVERAGE | 1.58 | 0.40 | 0.86 | 0.79 | 0.92 | 0.80 | 0.91 | 0.21 | 1.12 | 0.92 | 0.93 |
| | STAND. | | | | | | | | | | | |
| 21 | DEV. | 1.32 | 0.48 | 0.66 | 0.87 | 0.65 | 0.48 | 0.38 | 0.37 | 0.69 | 0.50 | 0.51 |
| GABBRO | AVERAGE | 6.18 | 0.23 | 0.80 | 0.43 | 0.93 | 1.49 | 1.02 | 0.63 | 1.08 | 0.97 | 0.98 |
| | STAND. | | | | | | | | | | | |
| 15 | DEV. | 2.75 | 0.21 | 0.59 | 0.40 | 0.58 | 0.56 | 0.82 | 0.66 | 0.55 | 0.46 | 0.49 |

## 6.6 Summary and Discussion

The major element oxides variations display negative correlation with MgO for $SiO_2$, $TiO_2$, $Na_2O$ and CaO and a weak or no significant correlation with $K_2O$ and $TiO_2$, Mg# and total Fe (FeO plus $Fe_2O_3$) has a weak positive correlation with MgO. The negative correlations are a result of the different controls for the major phases in the rock. Also it is a result of a high proportion of the ferro-magnesian minerals (olivine and pyroxene) displacing the trapped liquid. So orthocumulates have a high proportion of trapped liquids compared with adcumulates and so have higher concentrations of incompatible elements. The gabbros plot away from the peridotites and pyroxenites. Gabbros have high $SiO_2$, CaO and Al because of the presence of plagioclase. The pyroxenites also have higher values of Ca and Al than peridotite because of the intercumulus plagioclase. The peridotites have high Mg#, MgO, Cr, Ni and Co are which typical of ultramafic cumulates.

The incompatible element distributions of Zr, Y, Rb, $K_2O$, $TiO_2$ generally tend to increase with differentiation and with higher trapped liquid component. Ba, Sr remains roughly constant in pyroxenites and peridotites because are incompatible in olivine and orthopyroxene but compatible to plagioclase hence occurs more in the gabbro. The chalcophile elements Ni, Sc, Co and Cr tend to decrease with differentiation. Ni and Co are mainly found in the crystal lattice of olivine. Sc and Cr are compatible in orthopyroxene and clinopyroxene and hence are found more in the pyroxenites and peridotites as compared feldspathic rocks. The high Ni and Cr in the ultramafic xenoliths values indicate the cumulate origin of the xenoliths.

Total REE are also incompatible elements and their content is highest in pyroxenites, followed by gabbros and lowest in the peridotites. The slight enrichment of total REE in pyroxenite as compared to peridotite is because of the presence of intercumulus liquid (orthocumulus component). The REEs patterns of the Unki xenoliths all show both LREE and HREE depletion. The pyroxenites and peridotites both negative Eu

anomalies is due to the removal of plagioclase by fractionation. To a lesser extent the presence of orthopyroxene and clinopyroxene may contribution to the negative Eu anomaly. The gabbro shows a positive Eu anomaly due to the fractionation of plagioclase during crystallisation.

The spider diagram patterns are characterised by moderate but significant enrichments in LILE Cs, Rb, Ba, T, U and LREE in gabbros (3 to 10X primitive average) relative to HFSE Nb, Th, Zr, Y. The negative Nb anomaly is characteristic of continental crust and may be an indicator of continental crust involvement in magma processes.

In conclusion, the geochemistry data shows that the Unki xenoliths are (1) be part of a coherent fractionating system that may have taken place outside of the Great Dyke, (2) the distribution of incompatible elements is largely related to the amount of trapped liquid in the original cumulates (3) the REE have essentially flat indicating a protolith with primitive mantle-type signatures and which contrast with the steeper pattern of the Great Dyke cumulates as typified in the PAR 11 section.

# CHAPTER 7: GEOCHEMICAL COMPARISON OF MR 92, PAR 11 AND THE XENOLITH SUITE

## 7.1 Introduction

This chapter will focus on the geochemical comparison of the PAR 11 borehole, Unki xenolith suite and the MR 92 borehole which intersected the P1 pyroxenite in the Selukwe Subchamber. The locations of the two boreholes and xenolith suite sample sites are in Appendix A, Map A.

The aim of this comparison is to display which part of the sequence within the Great Dyke, PAR 11 borehole and xenoliths comes from using MR 92 as the reference of the uppermost P1 pyroxenite. The Unki xenolith suite will also be plotted on chemical variation diagrams and their chemical compositions will be compared with that of the both boreholes PAR 11 and the MR 92. REE patterns and multi-element diagram for PAR 11 borehole are compared with the Unki xenolith suite.

## 7.2 Major Element Variations

This section compares the major element oxides of the PAR 11 and MR 92 borehole plotted against MgO. As described in the Chapter 5 the PAR 11 borehole is consist of pyroxenites and peridotites. The MR 92 borehole represents the P1 pyroxenite layer of most evolved series of the Selukwe Subchamber (Wilson, 2001). Variation diagrams in Fig. 7.1 display the comparison of the major element variations of the PAR 11 and MR 92 boreholes. There are three separate populations with peridotites of PAR 11 plotting far from the pyroxenites. The peridotites have higher MgO whereas the PAR 11 pyroxenites have a lower MgO and the MR 92 pyroxenites have the lowest MgO. The PAR 11 pyroxenites and peridotites plot away from each other with the MR 92 pyroxenites close to the PAR 11 pyroxenites. The PAR 11 and MR 92 pyroxenites have similar linear trends in all major oxides. The MR 92 pyroxenites

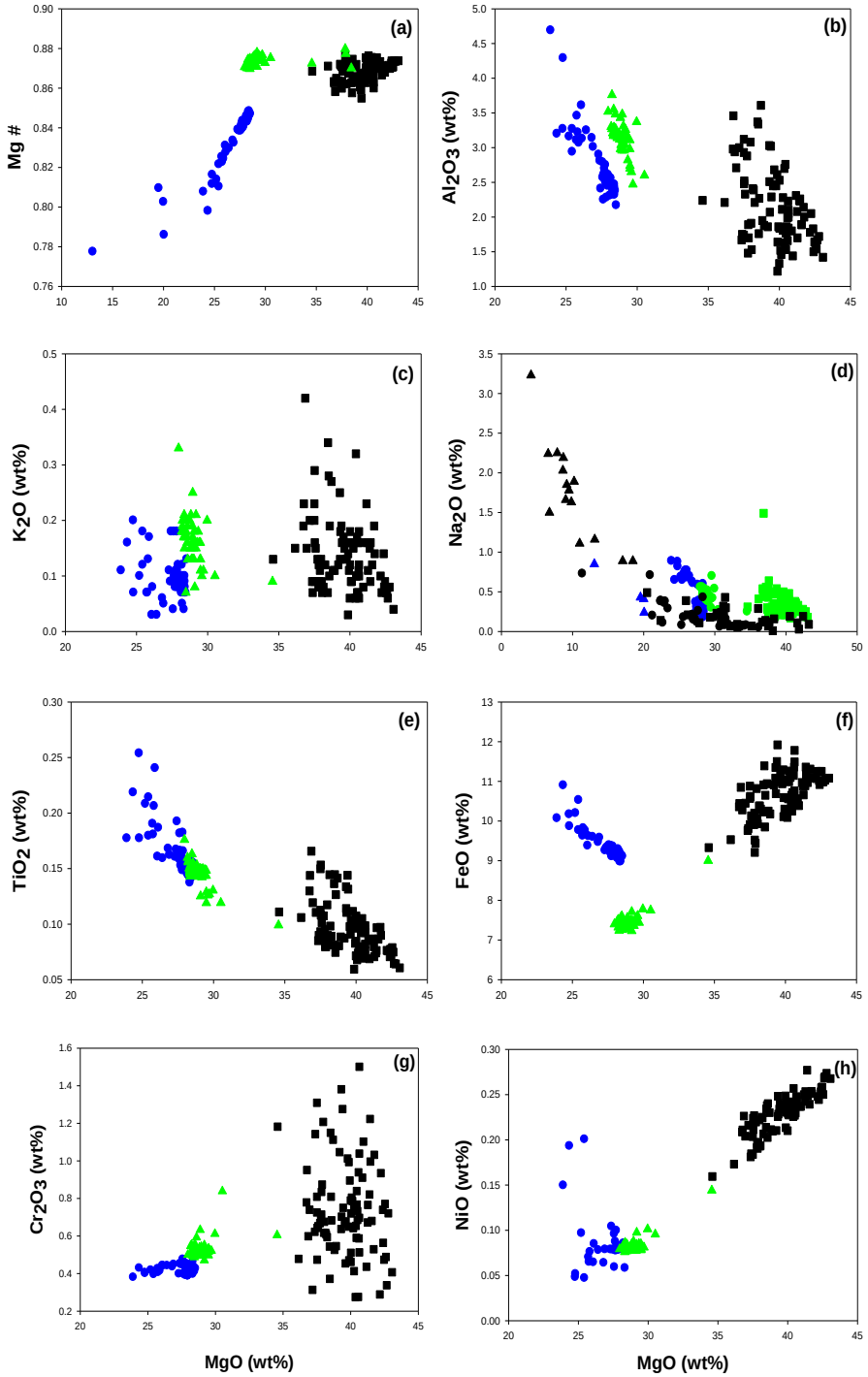


**Fig. 7.1.** Variation diagrams for major element oxides plotted against MgO for the PAR 11 and MR 92 samples. Closed squares (■) represent PAR 11 peridotites, green triangles (▲) represent PAR 11 pyroxenites and blue circles stars (●) represent MR 92 P1 pyroxenites.

are therefore more evolved, with lower Mg#, $Al_2O_3$, $K_2O$, $Na_2O$, $Cr_2O_3$, NiO and higher $TiO_2$, $Fe_2O_3$.

The variation diagrams in Fig. 7.2 display major element oxides PAR, MR 92 and the Unki xenoliths suite plotted together. The Unki xenoliths are describe in Chapter 6 as cumulates of a wide range of peridotites, pyroxenites and gabbros. The borehole samples (MR 92 and PAR 11) plot in separate but similar populations. There is a weak negative correlation with MgO for $Na_2O$, $SiO_2$, $TiO_2$, CaO and weak or no significant correlation with $K_2O$ and $TiO_2$. Mg# and FeO display positive correlation in the two boreholes.

## 7.3 Trace Element Variations

This section compares the selected trace elements oxides of the PAR 11, MR 92 borehole and the Unki xenoliths suite. As described in the Chapters 5 and 6, incompatible trace elements are mainly dependent on the amount of trapped liquid in the cumulate rocks. Variation diagrams in Fig. 7.3 display the comparison of the trace elements of the PAR 11 and MR 92 boreholes against MgO. There are negative correlations of Zr, Y, Ba, Sr, and Zn with MgO. There is positive correlation of Ni and MgO. Similar to the major element oxides plots, there are three separate populations of MR 92 pyroxenites plot away from the PAR 11 pyroxenites and PAR 11 peridotites.

Variation diagrams in Fig. 7.4 display the comparison of selected trace element oxides for PAR 11, MR 92 and the Unki xenoliths suite plotted together against MgO. Similar to the major element oxides plots, the trace elements of the MR 92 pyroxenites and PAR 11 pyroxenites plot separate but close together, and the peridotites plot away. The Unki xenolith samples show the widest range of compositions.

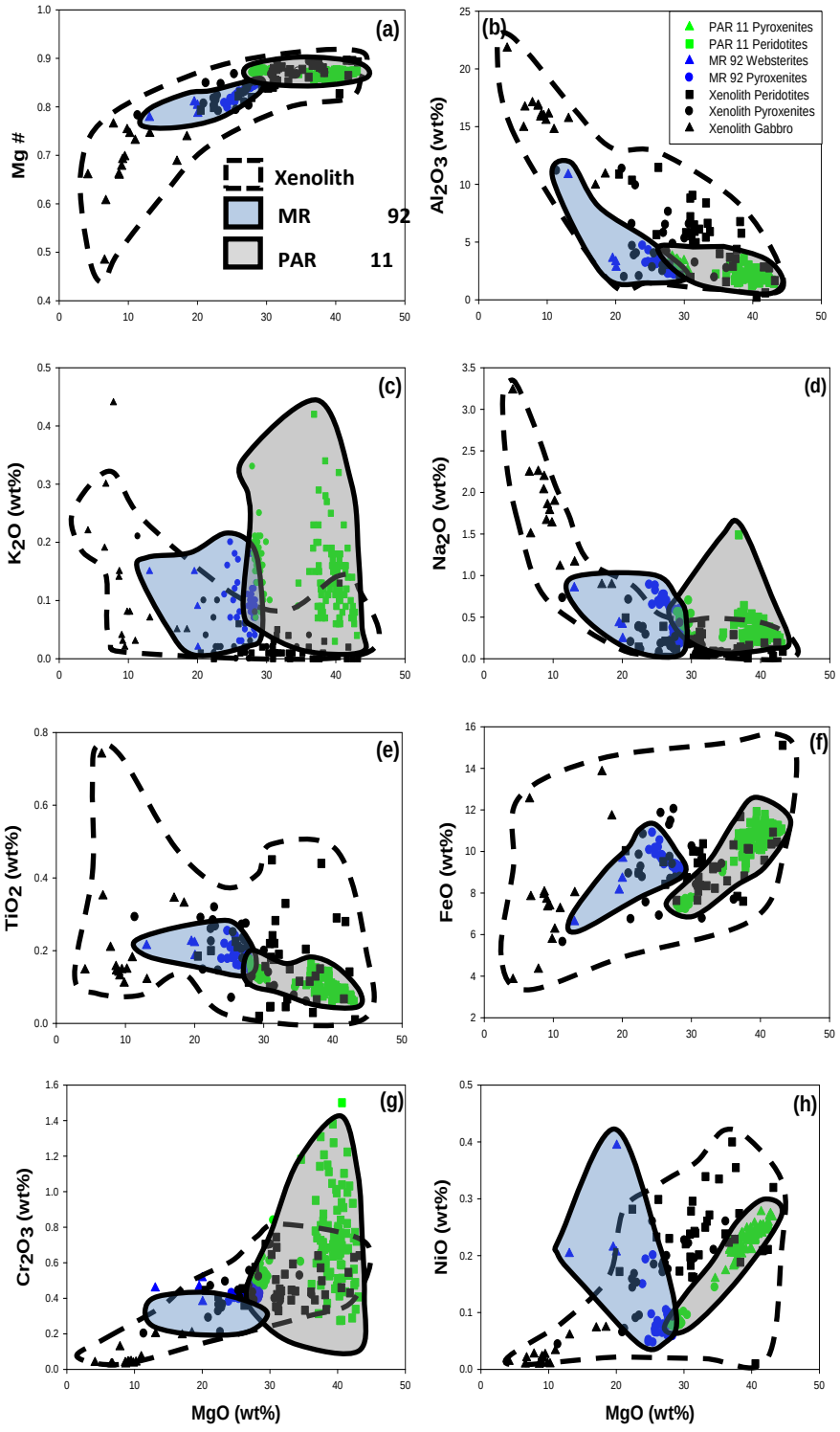


**Fig. 7.2.** Variation diagrams for major element oxides plotted against MgO for PAR 11 (grey field), MR 92 (blue field) and Unki xenolith samples (dotted field).

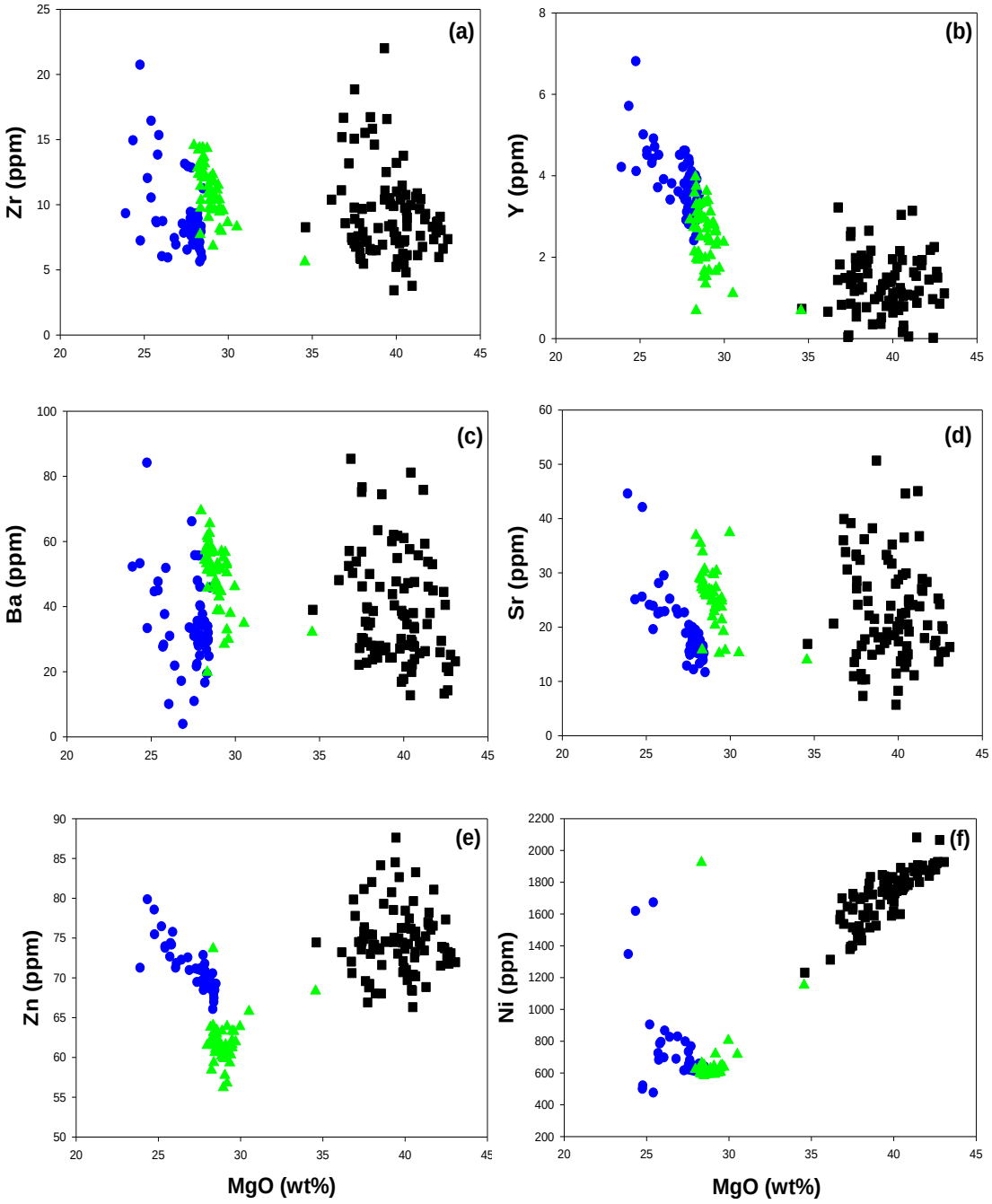


**Fig. 7.3.** Variation diagrams for trace elements plotted against MgO for the PAR 11 and MR 92 P1 pyroxenite samples. Closed squares (■) represent PAR 11 peridotites, green triangles (▲) represent PAR 11 pyroxenites and blue circles stars (●) represent MR 92 P1 pyroxenites.

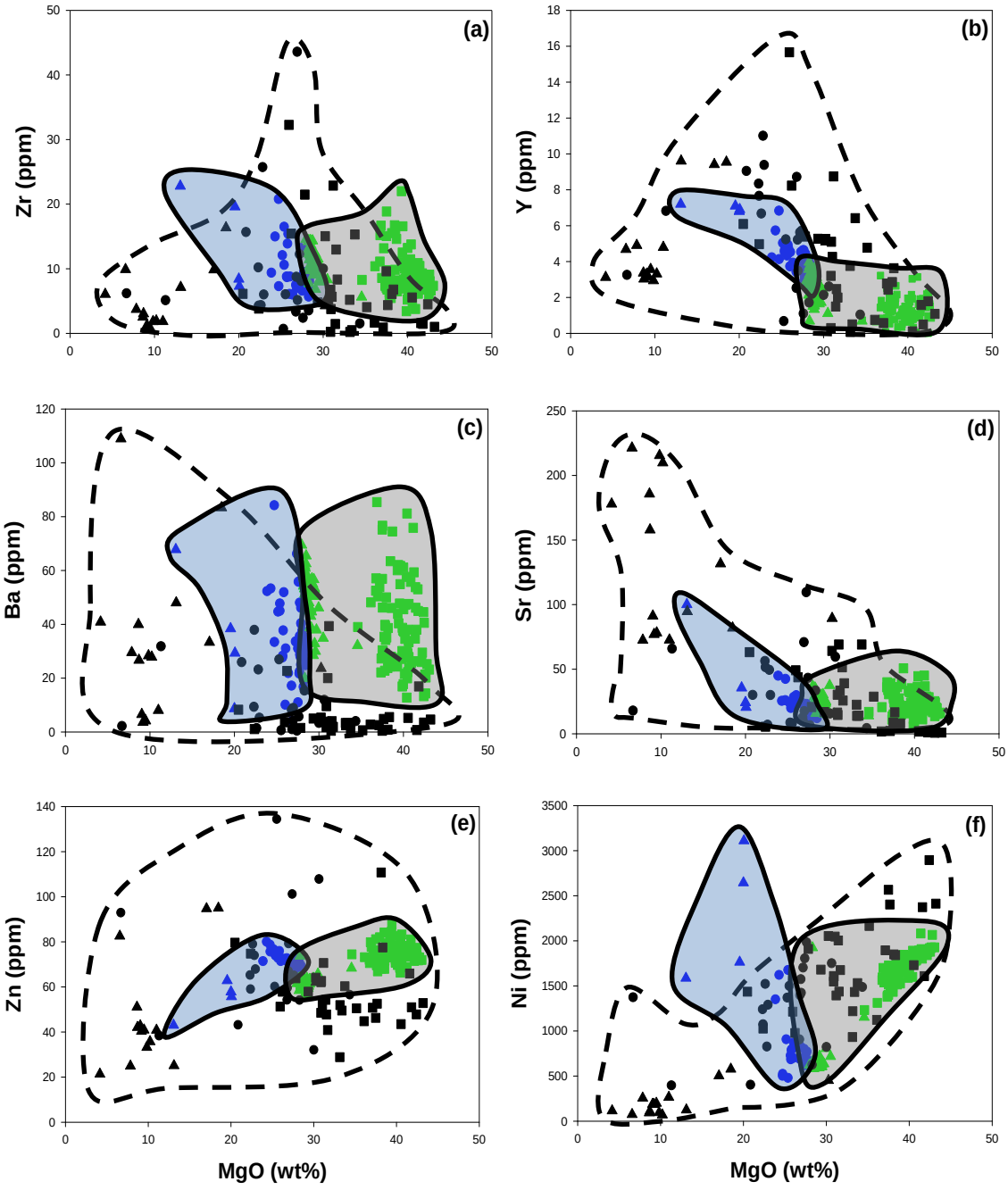


**Fig. 7.4.** Harker diagrams for trace elements plotted against MgO for the PAR 11 (grey field), MR 92 (blue field) and Unki xenolith samples (dotted field). See symbols in Fig 7.2.

## 7.4 Rare Earth Element Variations

The average PAR 11 samples and Unki xenoliths are normalised to Primitive Mantle after Sun and McDonough (1995) are displayed in Fig. 7.5. The PAR 11 samples which consist of peridotites and pyroxenites (represent by open circles and squares) are LREE enriched and HREE depleted with a negative Eu anomaly.

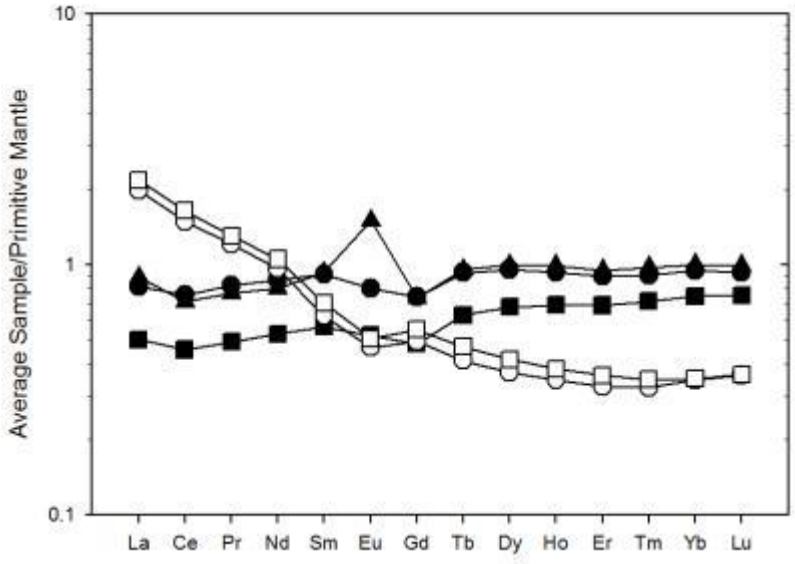


**Fig. 7.5.** Average REEs normalized to Primitive Mantle after Sun and McDonough (1995) of the PAR 11 samples and the Unki xenolith suite. Black symbols (■, ●, ▲) represent Unki xenolith samples and open symbols (□, ○) represent PAR 11 samples.

The Unki xenolith samples consist of peridotites, pyroxenites and gabbros (represented by black circles, squares and triangles). The peridotites are the most depleted with LREE and HREE depletion (less than 1). However there is slightly higher HREE contents than LREE and they display a negative Eu anomaly. The pyroxenites have a slightly higher content of REE as compared to the peridotites although they are also < 1. The pyroxenites display a depleted LREE with slight enrichment in HREEs and a negative anomaly. The Unki xenolith consist of gabbros

which are absent in the PAR 11 borehole. The gabbros are also LREE depleted with flat HREEs and a positive Eu anomaly.

## 7.5 Multi-Elements Variations

The average PAR 11 samples and Unki xenoliths normalised to Primitive Mantle after Sun and McDonough, (1989) are displayed in Fig. 7.6. The trace element of the PAR 11, peridotites and pyroxenites are similar in shape. The spider diagram displays a LREE and incompatible element enrichment with positive anomalies in Cs, K, Pb, U and negative Nb anomaly. There is strong HREE fractionation with a slight negative Eu anomaly and also a strong Y anomaly.

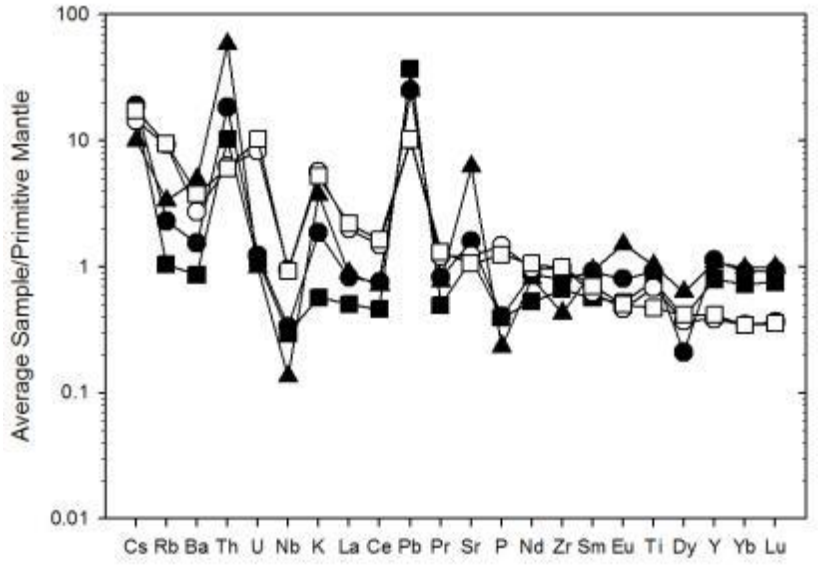


**Fig. 7.6.** Average trace elements normalised to Primitive Mantle after Sun and McDonough, (1989) of the PAR 11 samples and the Unki xenolith suite. Black symbols (■, ●, ▲) represent Unki xenolith samples and open symbols (□, ○) represent PAR 11 samples.

On contrast but similar the Unki xenolith suite displays relative enrichment of LILs and LREE, characterized by positive anomalies for Th, K, Pb, Sr and negative

anomalies for Nb, Pr and Dy. Overall for many elements the xenolith suite has relatively flat patterns with normalized values close to 1. Eu is positive in the gabbros and flat for peridotites and pyroxenite. The Unki xenoliths are generally depleted in trace element compared to the PAR 11 which has slightly higher values.

## 7.6 Summary and Discussion

The PAR 11 borehole represents ultramafic rocks that crystallized from a primitive magma similar that which crystallized the ultramafic sequence of the Great Dyke. Major and trace element compositions are different from those from the upper pyroxenites and represent a more primitive sequence compared with that of the P1 pyroxenite of the layered sequence. The pyroxenite and olivine-pyroxenite layers are more primitive with a lower MgO and Mg# as compared to the P1 pyroxenite layer represented by the MR 92 borehole. It also has layers of thick dunite and harzburgites which are unlike that of the P1 sequence. This clearly shows it is from the dunite succession within the ultramafic sequence. There are no gabbro layers in the PAR 11 borehole. The comparison illustrates that the PAR 11 ultramafic samples plot separately from MR 92 samples although they are all layered are a result of fractional crystallization and have a cumulate origin that may have been derived from the same source of magma parental to the Great Dyke. The Unki xenoliths are a wide range of rock types including peridotites, pyroxenites and gabbros. These rocks are more evolved (lower MgO and Mg#) as compared to the average rocks of the in the layered sequence of the Selukwe Subchamber and therefore may not have been derived from the same magma. Their location in the mafic sequence contributes to the reason why they are regarded as xenoliths. The REE pattern of PAR 11 samples with LREE enrichment and HREE depletion proves that they are from a source of similar composition as the Great Dyke. Therefore the PAR 11 borehole could be from the conduit of feeder dyke from lower levels of the Great Dyke from P2 pyroxenite down to P12 pyroxenite. In contrast the Unki xenoliths display a unique trace element

composition of depleted incompatible trace elements and relatively flat REE pattern. REEs upturned LREEs and flat HREEs that suggest that these are different to the Great Dyke ultramafic sequence and indicate a protolith with mantle-type signatures. It is suggested that these may have been derived from an unknown magma chamber underlying the Great Dyke layered sequence and possibly related to the older (SGB) even though there is no evidence of such rocks in the SGB.

# CHAPTER 8: MINERAL CHEMISTRY OF THE UNKI XENOLITH SUITE

## 8.1 Introduction

A total of 6 samples from the ultramafic – mafic xenolith suite were selected for this study on which for electron microprobe analyses (EMPA) was carried out on major mineral phases. Details of the electron microprobe analyses are in Appendix F. Two samples from each group peridotite (BC10/90/5, BC10/90/6), pyroxenite (USM 8, USM 65) and gabbro (USM 60, USM 66) are discussed in this chapter. While only 6 samples are not completely representative of the suite it reveals some important comparisons which could be further studied.

## 8.2 Orthopyroxene Compositions

Results of selected orthopyroxene analyses are shown in Appendix F, Table F1.1. Orthopyroxenes are mainly of enstatite (Mg-rich) composition and occur as tabular cumulus minerals. The Mg# of the orthopyroxene as [cation Mg/(Mg + $Fe^{2+}$)] values range from 74-86 (Fig. 8.1). The olivine rich rocks contain orthopyroxene with the highest values (~Mg# 86) and the lowest values in the gabbro with little or no orthopyroxene (~Mg# 74) indicating that the suite of rocks are derived from a coherent and integrated geological process. The range of all definitive orthopyroxene compositions is $En_{66-85}$ $Wo_{1-10}$ $Fs_{14-26}$. These values are much lower compared to orthopyroxene compositions in the layered series of the Great Dyke (Wilson, 1982) of $En_{85-91}$. The highest $En_{85}$ value is in harzburgites (BC/10/90/6) and the lowest of $En_{66}$ in gabbro (USM 66). Variations of Mg# for orthopyroxenes are (Fig. 8.2). The $Al_2O_3$ content in orthopyroxene shows a negative correlation with Mg# within the range of 1.33-4.44% $Al_2O_3$ with the highest in pyroxenite. The $Cr_2O_3$% content shows a negative correlation with Mg#, ranges from 0.14-0.77% with the highest range of values in pyroxenite (Mg#=0.77%) and the lowest values in gabbro (Mg#=0.14%).

This is surprising because for most layered intrusions pyroxene of highest Mg# also has the highest Cr content but may have been caused by increasing partition coefficient values at lower temperatures (A.H. Wilson, pers. comm.). The $TiO_2$ also shows a weak negative correlation with Mg# and ranges in values from 0.14-0.5. The CaO content shows an overall negative correlation with the gabbros ranging from 0.52-4.74%. The Mg# displays a strong positive correlation with Fo content of coexisting olivines (Fig. 8.2e). The Fo content in the olivines is $Fo_{70-85}$ but lower than values from the Great Dyke ($Fo_{84-90}$) after (Wilson, 1982). $Al_2O_3$ contents in orthopyroxene displays a positive correlation $TiO_2$ (Fig. 8.2f).

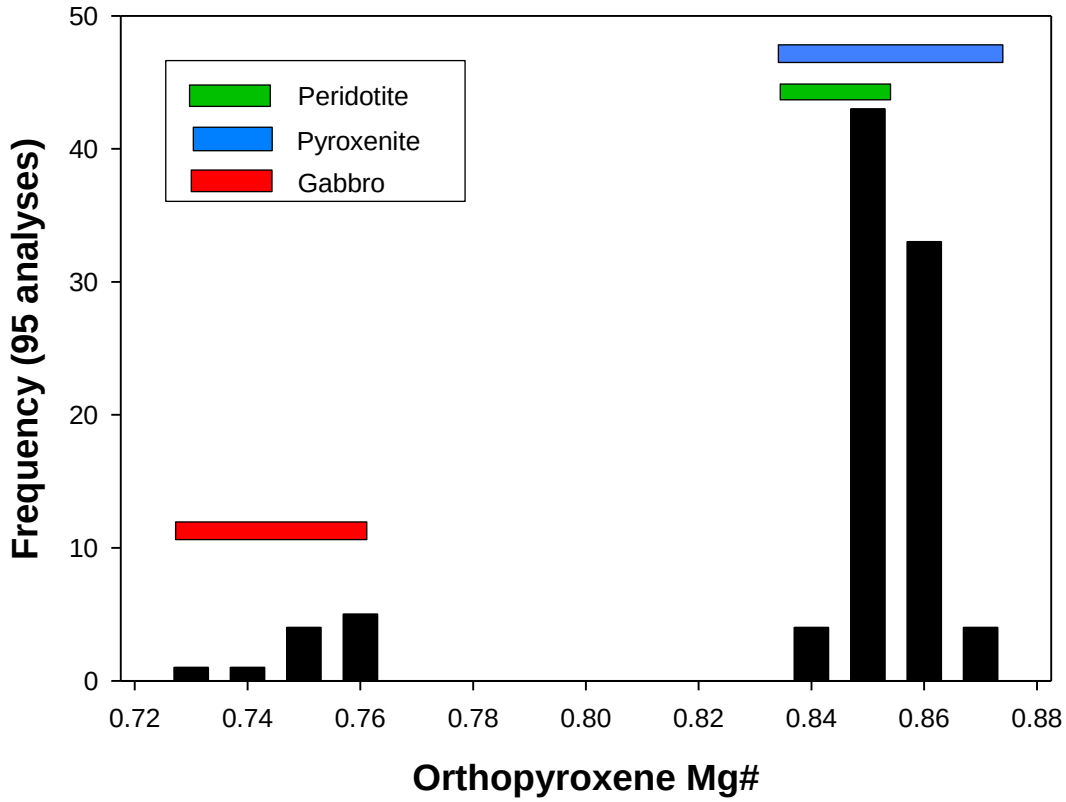


**Fig. 8.1.** The frequency distribution of orthopyroxene compositions based on 95 microprobe analyses. The range of the compositions is shown by the horizontal bars above the vertical bars. The peridotite has a range of Mg# 0.84-0.85; pyroxenites 0.84-0.86 and the gabbro have a lower Mg# 0.73-0.76.

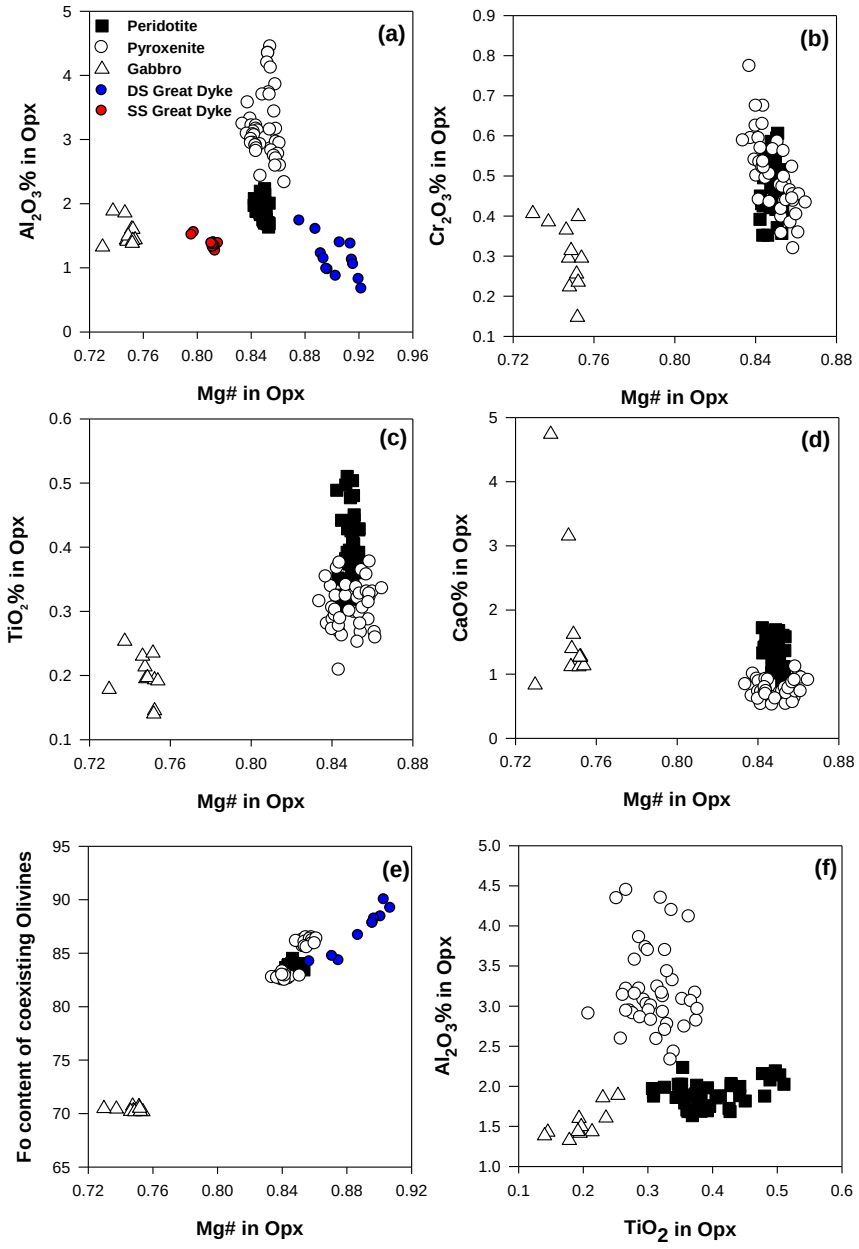


**Fig. 8.2.** Variation of Mg# in orthopyroxene with (a) $Al_2O_3$% (b) $Cr_2O_3$% (c) $TiO_2$% (d) CaO (e) Fo content of coexisting olivine and (f) $Al_2O_3$ vs $TiO_2$ in orthopyroxene. These are compared with orthopyroxene compositions from the Selukwe Subchamber (SS) red circles (Coghill, 1994) and Darwendale Subchamber, Great Dyke (DS) (Wilson, 1982) blue circles.

## 8.3 Olivine Compositions

Olivine is the most predominant mineral in the xenolith suite. The olivine is generally fresh, with some samples partially or completely serpentinized. Analyses of olivine from selected samples from the xenolith suite are given in Table F1.2. The range in Fosterite (Fo calculated as cation $Mg/(Mg+Fe^{2+})$ values in peridotite is Fo 0.83-0.85, in pyroxenite the range in values is Fo 0.82-0.86 and in the gabbro samples the range in values is Fo 0.70-0.71. The Fo values are much lower than the value observed in the Great Dyke (Wilson, 1982) of 0.88-0.92. The range in MgO in the olivine composition in the xenolith suite is high 31 to 46wt%. Ni contents in olivine display a wide range in values is 1390-4980 ppm. The peridotites and pyroxenite values overlap and the range in values is 3420-4980 ppm. The gabbro olivine contents are much lower in the range of 1390-2120 ppm. MnO and TiO contents range in values from 0.14-0.7% and 0-0.59% respectively.

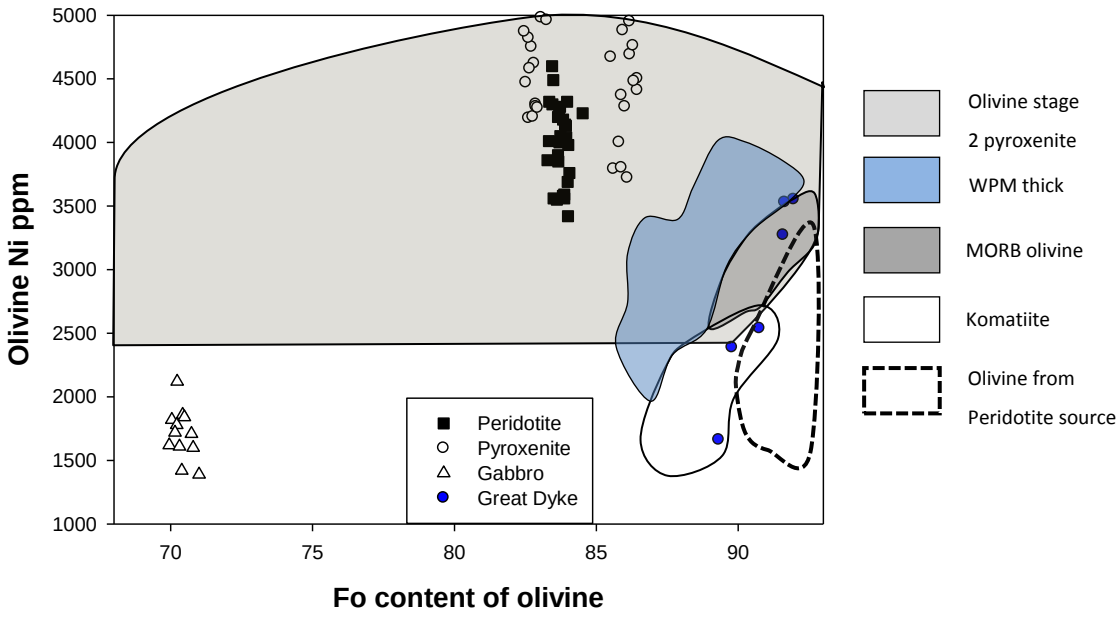


**Fig. 8.3.** Variation of Ni vs Fo content of olivine in the xenolith suite. The xenoliths are highly enriched in Ni and lie in the field of pyroxenite mantle source derived from subducted oceanic crust (Herzberg, 2011; Wilson, 2012).

## 8.4 Clinopyroxene Compositions

In the ultramafic cumulates clinopyroxene is found as an interstitial phase whereas in the mafics cumulate it occurs as a cumulus mineral, or as oikocryts. A dark green clinopyroxene with abundant exsolution lamellae is found in Unki xenolith suite and occurs mainly as oikocryts. Results of selected clinopyroxene analyses are shown in Table F1.3. The clinopyroxene occurs as diopside, augite and inverted pigeonite (Fig. 8.4) with a wide variation $En_{32-47}$ $Wo_{5-46}$ $Fs_{19-47.}$ As for orthopyroxene, it exhibits a wide range of compositions although not clearly zoned.

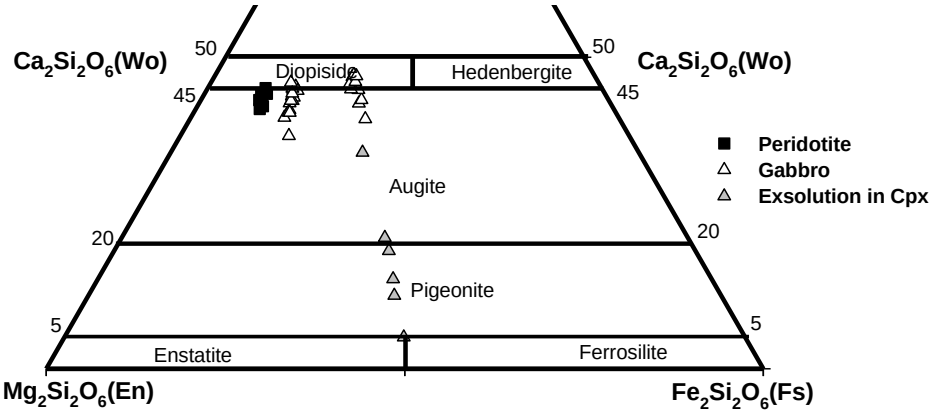


**Fig. 8.4.** The xenolith suite clinopyroxene occurs as diopside, augite and inverted pigeonite. The grey triangles are exsolution lamellae in the clinopyroxene.

The Mg# of clinopyroxene is relatively low at 49 - 85, typical of mafic cumulates. The harzburgite (BC/10/90/5) has the higher Mg# of 85-86 whereas the range in gabbros (USM 60, USM 66) is lower at 49 - 79. $Al_2O_3$ contents range from 1.89 to 16.93 with displays a negative correlation with Mg#. The high $Al_2O_3$ content of 6-16.93% in some of the clinopyroxene are exsolved phases. The $Al_2O_3$ values of the xenolith suite have been compared with much lower values of the Darwendale Subchamber, Great Dyke (Wilson, 1982) and the Selukwe Subchamber (Coghill, 1994) (Fig. 8.5). The $Cr_2O_3$ content range in values is 0-0.9% and correlate positively with Mg#. $TiO_2$ contents are 0.09 -0.9 wt% and correlate negatively with Mg#.

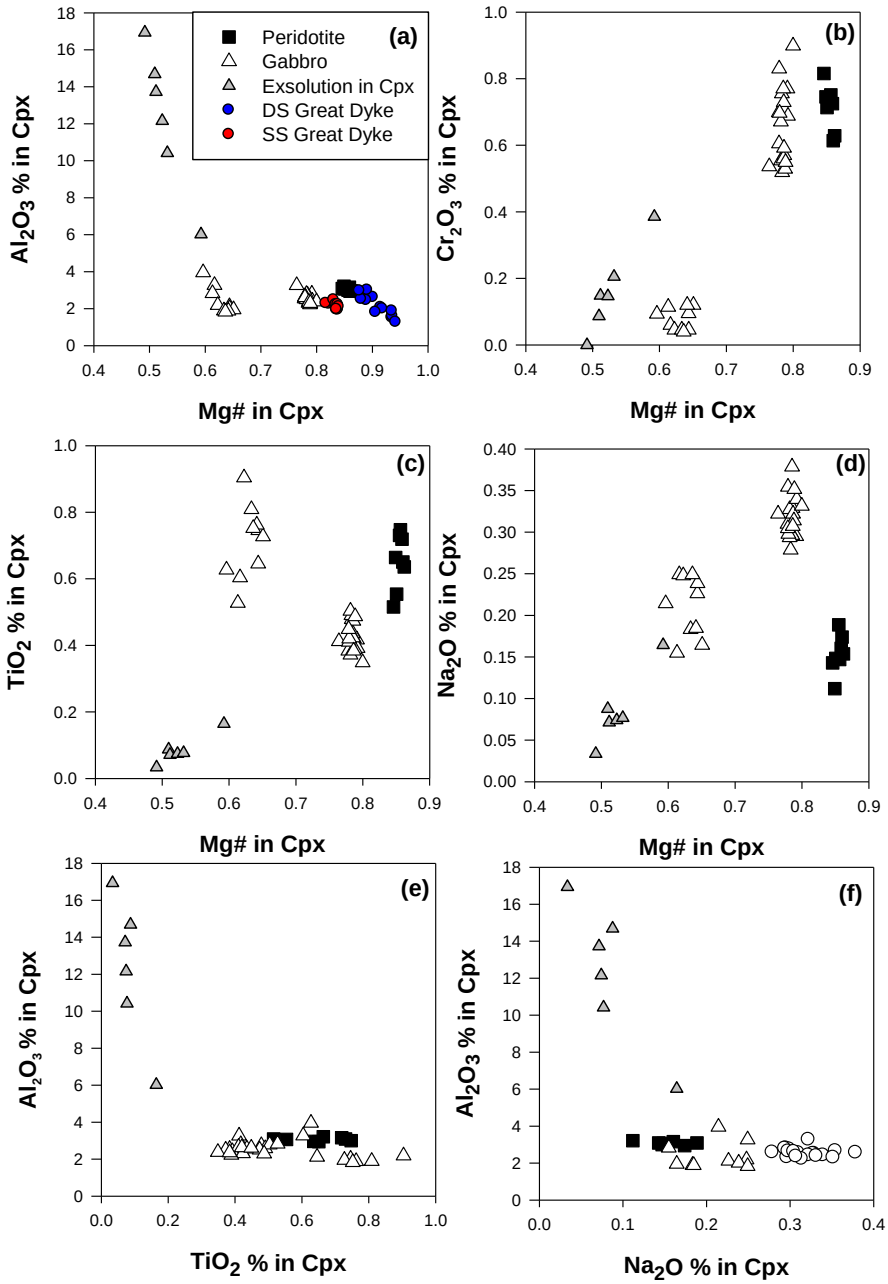


**Fig. 8.5.** Variation of Mg # in clinopyroxene with (a) $Al_2O_3$% (b) $Cr_2O_3$% (c) $TiO_2$% (d) $Na_2O$% (e) $Al_2O_3$% vs $TiO_2$% and (f) $Al_2O_3$% vs $Na_2O$% in clinopyroxene compared with clinopyroxene compositions from the Selukwe Subchamber (SS) (Coghill, 1994) red circles and Darwendale Subchamber, Great Dyke (DS) (Wilson, 1982) blue circles.

The clinopyroxene has $Na_2O$ contents that vary from 0.07- 0.24% with a strong positive correlation with Mg# with the gabbros. The CaO contents range in values from 2.06 – 21.98%. $Al_2O_3$ displays a negative correlation with $TiO_2$ and $Na_2O$. The Mg# of clinopyroxene show a positive correlation the (En) value of coexisting orthopyroxene and Fo content of olivine (Fig 8.6). Values from the Great Dyke (Wilson, 1982) show much higher values of Mg# of clinopyroxene, En content and Fo content.

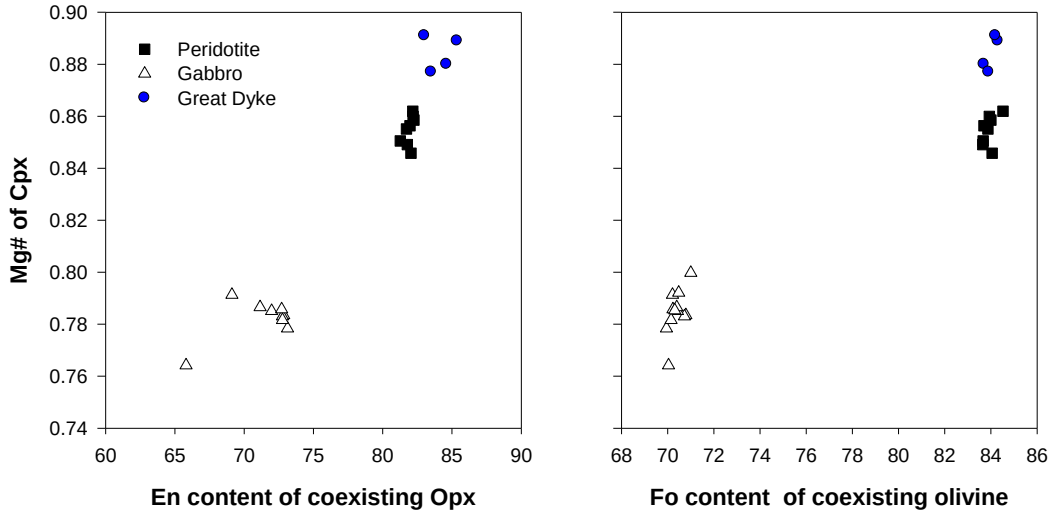


**Fig. 8.6.** Variation of Mg # for orthopyroxene (En) and olivine (Fo) with that of coexisting clinopyroxene plotted with values in the Great Dyke (Wilson, 1982).

## 8.5 Feldspar Compositions

In the ultramafic cumulates plagioclase is found as an interstitial phase, or derived from the trapped liquid and only appears as a cumulus phase in the gabbronorites. Analyses of plagioclase from the xenolith suite are given in Table F1.4. The plagioclase is clearly zoned, with oscillatory zoning developed in the mafic rocks. The Ca# of plagioclase as [molecular CaO/(CaO+Na2O)] in the ultramafic xenoliths ranges from 46-98. The highest Ca# plagioclase compositions are in the range 0.86-0.98 and come from pyroxenite samples (USM 8, USM 65). The Ca# of range 0.82-0.94 is observed for peridotite samples (BC/10/90/5, BC10/90/6). The gabbro is more

evolved with the lower Ca# 0.4-0.85 (USM 60, USM 66). In the feldspathic group, the clinopyroxene crystallized together with plagioclase throughout, because of the presence of clinopyroxene oikocrysts, while in the peridotites and pyroxenite, the plagioclase crystallized from the more primitive magma.

## 8.6 Spinel Compositions

Spinel occurs as small euhedral crystals enclosed or interstitial to the olivine, orthopyroxene and clinopyroxene crystals. Analyses of spinel from the xenolith suite are given in Table F1.5. The spinel probe compositions were recalculated to give $Fe^{2+}$ and $Fe^{3+}$ on the basis of charge balance. The spinels have a variable Cr# as 100 x Cr/(Cr + Al) that ranges from 0.27-0.73. The Cr# range in for spinels in peridotite is 0.58-0.62, while in pyroxenite it is 0.27-0.61 and in gabbro 0.62-0.73. The Cr# displays a negative correlation when plotted against $Mg/(Mg+Fe^{2+})$ (Fig. 8.7a). The xenoliths have much lower values as compared with the Great Dyke (Wilson, 1982) and there is no overlap. The distribution of the trivalent cations for chromitites from the xenolith suite compared with the Great Dyke (Wilson, 1982) is shown in Fig 8.7b. There is no overlap between the Great Dyke and the xenolith suite. The xenoliths also do not show any of the trends (Fe-Ti trend or Cr-Al trend) as that described by (Barnes and Roeder, 2001). The gabbros have the highest $Fe^{3+}$ content. $TiO_2$ contents range in values is 0.73 – 4.95% with the highest value in gabbro.

## 8.7 Summary and Discussion

All the xenoliths contain combinations of the three minerals, olivine, orthopyroxene, plagioclase and clinopyroxene as primary minerals indicating that they formed from a mafic magma. Orthopyroxene is mainly enstatite with Mg# between 74-86. The En values range in values $En_{66-85}$ compared to the Great Dyke $En_{91-85}$. Olivine has a wide Fo content range from 70-86 wt% and is highly enriched in NiO compared to the

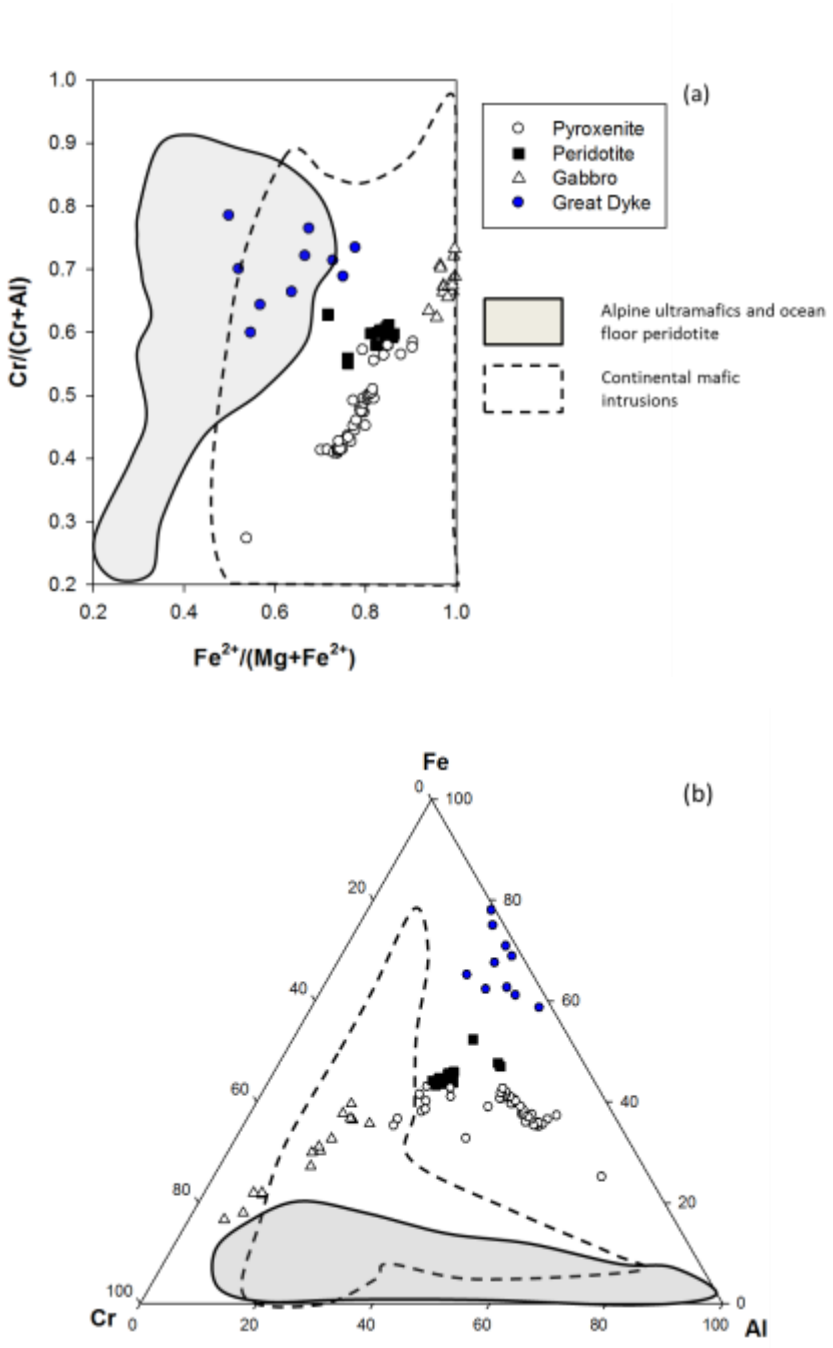


**Fig. 8.7.** Chromite variations for the xenolith suite in terms of the ratios (a) Cr/(Cr+Al) vs $Fe^{2+}$/(Mg+$Fe^{2+}$) (b) Plot of the trivalent cations $Al^{3+}$-$Cr^{3+}$-$Fe^{3+}$ compared with Great Dyke (Wilson, 1982) chromitites, alpine ultramafics, ocean floor peridotite and continental mafic intrusions (Barnes and Roeder, 2001).

the Fo content may be an important indicator of the source of the xenoliths (Sobolev *et al.*, 2007; Herzberg, 2011; Wilson, 2012). The xenolithic olivines are highly olivines of the layered sequence of the Great Dyke. These are typical of pyroxenite mantle source (Sobolev *et al.*, 2005; Herzberg, 2011). The relationship of the Ni and enriched in Ni and lie within the field defined by a pyroxenite mantle source (Fig.8.3) derived from a subducted oceanic crust as shown in stage 2 melts (Herzberg, 2011; Wilson, 2012). The olivine compositions have a much higher Ni compared with MORB, Archean komatiites, Great Dyke (A H Wilson unpublished data) and olivine derived from a peridotite source (Wilson, 2012; Sobolev *et al.*, 2007). Clinopyroxenes are mainly augite, diopside and inverted pigeonite. It occurs as large oikocrysts with abundant exsolution lamellae. The Mg# of clinopyroxene is low 49-85. The clinopyroxene also have high values of $Al_2O_3$ that range from 1.89 to 16.93 which are much higher than those of the Great Dyke. Plagioclase compositions have higher Ca# range in values 0.73–0.98 compared with the Great Dyke of Ca# 0.64-0.88 (Wilson, 1982) The more calcic plagioclase Ca# 0.98 occurs as postcumulus phases in pyroxenites while the evolved Ca# 0.73 occurs as cumulates in gabbro and olivine bearing gabbro. This is because it occurs in the primitive dunites to the most evolved gabbro and olivine bearing gabbro. The spinels have Cr# ranges in value is 0.27-0.67. The xenolith suite plot does not overlap with the Great Dyke (Wilson, 1982) compositions in the $Mg/(Mg+Fe^{2+})$ vs $Cr/(Cr+Al)$ and trivalent cations $Al^{3+}$-$Cr^{3+}$-$Fe^{3+}$ diagram. A combination of the Cr# of spinel and the Fo content of coexisting olivine has been discussed by Arai (1987, 1994) in an olivine-spinel mantle array (OSMA) diagram. The xenolith suite plots off the olivine spinel mantle array within the or in the low Fo area (Wilson, 1982; Arai, 1994). The mineral compositions values are not parallel with those of the Great Dyke therefore the xenoliths are conjectured not to have formed from the primitive Great Dyke magma source but from magma possibly similar to komatiite magma. The xenoliths do not

have mineral compositions that are similar to the Great Dyke and therefore were not derived from Great Dyke magma. This also precludes them as being derived from the Great Dyke Marginal Facies. They do not show similar Fe-Ti trend or Cr-trend in the trivalent ion plot. Therefore they were inherited from another source which also does not appear to be the SGB because there is no report of such rock types (other than peridotite) in the SGB. They are also not mantle derived.

# CHAPTER 9: ORIGINS OF THE UNKI ENCLAVES

## 9.1 Introduction

The Unki xenolith enclaves in Selukwe Subchamber are possibly of mixed origins and are found mainly on the western margin of the Subchamber, on the gabbro succession intermingled with the P1 pyroxenite. The Unki mafic and ultramafic xenolith suite could have originated from three possible sources; (1) ultramafic xenoliths from within the Great Dyke (including the PAR 11 borehole section) as autoliths derived from early crystallization stages, (2) ultramafic cumulates brought up from the source region of the Great Dyke magma (possibly mantle), and (3) fragments derived from the adjacent Shurugwi Greenstone Belt (SGB).

The ultramafic cumulate sequence represented by the PAR 11 borehole appears to be different from other xenolithic fragments and may have formed elsewhere in the Great Dyke and transported during the emplacement of the main layered series. It may also have been a later intrusion of Great Dyke magma which was emplaced before the layered sequence had cooled completely as these rocks are coarse-grained with no evidence of chilled margins. Greenstone belt fragments and metasedimentary rocks (not the subject of this study) would have been inherited from the Shurugwi Greenstone fragment and were ripped off from the walls during the Great Dyke magmatic event. The various possibilities are discussed below.

## 9.2 Ultramafic Cumulates from within the Great Dyke as seen in the PAR 11 borehole

The PAR 11 borehole is composed of cumulate peridotites and pyroxenites. These are cumulates that are similar in texture and composition to the ultramafic succession of the Great Dyke. The peridotites and pyroxenites are coarse grained (grain-size 2-5mm) with cumulate olivine, orthopyroxene and postcumulus plagioclase and

clinopyroxene. Texturally the PAR 11 cumulates show recrystallization textures and greater development of polygonal grain boundaries which may indicate that the unit pre-dated the layered sequence of the Great Dyke and was subject to prolonged heating (and cooling) with the Great Dyke rocks as described in Chapter 4. The pyroxenites are distinctly different to the peridotites with lower MgO, high Mg# and variable contents of Ca, Al, Ti. The peridotites are characterized by the presence of chromite, have high MgO, high Mg#, and Ni because of the presence of olivine. Generally, the PAR 11 samples are characterized by (1) high Mg # (0.78-0.80), (2) high Cr > 3000 ppm and (3) Ni > 1000 ppm content.

The incompatible trace element contents in these rocks are almost entirely dependent on the amount of trapped liquid. Variations with depth of Zr, Y, Rb, K and Ti show similar trends or gradual decrease upward with higher ranges in pyroxenite than peridotites. The REE pattern of the PAR 11 peridotites and pyroxenites show LREE enrichment and HREE depletion with a negative Eu anomaly. Total REE in peridotites content is 3.52 to 13.581 ppm with a LaN/YbN average of 3.52 to 13.581 ppm. Total REE in pyroxenites content is 4.15 to 17.5 ppm with a LaN/YbN average of 3.50 to 4.71. The enriched patterns of LREEs relative to HREEs are a result of the fractionation of orthopyroxene and clinopyroxene. The very low partition coefficients for the REE in olivine means that this mineral would not have had a significant influence on the patterns.

Isotopic studies using Rb-Sr, Sm-Nd, and Pb-Pb (Mukasa *et al.*, 1998; Oberthür *et al.*, 2002) reveal that the Great Dyke magma was either uncontaminated from an enriched mantle source or was slightly crustally contaminated asthenospheric mantle–derived intrusion. However (Schoenberg *et al.*, 2003) proposed that the Great Dyke was a result of a large mantle upwelling plume akin to a failed rifting system with no SCLM contamination. The PAR 11 borehole REE patterns are similar to those described above, as being slightly contaminated or enriched comparable to those that gave rise to the Great Dyke.

## 9.3 Ultramafic Cumulates of the Xenolith Suite

Ultramafic cumulates, similar to those of the xenolith suite, have not been described in the Shurugwi Greenstone Belt (Stowe, 1974). Some similar rocks have been previously described by (Wilson, 1993) in the Marginal Border Group of the Great Dyke therefore this should be considered as a source of autoliths. The ultramafic xenoliths are divided into three groups; peridotites, pyroxenites and gabbros. The main phases are olivine, orthopyroxene, clinopyroxene, plagioclase and spinel. The ultramafic cumulates are fine grained with polygonal textures. The possibility is that these rocks representing a wall-rock facies of the Great Dyke that were ripped from the walls and heated by the filling magma chamber.

Major and trace element show a wide range of compositional variations in the ultramafic rocks. The major element oxides variations display negative correlation with MgO for $SiO_2$, $TiO_2$, $Na_2O$ and CaO and a weak or no significant correlation with $K_2O$ and $TiO_2$, Mg# and total Fe (FeO plus $Fe_2O_3$) has a weak positive correlation with MgO. The correlations would be consistent with the xenoliths as resulting from fractional crystallization in the magma chamber.

The incompatible elements distributions of Zr, Y, Rb, $K_2O$, and $TiO_2$ generally tend to increase with the more evolved rock-types and could be the result of differentiation of the Great Dyke magma. Current studies of trace elements reveal that the xenoliths are characterized by mineral compositions with unique trace element contents and ultra-depleted in all incompatible elements including REEs. Total REE contents of peridotites content are 0.370 to 40.923 with a LaN/YbN average of 0.855. Total REE of pyroxenites content is 1.633 to 40.923 with a LaN/YbN average of 0.972. Total REE of gabbros content is 7.211 to 29.080 with a LaN/YbN average of 0.886. The REE patterns show that the xenoliths are not similar to the Great Dyke which has slightly elevated LREE patterns with CeN/YbN~12 (Hamilton, 1977). The patterns observed for the ultramafic xenoliths are similar to those of primitive komatiites that are depleted in LREEs and have flat HREEs. These patterns are similar to komatiitic

compositions (Arndt, 1977) and therefore peridotitic komatiite may be a possible link to these fragments. While there is no published information on the dunites that occur in the Shurugwi Greenstone Belt it is generally assumed that they were associated with primitive komatiitic-type magmas.

## 9.4 Summary and Discussion

There are two types of rocks in the PAR 11 borehole, peridotites and pyroxenites. These xenoliths are all interpreted as cumulates and contain these main phases olivine, orthopyroxene, clinopyroxene, plagioclase and spinel. Major and trace element geochemistry of PAR 11 and the MR 92 data of Coghill (1994) reveals that they be similar but less evolved. The PAR 11 pyroxenite samples plot separately but close to the MR 92 P1 pyroxenite. REE patterns are typical of an enriched source or crustally contaminated source with LREE enrichment, HREE depletion and a slight negative anomaly in both rock types. The mineral assemblages and proportions of phases in PAR 11 borehole samples are indicative of essentially the same composition as that which formed the layered sequence of the Great Dyke at depth and been transported to their present locality or emplaced at the later stage within the Great Dyke cumulates. Therefore on the basis of the rocks types and chemical compositions the PAR 11 body and the Great Dyke cumulates appear to be petrologically and chemically similar.

There are three main rock types of ultramafic-mafic xenoliths that have been observed in the mafic succession of the Unki area; peridotites, pyroxenites and gabbros. These xenoliths contain the main phases olivine, orthopyroxene, clinopyroxene, plagioclase and spinel. There is an absence hydrous minerals implying dry conditions during the formation of xenoliths. Major and trace elements show a wide range of compositions that have $CaO/Al_2O_3 \sim 1$ which are dissimilar to both PAR 11 and MR 92 borehole data. REE patterns show depletion of LREE with flat HREEs indicating a different magma to that which gave rise to the Great Dyke. The

peridotites with the highest MgO 30-40% are the most depleted followed by the pyroxenites with MgO 20-30%. The gabbros have the lowest MgO < 20% and the least depleted in incompatible elements with a positive Eu anomaly. Such flat patterns are typical of a primitive mantle source similar to that of komatiite magma. Komatiite compositions have not been documented in the SGB. Stowe (1974) describes dunite and chromite in the SGB and does not describe pyroxenites and gabbros. However, that does not mean that these rock types did not occur in the SGB. And if they did maybe they may have come from an intrusion within the SGB that is at depth and never been seen before.

The metasedimentary rocks are banded iron formation and quartzites and are all clearly derived from the different formations of the SGB. The quartzites are from the Mont d'Or Formation and Wanderer Formation. The BIFs are from the Upper Greenstone and Wanderer Formation. The Shurugwi Greenstones were stripped off from the western flank as compared to the Archean granitoids to the eastern flanks of the Great Dyke which were not affected by the magmatic event.

In summary, the results from this study enable us to discuss five hypotheses for the origin of the xenoliths in Selukwe Subchamber of the Great Dyke;

1. The PAR 11 body, although clearly different to the enclosing gabbros of the Great Dyke, has chemical trends and rock-types similar to those of the Great Dyke and therefore there is strong evidence that it was either a displaced fragment of the layered sequence or was a separate intrusion of Great Dyke magma,

2. The xenolithic fragments are autoliths derived from the marginal crystallization sequence of the Great Dyke. The chemical and mineral compositions within the xenoliths are not similar to those of the Great Dyke and therefore this must be viewed as a low possibility.

3 The mafic and ultramafic xenoliths were derived from the SGB from an unknown source within that belt, possibly part of a layered intrusion. The primitive

compositions are consistent with a komatiite-type source that would be appropriate for the SGB.

4. The ultramafic enclaves are derived from the mantle source region of the Great Dyke magma. This is probably the least likely possibility because the compositions are more evolved (MgO contents and Mg#) than would be expected from such a source. However, the primitive REE patterns and high Al contents of some of the pyroxenes may support such an origin.

5. The metasedimentary and banded iron formation xenoliths are clearly derived from the SGB.

# CHAPTER 10: DISCUSSION AND PETROGENESIS OF THE ULTRAMAFIC AND MAFIC ENCLAVES

## 10.1 Introduction

This dissertation describes the geology, field relationships, petrography, geochemistry and the origins of the enclaves in the Selukwe Subchamber. The PAR 11 borehole appears to be different to the rest of the xenolith suite and will be considered separately. The Unki enclaves display diverse patterns of compositional variation in both major and trace elements. The xenoliths may have formed from one or a combination, of several petrogenetic processes. The constraints that are required by applying petrogenetic models to the compositional variations are reviewed in this chapter. The phase relations and experimental and theoretical melting studies of simplified and natural peridotites are evaluated in terms of the modal and chemical variations observed in the xenolith samples. The results are compared to yield a model for the evolution of the xenolith suite and the PAR 11 borehole.

It is necessary to discuss the relationship of the xenoliths and the host rocks, in the context of the ultramafic and mafic rocks of the Great Dyke. The petrogenesis of the Selukwe Subchamber has been described by (Coghill *et al.*, 1993, Coghill, 1994, Wilson, 1996, Wilson *et al.*, 2000a; 2000b, Wilson, 2001) and will be summarized below. Current studies reveal more light on the petrogenesis of the xenoliths. The following will be considered: the xenoliths are (1) samples are cognate or autoliths that bear a direct genetic relationship with the Great Dyke layered sequence and (2) samples are represent true xenoliths as foreign rocks accidentally incorporated in the rising host magma with no relationship with the host rocks.

Two petrogenetic models have therefore been proposed for the genesis of the ultramafic enclaves of the Selukwe Subchamber.

1. A petrogenesis model for the PAR 11 body that intruded the pre-existing rocks of the Great Dyke and is therefore part of the Great Dyke, but not part of the regular layered sequence.
2. A petrogenesis model for the xenolith suite that came from outside the Great Dyke and therefore true xenoliths.

## 10.2 Petrogenesis Model for the Selukwe Subchamber in the Great Dyke.

The petrogenesis of the Great Dyke has been described by (Worst, 1960; Wilson, 1982; 1996; Coghill and Wilson, 1993; Prendergast and Wilson, 1989). Similar petrogenesis processes have been observed in the Munni Munni Complex, Stillwater Complex, Bushveld Complex and other layered intrusions (Cawthorn *et al.*, 1981; Barnes, 1993). The Bushveld and Stillwater Complexes, however, have a more extensive and thicker mafic unit compared to the Great Dyke (Wilson, 1996). The order of crystallization of in the Great Dyke magma chamber is chromite – olivine - orthopyroxene – clinopyroxene – plagioclase – pigeonite – magnetite and this order has been observed in the cumulus phases in all the five magma chambers (Fig 10.1).

It has been accepted that the most likely composition of the Great Dyke is similar to the East Dyke chill phase which contains 15.6% MgO, olivine $Fo_{91.6}$ and orthopyroxene $En_{91.2}$ micro-phenocryst composition. Such values are equivalent to the most magnesian mineral compositions in the Darwendale Subchamber (Wilson, 1982; Wilson and Prendergast, 1989; Wilson, 1996). The evolutionary path of the Great Dyke magma has been projected in phase diagrams (Fig 10.2) in a basaltic tetrahedron after (Irvine, 1970; 1979). Similar to other layered intrusions as the magma composition approached its phase boundary for each cumulus phase (olivine, orthopyroxene, clinopyroxene and plagioclase), the mineral first appears as a postcumulus phase, then subsequently as an oikocrysts and lastly as a discrete cumulus phase (Wilson, 1996). This is has been observed in all five subchambers of

the Great Dyke in orthopyroxene in each cyclic unit of the ultramafic sequence in the poikilitic harzburgite, clinopyroxene as nodules in the websterite and plagioclase in the nodular pyroxenite just before the appearance of the mafic rocks (Wilson, 1996).

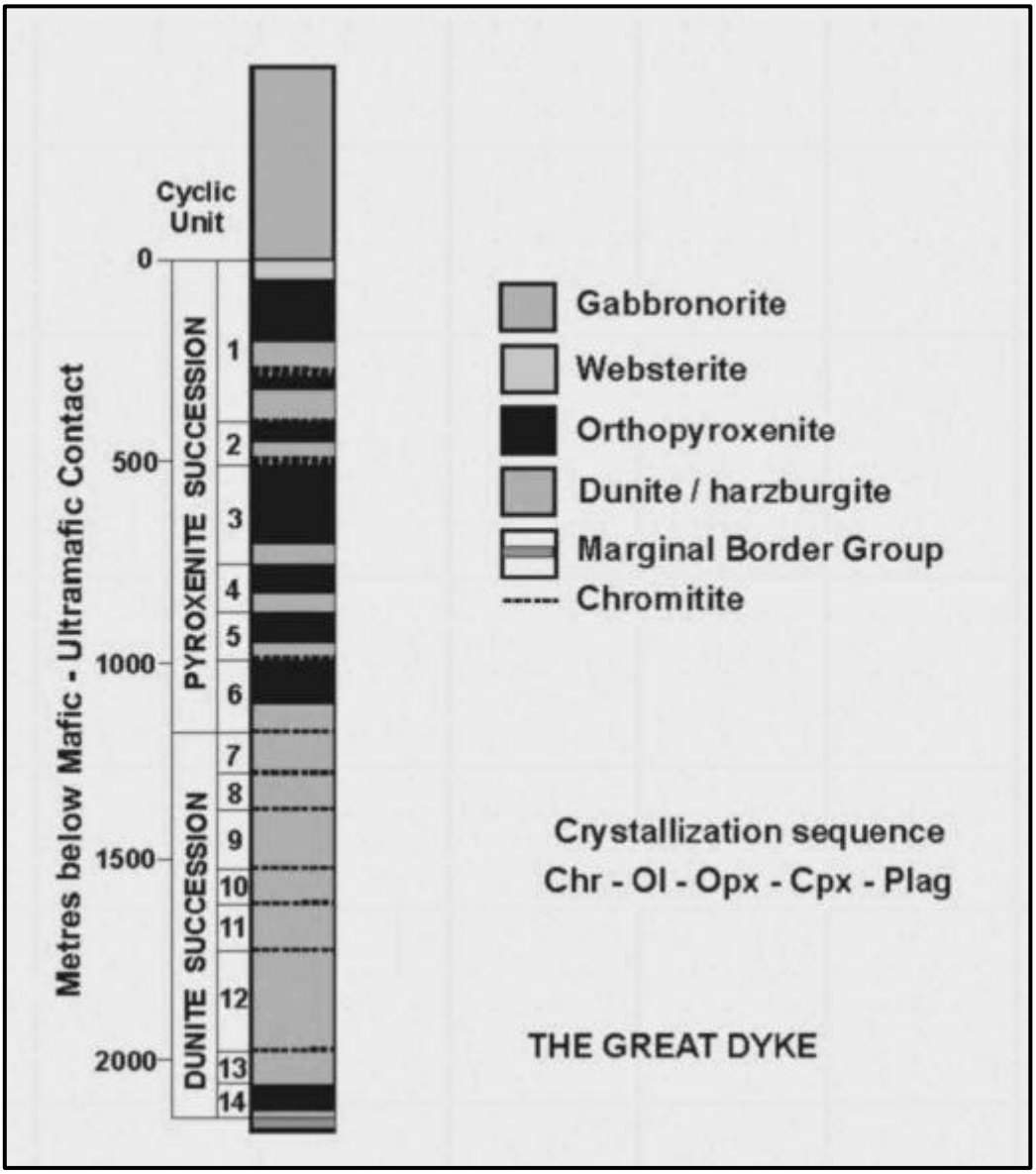


**Fig 10.1.** Crystallization sequence of the Great Dyke (Coghill *et al.,* 1993) as observed in the cyclic units of the Darwendale Subchamber. The order of crystallization in all five subchambers is chromite, olivine, orthopyroxene, clinopyroxene and plagioclase.

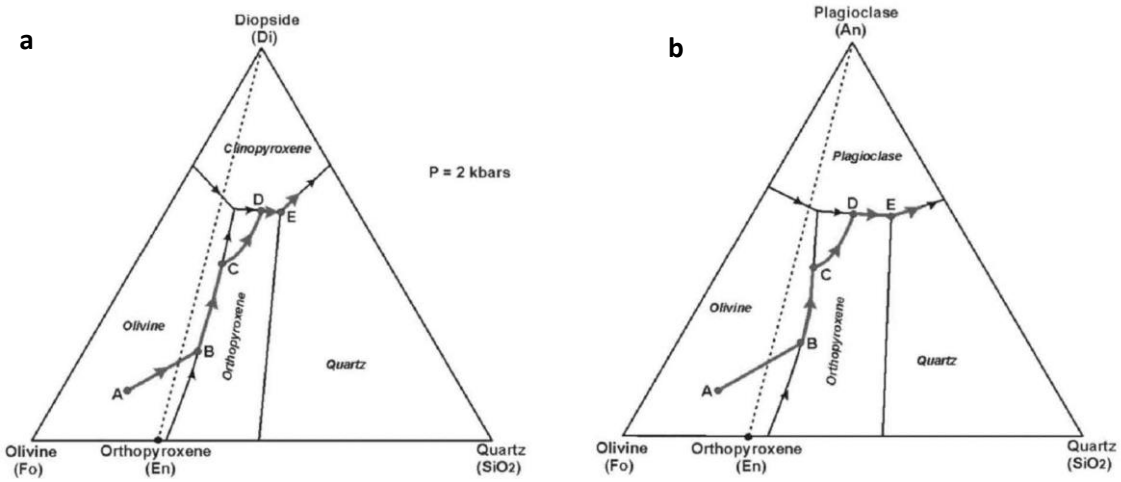


**Fig 10.2.** The modelled evolutionary path of the chill phase of the East Dyke offshoot (Wilson, 1982; 1996; Wilson and Prendergast, 1989). (a-b) are projections respectively from plagioclase and clinopyroxene in the basaltic tetrahedron (Irvine, 1970; 1979) and provide the phase diagram controls on the liquid paths.

The emplacement mechanisms of the Great Dyke have been proposed by (Worst, 1958; 1960; Hess, 1960; Wilson, 1996; Wilson and Prendergast, 1989). The Great Dyke magma was fed into an expanding chamber through a feeder dyke below the layered sequence. The magma expansion of the magma chamber was mainly due to subsidence of the floor and elevation of the roof. The hot magma may have carried with it large xenoliths from the side walls of which some where completely digested or preserved. These xenoliths have been observed in both the North and the South chambers and caused contamination of the magma.

The emplacement probably took place from the north to south, with the north having the largest compartments more developed in the north. During the early stages of the emplacement the north and the south were separated by the floor regularities and not linked. With time the North and South were subsequently linked, the Darwendale and Sebakwe and the Selukwe and the Wedza with also the barrier between the North and South Subchamber opened at the level that parallels with the Cyclic Unit 2.

Comparable to other layered intrusions it has been proposed that the Great Dyke developed from a stratified magma chamber (Huppert and Sparks, 1980; Coghill, 1994). The crystallization in the magma took place from a single layer double diffusive convection cells near the base of the subchamber (Irvine, 1980; McBirney and Noyes, 1979) with heat and matter transmitted through the magma column in steps by diffusion and small-scale convection. Fractional crystallization then gave rise to the individual units. Repeated injection of primitive magma of the same or similar composition as the initial liquid gave rise to the micro-cyclic layering observed in ultramafic sequence of the Great Dyke. Primitive high-magnesian magma was repeatedly injected in the early history of the intrusion into the subchamber giving rise to the ultramafic sequence (Wilson, 1996). This was followed by crystallization of an evolved phase of the magma melt which gave rise to the Mafic Sequence (Coghill and Wilson, 1993; Wilson, 1996). In the layered complexes the ultramafic sequence is made up of the Dunite Succession (basal chromitites, dunites and pyroxenites) and overlain by more evolved rocks of the Pyroxenite Succession (harzburgites, olivine-pyroxenites, pyroxenites) (Prendergast and Wilson, 1989). The lower most layers of the Ultramafic Sequence are not exposed in the field as they die out against the inclined walls of the subchambers and are only intersected by boreholes (Prendergast and Wilson, 1989; Coghill and Wilson, 1993).

Geochemical analyses displays an overall upward Mg # depletion trend in the pyroxenites from 0.89 (lower pyroxenites) to 0.79 (websterite in the P1 pyroxenite). The compositional reversals correspond with the bases of the cyclic units and are evidence for repeated injections of primitive magma into magma chamber. The mixing of the resident magma with the primitive magma caused the small increase in Mg# of the magnesian minerals, which would subsequently have started decreasing again with uninterrupted fractionation. As a result, each major influx would have given to a new cyclic (Coghill, 1994).

In all five subchambers cyclic unit 1 (CU 1) of the pyroxenite succession is similar and principle stratigraphic units can be correlated (ie chromite seams C1c and C1d, P1 pyroxenite, MSZ, LSZ and websterite layer). This indicates that the C1 represents the point and time when all the subchambers coalesced and after magma emplacement and crystallization took place in one single large chamber (Wager and Brown, 1968; Coghill, 1994; Wilson & Prendergast 1989). The last major batch of primitive magma was therefore emplaced at the base of the C1, approximately at the level of the chromite level C1c (Wilson *et al.*, 1989; Wilson and Tredoux, 1990; Coghill, 1994). The resident magma at this point would have been light and cool as a result of the crystallization of the olivine and orthopyroxene. Injection of a new and final hotter denser magma entered the magma chamber as a fountain, with some mixing occurring before it dropped back to the floor of the magma as a dense hybrid layer (Campbell and Turner, 1986b; Coghill and Wilson, 1993). There was change of the temperature and composition in the hybrid layer hence destroying the double diffusive convection cells. As the crystallization of the individual layering units then proceeded from the basal layer upward with chromite crystallization first in the hybrid layer due to chromite saturated in the mixing process (Irvine, 1979). The cooling of the last primitive magma due to Rayleigh fractionation produced dunite, harzburgite and pyroxenite of the cyclic unit 1 (Wilson, 2001). The P1 pyroxenite is composed of olivine-pyroxenite, pure pyroxenite and finally websterite being the most evolved in the Ultramafic Sequence. Due to compaction the intercumulus fluid moved upward through the cumulus pile to be trapped beneath the plagioclase cumulate of the gabbroic rocks. The volatile fluids therefore manifested themselves in the pegmatoidial pyroxenite just below the contact with the overlying mafic rocks. Fractionation then continued along the pyroxene plagioclase cotectic as represented in Fig. 10.2b, giving rise to the gabbro of the mafic sequence as plagioclase became the most dominant cumulus phase (Wilson and Tredoux, 1990; Coghill, 1994).

The Marginal Border Group (MBG) was a first crystallization stage of the Great Dyke and formed layered gabbros at the margins with the country rock (Wilson and Prendergast, 1989). In some places the MGB is not preserved and it is possible that some large fragments of it may have been preserved in some situations where the magma chamber was narrow and had highest heat flow. Some of the xenolithic fragments observed in the Selukwe Subchamber may have been autoliths derived from this suite.

## 10.3 Petrogenesis Model for the Par 11 Borehole

Petrographic and geochemical studies in this dissertation show that the order of crystallization of the borehole is similar to that described by (Wilson, 1982) for the layered sequence of the Great Dyke, as chromite – olivine - orthopyroxene – clinopyroxene – plagioclase. The rock types include peridotites (dunites, harzburgites) and pyroxenites (olivine-pyroxenites, pyroxenites). Stratigraphic variation of Mg# indicates repeated injection of primitive magma to give a series of units which are similar to the cyclic units of the Ultramafic Sequences in the Selukwe Subchamber (Coghill and Wilson, 1993; Wilson, 1996, Wilson and Prendergast, 1989). The PAR 11 samples show textures of orthocumulates result from slow cooling, similar to that observed in the axial facies as described by (Wilson, 1991) except that it is a sequence surrounded by gabbroic rocks of the Mafic Sequence. The PAR 11 borehole series is mainly composed of repeated cyclic units of peridotites that grade to olivine-pyroxenite then pure pyroxenite. There is no mafic sequence in the PAR 11 borehole sequence but such a sequence could also have been eroded from higher levels.

Major, minor elements and REEs and mineralogy are consistent with the development of sequence by crystal fractionation from a primitive magma the same or similar to that of layered sequence of the Great Dyke. The boundary of the ultramafic fragment that is studied here in the PAR 11 borehole is not exposed but it

is surrounded by gabbro of the Mafic Sequence of the Selukwe Subchamber. It has also been shown that the rock-types, compositions, and rock sequences observed in the section are remarkably similar to parts of the Ultramafic Sequence of the Great Dyke. Therefore several possibilities arise for the origin of the PAR 11 ultramafic body: (1) The body is a xenolith derived from a pre-existing layered sequence or from the Selukwe Greenstone Belt, (2) that it is an autolith derived from the Marginal Border Group, (3) that it is a structurally dismembered part of the Ultramafic Sequence, (4) it is later intrusion of Great Dyke magma that gave rise to a layered sequence within a pipe-like body of restricted size. The compositions, textures and rock-types observed in the PAR 11 section are completely different to those of the xenolith suite and it is unlikely to have had the same paragenesis. Therefore the first possibility is discounted. Comparison of the PAR 11 section to other sections of the Great Dyke in the area (MR 92 borehole) shows distinct parallels although not identical compositions. While the Marginal Border Group may have also had a sequence of layered ultramafic rocks associated with it, there is no evidence elsewhere for such a sequence to be present. The third possibility that it is structurally emplaced section of layered ultramafic rocks from depth, this is also discounted on the basis that the vertical displacement would have been at least 400 m (this being the distance from the base of the Mafic Sequence to the base of the P1 pyroxenite (Coghill, 1994). There is evidence for such a fault structure which also have serious implications for mining of the MSZ platinum horizon in the area. The final possibility of a pipe-like feeder has probably the greatest credence which produced a coarse-grained layered sequence while the surrounding cumulates were still hot.

## 10.4 Petrogenesis of the Xenolith Suite

The xenolith suite has a wide range of rock-types encompassing peridotites, pyroxenites and gabbros which could have been associated as a result of differentiation from a primitive parental magma. Assuming this to be a cognitive

suite, petrographic and geochemical studies show that the order of crystallization of the Unki xenolith suite is chromite – olivine - orthopyroxene – clinopyroxene – plagioclase – pigeonite – magnetite, which is the same as that of the layered sequence of the Great Dyke and for many continental tholeiitic magmas. In detail the rock types include peridotites (dunite, harzburgite, and lherzolite), pyroxenite (olivine-websterite, olivine-pyroxenite, pyroxenite, and olivine-clinopyroxenite) and gabbro (gabbro, olivine gabbro). The gabbroic fragments have large oikocrysts of clinopyroxene and plagioclase. The ultramafic cumulates are clearly distinguished from the Great Dyke ultramafic/mafic sequence by their generally finer grain size.

Several possibilities arise for the origin of the xenoliths. These are: (1) they were derived from the sidewall Marginal Border Group of the Great Dyke, (2) they were derived entirely from the lavas and coarse grained ultramafic rocks of the Shurugwi Greenstone Belt, (3) they were derived from a pre-existing magma chamber to the Great Dyke, or (4) a combination of several of these sources. Support of the first concept is that many of the fragments are fine grained and unlike the coarse grained rocks of the PAR 11 borehole. This is particularly the case for the gabbroic rocks. It has been shown that the chemical trends and signatures of the xenolith suite do not match those of the Great Dyke. The REE patterns indicate a primitive flat pattern whereas that for the Great Dyke rocks is LREE enriched as is typical for late Archaean and Proterozoic continental layered intrusions. While location would support the xenoliths has having been derived from the Shurugwi Greenstone Belt there is no evidence that such a suite of rocks formed part of that greenstone belt particularly as it well mapped and deformed to expose most rock units (Stowe, 1968). Banded iron stone and metasedimentary quartzite xenoliths are clearly derived from identifiable units in the SGB. It is therefore suggested that the most likely possibility is that xenoliths represent an extensive layered intrusion underlying both the Great Dyke and the greenstone belt and possibly even at the base of the crust. The high aluminous pyroxene compositions (unlike any from the Great Dyke) would support a high pressure environment. The last possibility is that a number of the listed possible

sources of the xenolithic fragments may have contributed to the observed suite. This cannot be ruled out but further detailed studies will be required to prove this.

# CHAPTER 11: SUMMARY AND FINAL CONCLUSIONS

## 11.1 Summary of Important Points

1. The PAR 11 section is a succession of ultramafic rocks within a body entirely enclosed within the gabbros of the Mafic Sequence of the Selukwe Subchamber.

2. The PAR 11 body is the only know occurrence of dunite and harzburgites in the Mafic Succession.

3. The PAR 11 body has mineral and chemical trends of rocks similar to those observed in the ultramafic sequence of the Great Dyke.

4. The PAR 11 body was derived from within the Great Dyke magma chamber.

5. The REE pattern of the PAR 11 body shows enrichment in LREEs which is typical of all mafic magma and similar to that of the Great Dyke.

6. The PAR 11 body also may be also from a later intrusion of the Great Dyke which was emplaced before the main layered sequence had cooled completely as these rocks are coarse grains with no evidence of a chilled margin.

7. The Unki xenolith suite is clearly derived from outside Great Dyke magma chamber.

8. The Unki xenoliths have mineral compositions and chemical trends that do not parallel rocks from the Great Dyke and therefore not from the Great Dyke.

9. Pyroxenites and gabbros with these compositions have not been reported in the Shurugwi Greenstone Belt.

10. The REE patterns of xenoliths show depletion indicating a different magma source to that of the PAR 11 body.

11. The Unki xenoliths are depleted in LREEs, flat HREEs similar to primitive komatiite magma and therefore peridotite komatiite may a possible link to these fragments even though slightly LREEs enriched are found in the Mendon Formation of Barberton Greenstone Belt (Lahaye *et al*., 1995).

12 The Unki xenoliths were inherited from another source that does not appear to be the Shurugwi Greenstone Belt not reported in the SGB.

13. The metasedimentary quartzites and banded iron formation are clearly from SGB.

## 11.2 Summary of Conclusions

In summary, the results from this study enable us to conclude that; the PAR 11 body has chemical trends and rock-types similar to those of the Great Dyke and therefore there is strong evidence that it was either a displaced fragment of the layered sequence or was a separate intrusion of Great Dyke magma.

The mafic and ultramafic xenoliths were derived from the SGB or from an unknown source within that belt, or possibly part of a separate and unknown layered intrusion. The primitive compositions are consistent with a komatiite-type source that would be appropriate for the SGB. This is probably the least likely possibility because the compositions are more evolved (MgO contents and Mg#) than would be expected from such a source. However, the primitive REE patterns and high Al contents of some of the pyroxenes may support such an origin. The metasedimentary xenoliths and banded iron formation are all derived from the SGB.

# REFERENCES


Allsopp, H. L. (1965). Rb-Sr and K-Ar age measurements on the Great Dyke of Southern Rhodesia. *Journal of Geophysical Research* **70,** 977-984.

Arndt, N. T. (1977). Ultrabasic magmas and high-degree melting of the mantle. *Contributions to Mineralogy and Petrology* **64,** 205-221.

Barnes, S. J. (1993). Partitioning of the platinum group elements and gold between silicate and sulphide magmas in the Munni Munni Complex, Western Australia. *Geochimica et Cosmochimica Acta* **57,** 1277-1290.

Campbell, I. H. & Turner, J. S. (1986a). The influence of viscosity on fountains in magma chambers. *Journal of Petrology* **27,** 1-30.

Campbell, I. H. & Turner, J. S. (1986b). The role of convection in the formation of platinum and chromitite in layered intrusions. *In:* SCARFE, C. M. (ed.) *Short Course in Silicate Melts.* Ottawa: Mineralogical Society of Canada **12**, 236-278.

Cawthorn, R. G., Davies, G., Clubley-Armstrong, A. & McCarthy, T. S. (1981). Sills associated with the Bushveld Complex, South Africa: an estimate of parental magma composition. *Lithos* **14,** 1-16.

Coghill, B. (1994). *Aspects of the Ultramafic Rocks and PGE Mineralization of the Selukwe Subchamber, Great Dyke.* Unpublished Ph.D. thesis, University of Natal, Durban.

Coghill, B. M. & Wilson, A. H. (1993). Platinum group minerals in the Selukwe Subchamber, Great Dyke, Zimbabwe: implications for PGE collection

mechanisms and post-formational redistribution. *Mineralogical Magazine* **57,** 613-633.

Davies, R. D., Allsopp, H. L., Erlank, A. J. & Manton, W. I. (1970). Sr isotopic studies on various layered mafic intrusions in Southern Africa. *Special Publication of the Geological Society of South Africa* **1,** 576-593.

Hamilton, J. (1977). Strontium isotope and trace element studies on the Great Dyke and Bushveld mafic phase and their relation to early Proterozoic magma genesis in southern Africa. *Journal of Petrology* **18,** 24-52.

Herzberg, C. (2011). Identification of Source Lithology in the Hawaiian and Canary Islands: Implications for Origins. *Journal of Petrology* **0,** 1-34.

Hess, H. H. (1960). Stillwater igneous complex, Montana, a quantitative mineralogical study. U.S.G.S.

Huppert, H. E. & Sparks, R. S. (1980). The fluid dynamics of a basaltic magma chamber replenished by influx of hot, dense, ultrabasic magma. *Contributions to Mineralogy and Petrology* **75,** 279-289.

Huppert, H. E. & Sparks, R. S. (1984). Double-diffusive convection due to crystallization in magmas. *Annual Review of Earth And Planetary Sciences* **12,** 11-37.

Irvine, T. N. (1970). Crystallization sequences in the Muskox Intrusion and other layered intrusions. I. Olivine-pyroxene-plagioclase relations. *Symposium on the Bushveld Igneous Complex and other layered intrusions.* Geological Society of South Africa **Special Publication, No. 1**, 441-476.

Irvine, T. N. (1979). Experimental modeling of convection in layered intrusions and convection and mixing in layered liquids. *Carnegie Institution of Washington Yearbook* **79,** 247-256.

Irvine, T. N. (1980). Magmatic infiltration metasomatism, double-diffusive fractional crystallization and adcumulus growth in the Muskox intrusion and other layered intrusions. *In:* HARGRAVES, R. B. (ed.) *Physics of Magmatic Processes.* Princeton, N.J.: Princeton University Press, 325 - 384.

Lahaye, Y., Arndt, N., Byerly, G., Chauvel, C., Fourcade, S., Gruau, G. (1995). The influence of alteration on the trace elements and Nd isotopic compositions in komatiites. *Chemical Geology* **126,** 43-64.

Le Maitre, R. W. (ed.) 1989. *A Classification of Igneous Rocks and Glossary of Terms,* Oxford: Blackwell Scientific.

McBirney, A. R. & Noyes, R. M. (1979). Crystallization and layering of the Skaergaard intrusion. *Journal of Petrology* **20,** 387-554.

McDonough, W. F. & Sun, S.-s. (1995). The composition of the Earth. *Chemical Geology* **120,** 223-253.

Mennel, F. P., Frost, A (1925). Notes on the Occurance of Platinum in the gret Dyke with special reference to Belingwe and Selukwe. *Proceedings of the Rhodesia Scientific Association* **XXV**.

Mukasa, S. B., Wilson, A. H. & Carlson, R. W. (1998). A multielement geochronological study of the Great Dyke, Zimbabwe: significance of the reset and robust ages. *Earth and Planetary Science Letters* **164,** 353-369.

Oberthür, T., Davis, D. W., Blenkinsop, T. G. & Hohndörf, A. (2002). Precise U-Pb mineral ages, Rb-Sr and Sm-Nd syetmatics for the Great Dyke, Zimbabwe - contraints on late Archean events in the Zimbabwe Craton and Limpopo belt. *Prembrian Research* **113,** 293-305.

Podmore, F. & Wilson, A. H. (1987). A reappraisal of the structure, geology and emplacement of the Great Dyke, Zimbabwe. *In:* HALLS, H. C. & FAHRIG, W. F. (eds.) *Mafic Dyke Swarms.* Geological Association of Canada Special Paper **34**, 433-444.

Prendergast, M. D. & Wilson, A. H. (1989). The Great Dyke of Zimbabwe II: Mineralisation and mineral deposits. *In:* PRENDERGAST, M. D. & JONES, M. J. (eds.) *Magmatic Sulphides - The Zimbabwe Volume.* London: Institution of Mining and Metallurgy, 21-42.

Rollinson, H. (1993). *Using geochemical data: evaluation, presentation, interpretation.*. New York: John Wiley and Sons.

Schoenberg, R., Nagler, T. F., Gnos, E., Kramers, J. D. & Kamber, B. S. (2003). The Source of the Great Dyke, Zimbabwe, and Its Tectonic Significance:Evidence from Re-Os Isotopes. *The Journal of Geology* **111,** 565-578.

Sobolev, A. V., Hofmann, A. W., Kuzmin, D. V., Yaxley, G. M., Arndt, N. T., Chung, S.-L., Danyushevky, L. V., Elliot, T., Frey, F. A., Garcia, M. O., Gurenko, A. A., Kamenetsy, V. S., Kerr, A. C., Krivolutskaya, N. A., Matvienkov, V. V., Nikogosian, I. K., Rocholl, A., Sigurdsson, I. A., Sushchevskaya, N. M. & Teklay, M. (2007). The Amount of Recycled Crust in Sources of Mantle-Derived Melts. *Science* **316,** 412-417.

Sobolev, A. V., Hofmann, A. W., Sobolev, S. V. & Nikogosian, I. K. (2005). An Olivine-free mantle source of the Hawaiian sheild basalts. *Nature* **1344,** 1-8.

Stowe, C. W. (1968). *The geology of the country south and west of Selukwe.* Rhodesia Geological Survey Bulletin.

Stowe, C. W. (1974). Alpine-type structures in the Rhodesian basement complex Selukwe. *Journal of Geological Society* **130,** 411-425.

Sun, S.-s. & McDonough, W. F. (1989). Chemical and isotopic systematics of oceanic basalts: implications for mantle composition and processes. *In:* SAUNDERS, A. D. & NORRY, M. J. (eds.) *Magmatism in the Ocean Basins.* Geological Society, London Special Publications **42**, 313-345.

Wager, L. R. & Brown, G. M. (1968). *Layered Igneous Rocks.* Edinburgh: Oliver and Boyd.

Wilson, A. H. (1982). The Geology of the Great 'Dyke', Zimbabwe: The Ultramafic Rocks. *Journal of Petrology* **23,** 240-292.

Wilson, A. H. (1991). The Geology of the Great Dyke, Zimbabwe: Crystallization, Layering, and the Cumulate Formation in the P1 Pyroxenite of Cyclic Unit 1 of the Darwendale Subchamber. 611-663.

Wilson, A. H. (1992). The Geology of the Great Dyke, Zimbabwe: Crystallisation, Layering, and Cumulate Formation in the P1 Pyroxenite of the Cyclic Unit 1 of the Darwendale Subchamber. *Journal of Petrology* **33,** 611-663.

Wilson, A. H. (1996). The Great Dyke of Zimbabwe. *Developments in Petrology* **15,** 365-402.

Wilson, A. H. (2001). Compositional and Lithological Controls on the PGE- Bearing Sulphide Zones in the Selukwe Subchamber, Great Dyke: a Combined Equilibrium - Rayleight Fractionation Model. *Journal of Petrology* **42,** 1845-1867.

Wilson, A. H. (2012). A Chill Sequence to the Bushveld Complex: Insight into the First Stage of Emplacement and Implications for the Parental Magmas. *Journal of Petrology* **0,** 1-46.

Wilson, A. H., Murahwi, C. Z. & Coghill, B. (2000a). Stratigraphy, geochemistry and platinum group element mineralisation of the central zone of the Selukwe Subchamber of the Great Dyke, Zimbabwe. *Journal of African Earth Sciences***,** 833-853.

Wilson, A. H., Murahwi, C. Z. & Coghill, B. M. (2000b). The geochemistry of the PGE Subzone in the Selukwe Subchamber, Great Dyke: an intraformational layer model for Platinum Group Element enrichment in layered intrusions. *Mineralogy and Petrology* **68,** 115 - 140.

Wilson, A. H., Naldrett, A. J. & Tredoux, M. (1989). Distribution and Controls of Platinum Group Element and Base Metal Mineralization in the Darwendale Subchamber of the Great Dyke, Zimbabwe. *Geology* **17,** 649-652.

Wilson, A. H. & Prendergast, M. (1989). The Great Dyke of Zimbabwe I: Tectonic setting, stratigraphy, petrology, structure, emplacement and crystallization. *In:* PRENDERGAST, M. D. & JONES, M. J. (eds.) *Magmatic Sulphides - the Zimbabwe Volume.* London: Institute of Mining and Metallurgy, 1-20.

Wilson, A. H. & Prendergast, M. D. (2001). Platinum- Group Element Mineralisation in the Great Dyke, Zimbabwe, and its Relationship to Magma Evolution and Magma Chamber structure. *South African Journal of Geology* **104,** 319-342.

Wilson, A. H. & Tredoux, M. (1990). Lateral and vertical variation of the platinum - group elements, and petrogenetic controls on the sulphide mineralisation in the P1 Pyroxenite Layer of the Darwendale Subchamber of the Great Dyke, Zimbabwe. *Economic Geology* **85,** 556-584.

Wingate, M. T. D. (2000). Ion - microprobe U - Pb zircon and baddeleyite ages for the Great Dyke and its satellite dykes, Zimbabwe. *South African Journal of Geology* **103,** 74 - 80.

Worst, B. G. (1958). The differentiation and structure of the Great Dyke of Southern Rhodesia. *Transactions of the Geological Society of South Africa* **61,** 283-354.

Worst, B. G. (1960). The Great Dyke of Southern Rhodesia. *Southern Rhodesia Geological Survey Bulletin* **47,** 130-143.

Zealley, A. E. V. (1919). The Geology ot the Selukwe Mineral Belt. *Southern Rhodesian Geological Survey Bulletin* **3,** 55-59.

# APPENDIX A – MAP

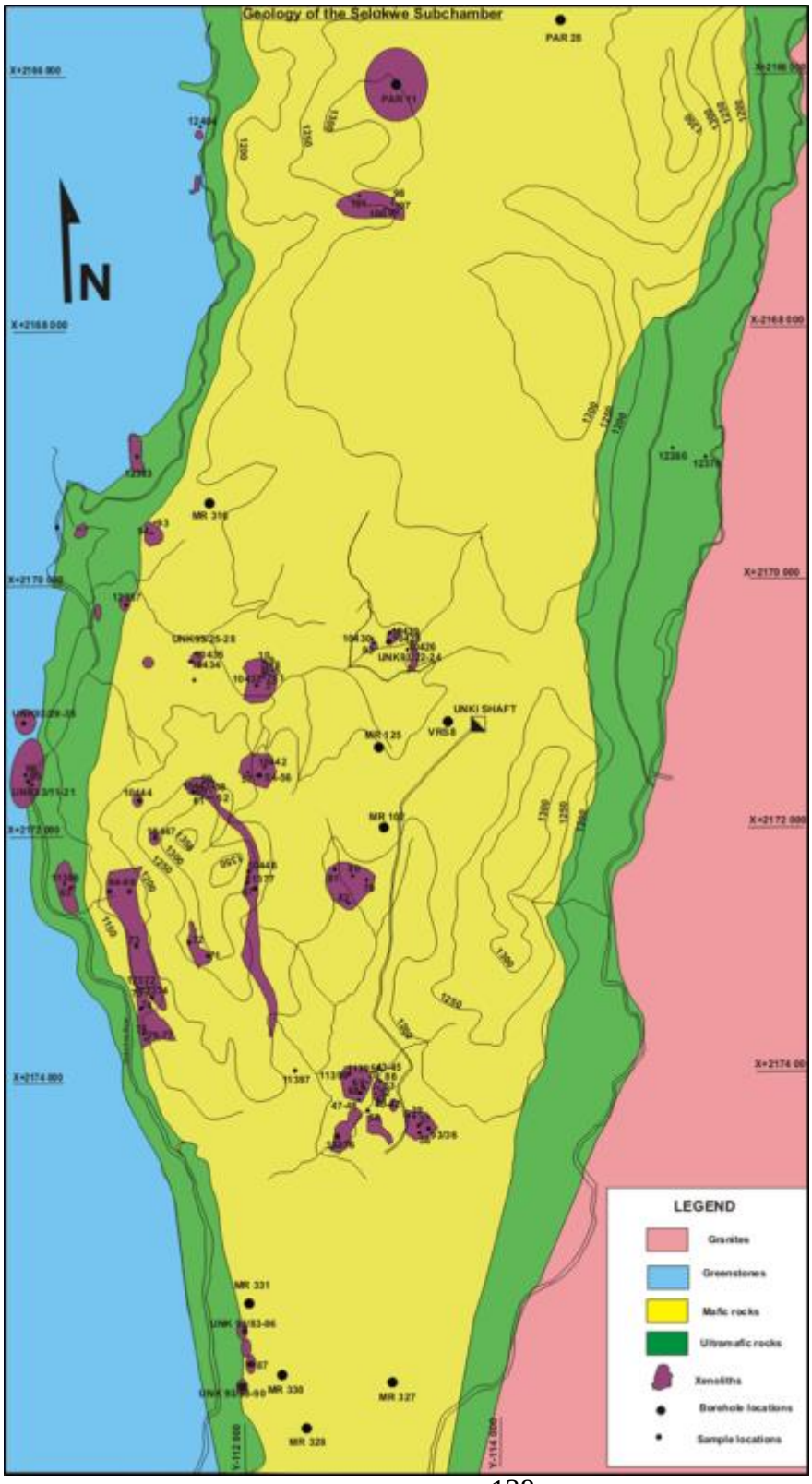
Geology of the Selokwe Subchamber
PAR 26
PAR 11
N
X+2166 000
X+2168 000
X+2170 000
X+2172 000
X+2174 000
MR 316
UNKI SHAFT
VRS8
MR 125
MR 100
MR 331
MR 330
MR 327
MR 328
LEGEND
Granites
Greenstones
Mafic rocks
Ultramafic rocks
Xenoliths
Borehole locations
Sample locations

# APPENDIX B-METHODOLOGY

**Sample selection**

A total of 159 samples were collected from borehole core of which most 152 of the samples were taken from the main borehole of study PAR 11. A detailed lithological core logging of the PAR 11 was done at the Prospecting Ventures Ltd in Harare, Zimbabwe where the core is kept. The samples were taken at least one in every metre. Twenty to thirty samples was randomly chosen for thin sections for the PAR 11 borehole. Other samples were taken from boreholes with xenoliths in the surrounding area shown in the diagram in the map in Appendix A. These boreholes are VS8, PAR 28, MR 33, MR 102, MR 125, MR 316, MR 327, MR 328, MR 330 and MR 331. The core logging of these borehole samples of xenoliths was done at the Unki Mine, where the mining core is kept. The samples were then air freighted to the Earth Laboratory, School of Geosciences, University of Witwatersrand, Johannesburg for geochemical analyses.

**Analytical techniques**

The rock samples were cut and cleaned to remove any traces of cutting fluids and contamination. Selected sampled were cut in thin blocks for to thins section and polished sections for petrographic studies and microprobe analyses. The rest were crushed using a Mo-steel jaw crusher to fragments less than a 1cm. During sample exchange the jaw-crusher was stripped, scrubbed with a wire brush. The sample pan was washed with water, vacuumed and cleaned with acetone. The samples were then coarse milled and only 80g was fine milled in a carbon case-hardened pure iron rotary mill to produce a powder to as a preparation for X-ray Fluorescence (XRF) and Inductively Coupled Plasma Mass Spectrometry (ICP-MS).

**X-ray Fluorescence (XRF**)

Whole rock analysis was then done using Panalytical PW2404 X-ray Fluorescence (XRF) spectrometer to determine major and trace element chemistry of each rock sample. The rock sample were prepared in two different forms using milled samples, a pressed powder disc for trace element analysis and a glass bead made from the

powdered sample fused with lithium metaborate or tetraborate for major element analysis. The spectrometer excites samples using X-ray where primary X-rays beam excites a secondary X-ray which determines the concentrations elements present using intensity. The major element oxides were fused using Johnson Matthey Spectroflux 105 at 1100°C. Trace element (Zr, Cr, Ni and Cl) were pressed pellets using 8g of powder diameter disk and calculated using XRF Panalytical ProTrace program.

**Inductively Coupled Plasma Mass Spectrometry (ICP-MS)**

The ICP-MS was used to determine the concentrations of other trace elements and rare earth elements (REE) using a Perkin Elmer Elan Instrument. The samples were prepared by HF-$HNO_3$ digestion using the CEM Mars microware system and after drying down were taken up into solution with 2% $HNO_3$. The samples were diluted 1000 times for ICP-MS analysis and mixed with internal Re, Rh, Bi and in standard to cover the requires mass range. Primary external calibration standards were made up over the range 5-100 ppb. Every ICP-MS determined was accompanied by control standards from the US Geological Survey Analysed Basalt BCR-1, Hawaiian Basalt BHVO-1, Icelandic Basalt BIR-1 and for all elements the deviation was less than 10% from recommended values. It has very low detection limits and good accuracy and precision. Sulphur analyses were done on the milled samples using the Lincoln Electric Co. CS244 infra-red spectrometer and an induction furnace in an oxygen atmosphere at 1340°C.

The mineral analyses were performed by using a CAMECA CAMEBEX SX50 electron microscope at the University of Kwazulu Natal. Standard operating conditions included a filament current of 1200nA at 20kV and a beam diameter of 15µm.

# APPENDIX C – PAR 11 BOREHOLE LOG

Easting : -97004.26

Northing : -2166419.69

## Wizard Log Sheet

Drill Hole PAR 11

Total Depth : 230.22m

| Depth (m) : | Drill Hole From | To | Rock Type | Rock Description Comments | Thin Sections Depth of reading. | Sample No. |
|---|---|---|---|---|---|---|
| 5 | | | | | | |
| | 0 | 16 | | Highly weathered Pyroxenite | | |
| 10 | | | | | | |
| 15 | | | | | | |
| | | | | | 18.94 | PAR 11/1 |
| 20 | | | | | | |
| | 16 | 30.26 | | Homogenous Pyroxenite | | |
| 25 | | | | | 24.32 | PAR 11/4 |
| 30 | 30.26 | 30.49 | | Olivine Pyroxenite | | |
| | | | | | 34.63 | PAR 11/12 |
| 35 | 30.49 | 76.96 | | Dunite/Harzburgite | 35.69 | PAR 11/13 |

| Depth (m) : | Drill Hole | | | Rock Description Comments | Thin Sections | |
|---|---|---|---|---|---|---|
| | From | To | Rock Type | | Depth of reading. | Sample No. |
| 45 | | | | | 46.4 | PAR 11/20 |
| | | | | | 48.73 | PAR 11/22 |
| 50 | | | | | | |
| | | | | | 53.33 | PAR 11/25 |
| 55 | | | | | | |
| | 30.49 | 76.96 | | Dunite/Harzburgite | | |
| 60 | | | | | | |
| | | | | | 64.41 | PAR 11/33 |
| 65 | | | | | | |
| 70 | | | | | | |
| | | | | | 71.57 | PAR 11/38 |
| 75 | | | | | | |
| | 76.96 | 85 | | Dunite/ Harzburgite with patches of olivine-pyroxenite 10cm across | | |

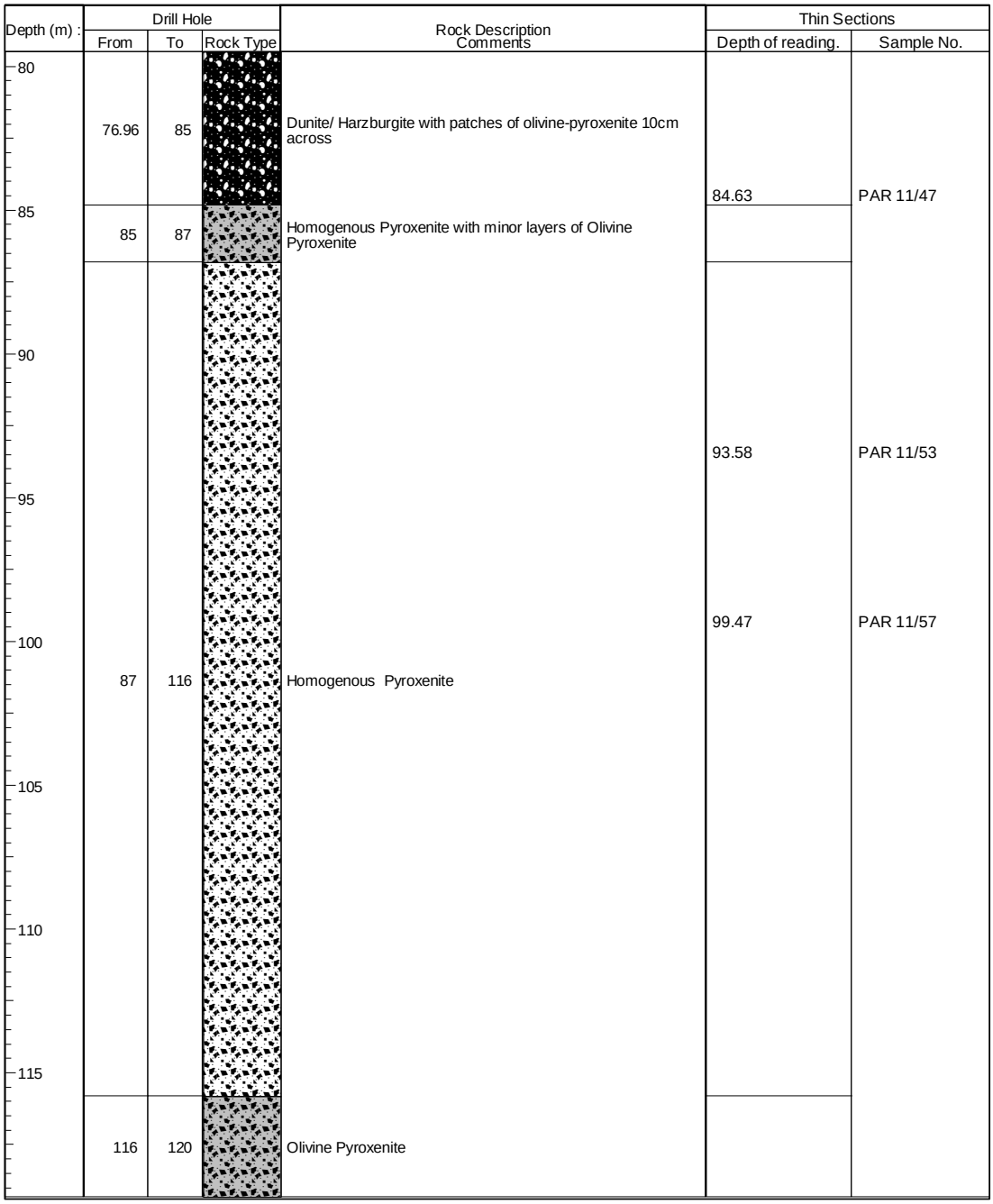
Depth (m) :
Drill Hole
From
To
Rock Type
Rock Description
Comments
Thin Sections
Depth of reading.
Sample No.
80
85
90
95
100
105
110
115
76.96
85
Dunite/ Harzburgite with patches of olivine-pyroxenite 10cm across
84.63
PAR 11/47
85
87
Homogenous Pyroxenite with minor layers of Olivine Pyroxenite
93.58
PAR 11/53
99.47
PAR 11/57
87
116
Homogenous Pyroxenite
116
120
Olivine Pyroxenite

| Depth (m) : | Drill Hole | | | Rock Description Comments | Thin Sections | |
|---|---|---|---|---|---|---|
| | From | To | Rock Type | | Depth of reading. | Sample No. |
| 120 | 116 | 120 | | Olivine Pyroxenite | | |
| 125 | | | | | 126.4 | PAR 11/76 |
| 130 | 120 | 143 | | Homogenous Pyroxenite | | |
| 135 | | | | | 135.93 | PAR 11/83 |
| 140 | | | | | | |
| 145 | 143 | 147 | | Olivine Pyroxenite | | |
| 150 | 147 | 165.27 | | Dunite/Harzburgite | | |
| 155 | | | | | 156.78 | PAR 11/98 |

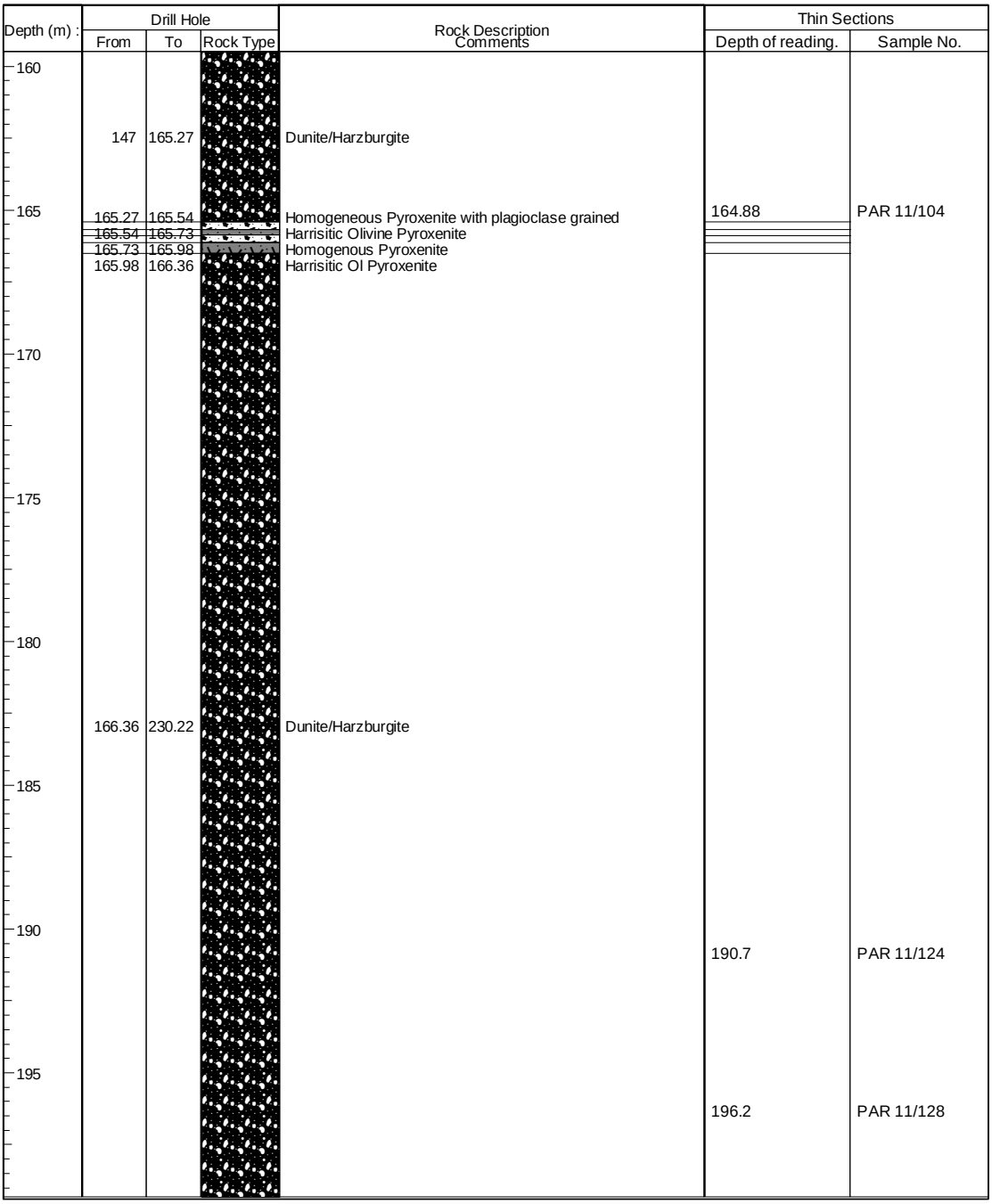
Depth (m) :
Drill Hole
From
To
Rock Type
Rock Description
Comments
Thin Sections
Depth of reading.
Sample No.
160
165
170
175
180
185
190
195
147
165.27
Dunite/Harzburgite
165.27
165.54
Homogeneous Pyroxenite with plagioclase grained
164.88
PAR 11/104
165.54
165.73
Harrisitic Olivine Pyroxenite
165.73
165.98
Homogenous Pyroxenite
165.98
166.36
Harrisitic Ol Pyroxenite
166.36
230.22
Dunite/Harzburgite
190.7
PAR 11/124
196.2
PAR 11/128

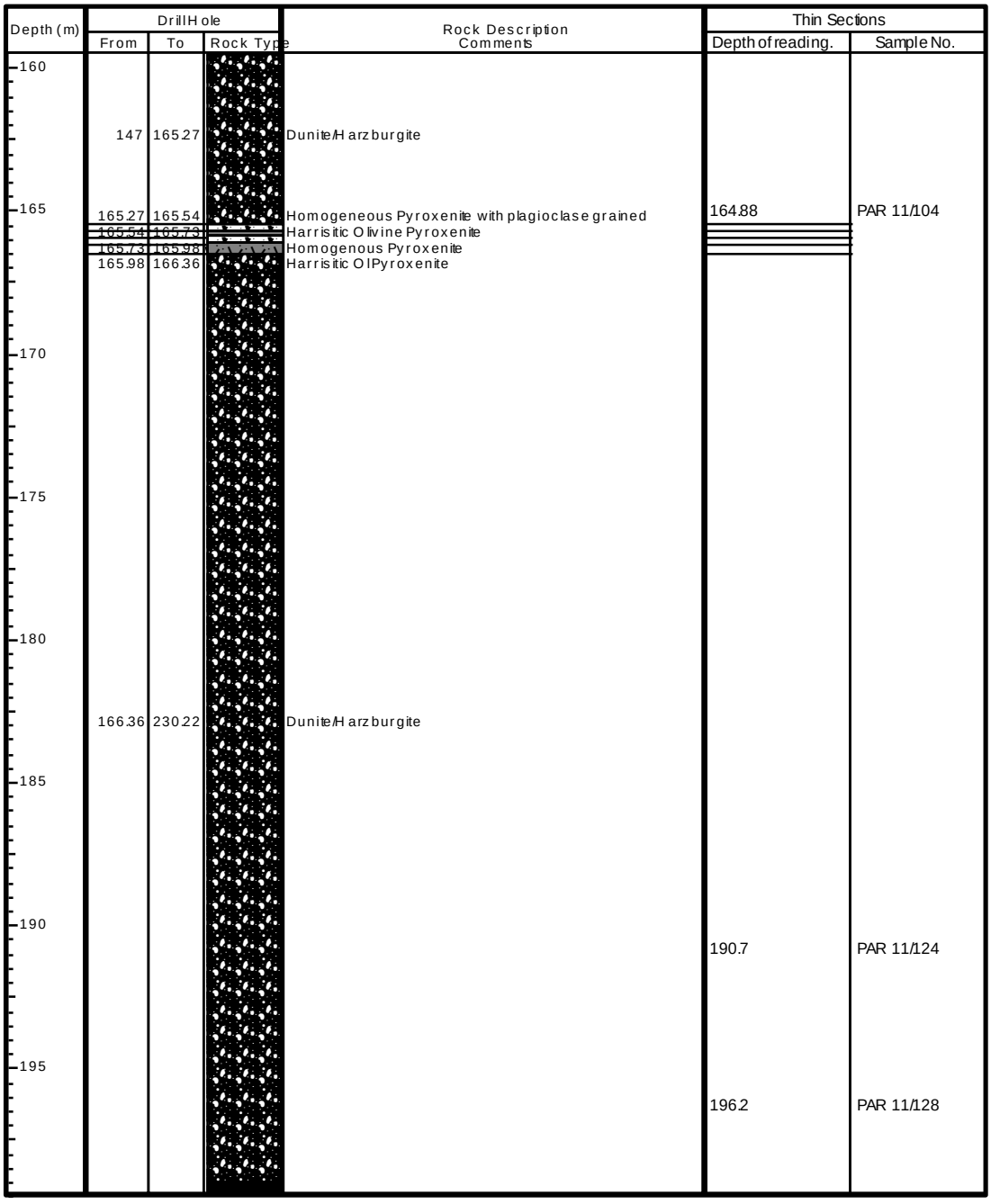
Depth (m)
Drill Hole
From
To
Rock Type
Rock Description
Comments
Thin Sections
Depth of reading.
Sample No.
160
165
170
175
180
185
190
195
147
165.27
Dunite/Harzburgite
165.27
165.54
Homogeneous Pyroxenite with plagioclase grained
164.88
PAR 11/104
165.54
165.73
Harrisitic Olivine Pyroxenite
165.73
165.98
Homogenous Pyroxenite
165.98
166.36
Harrisitic OlPyroxenite
166.36
230.22
Dunite/Harzburgite
190.7
PAR 11/124
196.2
PAR 11/128

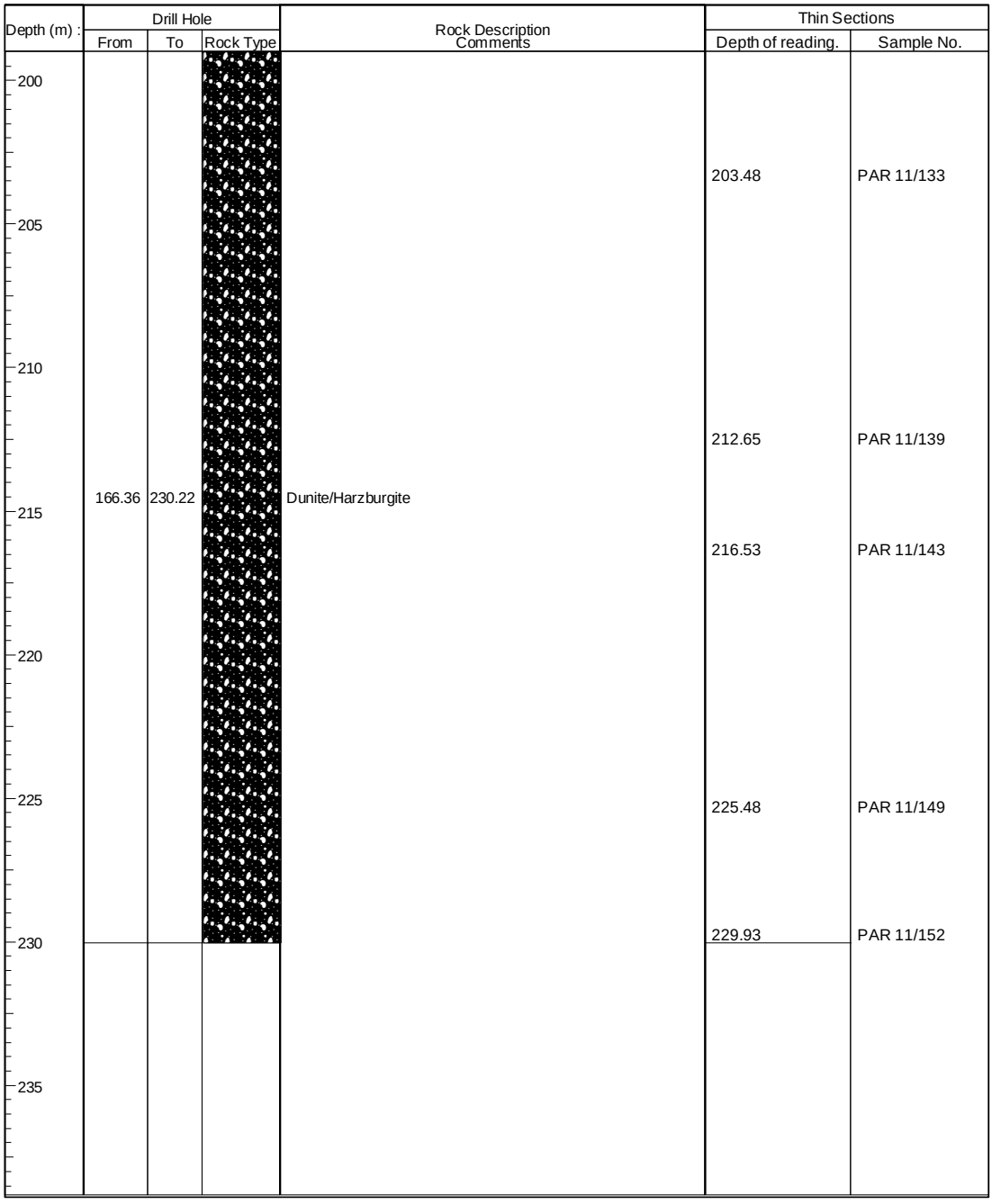
Depth (m) :
Drill Hole
From
To
Rock Type
Rock Description
Comments
Thin Sections
Depth of reading.
Sample No.
200
205
210
215
220
225
230
235
166.36
230.22
Dunite/Harzburgite
203.48
PAR 11/133
212.65
PAR 11/139
216.53
PAR 11/143
225.48
PAR 11/149
229.93
PAR 11/152

# APPENDIX D: -THIN SECTIONS DESCRIPTIONS

**BOREHOLE SAMPLES**

| SAMPLE # | ROCK TYPE | MAJOR MINERALS | MINOR MINERALS | TEXTURES |
|---|---|---|---|---|
| PAR 11/1 | Pyroxenite | Opx | Cpx, Plag, Biot | Cumulus Opx, Cpx Polygonal grains of Opx, granular |
| PAR 11/4 | Pyroxenite | Opx | Cpx, Plag | Cumulus polygonal grains of Opx granular |
| PAR 11/12 | Harzburgite | Ol,Opx | Plag, Chr | Ol serpentinized |
| PAR 11/13 | Harzburgite | Ol, Opx | Chr | Ol totally serpentinized |
| PAR 11/20 | Dunite | Ol | Chr, Biot | Poikilitic Chr enclosing Ol. Ol partially |
| PAR 11/22 | Dunite | Ol | Opx, Chr | Recrystallisation texture |
| PAR 11/25 | Harzburgite | Ol, Opx | Opx, Biot, Calcite, Chr | Ol serpentinized Chr grains |
| PAR 11/33 | Dunite | Ol | Opx, Chr | Granular Ol serpentinized |
| PAR 11/38 | Harzburgite | Ol, Opx | Chr, Biot, Plag | Granular, Ol serpentinized |
| PAR 11/47 | Harzburgite with Olivine-pyroxenite | Ol, Opx | Chr, Plag | Ol serpentinized optically continuous Opx |
| PAR 11/53 | Pyroxenite | Opx, | Cpx | Tabular Opx with interstitial Plag |
| PAR 11/57 | Pyroxenite | Opx | Cpx, Plag | Granophyric Plag |
| PAR 11/76 | Pyroxenite | Opx | Cpx, Plag | intergrowth of Opx and Cpx texture like granophyric texture |
| PAR 11/83 | Pyroxenite | Opx | Cpx, Plag, Ol | Optically continuous Opx |
| PAR 11/98 | Harzburgite | Ol | Chr | Poikilitic Chromite |
| PAR 11/104 | Dunite | Ol | Chr, Biot, | Ol partially altered |

**BOREHOLE SAMPLES CONTINUED.**

| SAMPLE # | ROCK TYPE | MAJOR MINERALS | MINOR MINERALS | TEXTURES |
|---|---|---|---|---|
| PAR 11/124 | Dunite | Ol | Plag | Ol totally serpentinized |
| PAR 11/139 | Dunite | Ol | Chr | Chromite grains surrounding Ol grains. Ol serpentinized |
| PAR 11/143 | Harzburgite | Ol | Opx, Chr | Ol totally serpentinized |
| PAR 11/149 | Olivine-pyroxenite | Ol, Opx | Chr | Optically continuous Opx, Ol |
| PAR 11/152 | Harzburgite | Ol, Opx | Chr, Plag | Coarse grained |
| VRS 8/154 | Replacement pegmatoid | Ol | - | Ol totally altered |
| PAR 28/156 | Serpentinite | Ol | Chr | Ol totally altered |
| MR 328/157 | Serpertinite | Opx, Cpx | | Fine grained |
| MR 33/1 | Harzburgite | Ol, Opx | Chr | Extensively serpentinized fine grained polygonal crystals |
| MR 33/2 | Serpentinized Dunite | Ol | Chr | Polygonal grains now serpentinized |
| MR 33/3 | Harzburgite | Ol, Opx | Chr | Medium to fine grained granular |
| MR 102/1 | Olivine-websterite | Ol, Opx, Cpx | Mag, Plag | Polygonal grains of variable size |
| MR 102/2 | Olivine-websterite | Ol, Opx, Cpx | - | Granular medium-grained |
| MR 102/3 | Olivine-websterite | Ol, Opx, Cpx | - | Fine-grained granular |
| MR125/1 | Olivine-websterite | Ol, Opx, Cpx | Chr, Plag | Granular subhedral Ol, Opx, |
| MR 125/2 | Olivine-websterite | Ol, Opx, Cpx | Plag | Fine-grained granular Ol, Opx |

**UNKI XENOLITH SUITE SAMPLES**

| SAMPLE # | ROCK TYPE | MAJOR MINERALS | MINOR MINERALS | TEXTURES |
|---|---|---|---|---|
| UNK 93/2A | Olivine-pyroxenite | Ol, Opx | Cpx, Chr | Cumulus Opx , Fine grained |
| UNK 93/4 | Olivine-pyroxenite | Ol, Opx | Chr | Fine grained polygonal grains. |
| UNK 93/7 | Olivine-pyroxenite | Ol, Opx | Chr | Phenocrysts of Chr, Interstitial Chr |
| UNK 93/13 | Harzburgite | Ol, Opx | Chr | Cumulus Opx, Phenocrysts of serpentinized Ol |
| UNK 93/15 | Olivine-pyroxenite | Ol, Opx | Chr | Polygonal grains of Opx |
| UNK 93/16 | Harzburgite | Ol, Opx | Chr | Bands of Ol pyroxenite and harzburgite. Ol serpentinized, Polygonal Opx |
| UNK 93/20 | Olivine pyroxenite | Opx | Chr | Fine grained |
| UNK 93/23 | Norite | Opx, Plag, | Cpx, Pigeonite | Cumulus Plag with triple point junctions |
| UNK 93/24 | Gabbro | Plag, Cpx | Opx | Large oikocrysts of Cpx with exsolution lamellae |
| UNK 93/26 | Harzburgite | Ol, Opx | Cpx, Chr | Fine grained, Polygonal grains. Cumulus Opx, Cpx |
| UNK 93/29 | Pyroxenite | Opx | - | Completely altered |
| UNK 93/32 | Spinel pyroxenite | Opx, Chr | - | Very altered Opx |
| UNK 93/34 | Harzburgite | Ol, Opx | Chr | Ol partly serpentinized |

**UNKI SURFACE SAMPLES CONTINUED.**

| SAMPLE # | ROCK TYPE | MAJOR MINERALS | MINOR MINERALS | TEXTURES |
|---|---|---|---|---|
| UNK 93/46 | Lherzolite | Ol, Opx, Cpx | Chr | Partially serpentinized polygonal grains of Ol, oikocrysts of Cpx Optically continuous Opx, |
| UNK 93/47 | Olivine-websterite | Opx, Cpx, Ol | Chr | Fine-medium of cumulus Opx, Cpx and Ol. Poikilitic Cpx enclosing serpentinized Ol. |
| UNK 93/53 | Olivine-websterite | Ol, Opx, Cpx | Chr | Polygonal Opx |
| UNK 93/54 | Gabbronorite | Cpx, Plag, Inverted Pigeonite | Opx | Cumulus Plag with optically continuous grains of Cpx |
| UNK 93/58 | Olivine-pyroxenite | Ol, Opx | Chr | Polygonal grains of Opx, fine grained serpentinized Ol |
| UNK 93/59 | Harzburgite | Ol, Opx | Cpx, Chr | Very fine grained |
| UNK 93/61 | Lherzolite | Ol, Opx, Cpx | Chr | Totally serpentinized Ol, Fine grained |
| UNK 93/64 | Lherzolite | Ol, Opx, Cpx | Chr | Ol totally serpentinized |
| UNK 93/65 | Olivine-websterite | Ol, Opx, Cpx | Chr | Fine grained polygonal grains |
| UNK 93/69 | Pyroxenite | Opx | Cpx | Tabular, polygonal Opx grains |
| UNK 93/76 | Metaquartzite | Quartz, Cpx | - | Subrounded quartz surrounded by prismatic Cpx grains |

**SURFACE SAMPLES CONTINUED**

| SAMPLE # | ROCK TYPE | MAJOR MINERALS | MINOR MINERALS | TEXTURES |
|---|---|---|---|---|
| UNK 93/78 | Olivine-pyroxenite | Opx, Ol | Chr | Ol partially serpertinized with tabular, polygonal Opx grains |
| UNK 93/83 | Ol pyroxenite | Opx, Ol | Chr | Very altered Ol and Opx |
| UNK 93/86 | Lherzolite | Ol, Opx, Cpx | Chr | Fine to medium polygonal Ol, Opx, Cpx grains |
| UNK 93/88 | Websterite | Ol, Opx, Cpx | Chr | Fine grained Ol totally serpentinized |
| UNK 93/90 | Pyroxenite | Opx | Ol, Chr | Fine grained with polygonal grains of Opx |
| UNK 93/93 | Harzburgite | Ol, Opx | Chr | Ol totally serpentinized |
| UNK 93/94 | Olivine-pyroxenite | Ol, Opx | Chr | Fine grained with polygonal grains Opx, Ol partially to completely serpentinized |
| UNK 93/100 | Olivine-pyroxenite | Ol, Opx | Chr | Medium to coarse grained Ol partially serpentinized. Polygonal grains of Ol and Opx |
| 10442-USM 17 | Poikilitic olivine gabbronorite | Ol, Opx, Cpx, Plag | Mag, Biot | Large poikilitic crystals of primary Opx with rounded grains of Ol, Cpx and Plag |
| 10443-USM 18 | Olivine-pyroxenite | Ol, Opx | Chr | Fine-grained granular with strong fabric |
| 10444-USM 19 | Harzburgite | Ol, Opx | Chr | Very fine-grained granular Ol totally serpentinized |

**SURFACE SAMPLES CONTINUED**

| SAMPLE # | ROCK TYPE | MAJOR MINERALS | MINOR MINERALS | TEXTURES |
|---|---|---|---|---|
| 11376-USM 26 | Quartzite | No thin section | - | - |
| 11377-USM 27 | Olivine-pyroxenite | Ol, Opx | Chr, Biot, Plag | Very fine-grained granular |
| 11378-USM 28 | Banded Ironstone | No thin section | - | - |
| 11379-USM 29 | Quartzite | No thin section | - | - |
| 11384-USM 34 | Olivine-pyroxenite | Ol, Opx | Chr, Mag | Fine-grained granular |
| 11386-USM 36 | Serpentinized granular harzburgite | Ol, Opx, Chr | Plag, Biot | Granular |
| 11388-USM 38 | Magnetite Norite | Mag, Opx, Cpx, Plag | Biot, Ap | Poikilitic Opx. Granular Plag and Cpx |
| 11389-USM 39 | Quartzite | No thin section | - | - |
| 12367-USM 55 | Olivine-pyroxenite | Ol, Opx | Mag | Fine polygonal grains |
| 12371-USM 60 | Gabbro | Cpx, Plag | Alteration products of Cpx | Coarse-grained Cpx in fine interlocking networking of Plag crystals |
| 12373-USM 61 | Olivine-pyroxenite | Ol, Opx | Chr | Fine-grained rock with micro-layering |
| 12372-USM 62 | Spinel harzburgite | Ol, Opx, Sp | - | Very fine-grained granular |
| 11395-USM 65 | Feldspathic olivine pyroxenite | Ol, Opx, Plag | Chr, Cpx | Large poikilitic olivine in granular matrix of Opx and interstitial Plag |
| 11396-USM 66 | Olivine gabbro | Ol, Cpx, Plag | - | Interlocking subhedral |
| 11397-USM 67 | Layered granular harzburgite | No thin section | - | - |

**SURFACE SAMPLES CONTINUED.**

| SAMPLE # | ROCK TYPE | MAJOR MINERALS | MINOR MINERALS | TEXTURES |
|---|---|---|---|---|
| 11398-USM 68 | Olivine gabbronorite | Ol, Opx, Cpx, Plag | - | Fine-grained granular |
| 12376-USM 71 | Serpentinite | No thin section | - | - |
| 12356-USM 74 | Websterite | Opx, Cpx | - | Fine-grained granular |
| 12378-USM 76 | Amygdaloidal meta-basalt | No thin section | - | - |
| 12380-USM 78 | Dunite | Ol, Chr | Chr | Microgranular Ol, serpentinized |
| 12383-USM 81 | Harzburgite | Ol, Opx | Chr | Poikilitic olivine with small rounded Opx enclosed in Plag |
| 12404-USM 102 | Tremolite schist | Amphibole talc | Chl | Small laths in a chlorite matrix |

# APPENDIX E:-WHOLE ROCK ANALYSES RESULTS

Symbols used wt% = weight percent, ppm = parts per million and ND = Not detected

## Table E1.1: Whole rock major element (wt%) for PAR 11 borehole by XRF.

| Sample # | DPF(m) | DPT(m) | Lithology | $SiO_2$ | $Al_2O_3$ | $Fe_2O_3$ | FeO | MnO | MgO | CaO | $Na_2O$ | $K_2O$ | $TiO_2$ | $P_2O_5$ | $Cr_2O_3$ | NiO | TOTAL | LOI |
|---|---|---|---|---|---|---|---|---|---|---|---|---|---|---|---|---|---|---|
| PAR 11/1 | 18.77 | 18.94 | Pyroxenite | 55.6 | 2.7 | 0.9 | 7.6 | 0.2 | 29.6 | 2.2 | 0.7 | 0.1 | 0.1 | ND | 0.5 | 0.1 | 100.3 | 0.3 |
| PAR 11/2 | 20.78 | 20.96 | Pyroxenite | 55.5 | 3.0 | 0.9 | 7.5 | 0.2 | 29.1 | 2.3 | 0.4 | 0.1 | 0.1 | ND | 0.5 | 0.1 | 99.6 | 0.5 |
| PAR 11/ 3 | 23.25 | 23.36 | Pyroxenite | 55.4 | 2.7 | 0.9 | 7.5 | 0.2 | 29.5 | 2.1 | 0.3 | 0.1 | 0.1 | ND | 0.5 | 0.1 | 99.5 | 0.7 |
| PAR 11/ 4 | 24.12 | 24.32 | Pyroxenite | 55.6 | 2.5 | 0.9 | 7.4 | 0.2 | 29.7 | 2.0 | 0.4 | 0.1 | 0.1 | ND | 0.5 | 0.1 | 99.5 | 0.4 |
| PAR 11/ 5 | 25.49 | 25.69 | Pyroxenite | 55.3 | 2.7 | 0.9 | 7.6 | 0.2 | 29.5 | 2.0 | 0.4 | 0.1 | 0.1 | ND | 0.5 | 0.1 | 99.4 | 0.5 |
| PAR 11/ 6 | 27.14 | 23.37 | Pyroxenite | 55.4 | 3.6 | 0.9 | 7.5 | 0.2 | 28.4 | 2.7 | 0.5 | 0.2 | 0.1 | ND | 0.5 | 0.1 | 100.1 | 0.8 |
| PAR 11/ 7 | 29.15 | 29.35 | Pyroxenite | 55.6 | 3.5 | 0.9 | 7.4 | 0.2 | 28.0 | 2.5 | 0.6 | 0.3 | 0.2 | 0.1 | 0.5 | 0.1 | 99.8 | 0.8 |
| PAR 11/ 8 | 30.35 | 30.60 | Pyroxenite | 53.4 | 3.4 | 1.0 | 7.8 | 0.2 | 30.0 | 2.4 | 0.5 | 0.2 | 0.1 | ND | 0.6 | 0.1 | 99.7 | 0.9 |
| PAR 11/ 9 | 30.77 | 31.02 | Harzburgite | 46.6 | 1.5 | 1.2 | 9.9 | 0.2 | 37.8 | 1.2 | 0.2 | 0.1 | 0.1 | ND | 0.7 | 0.2 | 99.6 | 4.5 |
| PAR 11/ 10 | 32.10 | 32.33 | Harzburgite | 44.5 | 2.4 | 1.3 | 10.4 | 0.2 | 38.2 | 2.0 | 0.3 | 0.1 | 0.1 | ND | 0.6 | 0.2 | 100.3 | 4.7 |
| PAR 11/ 11 | 33.21 | 33.43 | Harzburgite | 43.2 | 2.3 | 1.3 | 10.7 | 0.2 | 38.6 | 1.8 | 0.3 | 0.2 | 0.1 | ND | 0.7 | 0.2 | 99.6 | 5.1 |
| PAR 11/ 12 | 34.37 | 34.63 | Lherzolite | 44.7 | 2.3 | 1.3 | 10.1 | 0.2 | 37.6 | 2.4 | 0.6 | 0.2 | 0.1 | ND | 0.7 | 0.2 | 100.4 | 4.7 |
| PAR 11/ 13 | 35.48 | 35.69 | Harzburgite | 44.1 | 1.8 | 1.3 | 10.6 | 0.2 | 40.0 | 1.3 | 0.3 | 0.1 | 0.1 | ND | 0.5 | 0.2 | 100.7 | 5.9 |
| PAR 11/ 14 | 37.24 | 37.44 | Harzburgite | 43.5 | 2.1 | 1.3 | 10.7 | 0.2 | 39.3 | 1.4 | 0.3 | 0.2 | 0.1 | ND | 0.7 | 0.2 | 100.0 | 5.2 |
| PAR 11/ 15 | 38.61 | 38.82 | Harzburgite | 43.0 | 1.8 | 1.4 | 11.0 | 0.2 | 40.2 | 1.4 | 0.4 | 0.2 | 0.1 | ND | 0.7 | 0.2 | 100.7 | 6.4 |
| PAR 11/ 16 | 40.32 | 40.61 | Harzburgite | 44.2 | 1.6 | 1.3 | 10.6 | 0.2 | 39.9 | 1.1 | 0.2 | 0.1 | 0.1 | ND | 0.5 | 0.2 | 100.1 | 5.1 |
| PAR 11/ 17 | 41.43 | 41.69 | Dunite | 41.5 | 2.6 | 1.4 | 11.3 | 0.2 | 39.8 | 1.6 | 0.4 | 0.2 | 0.1 | ND | 0.6 | 0.2 | 99.9 | 6.8 |
| PAR 11/ 18 | 43.12 | 43.37 | Dunite | 41.8 | 2.2 | 1.4 | 11.4 | 0.2 | 40.6 | 1.4 | 0.2 | 0.1 | 0.1 | ND | 0.6 | 0.2 | 100.3 | 6.0 |
| PAR 11/ 19 | 44.70 | 44.96 | Dunite | 42.4 | 1.7 | 1.4 | 11.2 | 0.2 | 40.6 | 1.1 | 0.2 | 0.1 | 0.1 | ND | 0.9 | 0.2 | 100.0 | 5.9 |
| PAR 11/ 20 | 46.12 | 46.40 | Dunite | 41.6 | 2.5 | 1.4 | 11.4 | 0.2 | 39.3 | 1.3 | 0.2 | 0.1 | 0.1 | ND | 1.4 | 0.2 | 99.7 | 5.7 |
| PAR 11/ 21 | 47.37 | 47.69 | Dunite | 42.8 | 2.5 | 1.4 | 11.0 | 0.2 | 39.6 | 1.2 | 0.3 | 0.2 | 0.1 | ND | 0.7 | 0.2 | 100.1 | 4.8 |
| PAR 11/ 22 | 48.45 | 48.73 | Dunite | 42.4 | 3.4 | 1.3 | 10.9 | 0.2 | 38.5 | 1.8 | 0.5 | 0.3 | 0.1 | ND | 0.4 | 0.2 | 100.1 | 4.9 |
| PAR 11/ 23 | 50.13 | 50.37 | Dunite | 41.6 | 2.1 | 1.4 | 11.5 | 0.2 | 40.6 | 1.5 | 0.2 | 0.1 | 0.1 | ND | 0.5 | 0.2 | 100.0 | 5.3 |
| PAR 11/ 24 | 51.60 | 51.83 | Dunite | 41.0 | 3.3 | 1.4 | 11.4 | 0.2 | 38.5 | 1.7 | 0.3 | 0.3 | 0.1 | ND | 1.1 | 0.2 | 99.7 | 4.6 |

## Table E1.1: Whole rock major element (wt%) for PAR 11 borehole by XRF.

| Sample # | DPF(m) | DPT(m) | Lithology | $SiO_2$ | $Al_2O_3$ | $Fe_2O_3$ | FeO | MnO | MgO | CaO | $Na_2O$ | $K_2O$ | $TiO_2$ | $P_2O_5$ | $Cr_2O_3$ | NiO | TOTAL | LOI |
|---|---|---|---|---|---|---|---|---|---|---|---|---|---|---|---|---|---|---|
| PAR 11/25 | 53.06 | 53.33 | Harzburgite | 43.7 | 1.8 | 1.4 | 11.0 | 0.2 | 40.0 | 1.2 | 0.3 | 0.2 | 0.1 | ND | 0.7 | 0.2 | 100.9 | 3.3 |
| PAR 11/26 | 54.67 | 54.93 | Harzburgite | 47.1 | 1.7 | 1.2 | 9.9 | 0.2 | 37.5 | 1.3 | 0.2 | 0.1 | 0.1 | ND | 0.8 | 0.2 | 100.4 | 2.3 |
| PAR 11/27 | 55.96 | 56.03 | Harzburgite | 43.8 | 3.5 | 1.3 | 10.4 | 0.2 | 36.8 | 2.6 | 0.5 | 0.2 | 0.1 | ND | 1.0 | 0.2 | 100.6 | 3.7 |
| PAR 11/28 | 57.01 | 57.38 | Harzburgite | 43.8 | 3.1 | 1.3 | 10.9 | 0.2 | 37.5 | 1.8 | 0.4 | 0.2 | 0.1 | ND | 1.3 | 0.2 | 100.9 | 2.9 |
| PAR 11/29 | 58.49 | 58.82 | Dunite | 41.8 | 3.0 | 1.4 | 11.5 | 0.2 | 39.4 | 1.6 | 0.5 | 0.2 | 0.1 | ND | 1.3 | 0.2 | 101.3 | 3.4 |
| PAR 11/30 | 59.74 | 59.99 | Harzburgite | 44.4 | 2.7 | 1.3 | 10.3 | 0.2 | 37.0 | 1.9 | 0.4 | 0.2 | 0.1 | ND | 0.7 | 0.2 | 99.4 | 2.8 |
| PAR 11/31 | 61.10 | 61.36 | Harzburgite | 43.8 | 3.0 | 1.3 | 10.4 | 0.2 | 36.7 | 2.1 | 0.5 | 0.2 | 0.1 | ND | 0.8 | 0.2 | 99.3 | 3.9 |
| PAR 11/32 | 62.73 | 63.00 | Dunite | 42.7 | 3.0 | 1.3 | 10.5 | 0.2 | 37.2 | 1.9 | 0.6 | 0.2 | 0.1 | ND | 0.3 | 0.2 | 98.1 | 2.9 |
| PAR 11/33 | 64.12 | 64.41 | Harzburgite | 44.6 | 2.2 | 1.3 | 10.3 | 0.2 | 38.3 | 1.6 | 0.4 | 0.1 | 0.1 | ND | 0.6 | 0.2 | 99.8 | 3.1 |
| PAR 11/34 | 65.76 | 66.03 | Harzburgite | 46.2 | 1.5 | 1.2 | 9.9 | 0.2 | 38.1 | 1.2 | 0.3 | 0.1 | 0.1 | ND | 0.7 | 0.2 | 99.7 | 1.8 |
| PAR 11/35 | 66.67 | 66.90 | Harzburgite | 46.8 | 1.8 | 1.2 | 9.8 | 0.2 | 37.4 | 1.3 | 0.3 | 0.1 | 0.1 | ND | 1.1 | 0.2 | 100.1 | 1.8 |
| PAR 11/36 | 68.18 | 68.41 | Dunite | 43.0 | 3.1 | 1.3 | 10.8 | 0.2 | 38.0 | 2.0 | 0.5 | 0.1 | 0.1 | ND | 1.2 | 0.2 | 100.6 | 1.8 |
| PAR 11/37 | 69.75 | 70.00 | Harzburgite | 48.0 | 2.2 | 1.2 | 9.5 | 0.2 | 36.2 | 1.5 | 0.4 | 0.2 | 0.1 | ND | 0.5 | 0.2 | 100.1 | 1.0 |
| PAR 11/38 | 71.27 | 71.57 | Dunite | 42.1 | 2.3 | 1.4 | 11.3 | 0.2 | 40.3 | 1.3 | 0.5 | 0.2 | 0.1 | ND | 0.4 | 0.2 | 100.2 | 1.8 |
| PAR 11/39 | 72.45 | 72.71 | Harzburgite | 47.2 | 1.7 | 1.2 | 9.8 | 0.2 | 37.3 | 1.4 | 0.3 | 0.1 | 0.1 | ND | 0.6 | 0.2 | 100.0 | 1.3 |
| PAR 11/40 | 73.63 | 73.96 | Dunite | 41.5 | 2.7 | 1.4 | 11.2 | 0.2 | 39.6 | 1.9 | 0.5 | 0.2 | 0.1 | ND | 0.7 | 0.2 | 100.1 | 2.1 |
| PAR 11/41 | 75.22 | 75.46 | Harzburgite | 46.1 | 1.9 | 1.3 | 10.2 | 0.2 | 37.8 | 1.5 | 0.3 | 0.1 | 0.1 | ND | 0.7 | 0.2 | 100.3 | 1.9 |
| PAR 11/42 | 76.39 | 76.67 | Harzburgite | 44.6 | 2.9 | 1.3 | 10.6 | 0.2 | 37.5 | 1.6 | 0.6 | 0.2 | 0.1 | ND | 0.7 | 0.2 | 100.5 | 2.0 |
| PAR 11/42a | 78.07 | 78.30 | Harzburgite | 46.3 | 1.9 | 1.3 | 10.1 | 0.2 | 38.0 | 1.4 | 0.3 | 0.1 | 0.1 | ND | 0.6 | 0.2 | 100.4 | 0.8 |
| PAR 11/43 | 79.57 | 79.94 | Dunite | 43.1 | 2.5 | 1.4 | 11.1 | 0.2 | 39.6 | 1.4 | 0.5 | 0.2 | 0.1 | ND | 0.5 | 0.2 | 100.6 | 4.1 |
| PAR 11/44 | 80.63 | 80.90 | Dunite | 43.1 | 2.9 | 1.3 | 10.9 | 0.2 | 36.9 | 1.6 | 1.5 | 0.4 | 0.2 | 0.1 | 0.6 | 0.2 | 99.8 | 2.7 |
| PAR 11/45 | 81.73 | 82.00 | Harzburgite | 49.1 | 2.2 | 1.2 | 9.3 | 0.2 | 34.6 | 1.6 | 0.3 | 0.1 | 0.1 | ND | 1.2 | 0.2 | 100.1 | 1.6 |
| PAR 11/46 | 83.57 | 83.84 | Olivine-pyroxenite | 49.9 | 2.0 | 1.1 | 9.0 | 0.2 | 34.6 | 1.6 | 0.3 | 0.1 | 0.1 | ND | 0.6 | 0.1 | 99.5 | 1.8 |
| PAR 11/47 | 84.35 | 84.63 | Olivine-pyroxenite | 45.6 | 1.6 | 1.3 | 10.2 | 0.2 | 38.4 | 1.4 | 0.2 | 0.1 | 0.1 | ND | 0.5 | 0.2 | 99.7 | 4.7 |

## Table E1.1: Whole rock major element (wt%) for PAR 11 borehole by XRF.

| Sample # | DPF(m) | DPT(m) | Lithology | $SiO_2$ | $Al_2O_3$ | $Fe_2O_3$ | FeO | MnO | MgO | CaO | $Na_2O$ | $K_2O$ | $TiO_2$ | $P_2O_5$ | $Cr_2O_3$ | NiO | TOTAL | LOI |
|---|---|---|---|---|---|---|---|---|---|---|---|---|---|---|---|---|---|---|
| PAR 11/48 | 86.36 | 86.56 | Pyroxenite | 55.2 | 3.0 | 0.9 | 7.5 | 0.2 | 28.8 | 2.4 | 0.4 | 0.2 | 0.2 | ND | 0.5 | 0.1 | 99.3 | 1.1 |
| PAR 11/49 | 87.36 | 87.58 | Pyroxenite | 55.4 | 3.0 | 0.9 | 7.6 | 0.2 | 28.9 | 2.3 | 0.5 | 0.1 | 0.1 | ND | 0.6 | 0.1 | 99.8 | 0.7 |
| PAR 11/50 | 89.04 | 89.26 | Pyroxenite | 55.5 | 3.3 | 0.9 | 7.5 | 0.2 | 28.2 | 2.5 | 0.6 | 0.2 | 0.2 | ND | 0.5 | 0.1 | 99.6 | 0.5 |
| PAR 11/51 | 90.64 | 90.87 | Pyroxenite | 55.6 | 3.3 | 0.9 | 7.5 | 0.2 | 28.4 | 2.5 | 0.5 | 0.2 | 0.1 | ND | 0.5 | 0.1 | 99.6 | 0.7 |
| PAR 11/52 | 91.91 | 92.16 | Pyroxenite | 56.1 | 3.2 | 0.9 | 7.6 | 0.2 | 28.5 | 2.4 | 0.5 | 0.2 | 0.2 | ND | 0.6 | 0.1 | 100.4 | 0.9 |
| PAR 11/53 | 93.34 | 93.58 | Pyroxenite | 54.7 | 3.2 | 1.0 | 7.7 | 0.2 | 29.2 | 2.4 | 0.5 | 0.2 | 0.1 | ND | 0.5 | 0.1 | 99.6 | 0.5 |
| PAR 11/54 | 94.68 | 94.92 | Pyroxenite | 55.7 | 3.3 | 0.9 | 7.5 | 0.2 | 28.2 | 2.5 | 0.6 | 0.2 | 0.2 | ND | 0.6 | 0.1 | 99.9 | 0.5 |
| PAR 11/55 | 96.12 | 96.42 | Pyroxenite | 55.6 | 3.2 | 0.9 | 7.4 | 0.2 | 28.4 | 2.4 | 0.5 | 0.2 | 0.2 | ND | 0.5 | 0.1 | 99.6 | 0.5 |
| PAR 11/56 | 97.76 | 98.00 | Pyroxenite | 55.8 | 3.3 | 0.9 | 7.4 | 0.2 | 28.3 | 2.6 | 0.5 | 0.2 | 0.1 | ND | 0.5 | 0.1 | 100.0 | 0.5 |
| PAR 11/57 | 99.23 | 99.47 | Pyroxenite | 56.1 | 3.2 | 0.9 | 7.4 | 0.2 | 28.4 | 2.5 | 0.5 | 0.2 | 0.2 | ND | 0.5 | 0.1 | 100.1 | 0.5 |
| PAR 11/58 | 100.64 | 100.85 | Pyroxenite | 55.8 | 3.2 | 0.9 | 7.6 | 0.2 | 28.4 | 2.4 | 0.5 | 0.2 | 0.1 | ND | 0.5 | 0.1 | 100.0 | 0.5 |
| PAR 11/59 | 102.14 | 102.40 | Pyroxenite | 55.7 | 3.2 | 0.9 | 7.5 | 0.2 | 28.5 | 2.4 | 0.5 | 0.2 | 0.2 | ND | 0.5 | 0.1 | 99.9 | 0.4 |
| PAR 11/60 | 103.37 | 103.54 | Pyroxenite | 55.9 | 3.2 | 0.9 | 7.5 | 0.2 | 28.6 | 2.4 | 0.5 | 0.2 | 0.2 | ND | 0.5 | 0.1 | 100.1 | 0.5 |
| PAR 11/61 | 104.98 | 105.19 | Pyroxenite | 55.7 | 3.3 | 0.9 | 7.3 | 0.2 | 28.3 | 2.4 | 0.5 | 0.2 | 0.1 | ND | 0.5 | 0.1 | 99.7 | 0.6 |
| PAR 11/62 | 106.35 | 106.54 | Pyroxenite | 55.2 | 3.2 | 0.9 | 7.4 | 0.2 | 28.3 | 2.4 | 0.5 | 0.2 | 0.1 | ND | 0.5 | 0.1 | 99.0 | 0.5 |
| PAR 11/63 | 107.57 | 107.76 | Pyroxenite | 55.6 | 3.2 | 0.9 | 7.4 | 0.2 | 28.6 | 2.3 | 0.5 | 0.2 | 0.1 | ND | 0.5 | 0.1 | 99.4 | 0.4 |
| PAR 11/64 | 109.00 | 109.42 | Pyroxenite | 55.3 | 3.2 | 0.9 | 7.3 | 0.2 | 28.4 | 2.5 | 0.4 | 0.2 | 0.2 | ND | 0.5 | 0.1 | 99.0 | 0.4 |
| PAR 11/65 | 110.41 | 110.64 | Pyroxenite | 55.2 | 3.2 | 0.9 | 7.2 | 0.2 | 28.3 | 2.4 | 0.5 | 0.2 | 0.2 | ND | 0.5 | 0.1 | 98.8 | 0.8 |
| PAR 11/66 | 111.57 | 111.78 | Pyroxenite | 55.7 | 3.3 | 0.9 | 7.4 | 0.2 | 28.5 | 2.4 | 0.5 | 0.2 | 0.2 | ND | 0.5 | 0.1 | 99.8 | 0.4 |
| PAR 11/67 | 113.25 | 113.50 | Pyroxenite | 55.8 | 3.2 | 0.9 | 7.3 | 0.2 | 28.5 | 2.4 | 0.5 | 0.2 | 0.2 | ND | 0.5 | 0.1 | 99.7 | 0.4 |
| PAR 11/68 | 114.38 | 114.59 | Pyroxenite | 55.6 | 3.1 | 0.9 | 7.3 | 0.2 | 28.6 | 2.5 | 0.5 | 0.1 | 0.1 | ND | 0.6 | 0.1 | 99.6 | 0.4 |
| PAR 11/69 | 115.54 | 115.88 | Pyroxenite | 55.8 | 3.2 | 0.9 | 7.3 | 0.2 | 28.7 | 2.3 | 0.5 | 0.2 | 0.1 | ND | 0.5 | 0.1 | 99.8 | 0.8 |
| PAR 11/70 | 117.26 | 117.49 | Pyroxenite | 55.0 | 3.0 | 0.9 | 7.3 | 0.2 | 28.9 | 2.3 | 0.4 | 0.2 | 0.1 | ND | 0.5 | 0.1 | 98.8 | 1.5 |
| PAR 11/71 | 118.65 | 118.88 | Pyroxenite | 54.2 | 2.6 | 1.0 | 7.8 | 0.2 | 30.5 | 1.9 | 0.3 | 0.1 | 0.1 | ND | 0.8 | 0.1 | 99.5 | 1.6 |

## Table E1.1: Whole rock major element (wt%) for PAR 11 borehole by XRF.

| Sample # | DPF(m) | DPT(m) | Lithology | $SiO_2$ | $Al_2O_3$ | $Fe_2O_3$ | FeO | MnO | MgO | CaO | $Na_2O$ | $K_2O$ | $TiO_2$ | $P_2O_5$ | $Cr_2O_3$ | NiO | TOTAL | LOI |
|---|---|---|---|---|---|---|---|---|---|---|---|---|---|---|---|---|---|---|
| PAR 11/72 | 119.73 | 119.97 | Pyroxenite | 55.6 | 2.8 | 0.9 | 7.4 | 0.2 | 29.3 | 2.2 | 0.4 | 0.2 | 0.1 | ND | 0.5 | 0.1 | 99.8 | 2.4 |
| PAR 11/73 | 121.25 | 121.46 | Pyroxenite | 55.7 | 3.0 | 0.9 | 7.4 | 0.2 | 29.0 | 2.3 | 0.4 | 0.2 | 0.1 | ND | 0.5 | 0.1 | 99.8 | 1.6 |
| PAR 11/74 | 122.50 | 122.78 | Pyroxenite | 55.9 | 3.1 | 0.9 | 7.3 | 0.2 | 28.9 | 2.4 | 0.5 | 0.1 | 0.1 | ND | 0.5 | 0.1 | 100.1 | 0.3 |
| PAR 11/75 | 124.14 | 124.39 | Pyroxenite | 55.3 | 3.0 | 0.9 | 7.5 | 0.2 | 29.5 | 2.3 | 0.4 | 0.1 | 0.1 | ND | 0.5 | 0.1 | 99.9 | 1.1 |
| PAR 11/76 | 126.21 | 126.40 | Pyroxenite | 55.6 | 3.1 | 0.9 | 7.4 | 0.2 | 28.8 | 2.5 | 0.4 | 0.2 | 0.1 | ND | 0.5 | 0.1 | 99.7 | 0.5 |
| PAR 11/77 | 127.14 | 127.34 | Pyroxenite | 55.4 | 3.2 | 0.9 | 7.4 | 0.2 | 28.6 | 2.3 | 0.5 | 0.2 | 0.2 | ND | 0.5 | 0.1 | 99.5 | 0.5 |
| PAR 11/78 | 128.71 | 128.93 | Pyroxenite | 55.7 | 3.1 | 0.9 | 7.5 | 0.2 | 28.9 | 2.5 | 0.4 | 0.2 | 0.1 | ND | 0.5 | 0.1 | 100.1 | 0.3 |
| PAR 11/79 | 129.68 | 129.85 | Pyroxenite | 55.4 | 3.1 | 0.9 | 7.4 | 0.2 | 29.0 | 2.4 | 0.4 | 0.2 | 0.1 | ND | 0.5 | 0.1 | 99.8 | 0.3 |
| PAR 11/80 | 131.36 | 131.55 | Pyroxenite | 55.5 | 3.1 | 0.9 | 7.5 | 0.2 | 29.1 | 2.4 | 0.4 | 0.2 | 0.1 | ND | 0.5 | 0.1 | 99.9 | 0.3 |
| PAR 11/81 | 132.74 | 132.98 | Pyroxenite | 55.6 | 3.1 | 0.9 | 7.5 | 0.2 | 29.0 | 2.4 | 0.4 | 0.2 | 0.1 | ND | 0.5 | 0.1 | 100.0 | 0.2 |
| PAR 11/82 | 134.24 | 134.52 | Pyroxenite | 56.3 | 3.1 | 0.9 | 7.5 | 0.2 | 29.5 | 2.4 | 0.4 | 0.2 | 0.1 | ND | 0.5 | 0.1 | 101.2 | 0.2 |
| PAR 11/83 | 135.66 | 135.93 | Pyroxenite | 56.4 | 3.1 | 0.9 | 7.5 | 0.2 | 29.4 | 2.4 | 0.4 | 0.2 | 0.1 | ND | 0.5 | 0.1 | 101.2 | 0.3 |
| PAR 11/84 | 136.61 | 136.82 | Pyroxenite | 56.2 | 3.3 | 0.9 | 7.5 | 0.2 | 29.1 | 2.5 | 0.5 | 0.2 | 0.1 | ND | 0.5 | 0.1 | 101.0 | -0.4 |
| PAR 11/85 | 138.67 | 138.94 | Pyroxenite | 56.2 | 3.2 | 0.9 | 7.5 | 0.2 | 29.3 | 2.5 | 0.4 | 0.2 | 0.1 | ND | 0.5 | 0.1 | 101.1 | 0.3 |
| PAR 11/86 | 140.18 | 140.42 | Pyroxenite | 55.9 | 3.3 | 0.9 | 7.5 | 0.2 | 29.0 | 2.6 | 0.5 | 0.1 | 0.1 | ND | 0.5 | 0.1 | 100.7 | 0.5 |
| PAR 11/87 | 141.64 | 141.88 | Pyroxenite | 55.3 | 3.5 | 0.9 | 7.4 | 0.2 | 28.5 | 2.6 | 0.5 | 0.1 | 0.1 | ND | 0.5 | 0.1 | 99.7 | 0.3 |
| PAR 11/88 | 142.96 | 143.21 | Pyroxenite | 55.5 | 3.8 | 0.9 | 7.3 | 0.2 | 28.2 | 2.6 | 0.5 | 0.2 | 0.2 | ND | 0.5 | 0.1 | 100.0 | 0.6 |
| PAR 11/89 | 144.48 | 144.72 | Pyroxenite | 55.5 | 3.5 | 0.9 | 7.4 | 0.2 | 29.0 | 2.5 | 0.4 | 0.3 | 0.1 | ND | 0.5 | 0.1 | 100.4 | 2.7 |
| PAR 11/90 | 145.81 | 146.11 | Pyroxenite | 55.5 | 3.4 | 0.9 | 7.3 | 0.2 | 28.8 | 2.5 | 0.5 | 0.2 | 0.1 | ND | 0.5 | 0.1 | 100.1 | 2.4 |
| PAR 11/91 | 147.31 | 147.57 | Pyroxenite | 55.5 | 3.3 | 0.9 | 7.2 | 0.2 | 29.2 | 2.5 | 0.4 | 0.2 | 0.1 | ND | 0.6 | 0.1 | 100.0 | 2.7 |
| PAR 11/92 | 148.85 | 149.21 | Harzburgite | 43.3 | 2.4 | 1.3 | 10.4 | 0.2 | 38.1 | 1.8 | 0.2 | 0.1 | 0.1 | ND | 0.6 | 0.2 | 98.8 | 4.9 |
| PAR 11/93 | 149.71 | 150.10 | Harzburgite | 44.8 | 2.9 | 1.2 | 10.1 | 0.2 | 37.7 | 1.7 | 0.3 | 0.1 | 0.1 | ND | 0.7 | 0.2 | 100.0 | 6.6 |
| PAR 11/94 | 151.57 | 151.84 | Harzburgite | 44.2 | 1.6 | 1.3 | 10.5 | 0.2 | 40.4 | 1.2 | 0.3 | 0.1 | 0.1 | ND | 0.7 | 0.2 | 100.7 | 4.3 |
| PAR 11/96 | 154.11 | 154.39 | Dunite | 42.1 | 1.9 | 1.4 | 11.0 | 0.2 | 41.6 | 1.2 | 0.3 | 0.1 | 0.1 | ND | 0.7 | 0.2 | 100.7 | 3.0 |

## Table E1.1: Whole rock major element (wt%) for PAR 11 borehole by XRF.

| Sample # | DPF(m) | DPT(m) | Lithology | $SiO_2$ | $Al_2O_3$ | $Fe_2O_3$ | FeO | MnO | MgO | CaO | $Na_2O$ | $K_2O$ | $TiO_2$ | $P_2O_5$ | $Cr_2O_3$ | NiO | TOTAL | LOI |
|---|---|---|---|---|---|---|---|---|---|---|---|---|---|---|---|---|---|---|
| PAR 11/97 | 155.35 | 155.67 | Dunite | 41.3 | 2.1 | 1.4 | 11.1 | 0.2 | 41.7 | 1.3 | 0.3 | 0.2 | 0.1 | ND | 0.5 | 0.3 | 100.6 | 2.5 |
| PAR 11/98 | 156.44 | 156.78 | Dunite | 42.8 | 2.5 | 1.4 | 10.9 | 0.2 | 39.8 | 1.4 | 0.3 | 0.1 | 0.1 | ND | 1.0 | 0.2 | 100.6 | 2.8 |
| PAR 11/99 | 158.07 | 158.36 | Dunite | 41.3 | 3.6 | 1.4 | 10.9 | 0.2 | 38.7 | 1.9 | 0.5 | 0.3 | 0.1 | ND | 1.1 | 0.2 | 100.3 | 3.3 |
| PAR 11/100 | 159.49 | 159.80 | Dunite | 45.2 | 1.9 | 1.3 | 10.2 | 0.2 | 38.9 | 1.4 | 0.3 | 0.1 | 0.1 | ND | 0.5 | 0.2 | 100.3 | 2.2 |
| PAR 11/101 | 161.01 | 161.35 | Dunite | 42.1 | 2.5 | 1.4 | 11.0 | 0.2 | 40.0 | 1.6 | 0.4 | 0.2 | 0.1 | ND | 0.5 | 0.2 | 100.2 | 2.8 |
| PAR 11/102 | 162.04 | 162.74 | Harzburgite | 44.9 | 2.0 | 1.3 | 10.3 | 0.2 | 38.8 | 1.6 | 0.3 | 0.1 | 0.1 | ND | 0.5 | 0.2 | 100.2 | 2.1 |
| PAR 11/103 | 163.57 | 163.89 | Dunite | 42.1 | 3.0 | 1.4 | 11.1 | 0.2 | 39.3 | 1.3 | 0.4 | 0.3 | 0.1 | ND | 0.6 | 0.2 | 100.0 | 2.7 |
| PAR 11/104 | 164.64 | 164.88 | Dunite | 41.3 | 2.3 | 1.5 | 11.9 | 0.2 | 39.4 | 1.7 | 0.3 | 0.2 | 0.1 | ND | 0.8 | 0.2 | 99.8 | 3.1 |
| PAR 11/111 | 172.39 | 172.72 | Dunite | 41.7 | 2.7 | 1.4 | 11.1 | 0.2 | 40.4 | 1.6 | 0.4 | 0.2 | 0.1 | ND | 0.3 | 0.2 | 100.2 | 2.6 |
| PAR 11/112 | 173.59 | 173.89 | Harzburgite | 43.9 | 2.5 | 1.3 | 10.6 | 0.2 | 37.5 | 2.0 | 0.5 | 0.3 | 0.2 | ND | 0.5 | 0.2 | 99.8 | 0.5 |
| PAR 11/113 | 174.92 | 175.20 | Harzburgite | 44.0 | 2.5 | 1.3 | 10.6 | 0.2 | 37.5 | 1.6 | 0.5 | 0.2 | 0.1 | ND | 0.6 | 0.2 | 99.4 | 0.8 |
| PAR 11/114 | 176.48 | 176.72 | Dunite | 43.7 | 2.0 | 1.3 | 10.5 | 0.2 | 40.6 | 1.4 | 0.4 | 0.2 | 0.1 | ND | 0.3 | 0.2 | 100.7 | 1.7 |
| PAR 11/115 | 178.10 | 178.37 | Harzburgite | 45.0 | 1.3 | 1.3 | 10.2 | 0.2 | 40.0 | 1.1 | 0.2 | 0.1 | 0.1 | ND | 0.8 | 0.2 | 100.4 | 0.6 |
| PAR 11/116 | 179.52 | 179.81 | Dunite | 42.6 | 1.9 | 1.3 | 10.7 | 0.2 | 40.5 | 1.5 | 0.3 | 0.2 | 0.1 | ND | 0.7 | 0.2 | 100.3 | 1.1 |
| PAR 11/117 | 181.03 | 181.32 | Dunite | 40.4 | 2.1 | 1.4 | 11.3 | 0.2 | 42.2 | 1.1 | 0.3 | 0.1 | 0.1 | ND | 0.9 | 0.2 | 100.2 | 2.7 |
| PAR 11/118 | 182.53 | 182.84 | Dunite | 41.6 | 1.8 | 1.4 | 11.1 | 0.2 | 42.2 | 1.2 | 0.3 | 0.1 | 0.1 | ND | 0.3 | 0.2 | 100.4 | 3.0 |
| PAR 11/119 | 183.73 | 183.99 | Dunite | 40.3 | 1.6 | 1.4 | 11.3 | 0.2 | 42.5 | 0.9 | 0.2 | 0.1 | 0.1 | ND | 0.8 | 0.3 | 99.5 | 3.4 |
| PAR 11/120 | 183.11 | 183.45 | Dunite | 40.3 | 2.2 | 1.4 | 11.4 | 0.2 | 41.4 | 1.1 | 0.3 | 0.1 | 0.1 | ND | 1.2 | 0.2 | 99.9 | 4.3 |
| PAR 11/121 | 185.99 | 186.3 | Dunite | 39.4 | 2.0 | 1.5 | 11.8 | 0.2 | 40.6 | 1.1 | 0.2 | 0.1 | 0.1 | ND | 1.5 | 0.2 | 98.8 | 3.9 |
| PAR 11/122 | 187.70 | 188.00 | Dunite | 43.3 | 1.9 | 1.4 | 10.9 | 0.2 | 39.2 | 1.5 | 0.3 | 0.1 | 0.1 | ND | 1.0 | 0.2 | 100.1 | 2.2 |
| PAR 11/123 | 189.25 | 189.50 | Dunite | 42.8 | 2.1 | 1.3 | 10.6 | 0.2 | 40.2 | 1.3 | 0.4 | 0.2 | 0.1 | ND | 0.6 | 0.2 | 99.8 | 2.5 |
| PAR 11/124 | 190.46 | 190.70 | Dunite | 44.4 | 1.2 | 1.3 | 10.1 | 0.2 | 39.9 | 1.0 | 0.2 | ND | 0.1 | ND | 1.0 | 0.2 | 99.6 | 2.9 |
| PAR 11/125 | 191.82 | 192.13 | Dunite | 40.8 | 2.1 | 1.4 | 10.9 | 0.2 | 41.3 | 1.4 | 0.3 | 0.2 | 0.1 | ND | 0.7 | 0.2 | 99.4 | 2.6 |
| PAR 11/126 | 193.24 | 193.50 | Dunite | 42.8 | 1.8 | 1.3 | 10.5 | 0.2 | 40.5 | 1.3 | 0.3 | 0.1 | 0.1 | ND | 0.7 | 0.2 | 99.7 | 3.6 |

## Table E1.1: Whole rock major element (wt%) for PAR 11 borehole by XRF.

| Sample # | DPF(m) | DPT(m) | Lithology | $SiO_2$ | $Al_2O_3$ | $Fe_2O_3$ | FeO | MnO | MgO | CaO | $Na_2O$ | $K_2O$ | $TiO_2$ | $P_2O_5$ | $Cr_2O_3$ | NiO | TOTAL | LOI |
|---|---|---|---|---|---|---|---|---|---|---|---|---|---|---|---|---|---|---|
| PAR 11/127 | 194.64 | 194.96 | Dunite | 45.6 | 1.8 | 1.2 | 9.9 | 0.2 | 38.6 | 1.5 | 0.3 | 0.1 | 0.1 | ND | 0.8 | 0.2 | 100.2 | 2.9 |
| PAR 11/128 | 195.92 | 196.20 | Dunite | 40.8 | 2.3 | 1.4 | 11.2 | 0.2 | 41.5 | 1.2 | 0.3 | 0.2 | 0.1 | ND | 1.0 | 0.3 | 100.2 | 3.3 |
| PAR 11/129 | 197.14 | 197.44 | Dunite | 40.7 | 2.0 | 1.4 | 11.3 | 0.2 | 41.7 | 1.2 | 0.3 | 0.1 | 0.1 | ND | 1.0 | 0.3 | 100.3 | 3.2 |
| PAR 11/130 | 198.74 | 198.98 | Dunite | 40.9 | 1.6 | 1.4 | 11.3 | 0.2 | 42.5 | 1.0 | 0.2 | 0.1 | 0.1 | ND | 0.5 | 0.3 | 100.0 | 3.2 |
| PAR 11/131 | 200.35 | 200.6 | Dunite | 41.5 | 2.3 | 1.4 | 11.0 | 0.2 | 41.2 | 1.5 | 0.4 | 0.2 | 0.1 | ND | 0.4 | 0.3 | 100.3 | 2.5 |
| PAR 11/132 | 201.40 | 201.98 | Dunite | 42.1 | 2.1 | 1.3 | 10.8 | 0.2 | 40.6 | 1.3 | 0.3 | 0.2 | 0.1 | ND | 1.0 | 0.2 | 100.2 | 2.5 |
| PAR 11/133 | 203.19 | 203.48 | Dunite | 46.9 | 1.7 | 1.2 | 9.5 | 0.2 | 37.8 | 1.5 | 0.3 | 0.1 | 0.1 | ND | 0.7 | 0.2 | 100.2 | 1.1 |
| PAR 11/134 | 204.50 | 204.76 | Dunite | 42.5 | 1.8 | 1.3 | 10.6 | 0.2 | 40.9 | 1.2 | 0.3 | 0.2 | 0.1 | ND | 0.9 | 0.2 | 100.1 | 3.1 |
| PAR 11/135 | 206.04 | 206.32 | Dunite | 40.9 | 1.8 | 1.4 | 11.0 | 0.2 | 42.4 | 1.1 | 0.3 | 0.1 | 0.1 | ND | 0.7 | 0.3 | 100.2 | 3.6 |
| PAR 11/136 | 207.00 | 207.42 | Dunite | 41.5 | 1.5 | 1.4 | 10.9 | 0.2 | 42.4 | 1.1 | 0.3 | 0.1 | 0.1 | ND | 0.6 | 0.3 | 100.2 | 4.5 |
| PAR 11/137 | 208.68 | 208.91 | Dunite | 42.7 | 1.4 | 1.3 | 10.4 | 0.2 | 40.9 | 1.1 | 0.2 | 0.1 | 0.1 | ND | 1.1 | 0.2 | 99.8 | 2.1 |
| PAR 11/138 | 210.14 | 210.45 | Dunite | 41.2 | 1.5 | 1.4 | 11.0 | 0.2 | 42.6 | 1.1 | 0.2 | 0.1 | 0.1 | ND | 0.5 | 0.3 | 100.1 | 4.4 |
| PAR 11/139 | 211.32 | 212.65 | Dunite | 41.3 | 1.4 | 1.4 | 11.1 | 0.2 | 43.1 | 1.0 | 0.2 | ND | 0.1 | ND | 0.4 | 0.3 | 100.3 | 5.0 |
| PAR 11/140 | 212.53 | 212.80 | Dunite | 41.3 | 1.7 | 1.4 | 11.0 | 0.2 | 42.7 | 1.1 | 0.2 | 0.1 | 0.1 | ND | 0.3 | 0.3 | 100.2 | 5.3 |
| PAR 11/141 | 213.74 | 213.98 | Harzburgite | 44.2 | 1.5 | 1.3 | 10.2 | 0.2 | 40.1 | 1.2 | 0.3 | 0.1 | 0.1 | ND | 0.8 | 0.2 | 100.0 | 2.4 |
| PAR 11/142 | 215.28 | 215.59 | Harzburgite | 43.9 | 1.5 | 1.3 | 10.3 | 0.2 | 40.5 | 1.2 | 0.3 | 0.1 | 0.1 | ND | 0.8 | 0.2 | 100.2 | 3.3 |
| PAR 11/143 | 216.53 | 216.80 | Harzburgite | 43.3 | 1.8 | 1.3 | 10.4 | 0.2 | 40.4 | 1.2 | 0.3 | 0.1 | 0.1 | ND | 0.8 | 0.2 | 100.1 | 3.1 |
| PAR 11/144 | 218.36 | 218.61 | Dunite | 42.8 | 1.7 | 1.3 | 10.7 | 0.2 | 41.3 | 1.2 | 0.4 | 0.1 | 0.1 | ND | 0.8 | 0.3 | 100.7 | 3.7 |
| PAR 11/145 | 219.50 | 219.76 | Dunite | 43.1 | 1.8 | 1.3 | 10.5 | 0.2 | 40.6 | 1.2 | 0.3 | 0.1 | 0.1 | ND | 0.7 | 0.2 | 100.1 | 4.1 |
| PAR 11/146 | 221.23 | 221.50 | Dunite | 42.0 | 2.8 | 1.3 | 10.7 | 0.2 | 40.4 | 1.4 | 0.5 | 0.3 | 0.1 | ND | 0.6 | 0.3 | 100.5 | 3.8 |
| PAR 11/147 | 222.44 | 222.69 | Dunite | 40.7 | 1.7 | 1.4 | 11.0 | 0.2 | 42.8 | 0.9 | 0.3 | 0.1 | 0.1 | ND | 0.7 | 0.3 | 100.1 | 3.3 |
| PAR 11/148 | 223.74 | 223.99 | Harzburgite | 44.4 | 1.5 | 1.3 | 10.1 | 0.2 | 40.1 | 1.2 | 0.2 | 0.1 | 0.1 | ND | 0.8 | 0.2 | 100.2 | 2.5 |
| PAR 11/149 | 225.20 | 225.48 | Ol-pyroxenite | 48.3 | 1.6 | 1.1 | 9.2 | 0.2 | 37.8 | 1.3 | 0.3 | 0.1 | 0.1 | ND | 0.8 | 0.2 | 100.9 | 1.5 |

## Table E1.1: Whole rock major element (wt%) for PAR 11 borehole by XRF.

| Sample # | DPF(m) | DPT(m) | Lithology | $SiO_2$ | $Al_2O_3$ | $Fe_2O_3$ | FeO | MnO | MgO | CaO | $Na_2O$ | $K_2O$ | $TiO_2$ | $P_2O_5$ | $Cr_2O_3$ | NiO | TOTAL | LOI |
|---|---|---|---|---|---|---|---|---|---|---|---|---|---|---|---|---|---|---|
| PAR 11/150 | 226.66 | 226.96 | Dunite | 40.6 | 2.2 | 1.4 | 10.9 | 0.2 | 41.4 | 1.1 | 0.4 | 0.2 | 0.1 | ND | 0.8 | 0.3 | 99.4 | 1.7 |
| PAR 11/151 | 228.12 | 228.39 | Olivine-pyroxenite | 46.4 | 1.5 | 1.2 | 9.4 | 0.2 | 37.9 | 1.1 | 0.2 | 0.1 | 0.1 | ND | 0.9 | 0.2 | 99.2 | 1.6 |
| PAR 11/152 | 229.65 | 229.93 | Harzburgite | 43.4 | 1.9 | 1.3 | 10.3 | 0.2 | 39.9 | 1.3 | 0.3 | 0.1 | 0.1 | ND | 0.9 | 0.2 | 99.9 | 2.6 |
| MR330 153 | 61.79 | 62.01 | Harzburgite | 46.4 | 9.3 | 1.4 | 11.4 | 0.2 | 25.1 | 5.3 | 0.5 | ND | 0.1 | ND | 0.2 | 0.1 | 100.2 | 3.0 |
| VR58 154 | 210.51 | 210.81 | Olivine-pyroxenite | 49.6 | 2.5 | 1.5 | 11.9 | 0.2 | 30.9 | 2.4 | 0.2 | 0.1 | 0.1 | ND | 0.2 | 0.3 | 100.0 | 4.1 |
| PAR316 155 | 107.6 | 107.99 | Harzburgite | 44.7 | 1.9 | 1.6 | 13.2 | 0.2 | 35.7 | 1.8 | 0.2 | ND | 0.1 | ND | 0.2 | 0.2 | 99.7 | 8.4 |
| PAR28 156 | 179.31 | 179.64 | Harzburgite | 45.1 | 6.5 | 1.4 | 11.5 | 0.2 | 31.2 | 3.5 | 0.3 | ND | 0.1 | ND | 0.3 | 0.2 | 100.2 | 6.7 |
| MR328 157 | 57.21 | 57.44 | Websterite | 49.7 | 3.6 | 1.4 | 10.9 | 0.2 | 22.9 | 8.7 | 0.1 | ND | 0.3 | ND | 0.5 | 0.2 | 98.4 | 1.6 |
| MR330 158 | 47.19 | 47.45 | Gabbro | 50.3 | 22.4 | 0.5 | 3.6 | 0.1 | 7.2 | 11.5 | 2.8 | 1.0 | 0.0 | ND | 0.2 | 0.1 | 99.4 | 3.5 |
| MR327 159 | 162.79 | 163.05 | Harzburgite | 43.6 | 2.2 | 1.6 | 12.7 | 0.2 | 37.7 | 1.3 | 0.1 | ND | 0.1 | ND | 0.5 | 0.3 | 100.2 | 8.8 |

## Table E1.2: Whole rock trace element and sulphur analyses (ppm) for PAR 11 borehole by XRF.

| Sample # | DPF(m) | DPT(m) | Lithology | Sc | V | Cr | Co | Ni | Cu | Zn | Ga | Rb | Sr | Y | Zr | Nb | Ba | Pb | S |
|---|---|---|---|---|---|---|---|---|---|---|---|---|---|---|---|---|---|---|---|
| PAR 11/1 | 18.77 | 18.94 | Pyroxenite | 19.6 | 89.2 | 3470.5 | 87.9 | 648.4 | 34.0 | 63.3 | 3.3 | 4.3 | 19.2 | 2.4 | 8.0 | 1.3 | 30.0 | 0.3 | 1238.0 |
| PAR 11/2 | 20.78 | 20.96 | Pyroxenite | 19.8 | 84.5 | 3402.7 | 88.9 | 643.0 | 31.7 | 61.6 | 4.6 | 5.7 | 20.4 | 1.7 | 6.8 | 1.1 | 38.7 | -0.1 | 1411.2 |
| PAR 11/3 | 23.25 | 23.36 | Pyroxenite | 21.7 | 82.4 | 3338.5 | 86.9 | 642.9 | 36.1 | 61.6 | 4.1 | 4.9 | 24.8 | 1.7 | 8.1 | 1.2 | 32.9 | 1.8 | 1378.8 |
| PAR 11/4 | 24.12 | 24.32 | Pyroxenite | 19.9 | 80.6 | 3429.4 | 87.7 | 636.8 | 27.9 | 62.0 | 2.5 | 5.8 | 15.7 | 1.7 | 9.5 | 1.1 | 37.9 | 1.9 | 1450.2 |
| PAR 11/5 | 25.49 | 25.69 | Pyroxenite | 19.9 | 79.1 | 3516.3 | 84.1 | 642.6 | 28.5 | 61.2 | 3.1 | 6.3 | 21.3 | 2.7 | 9.8 | 1.4 | 50.4 | 2.8 | 1361.0 |
| PAR 11/6 | 27.14 | 23.37 | Pyroxenite | 24.9 | 86.7 | 3424.1 | 82.9 | 612.6 | 33.4 | 61.5 | 4.3 | 8.2 | 33.9 | 2.9 | 9.8 | 0.8 | 45.7 | 1.6 | 5235.0 |
| PAR 11/7 | 29.15 | 29.35 | Pyroxenite | 22.3 | 95.3 | 3174.5 | 79.9 | 623.3 | 39.5 | 61.5 | 3.9 | 12.1 | 36.9 | 2.9 | 14.6 | 1.2 | 69.5 | 1.6 | 1622.2 |
| PAR 11/8 | 30.35 | 30.60 | Pyroxenite | 22.5 | 87.6 | 3715.1 | 94.1 | 805.7 | 31.3 | 63.9 | 4.7 | 7.9 | 37.4 | 2.4 | 8.6 | 1.1 | 46.1 | 2.3 | 1952.5 |
| PAR 11/9 | 30.77 | 31.02 | Harzburgite | 13.2 | 53.8 | 3678.2 | 131.3 | 1498.7 | 7.8 | 68.8 | 1.5 | 4.5 | 11.4 | 2.0 | 6.8 | 1.1 | 22.8 | 2.5 | 3326.5 |
| PAR 11/10 | 32.10 | 32.33 | Harzburgite | 8.7 | 47.5 | 2989.4 | 142.1 | 1705.7 | 35.2 | 68.1 | 2.2 | 5.5 | 24.8 | 1.3 | 7.2 | 1.2 | 38.6 | 2.8 | 3920.6 |
| PAR 11/11 | 33.21 | 33.43 | Harzburgite | 10.6 | 52.8 | 3286.3 | 153.0 | 1833.4 | 70.9 | 71.6 | 2.2 | 9.5 | 21.5 | 2.7 | 15.8 | 1.8 | 46.1 | 3.7 | 4495.8 |
| PAR 11/12 | 34.37 | 34.63 | Lherzolite | 15.9 | 60.8 | 3317.0 | 144.5 | 1707.0 | 74.0 | 69.6 | 2.7 | 6.1 | 24.1 | 1.4 | 6.8 | -0.4 | 30.2 | 2.5 | 4622.8 |
| PAR 11/13 | 35.48 | 35.69 | Harzburgite | 13.2 | 40.0 | 2386.9 | 143.1 | 1677.6 | 20.2 | 70.9 | 1.9 | 6.7 | 17.4 | 0.6 | 7.6 | -0.1 | 37.5 | 1.2 | 5232.0 |
| PAR 11/14 | 37.24 | 37.44 | Harzburgite | 8.3 | 48.3 | 3314.6 | 145.5 | 1740.5 | 27.1 | 75.1 | 1.0 | 9.2 | 19.1 | 0.5 | 11.1 | -0.3 | 43.8 | 1.7 | 4680.4 |
| PAR 11/15 | 38.61 | 38.82 | Harzburgite | 9.7 | 44.3 | 3389.5 | 152.4 | 1753.4 | 16.2 | 70.2 | 1.7 | 7.6 | 14.7 | 1.1 | 10.5 | 0.2 | 28.2 | 1.2 | 4590.8 |
| PAR 11/16 | 40.32 | 40.61 | Harzburgite | 9.6 | 41.9 | 2269.9 | 147.5 | 1692.5 | 17.1 | 72.1 | 1.5 | 8.0 | 11.5 | 1.4 | 7.9 | -0.3 | 38.7 | 1.3 | 4635.0 |
| PAR 11/17 | 41.43 | 41.69 | Dunite | 10.2 | 44.7 | 2834.4 | 158.7 | 1822.0 | 29.7 | 74.4 | 3.5 | 7.9 | 28.0 | 1.4 | 9.9 | -0.2 | 30.1 | 2.0 | 5265.8 |
| PAR 11/18 | 43.12 | 43.37 | Dunite | 6.2 | 35.1 | 2410.6 | 156.9 | 1806.6 | 22.8 | 73.3 | 1.8 | 6.7 | 24.8 | 1.0 | 9.5 | -0.3 | 33.8 | 1.1 | 5257.5 |
| PAR 11/19 | 44.70 | 44.96 | Dunite | 7.6 | 44.3 | 4178.8 | 152.4 | 1770.9 | 15.9 | 72.6 | 1.4 | 4.8 | 15.0 | 0.2 | 4.8 | -0.3 | 28.0 | 0.2 | 4654.9 |
| PAR 11/20 | 46.12 | 46.40 | Dunite | 10.0 | 66.0 | 6253.0 | 160.3 | 1845.9 | 37.9 | 74.5 | 2.5 | 7.9 | 17.7 | 1.2 | 10.4 | -0.4 | 24.4 | 1.9 | 4508.1 |
| PAR 11/21 | 47.37 | 47.69 | Dunite | 10.1 | 38.4 | 3084.4 | 148.6 | 1738.4 | 15.2 | 73.1 | 1.2 | 8.5 | 23.9 | 1.3 | 8.4 | -0.2 | 47.8 | 1.9 | 4168.8 |
| PAR 11/22 | 48.45 | 48.73 | Dunite | 6.4 | 35.7 | 1698.3 | 152.3 | 1747.2 | 18.8 | 73.5 | 3.7 | 15.2 | 38.2 | 1.9 | 16.7 | 0.1 | 63.5 | 0.8 | 4509.4 |
| PAR 11/23 | 50.13 | 50.37 | Dunite | 10.0 | 38.5 | 2322.8 | 164.6 | 1771.2 | 19.2 | 75.8 | 3.5 | 6.4 | 25.1 | 1.1 | 9.0 | -0.8 | 33.3 | 2.1 | 4789.0 |
| PAR 11/24 | 51.60 | 51.83 | Dunite | 7.5 | 52.3 | 5334.2 | 164.8 | 1791.8 | 23.3 | 84.2 | 2.7 | 12.7 | 152.8 | 1.6 | 9.9 | -0.3 | 461.5 | 0.5 | 4474.9 |

## Table E1.2: Whole rock trace element and sulphur analyses (ppm) for PAR 11 borehole by XRF.

| Sample # | DPF(m) | DPT(m) | Lithology | Sc | V | Cr | Co | Ni | Cu | Zn | Ga | Rb | Sr | Y | Zr | Nb | Ba | Pb | S |
|---|---|---|---|---|---|---|---|---|---|---|---|---|---|---|---|---|---|---|---|
| PAR 11/25 | 53.06 | 53.33 | Harzburgite | 12.6 | 51.2 | 3746.6 | 159.0 | 1727.5 | 21.2 | 76.3 | 1.2 | 9.4 | 19.6 | 1.0 | 11.0 | -0.3 | 45.6 | 2.0 | 4490.8 |
| PAR 11/26 | 54.67 | 54.93 | Harzburgite | 11.5 | 61.0 | 4503.0 | 140.2 | 1401.5 | 15.6 | 75.8 | 3.2 | 5.9 | 15.0 | 0.9 | 7.0 | 0.2 | 30.4 | 1.6 | 3769.5 |
| PAR 11/27 | 55.96 | 56.03 | Harzburgite | 13.1 | 64.1 | 4785.9 | 155.7 | 1594.8 | 32.7 | 70.6 | 4.7 | 11.7 | 39.9 | 3.2 | 15.2 | 1.1 | 57.1 | 2.1 | 4790.9 |
| PAR 11/28 | 57.01 | 57.38 | Harzburgite | 11.3 | 72.2 | 6770.1 | 156.8 | 1628.0 | 22.2 | 81.2 | 3.0 | 10.4 | 33.1 | 2.5 | 9.8 | 0.2 | 56.9 | 0.9 | 4409.0 |
| PAR 11/29 | 58.49 | 58.82 | Dunite | 6.6 | 68.8 | 6200.3 | 162.7 | 1783.8 | 24.5 | 84.5 | 3.4 | 9.9 | 32.4 | 1.3 | 12.5 | 0.3 | 62.0 | 3.9 | 4770.4 |
| PAR 11/30 | 59.74 | 59.99 | Harzburgite | 12.2 | 59.1 | 3917.9 | 147.5 | 1538.2 | 19.1 | 77.8 | 3.4 | 7.3 | 30.6 | 0.8 | 8.6 | 0.3 | 50.4 | 3.9 | 4353.6 |
| PAR 11/31 | 61.00 | 61.36 | Harzburgite | 10.4 | 57.6 | 4106.0 | 149.6 | 1566.6 | 22.8 | 72.0 | 3.0 | 10.0 | 36.0 | 1.4 | 11.1 | 0.3 | 52.5 | 3.5 | 4705.1 |
| PAR 11/32 | 62.73 | 63.00 | Dunite | 8.4 | 39.0 | 1718.0 | 153.1 | 1646.7 | 23.5 | 74.5 | 3.2 | 9.2 | 39.2 | 1.5 | 13.2 | 0.2 | 53.9 | 2.8 | 4451.3 |
| PAR 11/33 | 64.12 | 64.41 | Harzburgite | 9.2 | 49.8 | 3070.5 | 147.2 | 1578.0 | 22.1 | 73.7 | 1.6 | 6.7 | 22.1 | 1.8 | 7.2 | -0.5 | 26.0 | 2.7 | 4282.6 |
| PAR 11/34 | 65.76 | 66.03 | Harzburgite | 13.9 | 52.0 | 3702.3 | 140.4 | 1434.2 | 7.2 | 74.2 | 4.0 | 4.3 | 10.4 | -0.5 | 5.5 | 0.6 | 28.0 | 0.2 | 3282.2 |
| PAR 11/35 | 66.67 | 66.90 | Harzburgite | 12.4 | 70.8 | 6148.8 | 138.0 | 1394.4 | 12.1 | 74.6 | 1.6 | 4.3 | 13.6 | 0.1 | 7.3 | 0.9 | 27.3 | -0.2 | 3196.9 |
| PAR 11/36 | 68.18 | 68.41 | Dunite | 9.8 | 67.9 | 6535.2 | 161.5 | 1694.5 | 28.3 | 82.1 | 3.3 | 6.0 | 36.2 | 1.5 | 9.7 | 1.5 | 50.0 | 2.2 | 3837.3 |
| PAR 11/37 | 69.75 | 70.00 | Harzburgite | 13.5 | 56.6 | 2767.9 | 131.5 | 1312.7 | 16.0 | 73.2 | 2.6 | 8.3 | 20.7 | 0.7 | 10.4 | 0.5 | 48.1 | 1.5 | 2956.4 |
| PAR 11/38 | 71.27 | 71.57 | Dunite | 6.4 | 38.8 | 2130.1 | 166.9 | 1806.4 | 19.9 | 77.5 | 2.3 | 5.7 | 29.6 | 1.8 | 10.4 | 2.5 | 47.2 | 1.9 | 3458.0 |
| PAR 11/39 | 72.45 | 72.71 | Harzburgite | 13.8 | 62.6 | 3459.2 | 138.1 | 1379.6 | 17.4 | 73.6 | 0.8 | 3.9 | 11.0 | ND | 7.5 | 0.3 | 22.2 | 3.1 | 2890.7 |
| PAR 11/40 | 73.63 | 73.96 | Dunite | 6.6 | 43.6 | 3601.0 | 162.5 | 1772.1 | 31.9 | 82.7 | 3.1 | 6.9 | 35.2 | 1.5 | 10.0 | 0.4 | 61.7 | 2.0 | 4105.7 |
| PAR 11/41 | 75.22 | 75.46 | Harzburgite | 10.2 | 60.2 | 3816.2 | 141.2 | 1452.0 | 22.5 | 75.5 | 2.9 | 5.5 | 16.6 | 1.8 | 8.6 | 1.4 | 39.8 | 2.5 | 3639.6 |
| PAR 11/42 | 76.39 | 76.67 | Harzburgite | 7.8 | 44.5 | 3846.3 | 154.6 | 1516.0 | 17.4 | 74.9 | 3.4 | 10.1 | 33.4 | 1.3 | 15.1 | 1.4 | 75.2 | 2.6 | 3857.7 |
| PAR 11/42A | 78.07 | 78.30 | Harzburgite | 11.8 | 51.9 | 3499.8 | 138.8 | 1481.1 | 20.0 | 75.4 | 3.5 | 4.9 | 17.8 | 1.2 | 7.9 | 1.0 | 35.1 | 2.6 | 2404.6 |
| PAR 11/43 | 79.57 | 79.94 | Dunite | 7.2 | 32.9 | 2194.1 | 161.7 | 1719.7 | 16.9 | 75.0 | 1.9 | 7.0 | 31.7 | 0.8 | 10.5 | 1.0 | 54.9 | 3.5 | 4624.2 |
| PAR 11/44 | 80.63 | 80.90 | Dunite | 7.7 | 55.5 | 3047.3 | 158.3 | 1699.2 | 19.4 | 79.9 | 2.3 | 11.9 | 33.8 | 1.8 | 16.7 | 1.7 | 85.4 | 2.6 | 3687.6 |
| PAR 11/45 | 81.73 | 82.00 | Harzburgite | 14.1 | 82.1 | 6803.5 | 128.5 | 1231.9 | 19.8 | 74.5 | 2.5 | 6.1 | 16.9 | 0.7 | 8.3 | -0.9 | 39.0 | 0.1 | 2774.3 |
| PAR 11/46 | 83.57 | 83.84 | Harzburgite | 10.4 | 63.5 | 3564.0 | 123.5 | 1152.4 | 13.1 | 68.4 | 2.2 | 4.1 | 14.0 | 0.7 | 5.6 | 0.7 | 32.1 | 1.5 | 2765.7 |

## Table E1.2: Whole rock trace element and sulphur analyses (ppm) for PAR 11 borehole by XRF.

| Sample # | DPF(m) | DPT(m) | Lithology | Sc | V | Cr | Co | Ni | Cu | Zn | Ga | Rb | Sr | Y | Zr | Nb | Ba | Pb | S |
|---|---|---|---|---|---|---|---|---|---|---|---|---|---|---|---|---|---|---|---|
| PAR 11/47 | 84.35 | 84.63 | Harzburgite | 7.9 | 50.1 | 2861.7 | 151.1 | 1637.3 | 50.2 | 73.7 | 2.2 | 2.8 | 14.9 | 0.8 | 6.6 | 0.8 | 24.3 | 0.6 | 3960.5 |
| PAR 11/48 | 86.36 | 86.56 | Pyroxenite | 16.1 | 82.9 | 3414.6 | 84.6 | 614.1 | 30.6 | 61.5 | 3.3 | 6.2 | 26.6 | 1.7 | 11.4 | 0.6 | 51.0 | 2.4 | 1917.3 |
| PAR 11/49 | 87.36 | 87.58 | Pyroxenite | 22.2 | 87.4 | 4015.9 | 90.8 | 628.2 | 36.7 | 63.3 | 4.0 | 6.2 | 26.7 | 2.0 | 9.7 | 0.5 | 45.8 | -0.1 | 1816.5 |
| PAR 11/50 | 89.04 | 89.26 | Pyroxenite | 20.4 | 91.3 | 3492.0 | 88.6 | 622.5 | 37.4 | 63.8 | 3.7 | 7.8 | 29.0 | 2.7 | 12.8 | 1.4 | 54.2 | 2.4 | 2165.6 |
| PAR 11/51 | 90.64 | 90.87 | Pyroxenite | 21.3 | 83.9 | 3272.5 | 85.8 | 644.6 | 48.3 | 63.1 | 3.8 | 6.2 | 30.1 | 2.9 | 10.4 | 0.5 | 51.2 | 1.2 | 2030.6 |
| PAR 11/52 | 91.91 | 92.16 | Pyroxenite | 19.8 | 86.2 | 3517.9 | 84.7 | 650.2 | 49.9 | 62.7 | 4.4 | 7.4 | 27.5 | 2.1 | 13.6 | 0.9 | 65.5 | 1.2 | 1920.8 |
| PAR 11/53 | 93.34 | 93.58 | Pyroxenite | 19.4 | 83.0 | 3055.7 | 95.6 | 720.4 | 45.5 | 63.9 | 4.0 | 7.1 | 30.4 | 2.0 | 10.7 | 0.5 | 51.4 | 0.7 | 1652.5 |
| PAR 11/54 | 94.68 | 94.92 | Pyroxenite | 20.0 | 86.7 | 3485.6 | 82.1 | 635.6 | 45.1 | 62.3 | 3.6 | 7.2 | 28.8 | 2.1 | 12.4 | 1.3 | 57.2 | 0.5 | 1238.4 |
| PAR 11/55 | 96.12 | 96.42 | Pyroxenite | 19.3 | 92.5 | 3342.7 | 89.1 | 662.5 | 54.3 | 63.1 | 5.5 | 8.1 | 28.1 | 2.0 | 11.4 | 0.4 | 58.9 | 2.4 | 1682.8 |
| PAR 11/56 | 97.76 | 98.00 | Pyroxenite | 6.1 | 30.1 | 1961.6 | 167.7 | 1924.1 | 3.9 | 73.7 | 1.9 | 1.3 | 15.8 | 0.7 | 7.7 | 2.1 | 19.9 | 0.8 | 1567.0 |
| PAR 11/57 | 99.23 | 99.47 | Pyroxenite | 19.7 | 94.0 | 3271.3 | 83.0 | 611.6 | 28.9 | 61.6 | 4.8 | 7.3 | 26.9 | 2.7 | 13.3 | 0.4 | 54.5 | 1.2 | 1116.0 |
| PAR 11/58 | 100.64 | 100.85 | Pyroxenite | 18.4 | 88.9 | 3218.9 | 84.6 | 591.0 | 32.5 | 60.6 | 4.0 | 6.9 | 27.4 | 1.9 | 12.2 | 0.3 | 53.8 | 4.7 | 1293.6 |
| PAR 11/59 | 102.14 | 102.4 | Pyroxenite | 19.2 | 89.0 | 3311.5 | 89.8 | 610.2 | 30.6 | 62.6 | 4.1 | 8.1 | 27.6 | 2.1 | 12.3 | 1.0 | 62.5 | 3.0 | 1547.0 |
| PAR 11/60 | 103.37 | 103.54 | Pyroxenite | 21.0 | 83.3 | 3396.2 | 85.2 | 593.0 | 29.6 | 63.4 | 4.6 | 7.2 | 26.1 | 3.1 | 12.4 | 2.4 | 58.5 | 4.2 | 1441.5 |
| PAR 11/61 | 104.98 | 105.19 | Pyroxenite | 18.6 | 78.0 | 3282.6 | 87.6 | 599.4 | 32.6 | 62.0 | 3.8 | 7.6 | 28.8 | 3.3 | 12.9 | 2.1 | 51.3 | 2.9 | 1609.9 |
| PAR 11/62 | 106.35 | 106.54 | Pyroxenite | 20.4 | 86.8 | 3330.1 | 83.7 | 593.7 | 27.8 | 64.0 | 4.8 | 6.3 | 28.0 | 3.7 | 12.3 | 1.4 | 61.6 | 2.0 | 1184.9 |
| PAR 11/63 | 107.57 | 107.76 | Pyroxenite | 18.6 | 80.6 | 3238.7 | 84.8 | 595.8 | 25.9 | 63.0 | 3.8 | 6.9 | 26.6 | 3.3 | 13.7 | 0.9 | 51.2 | 1.4 | 1294.5 |
| PAR 11/64 | 109.00 | 109.42 | Pyroxenite | 19.1 | 85.1 | 3262.3 | 86.2 | 602.6 | 27.3 | 59.4 | 4.2 | 6.8 | 28.0 | 3.1 | 13.4 | 1.6 | 60.9 | 2.0 | 1245.2 |
| PAR 11/65 | 110.41 | 110.64 | Pyroxenite | 19.5 | 85.1 | 3218.8 | 83.8 | 594.9 | 23.0 | 61.8 | 4.7 | 7.7 | 27.3 | 4.0 | 14.4 | 0.6 | 53.2 | 1.3 | 1310.5 |
| PAR 11/66 | 111.57 | 111.78 | Pyroxenite | 19.1 | 81.5 | 3347.4 | 86.1 | 598.7 | 26.8 | 61.9 | 3.9 | 7.2 | 27.3 | 3.3 | 14.4 | 0.8 | 53.3 | 2.8 | 1213.9 |
| PAR 11/67 | 113.25 | 113.50 | Pyroxenite | 18.6 | 86.9 | 3200.6 | 86.3 | 582.8 | 22.5 | 61.7 | 4.2 | 8.8 | 26.2 | 2.9 | 14.3 | 2.2 | 56.4 | 2.0 | 1125.4 |
| PAR 11/68 | 114.38 | 114.59 | Pyroxenite | 19.0 | 80.4 | 3772.4 | 82.9 | 590.9 | 28.0 | 62.4 | 3.6 | 6.3 | 26.2 | 2.0 | 13.1 | 2.9 | 50.3 | 2.9 | 1348.0 |
| PAR 11/69 | 115.54 | 115.88 | Pyroxenite | 16.6 | 79.8 | 3151.2 | 83.8 | 591.5 | 21.9 | 61.0 | 4.5 | 8.2 | 27.0 | 1.5 | 14.3 | 2.2 | 56.7 | 2.1 | 1527.0 |
| PAR 11/70 | 117.26 | 117.49 | Pyroxenite | 19.1 | 80.5 | 3215.1 | 84.3 | 593.8 | 27.3 | 60.0 | 4.2 | 7.1 | 21.9 | 1.5 | 12.1 | 1.7 | 53.1 | 1.4 | 1833.5 |

## Table E1.2: Whole rock trace element and sulphur analyses (ppm) for PAR 11 borehole by XRF.

| Sample # | DPF(m) | DPT(m) | Lithology | Sc | V | Cr | Co | Ni | Cu | Zn | Ga | Rb | Sr | Y | Zr | Nb | Ba | Pb | S |
|---|---|---|---|---|---|---|---|---|---|---|---|---|---|---|---|---|---|---|---|
| PAR 11/71 | 118.65 | 118.88 | Pyroxenite | 19.2 | 86.2 | 4839.8 | 96.0 | 717.4 | 20.5 | 65.8 | 2.6 | 3.8 | 15.3 | 1.1 | 8.3 | 1.9 | 34.9 | 2.5 | 2031.1 |
| PAR 11/72 | 119.73 | 119.97 | Pyroxenite | 18.0 | 75.7 | 3253.4 | 85.3 | 602.5 | 19.9 | 59.3 | 4.2 | 6.0 | 15.2 | 2.9 | 11.1 | 0.4 | 28.4 | 0.3 | 1816.5 |
| PAR 11/73 | 121.25 | 121.46 | Pyroxenite | 18.7 | 81.2 | 3216.2 | 85.9 | 595.1 | 24.8 | 57.8 | 3.7 | 6.8 | 22.9 | 3.4 | 10.6 | 0.3 | 45.7 | 4.0 | 1695.7 |
| PAR 11/74 | 122.50 | 122.78 | Pyroxenite | 19.9 | 77.9 | 3222.1 | 83.6 | 596.2 | 27.5 | 60.3 | 2.9 | 6.9 | 26.6 | 3.3 | 11.8 | 1.1 | 38.8 | 1.1 | 1354.7 |
| PAR 11/75 | 124.14 | 124.39 | Pyroxenite | 22.1 | 80.7 | 3252.7 | 85.8 | 631.4 | 21.9 | 62.2 | 3.4 | 6.3 | 23.7 | 2.6 | 10.4 | 0.5 | 52.9 | 1.7 | 1605.4 |
| PAR 11/76 | 126.21 | 126.40 | Pyroxenite | 20.6 | 83.4 | 3269.9 | 87.7 | 598.0 | 21.9 | 61.0 | 3.9 | 8.1 | 26.0 | 3.3 | 10.8 | 1.0 | 46.9 | 0.0 | 1434.2 |
| PAR 11/77 | 127.14 | 127.34 | Pyroxenite | 18.7 | 80.7 | 3246.4 | 87.1 | 591.5 | 22.2 | 61.3 | 4.2 | 7.4 | 25.8 | 2.5 | 12.1 | 2.4 | 51.1 | 2.9 | 1236.1 |
| PAR 11/78 | 128.71 | 128.93 | Pyroxenite | 20.7 | 84.8 | 3253.4 | 82.2 | 596.6 | 27.9 | 61.1 | 3.7 | 6.7 | 24.8 | 1.3 | 10.3 | 2.1 | 45.6 | 3.5 | 1073.0 |
| PAR 11/79 | 129.68 | 129.85 | Pyroxenite | 20.2 | 84.1 | 3271.1 | 90.7 | 606.2 | 23.6 | 60.7 | 3.0 | 7.8 | 25.3 | 2.7 | 12.1 | 2.4 | 44.9 | 1.4 | 1165.3 |
| PAR 11/80 | 131.36 | 131.55 | Pyroxenite | 22.1 | 91.1 | 3294.0 | 90.3 | 595.4 | 22.8 | 61.2 | 4.8 | 7.1 | 23.6 | 2.5 | 12.3 | 2.5 | 52.0 | 0.8 | 1208.5 |
| PAR 11/81 | 132.74 | 132.98 | Pyroxenite | 18.7 | 85.3 | 3242.4 | 85.7 | 594.6 | 21.1 | 59.9 | 3.3 | 6.5 | 26.4 | 2.5 | 11.0 | 3.2 | 44.9 | 1.2 | 1281.7 |
| PAR 11/82 | 134.24 | 134.52 | Pyroxenite | 18.4 | 89.2 | 3314.9 | 86.7 | 605.6 | 23.3 | 63.3 | 4.2 | 7.7 | 25.4 | 2.3 | 9.4 | 0.1 | 53.4 | 1.0 | 1052.4 |
| PAR 11/83 | 135.66 | 135.93 | Pyroxenite | 20.3 | 94.8 | 3380.3 | 85.8 | 602.5 | 20.2 | 60.3 | 3.3 | 6.9 | 24.9 | 2.8 | 11.5 | 0.0 | 56.6 | 1.2 | 1170.6 |
| PAR 11/84 | 136.61 | 136.82 | Pyroxenite | 21.1 | 82.1 | 3349.4 | 86.3 | 592.1 | 25.9 | 60.6 | 3.6 | 7.2 | 27.3 | 2.4 | 11.8 | 0.1 | 44.6 | 0.8 | 1179.5 |
| PAR 11/85 | 138.67 | 138.94 | Pyroxenite | 22.5 | 87.5 | 3374.6 | 84.3 | 601.9 | 20.6 | 60.8 | 4.1 | 7.0 | 24.7 | 2.8 | 10.4 | 0.2 | 55.0 | 1.8 | 1131.8 |
| PAR 11/86 | 140.18 | 140.42 | Pyroxenite | 20.5 | 87.5 | 3245.9 | 85.6 | 607.0 | 23.1 | 59.9 | 4.7 | 5.3 | 29.7 | 2.8 | 9.6 | 0.6 | 43.0 | 2.7 | 1340.5 |
| PAR 11/87 | 141.64 | 141.88 | Pyroxenite | 21.2 | 91.1 | 3367.4 | 82.7 | 605.7 | 24.2 | 61.1 | 4.2 | 4.5 | 30.7 | 3.0 | 12.9 | 2.0 | 56.6 | 1.7 | 1550.1 |
| PAR 11/88 | 142.96 | 143.21 | Pyroxenite | 24.3 | 96.8 | 3346.7 | 86.6 | 599.8 | 26.1 | 58.4 | 4.3 | 8.9 | 35.5 | 3.6 | 14.2 | 2.9 | 57.5 | 3.1 | 1508.6 |
| PAR 11/89 | 144.48 | 144.72 | Pyroxenite | 19.5 | 90.3 | 3421.6 | 82.8 | 608.6 | 20.3 | 56.2 | 4.1 | 8.9 | 29.8 | 3.6 | 9.7 | 2.8 | 51.9 | 1.4 | 1848.3 |
| PAR 11/90 | 145.81 | 146.11 | Pyroxenite | 21.4 | 95.4 | 3439.1 | 81.0 | 615.8 | 21.8 | 60.2 | 4.1 | 7.5 | 26.5 | 3.0 | 9.0 | 2.9 | 48.1 | 2.1 | 1771.3 |
| PAR 11/91 | 147.31 | 147.57 | Pyroxenite | 18.1 | 91.5 | 3495.2 | 82.9 | 610.3 | 21.3 | 56.8 | 4.1 | 7.0 | 24.4 | 3.1 | 9.6 | 2.7 | 56.9 | 1.5 | 1993.3 |
| PAR 11/92 | 148.85 | 149.21 | Harzburgite | 12.8 | 53.8 | 3115.3 | 142.4 | 1593.5 | 23.3 | 74.1 | 2.5 | 3.9 | 27.5 | 2.0 | 15.5 | 0.4 | 23.8 | 5.6 | 6895.2 |
| PAR 11/93 | 149.71 | 150.01 | Harzburgite | 9.6 | 49.2 | 3266.0 | 132.8 | 1502.2 | 32.7 | 66.9 | 3.2 | 6.8 | 32.4 | 1.2 | 7.6 | 1.0 | 35.4 | 3.6 | 6391.7 |

## Table E1.2: Whole rock trace element and sulphur analyses (ppm) for PAR 11 borehole by XRF.

| Sample # | DPF(m) | DPT(m) | Lithology | Sc | V | Cr | Co | Ni | Cu | Zn | Ga | Rb | Sr | Y | Zr | Nb | Ba | Pb | S |
|---|---|---|---|---|---|---|---|---|---|---|---|---|---|---|---|---|---|---|---|
| PAR 11/95 | 151.57 | 151.84 | Harzburgite | 11.1 | 49.7 | 3331.7 | 140.1 | 1599.5 | 11.8 | 68.5 | 2.1 | 4.1 | 12.7 | 0.8 | 6.2 | 1.0 | 12.8 | 1.8 | 4625.9 |
| PAR 11/96 | 154.11 | 154.39 | Dunite | 8.9 | 45.6 | 3292.0 | 159.4 | 1802.0 | 17.8 | 76.1 | 0.8 | 5.5 | 18.0 | 1.2 | 6.8 | 1.0 | 38.0 | 2.6 | 4995.2 |
| PAR 11/97 | 155.35 | 155.67 | Dunite | 6.8 | 34.1 | 2560.9 | 164.5 | 1876.9 | 17.9 | 76.6 | 0.9 | 8.8 | 28.3 | 1.8 | 8.9 | 1.2 | 53.0 | 0.6 | 5002.4 |
| PAR 11/98 | 156.44 | 156.78 | Dunite | 13.4 | 63.5 | 5209.8 | 160.1 | 1756.8 | 26.6 | 76.3 | 3.4 | 6.0 | 18.5 | 0.9 | 8.5 | 0.5 | 27.1 | -0.1 | 4540.9 |
| PAR 11/99 | 158.07 | 158.36 | Dunite | 11.4 | 64.4 | 5348.3 | 161.9 | 1723.4 | 20.6 | 79.3 | 4.1 | 10.3 | 50.7 | 2.2 | 14.6 | 1.5 | 74.5 | 3.2 | 5220.3 |
| PAR 11/100 | 159.49 | 159.80 | Dunite | 11.7 | 51.7 | 2970.5 | 146.2 | 1527.0 | 15.3 | 74.5 | 1.6 | 6.9 | 15.8 | 1.0 | 8.2 | 1.3 | 27.4 | 4.0 | 4377.5 |
| PAR 11/101 | 161.01 | 161.35 | Dunite | 9.6 | 43.6 | 2282.1 | 164.3 | 1740.8 | 22.2 | 78.5 | 1.5 | 8.2 | 28.8 | 1.1 | 13.2 | 1.5 | 61.1 | 1.5 | 3866.2 |
| PAR 11/102 | 162.04 | 162.74 | Harzburgite | 14.3 | 50.5 | 3027.5 | 152.5 | 1589.8 | 25.7 | 74.6 | 2.1 | 6.0 | 18.1 | 0.4 | 6.5 | 0.8 | 26.6 | 1.3 | 3673.8 |
| PAR 11/103 | 163.57 | 163.89 | Dunite | 8.2 | 50.0 | 3183.1 | 157.9 | 1740.2 | 20.5 | 78.5 | 2.2 | 11.5 | 33.3 | 0.4 | 22.0 | 0.2 | 60.1 | 4.0 | 4431.6 |
| PAR 11/104 | 164.64 | 164.88 | Dunite | 10.0 | 61.5 | 3906.7 | 163.9 | 1837.8 | 42.4 | 87.6 | 3.1 | 9.9 | 21.6 | 1.3 | 16.6 | 0.7 | 40.4 | 5.8 | 4172.6 |
| PAR 11/106 | 166.00 | 166.36 | Dunite | 11.9 | 50.3 | 1140.7 | 136.8 | 1459.2 | 43.8 | 74.6 | 3.8 | 11.6 | 37.9 | 2.2 | 21.5 | 0.9 | 73.5 | 2.6 | 3786.4 |
| PAR 11/107 | 166.74 | 167.03 | Dunite | 12.5 | 47.0 | 1808.0 | 154.3 | 1646.9 | 25.9 | 71.6 | 1.9 | 6.1 | 18.8 | 0.9 | 7.7 | 0.3 | 41.1 | 2.2 | 2878.6 |
| PAR 11/108 | 168.19 | 168.40 | Dunite | 10.8 | 43.4 | 3999.1 | 152.0 | 1638.4 | 23.9 | 76.4 | 2.5 | 3.7 | 24.9 | 0.7 | 6.4 | -0.1 | 20.9 | -1.0 | 2793.6 |
| PAR 11/109 | 169.40 | 169.68 | Dunite | 7.6 | 46.4 | 3744.3 | 170.8 | 1835.7 | 23.4 | 76.8 | 3.5 | 7.2 | 28.2 | 0.4 | 8.7 | 1.5 | 47.1 | 1.7 | 4002.3 |
| PAR 11/110 | 171.13 | 171.37 | Dunite | 9.3 | 43.2 | 2234.0 | 153.8 | 1647.6 | 12.5 | 77.0 | 3.0 | 14.0 | 45.8 | 1.8 | 17.3 | 1.9 | 81.2 | 2.1 | 3519.7 |
| PAR 11/111 | 172.39 | 172.72 | Dunite | 6.9 | 26.6 | 1486.0 | 162.7 | 1805.9 | 17.4 | 76.2 | 2.0 | 7.2 | 36.5 | 0.7 | 11.5 | 1.6 | 57.6 | 2.5 | 3720.1 |
| PAR 11/112 | 173.59 | 173.89 | Harzburgite | 10.6 | 55.8 | 2682.7 | 156.3 | 1727.4 | 41.7 | 76.4 | 2.6 | 12.9 | 27.1 | 2.6 | 18.9 | 2.4 | 76.6 | 3.3 | 2570.3 |
| PAR 11/113 | 174.92 | 175.20 | Harzburgite | 12.2 | 57.9 | 3665.2 | 155.0 | 1639.2 | 37.8 | 76.0 | 2.2 | 7.3 | 28.5 | 1.6 | 8.9 | 1.4 | 46.2 | 1.1 | 2943.6 |
| PAR 11/114 | 176.48 | 176.72 | Dunite | 10.0 | 42.1 | 1530.7 | 158.6 | 1758.1 | 20.3 | 75.3 | 2.1 | 7.0 | 20.5 | 1.9 | 10.8 | 2.8 | 38.0 | 1.5 | 3434.9 |
| PAR 11/115 | 178.10 | 178.37 | Harzburgite | 13.1 | 49.0 | 4543.8 | 146.2 | 1617.1 | 12.3 | 73.7 | 2.5 | 3.6 | 8.3 | 2.0 | 5.2 | 3.1 | 17.8 | 0.7 | 3290.3 |
| PAR 11/116 | 179.52 | 179.81 | Dunite | 8.5 | 51.5 | 3875.1 | 164.9 | 1791.0 | 17.8 | 79.7 | 2.9 | 6.0 | 16.5 | 3.0 | 9.8 | 2.9 | 29.2 | 2.2 | 3729.0 |
| PAR 11/117 | 181.03 | 181.32 | Dunite | 6.1 | 46.6 | 4433.5 | 167.9 | 1876.4 | 18.1 | 73.9 | 2.2 | 2.0 | 17.5 | 2.2 | 7.4 | 3.2 | 29.5 | -0.1 | 4724.9 |
| PAR 11/118 | 182.53 | 182.84 | Dunite | 8.5 | 26.9 | 1497.0 | 160.8 | 1840.4 | 19.6 | 71.5 | 1.4 | 4.5 | 16.7 | 1.5 | 8.3 | 2.8 | 26.0 | 2.3 | 5044.9 |
| PAR 11/119 | 183.73 | 183.99 | Dunite | 3.4 | 35.2 | 3602.5 | 167.0 | 1879.6 | 6.0 | 72.5 | 1.0 | 3.0 | 15.4 | -0.4 | 6.0 | 2.3 | 21.4 | ND | 3445.5 |

## Table E1.2: Whole rock trace element and sulphur analyses (ppm) for PAR 11 borehole by XRF.

| Sample # | DPF(m) | DPT(m) | Lithology | Sc | V | Cr | Co | Ni | Cu | Zn | Ga | Rb | Sr | Y | Zr | Nb | Ba | Pb | S |
|---|---|---|---|---|---|---|---|---|---|---|---|---|---|---|---|---|---|---|---|
| PAR 11/120 | 183.11 | 183.45 | Dunite | 8.4 | 44.3 | 5563.5 | 167.0 | 1842.2 | 9.6 | 76.7 | 2.7 | 4.7 | 28.9 | 0.9 | 7.6 | 1.7 | 53.8 | ND | 5407.3 |
| PAR 11/121 | 185.99 | 186.30 | Dunite | 5.2 | 59.3 | 7128.5 | 163.7 | 1862.2 | 29.4 | 83.3 | 1.5 | 4.0 | 24.2 | 0.2 | 6.1 | 1.7 | 23.9 | 1.6 | 5290.8 |
| PAR 11/122 | 187.70 | 188.00 | Dunite | 12.5 | 54.7 | 5321.1 | 154.7 | 1659.2 | 12.5 | 80.8 | 2.4 | 4.4 | 17.1 | 1.0 | 6.9 | 1.4 | 24.4 | 0.8 | 4081.3 |
| PAR 11/123 | 189.25 | 189.50 | Dunite | 9.0 | 41.7 | 3299.7 | 160.9 | 1744.1 | 19.0 | 74.3 | 2.3 | 5.3 | 22.5 | -0.2 | 7.0 | 0.8 | 34.6 | 1.0 | 4519.7 |
| PAR 11/124 | 190.46 | 190.70 | Dunite | 11.1 | 55.2 | 5086.5 | 149.9 | 1589.8 | 13.8 | 70.7 | 0.8 | 1.7 | 5.7 | 0.9 | 3.4 | 1.2 | 16.9 | 1.5 | 3604.7 |
| PAR 11/125 | 191.82 | 192.13 | Dunite | 9.1 | 38.9 | 3152.7 | 171.5 | 1874.2 | 16.4 | 75.2 | 1.1 | 4.9 | 36.8 | 1.6 | 10.9 | 1.9 | 59.3 | 1.7 | 4578.1 |
| PAR 11/126 | 193.24 | 193.50 | Dunite | 10.1 | 49.4 | 3350.6 | 156.9 | 1749.7 | 24.0 | 70.4 | 1.4 | 2.4 | 13.6 | 1.1 | 7.3 | 2.1 | 22.2 | 2.2 | 5142.0 |
| PAR 11/127 | 194.64 | 194.96 | Dunite | 12.3 | 59.6 | 4245.3 | 149.1 | 1515.5 | 23.7 | 68.0 | 1.5 | 5.6 | 19.1 | 2.0 | 6.5 | 1.5 | 28.0 | 0.3 | 4681.9 |
| PAR 11/128 | 195.92 | 196.20 | Dunite | 8.6 | 46.8 | 4435.0 | 172.3 | 1907.9 | 13.6 | 78.2 | 1.3 | 7.0 | 26.7 | 1.9 | 10.4 | 2.9 | 46.1 | 1.4 | 5478.3 |
| PAR 11/129 | 197.14 | 197.44 | Dunite | 6.9 | 46.3 | 4880.3 | 174.0 | 1905.1 | 15.3 | 81.1 | 0.9 | 5.6 | 20.3 | 1.9 | 9.3 | 1.3 | 45.0 | 1.6 | 4774.9 |
| PAR 11/130 | 198.74 | 198.98 | Dunite | 7.0 | 36.4 | 2233.5 | 175.5 | 1919.0 | 13.4 | 77.3 | 1.7 | 4.3 | 24.2 | 2.3 | 8.7 | 1.8 | 40.6 | -0.5 | 5566.3 |
| PAR 11/131 | 200.35 | 200.60 | Dunite | 6.7 | 31.3 | 2190.2 | 169.0 | 1892.2 | 20.1 | 73.4 | 2.1 | 9.0 | 45.1 | 3.1 | 10.6 | 1.5 | 75.8 | 1.5 | 4608.1 |
| PAR 11/132 | 201.40 | 201.98 | Dunite | 9.3 | 49.4 | 5171.1 | 167.8 | 1844.6 | 8.2 | 75.4 | 2.4 | 6.4 | 24.7 | 0.3 | 8.4 | 2.8 | 47.6 | 3.3 | 4567.8 |
| PAR 11/133 | 203.19 | 203.48 | Dunite | 14.6 | 59.4 | 4104.5 | 146.0 | 1467.5 | 16.1 | 68.9 | 1.3 | 6.0 | 16.5 | 0.8 | 6.3 | 2.3 | 39.4 | 1.3 | 3168.7 |
| PAR 11/134 | 204.50 | 204.76 | Dunite | 11.7 | 54.3 | 4584.6 | 161.6 | 1782.0 | 2.0 | 74.5 | 0.9 | 6.8 | 24.1 | 1.1 | 10.0 | 2.4 | 55.8 | 2.5 | 4976.7 |
| PAR 11/135 | 206.04 | 206.32 | Dunite | 4.0 | 36.6 | 3454.8 | 172.5 | 1906.3 | -3.2 | 73.8 | 1.2 | 6.1 | 25.3 | 1.0 | 7.9 | 2.6 | 44.5 | 0.5 | 5147.9 |
| PAR 11/136 | 207.00 | 207.42 | Dunite | 9.0 | 36.6 | 2593.0 | 165.0 | 1887.8 | 4.5 | 73.7 | 2.9 | 3.8 | 13.6 | ND | 8.7 | 2.3 | 13.3 | 1.3 | 5151.8 |
| PAR 11/137 | 208.68 | 208.91 | Dunite | 9.2 | 56.7 | 5679.6 | 157.8 | 1799.0 | 3.6 | 74.2 | 1.9 | 4.3 | 11.1 | 0.1 | 3.8 | 1.0 | 25.7 | 0.8 | 4412.0 |
| PAR 11/138 | 210.14 | 210.45 | Dunite | 8.4 | 31.6 | 2268.2 | 167.3 | 1918.9 | -1.1 | 73.3 | 2.3 | 3.0 | 20.2 | 1.6 | 9.1 | 1.3 | 14.3 | 2.6 | 5286.7 |
| PAR 11/139 | 211.32 | 212.65 | Dunite | 6.7 | 32.7 | 1958.4 | 160.8 | 1927.8 | 2.7 | 72.0 | 1.7 | 1.2 | 16.3 | 1.1 | 7.4 | 2.0 | 23.2 | 2.0 | 5231.9 |
| PAR 11/140 | 212.53 | 212.80 | Dunite | 8.9 | 27.9 | 1448.8 | 166.4 | 1928.3 | 7.2 | 71.8 | 1.9 | 3.7 | 19.7 | 1.5 | 8.1 | 1.4 | 20.2 | 2.0 | 5247.3 |
| PAR 11/141 | 213.74 | 213.98 | Harzburgite | 10.8 | 40.7 | 4190.7 | 155.3 | 1730.6 | 4.0 | 71.0 | 1.7 | 4.2 | 21.0 | 0.7 | 5.8 | 0.9 | 37.2 | 1.2 | 4057.1 |
| PAR 11/142 | 215.28 | 215.59 | Harzburgite | 11.5 | 41.2 | 3676.0 | 152.1 | 1786.0 | 8.8 | 66.3 | 1.8 | 4.8 | 29.9 | 1.2 | 5.5 | 1.1 | 19.9 | 2.9 | 4686.1 |
| PAR 11/143 | 216.53 | 216.80 | Harzburgite | 12.6 | 43.0 | 4119.3 | 162.8 | 1810.7 | 14.6 | 68.4 | 2.1 | 4.8 | 22.6 | 1.2 | 7.2 | 0.2 | 29.8 | 1.3 | 4337.1 |

## Table E1.2: Whole rock trace element and sulphur analyses (ppm) for PAR 11 borehole by XRF.

| Sample # | DPF(m) | DPT(m) | Lithology | Sc | V | Cr | Co | Ni | Cu | Zn | Ga | Rb | Sr | Y | Zr | Nb | Ba | Pb | S |
|---|---|---|---|---|---|---|---|---|---|---|---|---|---|---|---|---|---|---|---|
| PAR 11/144 | 218.36 | 218.61 | Dunite | 8.6 | 37.9 | 3640.9 | 163.1 | 1868.6 | 5.8 | 68.9 | 2.4 | 3.7 | 23.8 | 1.1 | 6.1 | 0.9 | 26.3 | 1.7 | 4727.6 |
| PAR 11/145 | 219.50 | 219.76 | Dunite | 10.9 | 41.6 | 3419.9 | 159.0 | 1816.1 | 11.1 | 70.2 | 1.2 | 5.0 | 19.2 | 0.8 | 9.0 | 1.8 | 27.7 | 1.5 | 4946.7 |
| PAR 11/146 | 221.23 | 221.50 | Dunite | 7.4 | 39.1 | 2767.7 | 167.3 | 1890.8 | 12.0 | 70.4 | 2.1 | 12.0 | 44.6 | 2.2 | 13.8 | 1.3 | 81.2 | 3.1 | 4957.1 |
| PAR 11/147 | 222.44 | 222.69 | Dunite | 3.8 | 34.4 | 3478.6 | 173.9 | 2066.0 | 11.0 | 73.1 | 2.8 | 2.0 | 15.4 | 0.9 | 6.6 | 1.2 | 25.2 | 0.1 | 5008.2 |
| PAR 11/148 | 223.74 | 223.99 | Harzburgite | 8.6 | 47.8 | 4145.3 | 153.8 | 1755.1 | 11.3 | 69.7 | 2.0 | 4.6 | 13.7 | 1.6 | 5.6 | 1.4 | 21.6 | 2.5 | 3883.2 |
| PAR 11/149 | 225.20 | 225.48 | Olivine-pyroxenite | 11.0 | 49.8 | 4606.4 | 134.4 | 1492.5 | 13.8 | 69.2 | 2.0 | 3.4 | 10.4 | 0.5 | 5.9 | 1.1 | 29.1 | 2.1 | 4003.7 |
| PAR 11/150 | 226.66 | 226.96 | Dunite | 5.1 | 46.6 | 4324.6 | 176.0 | 2081.7 | 21.7 | 77.0 | 2.3 | 5.5 | 27.0 | 1.5 | 9.7 | 1.7 | 34.7 | 1.9 | 4973.9 |
| PAR 11/151 | 228.12 | 228.39 | Olivine- pyroxenite | 11.5 | 50.9 | 4793.0 | 141.6 | 1523.5 | 12.9 | 73.0 | 1.6 | 5.7 | 7.3 | 1.2 | 5.8 | 0.4 | 34.2 | 1.7 | 3217.1 |
| PAR 11/152 | 229.65 | 229.93 | Harzburgite | 10.4 | 53.4 | 4466.3 | 158.7 | 1832.7 | 32.3 | 71.3 | 1.1 | 4.8 | 20.1 | 1.5 | 7.3 | 1.3 | 37.7 | 0.3 | 4450.5 |
| MR 330 153 | 61.79 | 62.01 | Harzburgite | 18.2 | 57.8 | 1003.9 | 121.5 | 900.3 | 185.2 | 81.1 | 7.0 | 0.7 | 40.5 | 0.1 | 0.7 | 0.5 | 8.4 | 2.3 | 3703.9 |
| VR58 154 | 210.51 | 210.81 | Olivine- pyroxenite | 17.6 | 77.5 | 1331.9 | 136.4 | 1938.1 | 236.0 | 82.3 | 3.7 | 3.9 | 19.3 | 0.7 | 7.7 | 0.4 | 30.2 | 2.1 | 6725.2 |
| PAR316 155 | 107.60 | 107.99 | Harzburgite | 12.4 | 54.1 | 868.8 | 142.2 | 1162.9 | 22.0 | 79.5 | 2.7 | 1.5 | 11.4 | 0.7 | 3.2 | 1.3 | 6.3 | 1.0 | 5511.4 |
| PAR28 156 | 179.31 | 179.64 | Harzburgite | 14.8 | 80.4 | 1769.3 | 107.5 | 1358.6 | 14.2 | 65.2 | 6.2 | 1.2 | 6.9 | 0.4 | 1.0 | 0.8 | 8.3 | 1.3 | 4881.0 |
| MR 328 157 | 57.21 | 57.44 | Websterite | 34.3 | 164.9 | 2852.7 | 105.6 | 1318.3 | 7.7 | 85.8 | 5.1 | 1.0 | 5.7 | 3.7 | 0.8 | 0.7 | 7.1 | 0.5 | 1813.1 |
| MR330 158 | 47.19 | 47.45 | Gabbro | 22.6 | 57.7 | 964.5 | 53.4 | 353.1 | 18.1 | 21.6 | 12.2 | 39.8 | 154.4 | -0.3 | 0.7 | 1.0 | 171.3 | -0.8 | 2101.5 |
| MR327 159 | 162.79 | 163.05 | Harzburgite | 14.6 | 70.1 | 2474.4 | 143.6 | 2242.7 | 70.0 | 73.5 | 4.0 | 0.9 | 5.4 | 1.0 | 3.9 | 1.6 | 10.6 | 2.5 | 4224.7 |

## Table E1.3: Trace elements for the PAR 11 borehole samples by ICP-MS (P-Sm).

| Sample # | DPF(m) | DPT(m) | Lithology | P | Ga | As | Rb | Sr | Y | Zr | Nb | Ba | Cs | La | Ce | Pr | Nd | Sm |
|---|---|---|---|---|---|---|---|---|---|---|---|---|---|---|---|---|---|---|
| PAR 11/1 | 18.77 | 18.94 | Pyroxenite | 47.19 | 1.33 | 0.71 | 1.92 | 14.88 | 1.05 | 7.71 | 1.08 | 7.70 | 0.18 | 0.83 | 1.53 | 0.19 | 0.77 | 0.16 |
| PAR 11/3 | 23.15 | 23.36 | Pyroxenite | 48.17 | 1.59 | 0.35 | 3.43 | 17.23 | 1.08 | 7.90 | 1.62 | 11.07 | 0.23 | 0.78 | 1.53 | 0.20 | 0.77 | 0.17 |
| PAR 11/5 | 25.49 | 25.69 | Pyroxenite | 64.79 | 2.06 | 0.27 | 5.16 | 21.82 | 1.56 | 10.59 | 0.42 | 16.98 | 0.44 | 1.29 | 2.68 | 0.34 | 1.34 | 0.27 |
| PAR 11/7 | 29.15 | 29.35 | Pyroxenite | 186.75 | 2.80 | 0.25 | 12.00 | 39.25 | 2.79 | 33.51 | 0.78 | 33.51 | 0.78 | 2.65 | 5.67 | 0.76 | 2.97 | 0.59 |
| PAR 11/9 | 30.77 | 31.02 | Harzburgite | 53.10 | 1.93 | 0.30 | 4.13 | 11.27 | 1.69 | 5.53 | 0.34 | 16.61 | 0.30 | 1.26 | 2.48 | 0.31 | 1.23 | 0.27 |
| PAR 11/11 | 33.21 | 33.43 | Harzburgite | 104.99 | 2.70 | 0.55 | 8.36 | 22.22 | 2.96 | 12.94 | 0.77 | 35.91 | 0.63 | 2.30 | 4.79 | 0.60 | 2.44 | 0.54 |
| PAR 11/13 | 35.48 | 35.69 | Harzburgite | 55.20 | 2.01 | 0.42 | 4.94 | 17.64 | 1.57 | 4.68 | 0.39 | 21.08 | 0.34 | 1.68 | 2.28 | 0.29 | 1.13 | 0.25 |
| PAR 11/15 | 38.61 | 38.82 | Harzburgite | 94.44 | 2.13 | 0.66 | 4.07 | 14.13 | 1.79 | 17.56 | 2.72 | 20.47 | 0.31 | 1.43 | 3.02 | 0.37 | 1.49 | 0.32 |
| PAR 11/17 | 41.43 | 41.69 | Dunite | 88.18 | 2.89 | 0.66 | 6.77 | 27.13 | 2.33 | 8.46 | 0.58 | 26.07 | 0.54 | 2.05 | 4.27 | 0.52 | 2.09 | 0.44 |
| PAR 11/19 | 44.70 | 44.96 | Dunite | 54.63 | 2.35 | 0.53 | 4.00 | 16.67 | 1.48 | 10.34 | 0.43 | 15.62 | 0.42 | 1.08 | 2.18 | 0.27 | 1.07 | 0.23 |
| /PAR 11/21 | 47.37 | 47.69 | Dunite | 83.92 | 2.70 | 0.53 | 6.77 | 24.26 | 2.02 | 7.06 | 0.41 | 32.90 | 0.61 | 1.80 | 3.59 | 0.44 | 1.71 | 0.36 |
| PAR 11/23 | 50.13 | 50.37 | Dunite | 90.69 | 2.36 | 0.56 | 5.42 | 23.84 | 2.39 | 13.52 | 0.58 | 21.62 | 0.56 | 1.76 | 3.60 | 0.44 | 1.75 | 0.39 |
| PAR 11/25 | 53.06 | 53.33 | Harzburgite | 94.79 | 2.41 | 0.58 | 7.42 | 18.79 | 2.29 | 9.16 | 0.53 | 25.39 | 0.64 | 2.50 | 3.79 | 0.46 | 1.85 | 0.39 |
| PAR 11/27 | 55.96 | 56.03 | Harzburgite | 117.05 | 3.25 | 0.60 | 7.47 | 35.38 | 3.25 | 28.19 | 2.73 | 30.31 | 0.67 | 2.42 | 5.06 | 0.64 | 2.68 | 0.60 |
| PAR 11/29 | 58.49 | 58.82 | Dunite | 121.23 | 3.89 | 0.62 | 9.15 | 32.74 | 2.53 | 9.50 | 0.66 | 33.43 | 0.77 | 2.57 | 5.20 | 0.61 | 2.38 | 0.48 |
| PAR 11/31 | 61.10 | 61.36 | Harzburgite | 130.22 | 3.41 | 0.45 | 7.42 | 35.58 | 2.85 | 21.69 | 0.57 | 34.39 | 0.63 | 2.31 | 4.68 | 0.58 | 2.35 | 0.51 |
| PAR 11/33 | 64.12 | 63.00 | Harzburgite | 79.73 | 2.47 | 0.36 | 5.18 | 23.09 | 1.84 | 6.43 | 0.38 | 25.29 | 0.43 | 1.46 | 2.92 | 0.36 | 1.44 | 0.31 |
| PAR 11/35 | 66.67 | 66.90 | Harzburgite | 63.50 | 2.38 | 0.34 | 3.21 | 13.52 | 1.27 | 6.10 | 0.31 | 14.18 | 0.24 | 1.04 | 2.11 | 0.26 | 1.01 | 0.21 |
| PAR 11/37 | 69.75 | 70.00 | Harzburgite | 86.52 | 2.10 | 0.41 | 7.32 | 19.83 | 1.70 | 8.95 | 0.60 | 24.11 | 0.52 | 1.61 | 3.27 | 0.39 | 1.49 | 0.31 |
| PAR 11/39 | 72.45 | 72.71 | Harzburgite | 65.10 | 1.92 | 0.32 | 4.01 | 11.38 | 1.44 | 8.36 | 0.32 | 16.22 | 0.29 | 1.14 | 2.26 | 0.28 | 1.11 | 0.24 |
| PAR 11/42 | 76.39 | 76.67 | Harzburgite | 68.51 | 2.04 | 0.43 | 3.87 | 17.01 | 1.23 | 5.24 | 0.31 | 14.82 | 0.28 | 1.05 | 2.20 | 0.26 | 1.01 | 0.21 |
| PAR 11/44 | 80.63 | 80.90 | Dunite | 185.13 | 3.30 | 0.56 | 11.77 | 34.12 | 3.04 | 19.51 | 0.96 | 52.18 | 0.68 | 3.41 | 7.09 | 0.86 | 3.34 | 0.67 |
| PAR 11/47 | 84.35 | 84.63 | Harzburgite | 58.88 | 2.05 | 0.71 | 3.01 | 14.06 | 1.19 | 4.07 | 0.29 | 17.64 | 0.17 | 0.78 | 1.55 | 0.19 | 0.75 | 0.18 |
| PAR 11/50 | 89.04 | 89.26 | Pyroxenite | 178.67 | 1.89 | 0.31 | 4.30 | 22.13 | 1.64 | 7.93 | 0.92 | 12.74 | 0.24 | 1.58 | 2.64 | 0.34 | 1.31 | 0.27 |

## Table E1.3: Continued (P-Sm).

| Sample # | DPF(m) | DPT(m) | Lithology | P | Ga | As | Rb | Sr | Y | Zr | Nb | Ba | Cs | La | Ce | Pr | Nd | Sm |
|---|---|---|---|---|---|---|---|---|---|---|---|---|---|---|---|---|---|---|
| PAR 11/53 | 93.34 | 93.58 | Pyroxenite | 86.50 | 2.62 | 0.34 | 6.05 | 28.53 | 1.60 | 8.15 | 0.47 | 16.91 | 0.30 | 1.49 | 2.81 | 0.32 | 1.20 | 0.24 |
| PAR 11/56 | 97.76 | 98.00 | Pyroxenite | 134.74 | 2.66 | 0.59 | 6.30 | 27.78 | 1.85 | 10.61 | 0.49 | 16.56 | 0.32 | 1.88 | 3.55 | 0.41 | 1.57 | 0.31 |
| PAR 11/59 | 102.14 | 102.4 | Pyroxenite | 130.72 | 2.08 | 0.34 | 4.66 | 22.30 | 1.49 | 8.44 | 0.95 | 19.42 | 0.26 | 1.24 | 2.20 | 0.28 | 1.11 | 0.24 |
| PAR 11/62 | 106.35 | 106.54 | Pyroxenite | 154.63 | 2.88 | 0.28 | 7.19 | 28.57 | 1.82 | 10.47 | 0.46 | 19.44 | 0.38 | 1.51 | 2.99 | 0.35 | 1.41 | 0.30 |
| PAR 11/65 | 110.41 | 110.64 | Pyroxenite | 195.50 | 2.79 | 0.31 | 7.81 | 29.50 | 1.78 | 10.68 | 0.55 | 19.71 | 0.41 | 1.59 | 3.24 | 0.41 | 1.62 | 0.32 |
| PAR 11/68 | 114.38 | 114.59 | Pyroxenite | 184.17 | 2.85 | 0.31 | 6.03 | 28.07 | 1.83 | 12.44 | 0.59 | 19.29 | 0.38 | 1.45 | 3.09 | 0.39 | 1.59 | 0.34 |
| PAR 11/71 | 118.65 | 118.88 | Pyroxenite | 134.08 | 3.27 | 0.67 | 3.54 | 16.01 | 1.43 | 8.50 | 0.34 | 20.17 | 0.19 | 0.85 | 1.75 | 0.21 | 0.85 | 0.19 |
| PAR 11/74 | 122.5 | 122.78 | Pyroxenite | 152.55 | 2.16 | 0.30 | 3.44 | 22.25 | 1.52 | 8.88 | 0.58 | 17.20 | 0.22 | 1.18 | 2.16 | 0.28 | 1.10 | 0.24 |
| PAR 11/77 | 127.14 | 127.34 | Pyroxenite | 180.70 | 3.07 | 0.37 | 7.93 | 29.55 | 1.94 | 12.11 | 0.65 | 23.34 | 0.43 | 1.56 | 3.17 | 0.39 | 1.49 | 0.32 |
| PAR 11/80 | 131.36 | 131.55 | Pyroxenite | 135.22 | 2.85 | 0.34 | 7.34 | 28.39 | 1.85 | 8.13 | 0.54 | 17.62 | 0.39 | 1.44 | 2.65 | 0.33 | 1.29 | 0.28 |
| PAR 11/83 | 135.66 | 135.93 | Pyroxenite | 122.35 | 2.17 | 0.30 | 4.02 | 22.50 | 1.57 | 11.42 | 0.71 | 12.50 | 0.22 | 1.23 | 2.09 | 0.25 | 0.99 | 0.22 |
| PAR 11/86 | 140.18 | 140.42 | Pyroxenite | 131.29 | 3.22 | 0.28 | 5.42 | 33.11 | 2.12 | 8.94 | 0.53 | 17.21 | 0.28 | 1.41 | 2.77 | 0.32 | 1.21 | 0.27 |
| PAR 11/89 | 144.48 | 144.72 | Pyroxenite | 141.88 | 4.50 | 0.78 | 8.72 | 34.11 | 2.46 | 10.93 | 0.48 | 38.82 | 0.30 | 1.28 | 2.39 | 0.28 | 1.11 | 0.27 |
| PAR 11/92 | 148.85 | 149.21 | Harzburgite | 244.08 | 4.31 | 0.82 | 5.47 | 29.01 | 2.36 | 13.57 | 1.18 | 25.12 | 0.33 | 2.30 | 4.50 | 0.54 | 2.09 | 0.45 |
| PAR 11/95 | 153.68 | 154.98 | Harzburgite | 128.90 | 3.38 | 0.94 | 3.57 | 13.62 | 1.75 | 5.96 | 0.43 | 15.86 | 0.36 | 0.85 | 1.75 | 0.21 | 0.87 | 0.21 |
| PAR 11/98 | 156.44 | 156.78 | Dunite | 185.44 | 4.81 | 0.69 | 5.33 | 19.36 | 2.06 | 13.15 | 0.57 | 24.06 | 0.27 | 1.44 | 2.78 | 0.32 | 1.26 | 0.29 |
| PAR 11/101 | 161.01 | 161.35 | Dunite | 196.22 | 4.13 | 1.01 | 8.03 | 30.45 | 2.59 | 9.89 | 0.80 | 43.88 | 0.43 | 1.78 | 3.56 | 0.43 | 1.68 | 0.41 |
| PAR 11/104 | 164.64 | 164.88 | Dunite | 457.04 | 5.78 | 1.19 | 6.84 | 22.95 | 3.03 | 35.38 | 1.55 | 56.40 | 0.48 | 1.99 | 4.52 | 0.53 | 2.23 | 0.51 |
| PAR 11/107 | 166.74 | 167.03 | Dunite | 181.79 | 2.77 | 0.91 | 5.91 | 19.63 | 2.46 | 7.62 | 0.57 | 25.30 | 0.29 | 1.27 | 2.65 | 0.33 | 1.40 | 0.34 |
| PAR 11/110 | 171.13 | 171.37 | Dunite | 239.92 | 4.81 | 0.85 | 14.65 | 46.58 | 2.57 | 23.59 | 1.27 | 69.83 | 0.78 | 2.48 | 4.84 | 0.55 | 2.05 | 0.42 |
| PAR 11/113 | 174.92 | 175.2 | Dunite | 88.48 | 2.42 | 0.86 | 4.62 | 44.48 | 1.49 | 6.16 | 0.66 | 30.01 | 0.29 | 1.05 | 2.06 | 0.25 | 0.95 | 0.22 |
| PAR 11/116 | 179.52 | 179.81 | Dunite | 98.86 | 2.59 | 0.62 | 7.12 | 14.44 | 1.74 | 4.06 | 0.38 | 19.48 | 0.32 | 1.02 | 2.06 | 0.24 | 0.99 | 0.23 |
| PAR 11/118 | 183.73 | 183.99 | Dunite | 80.19 | 2.60 | 0.87 | 2.98 | 13.60 | 1.25 | 3.41 | 0.29 | 14.91 | 0.23 | 0.96 | 1.81 | 0.21 | 0.81 | 0.17 |
| PAR 11/122 | 187.70 | 188.00 | Harzburgite | 77.99 | 2.83 | 0.72 | 4.68 | 16.71 | 1.46 | 4.81 | 0.30 | 18.80 | 0.20 | 0.84 | 1.68 | 0.21 | 0.84 | 0.20 |

## Table E1.3: Continued (P-Sm).

| Sample # | DPF(m) | DPT(m) | Lithology | P | Ga | As | Rb | Sr | Y | Zr | Nb | Ba | Cs | La | Ce | Pr | Nd | Sm |
|---|---|---|---|---|---|---|---|---|---|---|---|---|---|---|---|---|---|---|
| PAR 11/125 | 191.82 | 192.13 | Dunite | 116.31 | 2.74 | 0.63 | 6.24 | 27.78 | 1.57 | 6.13 | 0.38 | 27.54 | 0.29 | 1.02 | 2.03 | 0.24 | 0.92 | 0.21 |
| PAR 11/128 | 195.92 | 196.20 | Dunite | 134.45 | 3.37 | 0.85 | 6.48 | 21.92 | 1.68 | 7.56 | 0.48 | 29.22 | 0.31 | 1.30 | 2.50 | 0.30 | 1.13 | 0.24 |
| PAR 11/131 | 200.35 | 200.60 | Dunite | 124.58 | 2.08 | 0.73 | 6.02 | 31.02 | 1.55 | 7.14 | 0.57 | 36.88 | 0.24 | 1.15 | 2.26 | 0.28 | 1.06 | 0.24 |
| PAR 11/134 | 204.50 | 204.76 | Dunite | 114.88 | 2.80 | 0.95 | 7.05 | 19.77 | 1.58 | 4.65 | 0.38 | 30.44 | 0.31 | 1.00 | 2.00 | 0.24 | 0.98 | 0.22 |
| PAR 11/137 | 208.68 | 208.91 | Dunite | 198.52 | 2.54 | 0.94 | 3.62 | 10.35 | 1.10 | 4.73 | 0.17 | 14.54 | 0.21 | 1.64 | 1.30 | 0.15 | 0.64 | 0.15 |
| PAR 11/139 | 211.32 | 212.65 | Dunite | 105.50 | 2.01 | 0.69 | 3.87 | 17.27 | 1.88 | 56.28 | 0.51 | 13.22 | 0.33 | 1.29 | 2.45 | 0.29 | 1.16 | 0.24 |
| PAR 11/143 | 216.53 | 216.80 | Harzburgite | 91.44 | 2.49 | 0.93 | 4.65 | 20.45 | 1.25 | 5.40 | 0.50 | 21.91 | 0.23 | 0.88 | 1.77 | 0.22 | 0.83 | 0.18 |
| PAR 11/146 | 221.23 | 221.5 | Dunite | 143.21 | 2.88 | 1.07 | 12.79 | 39.92 | 2.17 | 8.60 | 1.02 | 54.33 | 0.55 | 2.04 | 3.94 | 0.46 | 1.76 | 0.39 |
| PAR 11/149 | 225.20 | 225.48 | Olivine pyroxenite | 55.12 | 2.01 | 0.67 | 4.03 | 9.47 | 0.99 | 4.43 | 0.24 | 13.86 | 0.21 | 0.68 | 1.37 | 0.16 | 0.59 | 0.13 |
| PAR 11/152 | 229.65 | 229.93 | Harzburgite | 80.71 | 2.57 | 1.18 | 5.49 | 17.24 | 1.22 | 5.37 | 0.44 | 19.91 | 0.29 | 0.89 | 1.84 | 0.22 | 0.86 | 0.19 |
| MR330/153 | 61.79 | 62.01 | Harzburgite | 20.25 | 6.89 | 0.51 | 0.53 | 42.57 | 0.52 | 0.53 | 0.01 | 2.18 | 0.02 | 0.07 | 0.12 | 0.02 | 0.08 | 0.03 |
| VR58/154 | 210.51 | 210.81 | Olivine pyroxenite | 79.79 | 2.74 | 0.56 | 3.09 | 18.47 | 1.32 | 5.90 | 0.23 | 10.62 | 0.18 | 0.68 | 1.51 | 0.17 | 0.67 | 0.15 |
| PAR316/155 | 107.60 | 107.99 | Harzburgite | 42.98 | 2.24 | 0.84 | 1.09 | 11.19 | 1.21 | 2.51 | 0.15 | 7.67 | 0.12 | 0.39 | 0.70 | 0.09 | 0.38 | 0.10 |
| PAR28/156 | 179.31 | 179.64 | Harzburgite | 47.96 | 4.21 | 0.56 | 0.34 | 4.79 | 0.34 | 1.08 | 0.18 | 10.11 | 0.03 | 0.12 | 0.24 | 0.03 | 0.12 | 0.03 |
| MR328/157 | 57.21 | 57.44 | Websterite | 6.90 | 5.66 | 0.28 | 0.70 | 6.37 | 4.11 | 1.60 | -0.01 | 3.16 | 0.18 | 0.05 | 0.19 | 0.06 | 0.47 | 0.27 |
| MR330/158 | 47.19 | 47.45 | Gabbro | 4.93 | 13.30 | 0.46 | 34.15 | 120.55 | 0.41 | 1.71 | -0.01 | 139.21 | 0.61 | 0.06 | 0.12 | 0.02 | 0.10 | 0.11 |
| MR327/159 | 162.79 | 163.05 | Harzburgite | 21.02 | 3.21 | 0.42 | 0.98 | 5.85 | 1.42 | 2.80 | 0.13 | 4.33 | 0.32 | 0.34 | 0.66 | 0.09 | 0.39 | 0.11 |

## Table E1.3: Continued (En-U).

| Sample # | DPF(m) | DPT(m) | Lithology | Eu | Gd | Tb | Dy | Ho | Er | Tm | Yb | Lu | Hf | Ta | W | Pb | Th | U |
|---|---|---|---|---|---|---|---|---|---|---|---|---|---|---|---|---|---|---|
| PAR 11/1 | 18.77 | 18.94 | Pyroxenite | 0.05 | 0.17 | 0.03 | 0.17 | 0.04 | 0.10 | 0.02 | 0.11 | 0.02 | 0.22 | 0.07 | 0.15 | 0.89 | 0.24 | 0.07 |
| PAR 11/3 | 23.15 | 23.36 | Pyroxenite | 0.06 | 0.17 | 0.03 | 0.17 | 0.04 | 0.11 | 0.02 | 0.11 | 0.02 | 0.22 | 0.10 | 0.09 | 0.87 | 0.24 | 0.13 |
| PAR 11/5 | 25.49 | 25.69 | Pyroxenite | 0.08 | 0.27 | 0.04 | 0.25 | 0.05 | 0.15 | 0.02 | 0.15 | 0.02 | 0.31 | 0.03 | 0.10 | 1.33 | 0.53 | 0.16 |
| PAR 11/7 | 29.15 | 29.35 | Pyroxenite | 0.14 | 0.56 | 0.08 | 0.47 | 0.09 | 0.26 | 0.04 | 0.25 | 0.04 | 0.98 | 0.06 | 0.16 | 1.89 | 1.07 | 0.30 |
| PAR 11/9 | 30.77 | 31.02 | Harzburgite | 0.07 | 0.28 | 0.04 | 0.28 | 0.06 | 0.17 | 0.03 | 0.17 | 0.03 | 0.07 | 0.02 | 0.10 | 1.03 | 0.34 | 0.13 |
| PAR 11/11 | 33.21 | 33.43 | Harzburgite | 0.13 | 0.55 | 0.09 | 0.52 | 0.10 | 0.28 | 0.04 | 0.24 | 0.04 | 0.36 | 0.07 | 0.20 | 1.95 | 1.35 | 0.50 |
| PAR 11/13 | 35.48 | 35.69 | Harzburgite | 0.07 | 0.25 | 0.04 | 0.26 | 0.05 | 0.15 | 0.02 | 0.16 | 0.03 | 0.14 | 0.03 | 0.11 | 1.09 | 0.41 | 0.13 |
| PAR 11/15 | 38.61 | 38.82 | Harzburgite | 0.08 | 0.32 | 0.05 | 0.31 | 0.06 | 0.17 | 0.02 | 0.16 | 0.02 | 0.48 | 0.22 | 0.15 | 1.22 | 0.52 | 0.24 |
| PAR 11/17 | 41.43 | 41.69 | Dunite | 0.12 | 0.44 | 0.07 | 0.40 | 0.08 | 0.23 | 0.03 | 0.20 | 0.03 | 0.23 | 0.04 | 0.13 | 1.12 | 0.53 | 0.21 |
| PAR 11/19 | 44.7 | 44.96 | Dunite | 0.07 | 0.24 | 0.04 | 0.24 | 0.05 | 0.14 | 0.02 | 0.15 | 0.02 | 0.26 | 0.04 | 0.12 | 0.93 | 0.38 | 0.14 |
| PAR 11/21 | 47.37 | 47.69 | Dunite | 0.10 | 0.35 | 0.06 | 0.34 | 0.07 | 0.19 | 0.03 | 0.19 | 0.03 | 0.20 | 0.03 | 0.12 | 1.76 | 0.48 | 0.22 |
| PAR 11/23 | 50.13 | 50.37 | Dunite | 0.11 | 0.41 | 0.07 | 0.40 | 0.08 | 0.23 | 0.04 | 0.22 | 0.04 | 0.39 | 0.05 | 0.21 | 1.13 | 0.55 | 0.19 |
| PAR 11/25 | 53.06 | 53.33 | Harzburgite | 0.09 | 0.40 | 0.06 | 0.38 | 0.08 | 0.22 | 0.03 | 0.21 | 0.03 | 0.25 | 0.04 | 0.17 | 1.05 | 0.50 | 0.21 |
| PAR 11/27 | 55.96 | 56.03 | Harzburgite | 0.15 | 0.60 | 0.10 | 0.58 | 0.12 | 0.31 | 0.04 | 0.26 | 0.04 | 0.89 | 0.26 | 0.62 | 2.53 | 0.73 | 0.32 |
| PAR 11/29 | 58.49 | 58.82 | Dunite | 0.13 | 0.47 | 0.08 | 0.43 | 0.09 | 0.24 | 0.03 | 0.22 | 0.03 | 0.27 | 0.05 | 0.19 | 1.57 | 0.75 | 0.27 |
| PAR 11/31 | 61.1 | 61.36 | Harzburgite | 0.14 | 0.51 | 0.08 | 0.49 | 0.10 | 0.27 | 0.04 | 0.25 | 0.04 | 0.53 | 0.05 | 0.16 | 1.75 | 0.62 | 0.25 |
| PAR 11/33 | 64.12 | 63 | Harzburgite | 0.09 | 0.32 | 0.05 | 0.31 | 0.06 | 0.18 | 0.03 | 0.17 | 0.03 | 0.16 | 0.03 | 0.14 | 1.30 | 0.35 | 0.15 |
| PAR 11/35 | 66.67 | 66.9 | Harzburgite | 0.06 | 0.22 | 0.04 | 0.22 | 0.04 | 0.13 | 0.02 | 0.13 | 0.02 | 0.16 | 0.02 | 0.23 | 0.83 | 0.29 | 0.15 |
| PAR 11/37 | 69.75 | 70 | Harzburgite | 0.08 | 0.31 | 0.05 | 0.29 | 0.06 | 0.16 | 0.02 | 0.15 | 0.02 | 0.24 | 0.05 | 0.16 | 1.34 | 0.45 | 0.19 |
| PAR 11/39 | 72.45 | 72.71 | Harzburgite | 0.06 | 0.25 | 0.04 | 0.24 | 0.05 | 0.14 | 0.02 | 0.14 | 0.02 | 0.27 | 0.02 | 0.10 | 0.96 | 0.35 | 0.13 |
| PAR 11/42 | 76.39 | 76.67 | Harzburgite | 0.06 | 0.22 | 0.03 | 0.21 | 0.04 | 0.12 | 0.02 | 0.12 | 0.02 | 0.14 | 0.02 | 0.09 | 1.52 | 0.31 | 0.13 |
| PAR 11/44 | 80.63 | 80.9 | Dunite | 0.16 | 0.65 | 0.10 | 0.54 | 0.10 | 0.28 | 0.04 | 0.23 | 0.04 | 0.49 | 0.08 | 0.20 | 1.88 | 0.87 | 0.40 |
| PAR 11/47 | 84.35 | 84.63 | Harzburgite | 0.05 | 0.18 | 0.03 | 0.18 | 0.04 | 0.10 | 0.02 | 0.11 | 0.02 | 0.11 | 0.02 | 0.09 | 1.23 | 0.25 | 0.12 |
| PAR 11/50 | 89.04 | 89.26 | Pyroxenite | 0.07 | 0.29 | 0.04 | 0.25 | 0.05 | 0.14 | 0.02 | 0.14 | 0.02 | 0.23 | 0.06 | 0.21 | 1.45 | 0.52 | 0.16 |

## Table E1.3: Continued (Eu-U).

| Sample # | DPF(m) | DPT(m) | Lithology | Eu | Gd | Tb | Dy | Ho | Er | Tm | Yb | Lu | Hf | Ta | W | Pb | Th | U |
|---|---|---|---|---|---|---|---|---|---|---|---|---|---|---|---|---|---|---|
| PAR 11/53 | 93.34 | 93.58 | Pyroxenite | 0.08 | 0.27 | 0.04 | 0.25 | 0.05 | 0.14 | 0.02 | 0.15 | 0.02 | 0.23 | 0.04 | 0.13 | 1.55 | 0.43 | 0.20 |
| PAR 11/56 | 97.76 | 98 | Pyroxenite | 0.08 | 0.34 | 0.05 | 0.29 | 0.06 | 0.16 | 0.03 | 0.17 | 0.03 | 0.32 | 0.04 | 0.14 | 1.85 | 0.60 | 0.22 |
| PAR 11/59 | 102.14 | 102.4 | Pyroxenite | 0.07 | 0.25 | 0.04 | 0.23 | 0.05 | 0.13 | 0.02 | 0.14 | 0.02 | 0.24 | 0.07 | 0.24 | 1.82 | 0.49 | 0.13 |
| PAR 11/62 | 106.35 | 106.54 | Pyroxenite | 0.08 | 0.32 | 0.05 | 0.29 | 0.06 | 0.16 | 0.03 | 0.17 | 0.03 | 0.32 | 0.04 | 0.19 | 2.07 | 0.58 | 0.17 |
| PAR 11/65 | 110.41 | 110.64 | Pyroxenite | 0.09 | 0.34 | 0.05 | 0.29 | 0.06 | 0.16 | 0.02 | 0.16 | 0.03 | 0.33 | 0.05 | 0.21 | 2.36 | 0.57 | 0.19 |
| PAR 11/68 | 114.38 | 114.59 | Pyroxenite | 0.09 | 0.35 | 0.05 | 0.30 | 0.06 | 0.16 | 0.03 | 0.17 | 0.03 | 0.40 | 0.05 | 0.20 | 2.22 | 0.62 | 0.16 |
| PAR 11/71 | 118.65 | 118.88 | Pyroxenite | 0.06 | 0.21 | 0.04 | 0.23 | 0.05 | 0.14 | 0.02 | 0.16 | 0.03 | 0.27 | 0.03 | 0.12 | 1.98 | 0.41 | 0.14 |
| PAR 11/74 | 122.5 | 122.78 | Pyroxenite | 0.07 | 0.26 | 0.04 | 0.24 | 0.05 | 0.14 | 0.02 | 0.15 | 0.02 | 0.29 | 0.05 | 0.17 | 1.86 | 0.51 | 0.12 |
| PAR 11/77 | 127.14 | 127.34 | Pyroxenite | 0.09 | 0.35 | 0.05 | 0.31 | 0.06 | 0.18 | 0.03 | 0.19 | 0.03 | 0.38 | 0.05 | 0.22 | 2.18 | 0.65 | 0.23 |
| PAR 11/80 | 131.36 | 131.55 | Pyroxenite | 0.08 | 0.30 | 0.05 | 0.28 | 0.06 | 0.16 | 0.02 | 0.17 | 0.03 | 0.24 | 0.09 | 0.35 | 1.99 | 0.49 | 0.18 |
| PAR 11/83 | 135.66 | 135.93 | Pyroxenite | 0.07 | 0.25 | 0.04 | 0.24 | 0.05 | 0.13 | 0.02 | 0.15 | 0.03 | 0.34 | 0.07 | 0.20 | 1.66 | 0.46 | 0.15 |
| PAR 11/86 | 140.18 | 140.42 | Pyroxenite | 0.09 | 0.31 | 0.05 | 0.32 | 0.07 | 0.19 | 0.03 | 0.20 | 0.03 | 0.27 | 0.06 | 0.19 | 2.32 | 0.45 | 0.18 |
| PAR 11/89 | 144.48 | 144.72 | Pyroxenite | 0.09 | 0.30 | 0.05 | 0.34 | 0.08 | 0.21 | 0.04 | 0.25 | 0.05 | 0.32 | 0.06 | 0.17 | 2.75 | 0.52 | 0.21 |
| PAR 11/92 | 148.85 | 149.21 | Harzburgite | 0.10 | 0.47 | 0.07 | 0.40 | 0.08 | 0.20 | 0.03 | 0.20 | 0.03 | 0.40 | 0.11 | 0.85 | 7.74 | 0.95 | 0.38 |
| PAR 11/95 | 153.68 | 154.98 | Harzburgite | 0.06 | 0.24 | 0.04 | 0.27 | 0.06 | 0.16 | 0.03 | 0.18 | 0.03 | 0.17 | 0.05 | 0.43 | 2.45 | 0.38 | 0.16 |
| PAR 11/98 | 156.44 | 156.78 | Dunite | 0.08 | 0.31 | 0.05 | 0.32 | 0.07 | 0.18 | 0.03 | 0.19 | 0.03 | 0.38 | 0.06 | 0.28 | 1.91 | 0.43 | 0.27 |
| PAR 11/101 | 161.01 | 161.35 | Dunite | 0.11 | 0.43 | 0.07 | 0.42 | 0.09 | 0.23 | 0.03 | 0.23 | 0.04 | 0.26 | 0.08 | 0.38 | 2.14 | 0.89 | 0.44 |
| PAR 11/104 | 164.64 | 164.88 | Dunite | 0.14 | 0.54 | 0.09 | 0.52 | 0.10 | 0.28 | 0.04 | 0.26 | 0.04 | 0.99 | 0.12 | 0.33 | 3.48 | 0.67 | 0.36 |
| PAR 11/107 | 166.74 | 167.03 | Dunite | 0.09 | 0.38 | 0.06 | 0.39 | 0.08 | 0.21 | 0.03 | 0.21 | 0.03 | 0.23 | 0.05 | 0.18 | 2.17 | 0.36 | 0.17 |
| PAR 11/110 | 171.13 | 171.37 | Dunite | 0.15 | 0.43 | 0.07 | 0.40 | 0.08 | 0.22 | 0.03 | 0.23 | 0.04 | 0.67 | 0.12 | 0.42 | 3.10 | 1.18 | 0.44 |
| PAR 11/113 | 174.92 | 175.2 | Dunite | 0.07 | 0.23 | 0.04 | 0.21 | 0.04 | 0.13 | 0.02 | 0.13 | 0.02 | 0.16 | 0.05 | 0.16 | 1.58 | 0.45 | 0.18 |
| PAR 11/116 | 179.52 | 179.81 | Dunite | 0.06 | 0.26 | 0.04 | 0.25 | 0.05 | 0.14 | 0.02 | 0.14 | 0.02 | 0.10 | 0.03 | 0.15 | 1.89 | 0.38 | 0.18 |
| PAR 11/118 | 183.73 | 183.99 | Dunite | 0.05 | 0.19 | 0.03 | 0.17 | 0.04 | 0.11 | 0.02 | 0.12 | 0.02 | 0.09 | 0.02 | 0.13 | 1.50 | 0.28 | 0.14 |
| PAR 11/122 | 187.7 | 188 | Harzburgite | 0.06 | 0.22 | 0.04 | 0.21 | 0.04 | 0.12 | 0.02 | 0.12 | 0.02 | 0.12 | 0.02 | 0.13 | 1.40 | 0.29 | 0.14 |

## Table E1.3: Continued (Eu-U).

| Sample # | DPF(m) | DPT(m) | Lithology | Eu | Gd | Tb | Dy | Ho | Er | Tm | Yb | Lu | Hf | Ta | W | Pb | Th | U |
|---|---|---|---|---|---|---|---|---|---|---|---|---|---|---|---|---|---|---|
| PAR 11/125 | 191.82 | 192.13 | Dunite | 0.07 | 0.23 | 0.04 | 0.22 | 0.05 | 0.13 | 0.02 | 0.13 | 0.02 | 0.13 | 0.03 | 0.17 | 2.40 | 0.34 | 0.23 |
| PAR 11/128 | 195.92 | 196.2 | Dunite | 0.07 | 0.26 | 0.04 | 0.24 | 0.05 | 0.14 | 0.02 | 0.14 | 0.02 | 0.19 | 0.04 | 0.20 | 2.09 | 0.46 | 0.19 |
| PAR 11/131 | 200.35 | 200.6 | Dunite | 0.07 | 0.26 | 0.04 | 0.22 | 0.05 | 0.13 | 0.02 | 0.12 | 0.02 | 0.19 | 0.04 | 0.14 | 1.89 | 0.40 | 0.16 |
| PAR 11/134 | 204.5 | 204.76 | Dunite | 0.06 | 0.24 | 0.04 | 0.23 | 0.05 | 0.13 | 0.02 | 0.13 | 0.02 | 0.12 | 0.03 | 0.83 | 2.75 | 0.48 | 0.23 |
| PAR 11/137 | 208.68 | 208.91 | Dunite | 0.04 | 0.17 | 0.03 | 0.15 | 0.03 | 0.09 | 0.01 | 0.10 | 0.02 | 0.12 | 0.01 | 0.11 | 4.96 | 0.23 | 0.11 |
| PAR 11/139 | 211.32 | 212.65 | Dunite | 0.07 | 0.28 | 0.04 | 0.25 | 0.05 | 0.16 | 0.03 | 0.17 | 0.03 | 1.09 | 0.04 | 0.17 | 1.39 | 0.58 | 0.24 |
| PAR 11/143 | 216.53 | 216.8 | Harzburgite | 0.05 | 0.20 | 0.03 | 0.17 | 0.04 | 0.10 | 0.02 | 0.11 | 0.02 | 0.14 | 0.04 | 0.13 | 1.56 | 0.45 | 0.19 |
| PAR 11/146 | 221.23 | 221.5 | Dunite | 0.11 | 0.40 | 0.06 | 0.32 | 0.07 | 0.18 | 0.03 | 0.16 | 0.03 | 0.23 | 0.08 | 0.26 | 2.10 | 0.65 | 0.25 |
| PAR 11/149 | 225.2 | 225.48 | Olivine Pyroxenite | 0.04 | 0.15 | 0.02 | 0.15 | 0.03 | 0.09 | 0.01 | 0.10 | 0.02 | 0.13 | 0.02 | 0.03 | 1.19 | 0.25 | 0.10 |
| PAR 11/152 | 229.65 | 229.93 | Harzburgite | 0.06 | 0.20 | 0.03 | 0.18 | 0.04 | 0.10 | 0.02 | 0.10 | 0.02 | 0.15 | 0.04 | 0.15 | 1.26 | 0.37 | 0.19 |
| MR330/153 | 61.79 | 62.01 | Harzburgite | 0.04 | 0.04 | 0.01 | 0.06 | 0.02 | 0.05 | 0.01 | 0.07 | 0.01 | 0.01 | 0.01 | -0.04 | 1.15 | 0.00 | 0.00 |
| VR58/154 | 210.51 | 210.81 | Olivine Pyroxenite | 0.05 | 0.18 | 0.03 | 0.18 | 0.04 | 0.12 | 0.02 | 0.14 | 0.02 | 0.15 | 0.03 | 0.20 | 2.01 | 0.28 | 0.14 |
| PAR316/155 | 107.6 | 107.99 | Harzburgite | 0.03 | 0.13 | 0.02 | 0.16 | 0.04 | 0.11 | 0.02 | 0.14 | 0.02 | 0.07 | 0.01 | ND | 0.80 | 0.11 | 0.05 |
| PAR28/156 | 179.31 | 179.64 | Harzburgite | 0.02 | 0.03 | 0.01 | 0.04 | 0.01 | 0.04 | 0.01 | 0.06 | 0.01 | 0.02 | 0.01 | ND | 2.32 | 0.03 | 0.02 |
| MR328/157 | 57.21 | 57.44 | Websterite | 0.09 | 0.43 | 0.09 | 0.61 | 0.13 | 0.35 | 0.05 | 0.35 | 0.06 | 0.10 | ND | ND | 0.70 | ND | ND |
| MR330/158 | 47.19 | 47.45 | Gabbro | 0.11 | 0.05 | 0.01 | 0.06 | 0.01 | 0.04 | 0.01 | 0.03 | 0.00 | 0.04 | ND | 0.05 | 28.50 | -0.01 | ND |
| MR327/159 | 162.79 | 163.05 | Harzburgite | 0.04 | 0.14 | 0.03 | 0.19 | 0.04 | 0.13 | 0.02 | 0.16 | 0.03 | 0.07 | 0.01 | 0.03 | 1.09 | 0.05 | 0.05 |

## Table E2.1: Whole rock major element oxides analyses (wt %) for the USM surface samples by XRF.

| USM | PV number | Lithology | $SiO_2$ | $Al_2O_3$ | $Fe_2O_3$ | FeO | MnO | MgO | CaO | $Na_2O$ | $K_2O$ | $TiO_2$ | $P_2O_5$ | $Cr_2O_3$ | NiO | Total |
|---|---|---|---|---|---|---|---|---|---|---|---|---|---|---|---|---|
| 1 | 10426 | Pyroxenite | 47.16 | 10.87 | 1.44 | 11.70 | 0.21 | 18.48 | 8.20 | 0.89 | 0.05 | 0.33 | 0.02 | 0.21 | 0.07 | 99.63 |
| 3 | 10428 | Gabbro | 52.42 | 15.52 | 0.71 | 5.76 | 0.15 | 9.83 | 13.20 | 1.63 | 0.08 | 0.11 | ND | 0.03 | 0.01 | 99.46 |
| 4 | 10429 | Gabbro | 50.26 | 14.73 | 0.89 | 7.24 | 0.17 | 11.00 | 14.32 | 1.11 | 0.03 | 0.18 | ND | 0.07 | 0.03 | 100.03 |
| 5 | 10430 | Gabbro | 51.22 | 15.81 | 0.95 | 7.69 | 0.18 | 9.04 | 12.57 | 1.66 | 0.04 | 0.14 | ND | 0.04 | 0.02 | 99.37 |
| 8 | 10433 | Pyroxenite | 47.92 | 7.20 | 1.03 | 8.35 | 0.18 | 30.88 | 3.49 | 0.07 | 0.01 | 0.19 | 0.02 | 0.54 | 0.20 | 100.08 |
| 9 | 10434 | Peridotite | 46.99 | 5.93 | 1.20 | 9.69 | 0.15 | 31.53 | 3.35 | 0.30 | 0.05 | 0.22 | 0.01 | 0.42 | 0.24 | 100.08 |
| 10 | 10435 | Peridotite | 45.86 | 5.65 | 1.23 | 10.00 | 0.22 | 25.95 | 10.22 | 0.32 | 0.01 | 0.45 | 0.01 | 0.34 | 0.16 | 100.43 |
| 17 | 10442 | Gabbro | 51.74 | 16.05 | 0.90 | 7.32 | 0.17 | 9.18 | 12.57 | 1.85 | 0.03 | 0.13 | ND | 0.04 | 0.02 | 100.02 |
| 18 | 10443 | Peridotite | 43.80 | 9.05 | 1.25 | 10.12 | 0.17 | 31.19 | 3.19 | 0.16 | 0.03 | 0.44 | 0.03 | 0.34 | 0.19 | 99.96 |
| 19 | 10444 | Peridotite | 42.24 | 5.77 | 1.25 | 10.14 | 0.18 | 38.33 | 0.98 | 0.01 | 0.01 | 0.15 | 0.01 | 0.42 | 0.27 | 99.77 |
| 22 | 10447 | Peridotite | 42.66 | 6.78 | 1.14 | 9.24 | 0.20 | 38.15 | 0.77 | 0.08 | 0.01 | 0.15 | 0.01 | 0.44 | 0.27 | 99.89 |
| 23 | 10448 | Pyroxenite | 49.08 | 11.34 | 1.10 | 8.94 | 0.18 | 20.92 | 7.27 | 0.71 | 0.10 | 0.29 | 0.02 | 0.29 | 0.07 | 100.30 |
| 27 | 11377 | Peridotite | 44.21 | 11.47 | 1.18 | 9.58 | 0.17 | 26.22 | 6.32 | 0.19 | 0.13 | 0.29 | 0.03 | 0.46 | 0.01 | 100.27 |
| 34 | 11384 | Pyroxenite | 48.57 | 6.55 | 1.04 | 8.40 | 0.16 | 30.70 | 3.95 | 0.06 | 0.01 | 0.14 | 0.01 | 0.40 | 0.22 | 100.21 |
| 36 | 11386 | Peridotite | 37.14 | 12.78 | 1.41 | 11.39 | 0.16 | 32.23 | 3.72 | 0.10 | 0.04 | 0.14 | 0.01 | 0.56 | 0.11 | 99.79 |
| 38 | 11388 | Gabbro | 50.47 | 14.91 | 1.55 | 12.52 | 0.23 | 6.57 | 10.24 | 2.24 | 0.19 | 0.74 | 0.01 | 0.03 | 0.01 | 99.71 |
| 65 | 11395 | Pyroxenite | 50.21 | 7.62 | 1.08 | 8.74 | 0.18 | 27.67 | 3.41 | 0.26 | 0.03 | 0.21 | 0.01 | 0.39 | 0.18 | 99.98 |
| 66 | 11396 | Gabbro | 46.71 | 15.68 | 0.99 | 8.01 | 0.23 | 13.11 | 13.06 | 1.16 | 0.07 | 0.12 | 0.01 | 0.20 | 0.06 | 99.42 |
| 68 | 11398 | Peridotite | 46.64 | 3.06 | 1.35 | 10.93 | 0.21 | 27.82 | 8.01 | 0.03 | 0.02 | 0.28 | 0.02 | 0.43 | 0.21 | 99.00 |
| 55 | 12367 | Pyroxenite | 50.03 | 2.75 | 0.95 | 7.68 | 0.13 | 36.18 | 1.51 | 0.05 | 0.04 | 0.06 | 0.01 | 0.42 | 0.26 | 100.07 |
| 60 | 12371 | Gabbro | 49.56 | 16.68 | 0.97 | 7.82 | 0.23 | 6.75 | 15.62 | 1.50 | 0.30 | 0.35 | 0.01 | 0.03 | 0.02 | 99.84 |
| 62 | 12372 | Greenstone | 30.36 | 19.40 | 1.99 | 16.15 | 0.24 | 30.25 | 0.29 | 0.06 | 0.01 | 1.24 | 0.04 | 0.06 | 0.03 | 100.12 |
| 61 | 12373 | Peridotite | 46.50 | 5.91 | 1.13 | 9.17 | 0.17 | 33.76 | 2.39 | 0.09 | 0.04 | 0.33 | 0.03 | 0.39 | 0.25 | 100.16 |
| 78 | 12380 | Peridotite | 40.59 | 0.23 | 1.87 | 15.11 | 0.08 | 40.55 | 0.02 | 0.09 | 0.00 | 0.01 | ND | 0.64 | 0.32 | 99.51 |

## Table E2.1: Whole rock major element oxides analyses (wt %) for the USM surface samples by XRF.

| USM | PV number | Lithology | SiO2 | Al2O3 | Fe2O3 | FeO | MnO | MgO | CaO | Na2O | K2O | TiO2 | P2O5 | Cr2O3 | NiO | Total |
|---|---|---|---|---|---|---|---|---|---|---|---|---|---|---|---|---|
| 97 | 12399 | Peridotite | 42.15 | 0.60 | 1.44 | 11.68 | 0.20 | 41.82 | 0.03 | 0.14 | ND | 0.03 | ND | 0.64 | 0.40 | 98.97 |
| 102 | 12404 | Greenstone | 48.95 | 6.67 | 1.37 | 11.06 | 0.21 | 20.64 | 10.04 | 0.10 | 0.03 | 0.61 | 0.04 | 0.29 | 0.07 | 100.07 |

## Table E2.2: Whole rock trace elements (ppm) analyses for the USM surface samples by XRF.

| USM | PV number | Lithology | Zr | Y | Sr | Rb | Zn | Cu | Ni |
|---|---|---|---|---|---|---|---|---|---|
| 1 | 10426 | Pyroxenite | 16.8 | 11.8 | 94.8 | 0.4 | 100.0 | 6.0 | 544.0 |
| 3 | 10428 | Gabbro | 2.5 | 5.6 | 225.3 | 1.6 | 35.0 | 64.0 | 83.0 |
| 4 | 10429 | Gabbro | 2.7 | 6.9 | 75.5 | 0.9 | 40.0 | 108.0 | 240.0 |
| 5 | 10430 | Gabbro | 2.1 | 5.4 | 91.0 | 0.6 | 45.0 | 153.0 | 162.0 |
| 8 | 10433 | Pyroxenite | 9.8 | 8.9 | 30.5 | 1.0 | 69.0 | 24.0 | 1634.0 |
| 9 | 10434 | Peridotite | 6.5 | 6.9 | 28.8 | 3.3 | 64.0 | 4.0 | 1894.0 |
| 10 | 10435 | Peridotite | 35.5 | 17.6 | 46.0 | 0.4 | 58.0 | 5.0 | 1274.0 |
| 17 | 10442 | Gabbro | 1.6 | 5.7 | 85.1 | 0.9 | 42.0 | 19.0 | 169.0 |
| 18 | 10443 | Peridotite | 26.6 | 1.8 | 34.5 | 1.3 | 72.0 | 33.0 | 1495.0 |
| 19 | 10444 | Peridotite | 8.7 | 13.8 | 8.5 | 1.4 | 83.0 | 11.0 | 2130.0 |
| 22 | 10447 | Peridotite | 8.1 | 5.5 | 6.3 | 1.0 | 138.0 | 6.0 | 2080.0 |
| 23 | 10448 | Pyroxenite | 16.8 | 4.9 | 36.8 | 3.4 | 61.0 | 11.0 | 513.0 |
| 27 | 11377 | Peridotite | 16.6 | 12.4 | 41.1 | 3.0 | 59.0 | 12.0 | 1067.0 |
| 34 | 11384 | Pyroxenite | 6.7 | 7.1 | 56.9 | 1.5 | 123.0 | 35.0 | 1753.0 |
| 36 | 11386 | Peridotite | 3.8 | 4.2 | 13.4 | 2.1 | 102.0 | ND | 888.0 |
| 38 | 11388 | Gabbro | 11.0 | 6.9 | 240.7 | 4.3 | 64.0 | 22.0 | 64.0 |
| 65 | 11395 | Pyroxenite | 7.7 | 6.6 | 16.8 | 1.3 | 106.0 | 60.0 | 1389.0 |
| 66 | 11396 | Gabbro | 6.1 | 9.4 | 104.3 | 1.6 | 67.0 | 1.0 | 457.0 |
| 68 | 11398 | Peridotite | 15.7 | 10.0 | 66.7 | 0.5 | 67.0 | 64.0 | 1567.0 |

**Table E2.2: Whole rock trace elements (ppm) analyses for the USM surface samples by XRF.**

| USM | PV number | Lithology | Zr | Y | Sr | Rb | Zn | Cu | Ni |
|---|---|---|---|---|---|---|---|---|---|
| 60 | 12371 | Gabbro | 13.0 | 12.9 | 149.2 | 12.8 | 48.0 | 15.0 | 145.0 |
| 62 | 12372 | Greenstone | 18.2 | 5.4 | 2.0 | 1.3 | 101.0 | 20.0 | 228.0 |
| 61 | 12373 | Peridotite | 27.2 | 10.3 | 21.7 | 0.9 | 67.0 | 16.0 | 1981.0 |
| 78 | 12380 | Peridotite | 0.3 | 2.3 | 1.3 | 1.5 | 44.0 | 11.0 | 2713.0 |
| 97 | 12399 | Peridotite | 1.4 | 2.3 | 2.7 | 0.7 | 50.0 | 14.0 | 1832.0 |
| 102 | 12404 | Greenstone | 39.3 | 13.7 | 21.5 | 1.9 | 97.0 | 33.0 | 485.0 |

## Table E2.3: Trace elements (ppm) for the USM surface samples by ICP-MS (Li-Cs).

| USM | PV number | Lithology | Li | P | Sc | Ti | V | Cr | Co | Ni | Cu | Zn | Ga | As | Rb | Sr | Y | Zr | Nb | Ba | Sn | Cs |
|---|---|---|---|---|---|---|---|---|---|---|---|---|---|---|---|---|---|---|---|---|---|---|
| 1 | 10426 | Pyroxenite | 2.80 | 76.40 | 25.90 | 2042.10 | 136.40 | 1568.20 | 86.10 | 577.20 | 7.30 | 95.00 | 12.20 | 0.30 | 0.60 | 81.90 | 9.50 | 16.40 | 0.20 | 83.30 | 0.20 | 0.10 |
| 3 | 10428 | Gabbro | 6.80 | 13.10 | 36.40 | 709.90 | 158.00 | 268.40 | 62.70 | 95.60 | 61.80 | 33.20 | 13.30 | 0.30 | 0.50 | 215.50 | 2.90 | 1.80 | ND | 28.30 | 0.20 | ND |
| 4 | 10429 | Gabbro | 3.20 | 9.60 | 47.70 | 1150.60 | 212.80 | 500.20 | 59.10 | 265.00 | 112.00 | 40.80 | 11.20 | 0.30 | 0.20 | 72.70 | 4.80 | 1.80 | ND | 8.10 | 0.10 | ND |
| 5 | 10430 | Gabbro | 5.40 | 9.70 | 40.20 | 876.70 | 152.10 | 312.60 | 54.90 | 187.60 | 149.30 | 42.80 | 13.00 | 0.40 | 0.20 | 91.20 | 3.30 | 1.10 | ND | 6.50 | 0.30 | ND |
| 8 | 10433 | Pyroxenite | 3.80 | 81.30 | 13.00 | 1150.60 | 105.10 | 3536.40 | 108.50 | 1610.20 | 21.20 | 62.10 | 5.30 | 0.30 | 0.40 | 30.30 | 3.20 | 6.70 | 0.20 | 9.60 | 0.40 | ND |
| 9 | 10434 | Peridotite | 2.20 | 46.20 | 12.10 | 1946.50 | 107.70 | 2183.90 | 85.10 | 1437.10 | 8.70 | 47.80 | 4.10 | 0.60 | 1.50 | 25.70 | 2.50 | 13.00 | 1.20 | 4.00 | 0.60 | 0.40 |
| 10 | 10435 | Peridotite | 1.90 | 48.50 | 27.80 | 2703.60 | 146.10 | 2156.70 | 91.20 | 1215.00 | 5.90 | 51.30 | 6.60 | 0.30 | 0.30 | 49.20 | 15.70 | 32.30 | 0.60 | 3.60 | 0.50 | 0.10 |
| 17 | 10442 | Gabbro | 4.00 | 5.50 | 35.60 | 828.60 | 163.70 | 304.70 | 54.20 | 186.90 | 20.60 | 40.40 | 12.20 | 0.40 | 0.10 | 76.90 | 3.10 | 1.10 | ND | 3.60 | 0.30 | 0.00 |
| 18 | 10443 | Peridotite | 7.70 | 137.30 | 18.10 | 2417.10 | 171.60 | 2120.90 | 97.10 | 1394.40 | 33.70 | 70.70 | 8.10 | 0.30 | 0.70 | 33.50 | 8.70 | 22.90 | 0.70 | 39.30 | 0.30 | 0.20 |
| 19 | 10444 | Peridotite | 7.80 | 31.10 | 9.20 | 743.70 | 104.40 | 2734.20 | 103.00 | 1840.90 | 12.70 | 77.50 | 4.80 | 0.30 | 1.00 | 8.00 | 3.60 | 6.80 | 0.10 | 5.50 | 1.40 | 1.90 |
| 22 | 10447 | Peridotite | 7.20 | 26.00 | 11.60 | 691.40 | 83.20 | 2734.60 | 107.80 | 1849.40 | 7.00 | 110.80 | 5.00 | 0.50 | 0.60 | 6.20 | 2.90 | 6.10 | 0.20 | 0.90 | 0.30 | 0.50 |
| 23 | 10448 | Pyroxenite | 11.10 | 77.30 | 25.30 | 1652.20 | 145.40 | 1458.80 | 53.50 | 397.30 | 12.30 | 42.90 | 6.40 | 0.30 | 1.80 | 29.60 | 9.00 | 15.60 | 0.60 | 25.70 | 0.60 | 1.00 |
| 27 | 11377 | Peridotite | 35.80 | 114.30 | 29.70 | 1600.20 | 158.90 | 3273.10 | 86.80 | 978.90 | 12.50 | 57.90 | 9.20 | 0.30 | 2.10 | 43.70 | 8.20 | 15.40 | 0.60 | 22.70 | 0.80 | 0.40 |
| 34 | 11384 | Pyroxenite | 6.70 | 32.40 | 13.50 | 856.90 | 77.90 | 2658.00 | 99.90 | 1745.10 | 34.30 | 107.60 | 4.50 | 3.10 | 0.50 | 59.10 | 2.60 | 4.60 | 0.10 | 11.70 | 0.70 | 0.30 |
| 36 | 11386 | Peridotite | 3.00 | 53.50 | 23.10 | 765.90 | 240.20 | 3418.10 | 120.00 | 797.60 | 1.00 | 96.30 | 11.90 | 0.40 | 1.20 | 14.50 | 2.30 | 4.20 | 0.30 | 14.00 | 1.30 | 0.20 |
| 38 | 11388 | Gabbro | 10.00 | 45.10 | 37.20 | 4813.70 | 540.60 | 262.20 | 81.40 | 74.50 | 23.90 | 82.60 | 18.50 | 0.60 | 3.20 | 221.30 | 4.70 | 9.90 | 0.40 | 108.90 | 0.70 | 1.20 |
| 65 | 11395 | Pyroxenite | 6.00 | -0.40 | 13.50 | 375.50 | 60.80 | 2819.50 | 108.50 | 1977.60 | 9.40 | 64.90 | 2.40 | 0.30 | 1.70 | 6.10 | 1.10 | 2.30 | 0.10 | 5.50 | 0.80 | 0.80 |
| 66 | 11396 | Gabbro | 10.80 | 38.50 | 50.80 | 1302.70 | 323.60 | 180.10 | 38.20 | 125.40 | 10.60 | 25.10 | 11.30 | 0.40 | 6.10 | 94.70 | 9.60 | 7.10 | 0.20 | 48.00 | 0.70 | 0.90 |
| 68 | 11398 | Peridotite | 5.00 | 120.90 | 14.80 | 1889.90 | 114.20 | 2634.10 | 113.00 | 1910.40 | 15.60 | 63.80 | 5.30 | 1.20 | 0.60 | 20.70 | 5.40 | 21.50 | 0.20 | 1.50 | 0.50 | 0.10 |
| 55 | 12367 | Pyroxenite | 7.50 | 148.50 | 35.80 | 7327.00 | 342.80 | 329.80 | 89.20 | 209.80 | 17.30 | 85.10 | 16.00 | 0.30 | 0.10 | 1.00 | 4.10 | 19.10 | 1.00 | 0.90 | 0.70 | ND |
| 60 | 12371 | Gabbro | 2.00 | 47.40 | 18.50 | 1225.60 | 104.10 | 2547.20 | 98.90 | 1368.00 | 54.40 | 92.70 | 6.00 | 1.20 | 1.10 | 17.50 | 3.20 | 6.10 | 0.30 | 2.00 | 1.50 | 0.60 |
| 62 | 12372 | Greenstone | 4.00 | 25.00 | 36.30 | 743.60 | 125.10 | 1401.10 | 78.90 | 451.70 | 3.10 | 62.00 | 11.40 | 0.30 | 0.60 | 89.40 | 5.10 | 4.30 | 0.10 | 23.70 | 0.40 | 0.20 |
| 61 | 12373 | Peridotite | 3.60 | 43.00 | 15.00 | 1563.30 | 77.20 | 2906.90 | 101.80 | 1531.60 | 60.90 | 60.30 | 4.70 | 0.50 | 0.30 | 69.10 | 6.40 | 15.30 | 0.20 | 1.10 | 0.40 | ND |
| 78 | 12380 | Peridotite | 0.80 | 17.00 | 6.30 | 613.90 | 28.10 | 3484.80 | 149.30 | 1730.20 | 10.60 | 43.50 | 0.90 | 0.70 | 0.10 | 1.70 | 0.10 | 5.50 | 0.20 | 5.20 | 0.20 | ND |

## Table E2.3: Trace elements (ppm) for the USM surface samples by ICP-MS (Li-Cs).

| USM | PV number | Lithology | Li | P | Sc | Ti | V | Cr | Co | Ni | Cu | Zn | Ga | As | Rb | Sr | Y | Zr | Nb | Ba | Sn | Cs |
|---|---|---|---|---|---|---|---|---|---|---|---|---|---|---|---|---|---|---|---|---|---|---|
| 97 | 12399 | Peridotite | 0.30 | 17.00 | 10.40 | 158.60 | 41.00 | 4693.00 | 146.50 | 1608.40 | 12.70 | 51.00 | 1.40 | 1.00 | 0.20 | 2.40 | 0.50 | 1.50 | ND | 16.90 | 2.20 | ND |
| 102 | 12404 | Greenstone | 10.80 | 177.50 | 31.60 | 3589.10 | 164.70 | 1986.50 | 78.40 | 496.40 | 36.30 | 92.10 | 8.60 | 1.30 | 1.10 | 24.10 | 13.50 | 39.40 | 1.80 | 2.40 | 0.50 | 0.30 |

## Table E2.3: Trace elements (ppm) for the USM surface samples by ICP-MS (La-U).

| USM | PV number | Lithology | La | Ce | Pr | Nd | Sm | Eu | Gd | Tb | Dy | Ho | Er | Tm | Yb | Lu | Hf | Ta | W | Au | Pb | Th | U |
|---|---|---|---|---|---|---|---|---|---|---|---|---|---|---|---|---|---|---|---|---|---|---|---|
| 1 | 10426 | Pyroxenite | 1.80 | 3.90 | 0.60 | 2.90 | 1.00 | 0.40 | 1.10 | 0.20 | 1.50 | 0.30 | 0.90 | 0.10 | 0.90 | 0.10 | 0.70 | ND | 0.10 | ND | 1.50 | 0.20 | 0.10 |
| 3 | 10428 | Gabbro | 0.40 | 0.90 | 0.10 | 0.80 | 0.30 | 0.20 | 0.40 | 0.10 | 0.50 | 0.10 | 0.30 | ND | 0.30 | ND | 0.10 | ND | 0.10 | ND | 2.00 | ND | ND |
| 4 | 10429 | Gabbro | 0.30 | 0.50 | 0.10 | 0.60 | 0.30 | 0.20 | 0.40 | 0.10 | 0.70 | 0.20 | 0.50 | 0.10 | 0.50 | 0.10 | 0.10 | ND | ND | ND | 1.50 | ND | ND |
| 5 | 10430 | Gabbro | 0.10 | 0.20 | ND | 0.30 | 0.20 | 0.20 | 0.30 | 0.10 | 0.50 | 0.10 | 0.30 | 0.10 | 0.40 | 0.10 | 0.10 | ND | 0.10 | ND | 1.80 | ND | ND |
| 8 | 10433 | Pyroxenite | 0.30 | 0.70 | 0.10 | 0.50 | 0.20 | 0.10 | 0.20 | 0.10 | 0.40 | 0.10 | 0.30 | 0.10 | 0.40 | 0.10 | 0.20 | ND | 0.70 | ND | 3.10 | ND | ND |
| 9 | 10434 | Peridotite | 0.40 | 0.90 | 0.10 | 0.50 | 0.10 | 0.10 | 0.20 | ND | 0.30 | 0.10 | 0.20 | ND | 0.30 | ND | 0.40 | 0.10 | 0.50 | ND | 3.70 | ND | ND |
| 10 | 10435 | Peridotite | 1.40 | 4.10 | 0.80 | 4.20 | 1.50 | 0.50 | 1.90 | 0.40 | 2.50 | 0.50 | 1.50 | 0.20 | 1.50 | 0.20 | 1.10 | ND | 0.20 | ND | 3.10 | 0.20 | 0.10 |
| 17 | 10442 | Gabbro | 0.10 | 0.20 | 0.00 | 0.30 | 0.10 | 0.20 | 0.20 | 0.10 | 0.50 | 0.10 | 0.30 | 0.10 | 0.40 | 0.10 | 0.10 | ND | 0.10 | ND | 2.30 | ND | ND |
| 18 | 10443 | Peridotite | 1.10 | 2.40 | 0.40 | 1.90 | 0.60 | 0.20 | 0.80 | 0.20 | 1.30 | 0.30 | 0.90 | 0.10 | 0.90 | 0.10 | 0.80 | 0.10 | 0.20 | ND | 5.20 | 0.10 | ND |
| 19 | 10444 | Peridotite | 0.20 | 0.30 | 0.10 | 0.30 | 0.10 | 0.10 | 0.20 | 0.10 | 0.50 | 0.10 | 0.40 | 0.10 | 0.40 | 0.10 | 0.20 | ND | 0.10 | ND | 19.10 | ND | ND |
| 22 | 10447 | Peridotite | 0.10 | 0.30 | 0.00 | 0.30 | 0.10 | 0.00 | 0.20 | 0.00 | 0.40 | 0.10 | 0.30 | 0.10 | 0.30 | 0.10 | 0.20 | ND | 0.10 | ND | 4.20 | ND | ND |
| 23 | 10448 | Pyroxenite | 1.70 | 3.20 | 0.50 | 2.20 | 0.60 | 0.20 | 0.90 | 0.20 | 1.30 | 0.30 | 0.80 | 0.10 | 0.90 | 0.10 | 0.50 | ND | 0.20 | ND | 3.70 | 0.10 | ND |
| 27 | 11377 | Peridotite | 1.20 | 2.60 | 0.40 | 1.80 | 0.50 | 0.10 | 0.70 | 0.10 | 1.10 | 0.30 | 0.80 | 0.10 | 0.90 | 0.10 | 0.50 | ND | 0.70 | ND | 4.20 | 0.30 | 0.10 |
| 34 | 11384 | Pyroxenite | 0.20 | 0.40 | 0.10 | 0.30 | 0.10 | 0.10 | 0.20 | ND | 0.30 | 0.10 | 0.20 | ND | 0.30 | 0.00 | 0.10 | ND | 0.40 | ND | 6.70 | ND | ND |
| 36 | 11386 | Peridotite | 0.70 | 1.40 | 0.20 | 0.80 | 0.20 | 0.10 | 0.20 | 0.00 | 0.30 | 0.10 | 0.20 | ND | 0.30 | 0.10 | 0.10 | ND | 0.20 | ND | 3.00 | 0.10 | ND |
| 38 | 11388 | Gabbro | 1.50 | 3.20 | 0.40 | 1.80 | 0.60 | 0.40 | 0.60 | 0.10 | 0.80 | 0.20 | 0.50 | 0.10 | 0.50 | 0.10 | 0.30 | ND | 0.10 | ND | 3.70 | 0.20 | 0.10 |
| 65 | 11395 | Pyroxenite | 0.20 | 0.30 | 0.00 | 0.20 | 0.10 | 0.00 | 0.10 | ND | 0.10 | ND | 0.10 | ND | 0.10 | ND | 0.10 | ND | 0.20 | ND | 3.40 | ND | ND |
| 66 | 11396 | Gabbro | 1.10 | 1.90 | 0.40 | 2.10 | 0.80 | 0.40 | 1.00 | 0.20 | 1.40 | 0.30 | 0.90 | 0.10 | 0.90 | 0.10 | 0.30 | ND | 0.10 | ND | 0.80 | 0.20 | ND |
| 68 | 11398 | Peridotite | 0.60 | 1.40 | 0.20 | 1.00 | 0.30 | 0.10 | 0.50 | 0.10 | 0.80 | 0.20 | 0.50 | 0.10 | 0.50 | 0.10 | 0.60 | ND | 0.50 | ND | 1.90 | ND | ND |

## Table E2.3: Trace elements (ppm) for the USM surface samples by ICP-MS (La-U).

| USM | PV number | Lithology | La | Ce | Pr | Nd | Sm | Eu | Gd | Tb | Dy | Ho | Er | Tm | Yb | Lu | Hf | Ta | W | Au | Pb | Th | U |
|---|---|---|---|---|---|---|---|---|---|---|---|---|---|---|---|---|---|---|---|---|---|---|---|
| 55 | 12367 | Pyroxenite | 0.10 | 0.10 | ND | ND | ND | ND | ND | ND | 0.30 | 0.10 | 0.60 | 0.10 | 1.00 | 0.20 | 0.80 | 0.10 | 0.10 | 0.00 | 16.40 | ND | ND |
| 60 | 12371 | Gabbro | 0.30 | 0.80 | 0.10 | 0.50 | 0.20 | 0.00 | 0.20 | ND | 0.40 | 0.10 | 0.30 | 0.10 | 0.40 | 0.10 | 0.20 | ND | 0.30 | ND | 6.60 | 0.10 | ND |
| 62 | 12372 | Greenstone | 0.70 | 1.40 | 0.20 | 1.10 | 0.40 | 0.20 | 0.50 | 0.10 | 0.70 | 0.20 | 0.50 | 0.10 | 0.50 | 0.10 | 0.20 | ND | 0.10 | ND | 6.60 | 0.10 | ND |
| 61 | 12373 | Peridotite | 0.80 | 2.70 | 0.50 | 2.50 | 0.80 | 0.20 | 0.90 | 0.20 | 1.00 | 0.20 | 0.60 | 0.10 | 0.50 | 0.10 | 0.50 | ND | 0.70 | ND | 2.10 | 0.10 | ND |
| 78 | 12380 | Peridotite | ND | 0.10 | ND | ND | ND | ND | ND | ND | ND | ND | ND | ND | ND | ND | 0.20 | ND | 0.10 | ND | 2.50 | ND | 0.10 |
| 97 | 12399 | Peridotite | 0.10 | 0.20 | ND | 0.10 | 0.00 | ND | ND | ND | 0.10 | ND | ND | ND | 0.10 | ND | ND | ND | ND | ND | 12.30 | ND | ND |
| 102 | 12404 | Greenstone | 2.60 | 6.30 | 1.00 | 4.70 | 1.40 | 0.40 | 1.70 | 0.30 | 2.10 | 0.40 | 1.20 | 0.20 | 1.20 | 0.20 | 1.10 | 0.10 | 0.60 | ND | 1.30 | 0.50 | 0.10 |

## Table E3.1: Whole rock major element oxides (wt %) for the UNK 93 surface samples by XRF.

| Sample # | Lithology | $SiO_2$ | $Al_2O_3$ | $Fe_2O_3$ | FeO | MnO | MgO | CaO | Na2O | $K_2O$ | $TiO_2$ | $P_2O_5$ | $Cr_2O_3$ | NiO | TOTAL |
|---|---|---|---|---|---|---|---|---|---|---|---|---|---|---|---|
| UNK 93/1 | Peridotite | 44.27 | 5.43 | 1.27 | 10.32 | 0.13 | 33.15 | 4.36 | 0.29 | 0.02 | 0.20 | 0.02 | 0.44 | 0.24 | 100.10 |
| UNK 93/2A | Pyroxenite | 49.12 | 5.31 | 1.26 | 10.24 | 0.17 | 30.07 | 2.57 | 0.18 | 0.02 | 0.20 | 0.02 | 0.70 | 0.23 | 100.10 |
| UNK 93/4 | Peridotite | 43.34 | 1.67 | 1.14 | 9.26 | 0.15 | 43.21 | 0.36 | 0.06 | 0.01 | 0.05 | 0.01 | 0.45 | 0.34 | 100.00 |
| UNK 93/5A | Pyroxenite | 50.77 | 1.94 | 1.16 | 9.40 | 0.19 | 34.41 | 1.59 | 0.08 | 0.02 | 0.08 | 0.01 | 0.53 | 0.21 | 100.40 |
| UNK 93/7 | Peridotite | 32.98 | 19.24 | 1.54 | 12.43 | 0.17 | 33.59 | 0.17 | 0.06 | 0.01 | 0.11 | 0.04 | 0.26 | 0.15 | 100.70 |
| UNK 93/9 | Peridotite | 32.38 | 20.62 | 3.41 | 27.64 | 0.13 | 3.44 | 9.83 | 1.44 | 0.07 | 1.42 | 0.01 | 0.03 | 0.04 | 100.50 |
| UNK 93/13 | Peridotite | 49.05 | 2.91 | 1.02 | 8.23 | 0.11 | 37.11 | 0.87 | 0.07 | ND | 0.07 | 0.01 | 0.59 | 0.26 | 100.30 |
| UNK 93/15 | Peridotite | 47.93 | 1.57 | 1.28 | 10.36 | 0.20 | 36.09 | 1.32 | 0.11 | ND | 0.07 | 0.01 | 0.55 | 0.21 | 99.67 |
| UNK 93/16 | Peridotite | 44.69 | 8.39 | 1.08 | 8.74 | 0.15 | 33.18 | 3.05 | 0.18 | 0.02 | 0.02 | 0.01 | 0.70 | 0.17 | 100.40 |
| UNK 93/18 | Pyroxenite | 51.83 | 4.84 | 1.08 | 8.78 | 0.20 | 28.34 | 3.63 | 0.43 | 0.08 | 0.13 | 0.01 | 0.52 | 0.09 | 99.98 |
| UNK 93/20A | Peridotite | 45.98 | 6.63 | 1.04 | 8.38 | 0.16 | 33.40 | 2.83 | 0.11 | 0.00 | 0.05 | 0.01 | 0.74 | 0.20 | 99.52 |
| UNK 93/23 | Gabbro | 52.39 | 16.08 | 0.77 | 6.25 | 0.16 | 10.22 | 12.29 | 1.89 | 0.08 | 0.15 | 0.01 | 0.04 | 0.01 | 100.30 |
| UNK 93/24 | Gabbro | 51.33 | 15.92 | 0.91 | 7.37 | 0.17 | 9.50 | 12.32 | 1.78 | 0.02 | 0.15 | 0.01 | 0.04 | 0.03 | 99.54 |
| UNK 93/29 | Pyroxenite | 54.78 | 2.81 | 0.85 | 6.91 | 0.13 | 25.35 | 8.04 | 0.08 | 0.02 | 0.07 | 0.01 | 0.44 | 0.26 | 99.76 |
| UNK 93/32 | Peridotite | 28.95 | 22.44 | 2.01 | 16.26 | 0.25 | 30.32 | 0.09 | 0.02 | 0.01 | 0.32 | 0.02 | 0.05 | 0.02 | 100.70 |
| UNK 93/34 | Peridotite | 44.22 | 2.85 | 1.06 | 8.59 | 0.15 | 41.59 | 0.17 | 0.07 | 0.01 | 0.12 | 0.01 | 0.33 | 0.34 | 99.48 |
| UNK 93/37 | Pyroxenite | 51.63 | 4.66 | 1.22 | 9.84 | 0.22 | 22.42 | 9.34 | 0.39 | 0.01 | 0.23 | 0.01 | 0.36 | 0.14 | 100.50 |
| UNK 93/39 | Pyroxenite | 50.48 | 6.56 | 1.10 | 8.92 | 0.20 | 22.37 | 9.41 | 0.38 | 0.07 | 0.26 | 0.01 | 0.33 | 0.16 | 100.20 |
| UNK 93/41 | Pyroxenite | 54.09 | 2.91 | 1.42 | 11.47 | 0.27 | 27.02 | 2.56 | 0.19 | 0.01 | 0.23 | 0.01 | 0.40 | 0.19 | 100.80 |
| UNK 93/42 | Pyroxenite | 54.17 | 2.49 | 1.39 | 11.28 | 0.26 | 26.83 | 2.46 | 0.21 | 0.02 | 0.20 | 0.01 | 0.41 | 0.18 | 99.92 |
| UNK 93/46 | Peridotite | 46.11 | 2.15 | 1.24 | 10.02 | 0.21 | 29.34 | 9.68 | 0.23 | 0.01 | 0.16 | 0.01 | 0.65 | 0.22 | 100.00 |
| UNK 93/47 | Peridotite | 45.62 | 1.95 | 1.29 | 10.45 | 0.19 | 30.92 | 8.73 | 0.19 | 0.00 | 0.14 | 0.01 | 0.63 | 0.21 | 100.30 |
| UNK 93/50 | Pyroxenite | 49.90 | 4.02 | 1.46 | 11.85 | 0.28 | 25.59 | 5.52 | 0.18 | 0.00 | 0.25 | 0.01 | 0.40 | 0.18 | 99.65 |
| UNK 93/52 | Pyroxenite | 49.84 | 2.97 | 1.20 | 9.74 | 0.25 | 26.88 | 8.08 | 0.20 | 0.01 | 0.27 | 0.01 | 0.47 | 0.17 | 100.10 |

## Table E3.1: Whole rock major element oxides (wt %) for the UNK 93 surface samples by XRF.

| Sample # | Lithology | $SiO_2$ | $Al_2O_3$ | $Fe_2O_3$ | FeO | MnO | MgO | CaO | Na2O | $K_2O$ | $TiO_2$ | $P_2O_5$ | $Cr_2O_3$ | NiO | TOTAL |
|---|---|---|---|---|---|---|---|---|---|---|---|---|---|---|---|
| UNK 93/53 | Pyroxenite | 50.40 | 4.02 | 1.34 | 10.83 | 0.20 | 23.02 | 9.39 | 0.38 | 0.02 | 0.27 | 0.01 | 0.37 | 0.15 | 100.40 |
| UNK 93/54 | Gabbro | 53.09 | 21.78 | 0.47 | 3.83 | 0.08 | 4.16 | 13.23 | 3.23 | 0.22 | 0.15 | 0.01 | 0.04 | 0.01 | 100.30 |
| UNK 93/56 | Pyroxenite | 47.22 | 9.91 | 1.71 | 13.83 | 0.22 | 17.04 | 8.98 | 0.89 | 0.05 | 0.34 | 0.02 | 0.19 | 0.07 | 100.50 |
| UNK 93/58 | Peridotite | 45.31 | 4.00 | 1.08 | 8.76 | 0.15 | 35.17 | 4.45 | 0.09 | 0.01 | 0.18 | 0.01 | 0.42 | 0.28 | 99.92 |
| UNK 93/59 | Pyroxenite | 51.01 | 5.79 | 1.07 | 8.68 | 0.18 | 26.98 | 5.32 | 0.15 | 0.06 | 0.18 | 0.03 | 0.55 | 0.17 | 100.20 |
| UNK 93/61 | Peridotite | 45.24 | 5.82 | 1.28 | 10.37 | 0.16 | 30.24 | 6.12 | 0.09 | 0.01 | 0.28 | 0.02 | 0.44 | 0.24 | 100.30 |
| UNK 93/64 | Peridotite | 44.11 | 2.77 | 1.09 | 8.82 | 0.13 | 42.41 | 0.10 | 0.12 | ND | 0.07 | 0.01 | 0.50 | 0.36 | 100.50 |
| UNK 93/65 | Peridotite | 33.80 | 17.93 | 1.62 | 13.10 | 0.11 | 32.75 | 0.28 | 0.07 | ND | 1.13 | 0.06 | 0.02 | 0.09 | 101.00 |
| UNK 93/67 | Pyroxenite | 50.46 | 9.91 | 1.08 | 8.77 | 0.20 | 22.89 | 5.93 | 0.36 | 0.10 | 0.32 | 0.04 | 0.35 | 0.09 | 100.50 |
| UNK 93/69 | Pyroxenite | 47.29 | 4.18 | 1.49 | 12.04 | 0.23 | 27.46 | 6.32 | 0.12 | 0.00 | 0.27 | 0.01 | 0.43 | 0.20 | 100.10 |
| UNK 93/73 | Peridotite | 46.49 | 5.55 | 0.94 | 7.61 | 0.25 | 31.05 | 7.25 | 0.07 | ND | 0.13 | 0.01 | 0.57 | 0.23 | 100.20 |
| UNK 93/75 | Peridotite | 30.40 | 18.82 | 1.94 | 15.67 | 0.17 | 31.44 | 0.23 | 0.10 | 0.01 | 1.09 | 0.05 | 0.06 | 0.03 | 100.00 |
| UNK 93/76 | Quartzite | 64.86 | 1.54 | 0.54 | 4.36 | 0.42 | 10.14 | 16.99 | 0.59 | 0.06 | 0.08 | 0.01 | 0.18 | 0.04 | 99.79 |
| UNK 93/78 | Peridotite | 47.16 | 4.96 | 0.95 | 7.66 | 0.18 | 31.69 | 5.60 | 0.09 | 0.02 | 0.10 | 0.01 | 0.51 | 0.24 | 99.17 |
| UNK 93/80 | Pyroxenite | 49.14 | 6.49 | 1.16 | 9.39 | 0.17 | 27.26 | 6.12 | 0.16 | 0.02 | 0.23 | 0.02 | 0.42 | 0.19 | 100.80 |
| UNK 93/84 | Pyroxenite | 52.94 | 3.85 | 1.14 | 9.27 | 0.19 | 22.68 | 9.37 | 0.11 | 0.02 | 0.28 | 0.01 | 0.21 | 0.17 | 100.30 |
| UNK 93/85 | Gabbro | 51.32 | 17.05 | 0.53 | 4.32 | 0.13 | 7.85 | 16.53 | 2.25 | 0.44 | 0.21 | 0.01 | 0.13 | 0.03 | 100.80 |
| UNK 93/86 | Peridotite | 45.48 | 10.89 | 1.18 | 9.52 | 0.22 | 20.48 | 11.21 | 0.43 | 0.04 | 0.18 | 0.01 | 0.45 | 0.16 | 100.30 |
| UNK 93/88 | Pyroxenite | 50.08 | 11.18 | 0.70 | 5.64 | 0.17 | 11.37 | 19.80 | 0.73 | 0.21 | 0.29 | 0.01 | 0.20 | 0.04 | 100.40 |
| UNK 93/90 | Peridotite | 46.85 | 10.36 | 1.24 | 10.04 | 0.24 | 22.37 | 8.00 | 0.49 | 0.01 | 0.19 | 0.01 | 0.45 | 0.17 | 100.40 |
| UNK 93/93 | Peridotite | 44.30 | 4.37 | 1.11 | 8.98 | 0.15 | 37.66 | 2.42 | 0.14 | ND | 0.20 | 0.01 | 0.41 | 0.28 | 100.00 |
| UNK 93/94 | Peridotite | 46.70 | 3.58 | 1.03 | 8.37 | 0.14 | 37.49 | 1.79 | 0.21 | 0.01 | 0.24 | 0.02 | 0.33 | 0.30 | 100.20 |
| UNK 93/96 | Peridotite | 47.01 | 8.81 | 1.00 | 8.09 | 0.13 | 30.87 | 3.50 | 0.15 | 0.03 | 0.05 | 0.01 | 0.69 | 0.18 | 100.50 |
| UNK 93/98 | Gabbro | 51.85 | 16.75 | 0.98 | 7.92 | 0.17 | 8.64 | 11.59 | 2.03 | 0.14 | 0.16 | 0.01 | 0.04 | 0.01 | 100.30 |

## Table E3.1: Whole rock major element oxides (wt %) for the UNK 93 surface samples by XRF.

| Sample # | Lithology | $SiO_2$ | $Al_2O_3$ | $Fe_2O_3$ | FeO | MnO | MgO | CaO | Na2O | $K_2O$ | $TiO_2$ | $P_2O_5$ | $Cr_2O_3$ | NiO | TOTAL |
|---|---|---|---|---|---|---|---|---|---|---|---|---|---|---|---|
| UNK 93/100 | Peridotite | 48.51 | 6.49 | 0.97 | 7.84 | 0.15 | 31.44 | 4.35 | 0.12 | ND | 0.12 | 0.01 | 0.39 | 0.22 | 100.60 |
| UNK 93/101 | Gabbro | 51.92 | 16.83 | 0.99 | 8.04 | 0.18 | 8.70 | 11.49 | 2.19 | 0.15 | 0.14 | 0.01 | 0.03 | 0.01 | 100.70 |

## Table E3.2: Whole rock trace elements (ppm) for the UNK 93 surface samples by XRF.

| Sample # | Lithology | Sc | V | Cr | Co | Ni | Cu | Zn | Ga | Rb | Sr | Y | Zr | Nb | Mo | Ba | Pb | Th |
|---|---|---|---|---|---|---|---|---|---|---|---|---|---|---|---|---|---|---|
| UNK 93/1 | Peridotite | 20.3 | 51.5 | 2504.0 | 114.4 | 1869.0 | 9.7 | 52.9 | 5.3 | 2.1 | 27.1 | 3.1 | 6.3 | 2.6 | 1.0 | 7.9 | ND | 5.6 |
| UNK 93/2A | Pyroxenite | 16.9 | 105.5 | 4450.0 | 120.5 | 1805.0 | 0.3 | 61.4 | 4.9 | 1.8 | 17.1 | 2.6 | 13.7 | 2.9 | 0.5 | 7.6 | 1.3 | 4.0 |
| UNK 93/4 | Peridotite | 6.8 | 29.0 | 2241.0 | 129.4 | 2514.0 | 12.6 | 47.7 | 0.2 | 1.9 | 0.9 | 0.2 | 1.3 | 2.1 | 0.4 | 12.2 | 2.7 | 4.8 |
| UNK 93/5A | Pyroxenite | 20.1 | 83.5 | 3010.0 | 114.2 | 1573.0 | 11.0 | 66.3 | 2.0 | 1.3 | 3.1 | 0.7 | 0.9 | 1.4 | 0.8 | 8.7 | 0.8 | 0.8 |
| UNK 93/7 | Peridotite | 14.5 | 93.9 | 1752.0 | 113.6 | 1130.0 | 5.4 | 550.2 | 38.4 | 1.6 | 0.1 | 88.7 | 95.0 | 12.4 | 0.4 | 3.1 | 14.2 | 9.6 |
| UNK 93/9 | Peridotite | 19.2 | 1419.0 | 62.3 | 84.0 | 164.0 | 10.6 | 128.9 | 35.5 | 2.8 | 242.4 | 3.1 | 1.9 | 2.8 | 0.4 | 30.3 | 2.9 | 2.0 |
| UNK 93/13 | Peridotite | 22.0 | 124.6 | 3375.0 | 110.9 | 1957.0 | 6.1 | 57.7 | 2.6 | 0.6 | 1.6 | 0.2 | 1.7 | 1.7 | 0.6 | 1.2 | 0.4 | 1.3 |
| UNK 93/15 | Peridotite | 15.4 | 67.7 | 3019.0 | 127.8 | 1559.0 | 6.0 | 67.6 | 1.1 | 2.0 | 1.4 | 1.2 | 1.1 | 1.1 | 0.6 | 10.8 | 1.2 | 0.3 |
| UNK 93/16 | Peridotite | 25.8 | 116.6 | 3724.0 | 105.0 | 1290.0 | 12.6 | 55.2 | 4.8 | 1.8 | 13.2 | 2.2 | 0.4 | 0.4 | 0.3 | 0.3 | 0.5 | 4.7 |
| UNK 93/18 | Pyroxenite | 22.8 | 119.7 | 3298.0 | 89.1 | 626.0 | 12.5 | 62.3 | 4.1 | 2.4 | 30.6 | 0.6 | 4.9 | 1.5 | 1.2 | 41.3 | 0.1 | 6.2 |
| UNK 93/20A | Peridotite | 16.2 | 78.6 | 3953.0 | 111.7 | 1488.0 | 9.3 | 54.5 | 3.4 | 2.0 | 12.6 | 1.1 | 0.2 | 0.2 | 0.1 | 0.7 | 1.5 | 4.4 |
| UNK 93/23 | Gabbro | 38.1 | 145.9 | 258.0 | 65.7 | 60.0 | 6.3 | 37.1 | 15.8 | 1.9 | 228.7 | 2.1 | 2.4 | 1.3 | 2.2 | 41.0 | 0.6 | 5.3 |
| UNK 93/24 | Gabbro | 41.2 | 162.6 | 279.9 | 47.6 | 183.3 | 129.9 | 44.0 | 12.8 | 0.2 | 84.9 | 2.1 | 0.3 | 0.7 | 0.0 | 7.2 | 0.1 | 3.0 |
| UNK 93/29 | Pyroxenite | 21.9 | 40.7 | 2825.0 | 116.2 | 1875.0 | 1.9 | 101.7 | 4.3 | 2.4 | 8.6 | 0.5 | 0.6 | 0.3 | 0.5 | 43.6 | 2.3 | 3.7 |
| UNK 93/32 | Peridotite | 69.4 | 363.5 | 276.9 | 90.3 | 139.9 | 0.6 | 182.3 | 12.6 | 1.1 | 1.0 | 1.5 | 2.1 | 0.3 | 0.4 | 19.4 | 0.1 | 3.6 |
| UNK 93/34 | Peridotite | 14.8 | 66.9 | 1897.0 | 110.6 | 2312.0 | 10.7 | 62.8 | 2.7 | 0.5 | 1.0 | 1.2 | 2.0 | 0.8 | 0.2 | 2.6 | 3.3 | 1.8 |
| UNK 93/37 | Pyroxenite | 33.9 | 138.6 | 2308.0 | 94.9 | 1093.0 | 33.0 | 69.2 | 5.7 | 2.4 | 47.4 | 5.2 | 4.4 | 1.3 | 1.7 | 64.6 | 2.5 | 7.3 |
| UNK 93/39 | Pyroxenite | 27.2 | 135.2 | 2134.0 | 99.8 | 1239.0 | 6.0 | 75.6 | 8.0 | 3.5 | 51.1 | 6.1 | 11.3 | 0.3 | 0.1 | 16.1 | 1.5 | 2.7 |
| UNK 93/41 | Pyroxenite | 18.4 | 84.4 | 2624.0 | 113.6 | 1484.0 | 12.1 | 93.8 | 4.4 | 0.4 | 17.6 | 2.3 | 6.5 | 1.8 | 0.3 | 27.8 | 2.3 | 1.4 |

## Table E3.2: Whole rock trace elements (ppm) for the UNK 93 surface samples by XRF.

| Sample # | Lithology | Sc | V | Cr | Co | Ni | Cu | Zn | Ga | Rb | Sr | Y | Zr | Nb | Mo | Ba | Pb | Th |
|---|---|---|---|---|---|---|---|---|---|---|---|---|---|---|---|---|---|---|
| UNK 93/42 | Pyroxenite | 13.3 | 94.3 | 2731.0 | 102.2 | 1442.0 | 2.7 | 94.5 | 3.6 | 0.5 | 14.6 | 1.5 | 3.5 | 1.9 | 0.5 | 30.7 | 1.4 | 4.2 |
| UNK 93/46 | Peridotite | 24.9 | 84.0 | 3679.0 | 114.2 | 1742.0 | 1.1 | 65.5 | 3.5 | 0.2 | 16.1 | 2.0 | 5.0 | 2.1 | 0.9 | 2.8 | 0.3 | 3.0 |
| UNK 93/47 | Peridotite | 24.0 | 82.8 | 3472.0 | 110.4 | 1614.0 | 2.9 | 71.5 | 2.4 | 0.4 | 13.9 | 2.1 | 3.4 | 1.6 | 1.2 | 8.8 | 0.3 | 1.4 |
| UNK 93/50 | Pyroxenite | 20.1 | 118.1 | 2601.0 | 116.5 | 1460.0 | 6.0 | 158.3 | 5.9 | 0.6 | 6.3 | 2.4 | 6.1 | 2.1 | ND | 1.0 | 0.2 | 2.3 |
| UNK 93/52 | Pyroxenite | 22.9 | 89.8 | 2856.0 | 107.8 | 1382.0 | 0.4 | 61.6 | 5.2 | 0.6 | 7.9 | 6.2 | 10.1 | 2.2 | 0.3 | 0.1 | 1.8 | 2.7 |
| UNK 93/53 | Pyroxenite | 25.8 | 102.7 | 2248.0 | 98.6 | 1237.0 | 0.3 | 68.4 | 4.0 | 0.6 | 27.4 | 6.1 | 6.8 | 2.7 | 0.9 | 5.4 | 2.6 | 1.0 |
| UNK 93/54 | Gabbro | 31.4 | 125.4 | 208.5 | 26.0 | 84.6 | 27.3 | 26.4 | 21.2 | 3.0 | 251.6 | 2.3 | 7.8 | 1.8 | 0.4 | 75.9 | 0.8 | 0.3 |
| UNK 93/56 | Pyroxenite | 25.4 | 130.3 | 1123.0 | 92.7 | 482.5 | 14.3 | 110.4 | 13.0 | 2.0 | 124.5 | 6.8 | 10.5 | 3.1 | 0.5 | 36.4 | 0.3 | 2.8 |
| UNK 93/58 | Peridotite | 16.6 | 84.8 | 2199.0 | 109.9 | 2208.0 | 4.2 | 45.9 | 3.7 | 0.3 | 29.0 | 4.4 | 5.1 | 1.5 | 0.2 | 3.6 | 0.8 | 0.2 |
| UNK 93/59 | Pyroxenite | 19.4 | 92.6 | 3613.0 | 111.2 | 1336.0 | 32.1 | 73.6 | 5.6 | 3.2 | 67.6 | 3.7 | 49.0 | 1.2 | 0.5 | 14.6 | 2.0 | 2.6 |
| UNK 93/61 | Peridotite | 19.8 | 108.9 | 2496.0 | 112.2 | 1839.0 | 33.4 | 56.2 | 7.3 | 1.7 | 64.0 | 3.9 | 18.0 | 1.3 | 1.3 | 11.8 | 2.5 | 2.8 |
| UNK 93/64 | Peridotite | 9.2 | 44.1 | 2697.0 | 115.6 | 2491.0 | 17.2 | 35.5 | 2.6 | 0.7 | 0.9 | 0.6 | 4.5 | 0.1 | 0.2 | 3.0 | 1.7 | 3.7 |
| UNK 93/65 | Peridotite | 23.1 | 206.2 | 171.4 | 118.1 | 652.7 | 8.4 | 85.3 | 12.8 | 1.0 | ND | 3.4 | 76.7 | 3.4 | 1.0 | 11.3 | 0.2 | 3.4 |
| UNK 93/67 | Pyroxenite | 27.0 | 158.6 | 2164.0 | 78.0 | 692.5 | 0.4 | 71.1 | 9.1 | 4.0 | 46.5 | 9.9 | 26.9 | 1.1 | 1.3 | 21.3 | 2.7 | 3.8 |
| UNK 93/69 | Pyroxenite | 19.9 | 83.9 | 2488.0 | 120.0 | 1511.0 | 62.1 | 98.6 | 6.5 | 1.3 | 40.9 | 4.5 | 8.1 | 2.1 | 0.5 | 10.9 | 0.1 | 7.9 |
| UNK 93/73 | Peridotite | 20.6 | 79.2 | 3566.0 | 112.7 | 1742.0 | 6.6 | 51.8 | 4.3 | 0.8 | 64.8 | 4.8 | 6.6 | 1.4 | 0.3 | 40.5 | 2.5 | 5.3 |
| UNK 93/75 | Peridotite | 43.3 | 343.6 | 397.8 | 79.2 | 169.4 | 10.0 | 64.6 | 19.1 | 1.9 | 0.7 | 5.4 | 15.7 | 2.2 | 0.1 | 7.5 | 0.4 | 5.8 |
| UNK 93/76 | Quartzite | 22.8 | 41.3 | 1143.0 | 42.7 | 312.2 | 0.6 | 20.1 | 0.5 | 3.0 | 11.3 | 2.4 | 6.8 | 2.2 | 1.3 | 0.7 | 1.6 | 6.5 |
| UNK 93/78 | Peridotite | 18.6 | 67.1 | 3048.0 | 116.4 | 1873.0 | 7.3 | 49.3 | 3.8 | 1.6 | 46.1 | 1.4 | 3.4 | 1.4 | 0.4 | 8.7 | 4.8 | 4.0 |
| UNK 93/80 | Pyroxenite | 24.0 | 118.6 | 2541.0 | 109.5 | 1443.0 | 6.3 | 65.8 | 5.5 | 1.2 | 100.3 | 2.9 | 13.6 | 0.2 | 0.5 | 2.8 | 1.7 | 0.4 |
| UNK 93/84 | Pyroxenite | 22.3 | 119.8 | 1345.0 | 89.3 | 1310.0 | 0.8 | 87.9 | 5.4 | 2.4 | 6.6 | 3.6 | 5.1 | 1.0 | 0.8 | 3.9 | 0.1 | 3.1 |
| UNK 93/85 | Gabbro | 61.1 | 228.2 | 834.3 | 41.5 | 223.9 | 0.1 | 23.3 | 11.7 | 19.4 | 75.9 | 2.9 | 3.4 | 0.5 | 0.6 | 32.1 | 1.0 | 0.1 |
| UNK 93/86 | Peridotite | 31.4 | 114.8 | 2666.0 | 110.8 | 1262.0 | 3.0 | 78.2 | 9.9 | 2.9 | 61.7 | 3.2 | 6.8 | 0.7 | 0.8 | 7.9 | 1.1 | 3.8 |
| UNK 93/88 | Pyroxenite | 58.2 | 325.1 | 1340.0 | 56.0 | 361.0 | 0.6 | 36.8 | 10.6 | 8.1 | 61.4 | 2.2 | 5.1 | 1.0 | 1.0 | 32.9 | 1.1 | 0.2 |

**Table E3.2: Whole rock trace elements (ppm) for the UNK 93 surface samples by XRF.**

| Sample # | Lithology | Sc | V | Cr | Co | Ni | Cu | Zn | Ga | Rb | Sr | Y | Zr | Nb | Mo | Ba | Pb | Th |
|---|---|---|---|---|---|---|---|---|---|---|---|---|---|---|---|---|---|---|
| UNK 93/90 | Peridotite | 25.7 | 141.3 | 2515.0 | 89.8 | 1344.0 | 5.9 | 110.8 | 8.9 | 1.0 | 5.7 | 3.1 | 1.7 | 1.8 | 0.8 | 6.6 | 1.9 | 6.4 |
| UNK 93/93 | Peridotite | 15.7 | 79.8 | 2132.0 | 111.5 | 2126.0 | 3.1 | 53.5 | 4.7 | 1.4 | 17.4 | 2.5 | 5.2 | 0.5 | 0.2 | 15.0 | 0.3 | 2.9 |
| UNK 93/94 | Peridotite | 15.3 | 81.1 | 1907.0 | 109.2 | 2193.0 | 2.1 | 48.0 | 4.4 | 1.8 | 9.0 | 3.6 | 13.9 | 1.8 | 0.1 | 8.6 | 1.5 | 2.8 |
| UNK 93/96 | Peridotite | 21.3 | 118.5 | 3850.0 | 103.0 | 1384.0 | 3.1 | 60.1 | 5.1 | 4.6 | 16.2 | 1.2 | 0.7 | 1.5 | 0.1 | 1.4 | 1.8 | 5.5 |
| UNK 93/98 | Gabbro | 34.5 | 144.2 | 190.1 | 66.2 | 75.8 | 73.1 | 52.9 | 16.4 | 4.1 | 205.9 | 1.8 | 3.1 | 1.2 | 0.7 | 58.2 | 0.2 | 4.8 |
| UNK 93/100 | Peridotite | 14.3 | 77.2 | 2351.0 | 99.9 | 1725.0 | 8.4 | 55.0 | 6.0 | 0.9 | 50.8 | 0.8 | 2.2 | 0.7 | 1.2 | 9.3 | 4.1 | 4.9 |
| UNK 93/101 | Gabbro | 36.4 | 160.1 | 181.6 | 65.9 | 71.7 | 83.6 | 52.3 | 13.6 | 1.0 | 211.2 | 1.1 | 3.2 | 0.9 | 0.5 | 41.1 | 0.8 | 5.7 |

## Table E3.3: Trace elements (ppm) for the UNK 93 surface samples by ICP-MS (Li-Cs).

| Sample # | Lithology | Li | P | Sc | Ti | V | Cr | Co | Ni | Cu | Zn | Ga | As | Rb | Sr | Y | Zr | Nb | Ba | Sn | Cs |
|---|---|---|---|---|---|---|---|---|---|---|---|---|---|---|---|---|---|---|---|---|---|
| UNK 93/1 | Peridotite | 2.89 | 33.35 | 15.59 | 931.20 | 54.14 | 1767.00 | 58.25 | 932.60 | 14.91 | 28.87 | 2.95 | 0.37 | 0.36 | 22.44 | 3.76 | 5.18 | 0.08 | 3.34 | 0.38 | 0.01 |
| UNK 93/2A | Pyroxenite | 1.58 | 31.57 | 8.31 | 941.90 | 80.49 | 2447.00 | 52.32 | 816.30 | 8.95 | 31.82 | 2.65 | 0.47 | 0.34 | 15.22 | 2.11 | 9.92 | 0.52 | 3.12 | 0.33 | 0.08 |
| UNK 93/4 | Peridotite | 1.82 | 6.14 | 9.88 | 212.90 | 30.92 | 2693.00 | 116.50 | 2413.00 | 4.74 | 52.85 | 1.52 | 0.70 | 0.15 | 0.94 | 1.08 | 1.00 | 0.06 | 4.64 | 0.90 | 0.05 |
| UNK 93/5A | Pyroxenite | 2.34 | 1.09 | 17.62 | 350.60 | 63.79 | 3099.00 | 101.70 | 1481.00 | 21.29 | 56.31 | 1.90 | 0.56 | 2.01 | 3.88 | 1.01 | 1.43 | 0.05 | 3.82 | 0.18 | 1.64 |
| UNK 93/7 | Peridotite | 1.56 | 138.70 | 6.82 | 424.60 | 61.58 | 861.00 | 66.16 | 773.60 | 4.82 | 202.60 | 14.58 | 1.14 | 0.26 | 0.84 | 90.92 | 93.62 | 12.22 | 0.85 | 7.83 | 0.02 |
| UNK 93/9 | Peridotite | 7.68 | 1.00 | 13.28 | 8092.00 | 1301.00 | 52.17 | 98.16 | 223.70 | 12.34 | 79.11 | 31.67 | 0.82 | 0.52 | 219.30 | 0.72 | 2.83 | 0.16 | 27.30 | 0.89 | 0.02 |
| UNK 93/13 | Peridotite | 1.92 | 3.20 | 16.39 | 303.20 | 95.74 | 3418.00 | 97.98 | 1895.00 | 1.21 | 50.79 | 2.49 | 0.45 | 0.72 | 2.17 | 0.57 | 0.89 | 0.04 | 2.57 | 0.15 | 0.54 |
| UNK 93/15 | Peridotite | 1.79 | 9.26 | 12.00 | 279.10 | 55.79 | 2621.00 | 89.52 | 1123.00 | 3.71 | 44.80 | 1.42 | 0.56 | 1.01 | 1.81 | 0.76 | 1.66 | 0.05 | 2.76 | 0.20 | 1.35 |
| UNK 93/16 | Peridotite | 1.89 | 0.86 | 14.50 | 74.29 | 96.21 | 3796.00 | 95.73 | 1219.00 | 1.03 | 51.95 | 4.61 | 0.26 | 1.28 | 13.84 | 0.09 | 0.22 | 0.03 | 2.47 | 0.15 | 0.92 |
| UNK 93/18 | Pyroxenite | 0.45 | 14.08 | 16.74 | 617.00 | 85.99 | 2832.00 | 84.41 | 619.30 | 14.57 | 53.93 | 3.29 | 0.23 | 3.07 | 33.04 | 1.69 | 3.46 | 0.12 | 15.15 | 0.20 | 0.66 |
| UNK 93/20A | Peridotite | 2.25 | 10.53 | 10.24 | 163.70 | 64.80 | 4544.00 | 102.10 | 1433.00 | 0.89 | 49.55 | 3.66 | 0.19 | 1.33 | 14.02 | 0.50 | 0.48 | 0.01 | 3.40 | 0.30 | 1.65 |
| UNK 93/23 | Gabbro | 6.16 | 3.49 | 33.71 | 762.90 | 140.30 | 273.80 | 59.98 | 69.98 | 5.92 | 35.74 | 12.96 | 0.33 | 0.69 | 209.80 | 3.31 | 1.93 | 0.04 | 27.83 | 0.36 | 0.04 |
| UNK 93/24 | Gabbro | 2.92 | 1.17 | 36.74 | 774.60 | 153.00 | 296.50 | 53.01 | 199.50 | 122.30 | 40.91 | 11.98 | 0.37 | 0.20 | 78.15 | 3.56 | 0.77 | 0.02 | 4.16 | 0.22 | 0.02 |
| UNK 93/29 | Pyroxenite | 28.33 | 15.22 | 18.70 | 273.30 | 32.86 | 2274.00 | 72.97 | 1364.00 | 1.47 | 59.91 | 3.53 | 0.32 | 1.18 | 8.12 | 0.65 | 0.60 | 0.02 | 26.74 | 0.35 | 1.82 |
| UNK 93/32 | Peridotite | 11.71 | 63.89 | 55.14 | 1526.00 | 350.90 | 231.20 | 89.40 | 136.80 | 5.93 | 195.10 | 10.86 | 0.49 | 0.48 | 1.92 | 2.88 | 2.62 | 0.01 | 9.90 | 0.12 | 0.55 |
| UNK 93/34 | Peridotite | 1.87 | 20.66 | 13.03 | 530.30 | 55.03 | 2158.00 | 109.80 | 2374.00 | 1.75 | 65.95 | 2.54 | 0.44 | 0.52 | 1.09 | 1.58 | 1.58 | 0.01 | 0.73 | 0.11 | 0.69 |
| UNK 93/37 | Pyroxenite | 0.65 | 22.44 | 33.18 | 1126.00 | 122.70 | 2436.00 | 88.41 | 1069.00 | 34.71 | 58.78 | 5.64 | 0.12 | 0.37 | 51.14 | 7.63 | 4.20 | 0.04 | 37.72 | 0.21 | 0.06 |
| UNK 93/39 | Pyroxenite | 0.97 | 18.44 | 27.22 | 1307.00 | 120.50 | 2220.00 | 89.52 | 1235.00 | 3.62 | 65.03 | 6.81 | 0.20 | 2.34 | 55.88 | 8.31 | 10.11 | 0.07 | 9.11 | 0.22 | 0.17 |
| UNK 93/41 | Pyroxenite | 0.22 | 21.69 | 5.04 | 979.00 | 67.48 | 2354.00 | 98.11 | 1417.00 | 14.62 | 78.97 | 3.68 | 0.12 | 0.43 | 17.05 | 3.45 | 5.06 | 0.14 | 8.69 | 0.21 | 0.06 |
| UNK 93/42 | Pyroxenite | 0.54 | 15.87 | 8.18 | 933.10 | 72.45 | 2010.00 | 66.35 | 900.50 | 7.70 | 54.00 | 3.06 | 0.16 | 0.39 | 12.08 | 2.50 | 3.28 | 0.09 | 7.99 | 0.20 | 0.09 |
| UNK 93/46 | Peridotite | 4.46 | 17.42 | 27.10 | 760.40 | 77.83 | 4208.00 | 106.20 | 1681.00 | 9.15 | 57.91 | 3.32 | 0.36 | 0.78 | 16.84 | 5.27 | 4.80 | 0.06 | 4.98 | 0.27 | 0.25 |
| UNK 93/47 | Peridotite | 3.20 | 16.73 | 21.48 | 669.40 | 72.22 | 4102.00 | 106.50 | 1605.00 | 5.84 | 62.67 | 2.96 | 0.34 | 0.43 | 14.56 | 5.10 | 3.76 | 0.04 | 3.83 | 0.37 | 0.19 |
| UNK 93/50 | Pyroxenite | 1.03 | 21.73 | 16.28 | 1290.00 | 100.20 | 2914.00 | 107.20 | 1493.00 | 4.30 | 134.20 | 5.06 | 0.15 | 0.20 | 7.59 | 5.21 | 5.95 | 0.09 | 0.43 | 0.29 | ND |
| UNK 93/52 | Pyroxenite | 2.20 | 20.02 | 22.56 | 1370.00 | 78.46 | 3115.00 | 104.80 | 1392.00 | 3.54 | 59.27 | 4.63 | 0.30 | 0.34 | 9.34 | 8.68 | 8.65 | 0.08 | 0.79 | 0.30 | 0.02 |

## Table E3.3: Trace elements (ppm) for the UNK 93 surface samples by ICP-MS (Li-Cs).

| Sample # | Lithology | Li | P | Sc | Ti | V | Cr | Co | Ni | Cu | Zn | Ga | As | Rb | Sr | Y | Zr | Nb | Ba | Sn | Cs |
|---|---|---|---|---|---|---|---|---|---|---|---|---|---|---|---|---|---|---|---|---|---|
| UNK 93/53 | Pyroxenite | 1.10 | 20.58 | 21.75 | 1353.00 | 91.80 | 2555.00 | 93.26 | 1285.00 | 7.17 | 67.66 | 5.34 | 0.20 | 0.44 | 29.52 | 9.35 | 5.93 | 0.05 | 5.07 | 0.21 | 0.15 |
| UNK 93/54 | Gabbro | 6.62 | 22.75 | 23.08 | 707.40 | 123.90 | 170.10 | 22.02 | 115.40 | 27.46 | 21.35 | 12.64 | 0.22 | 1.51 | 178.00 | 3.12 | 6.05 | 0.15 | 40.88 | 0.23 | 0.07 |
| UNK 93/56 | Pyroxenite | 4.32 | 38.86 | 30.90 | 1847.00 | 124.00 | 1297.00 | 98.19 | 503.80 | 16.50 | 94.72 | 12.22 | 0.27 | 0.62 | 131.60 | 9.41 | 9.84 | 0.10 | 33.36 | 0.19 | 0.05 |
| UNK 93/58 | Peridotite | 7.27 | 26.18 | 14.59 | 938.00 | 79.45 | 2688.00 | 106.80 | 2165.00 | 23.41 | 50.54 | 3.30 | 0.33 | 0.31 | 28.74 | 4.77 | 4.06 | 0.05 | 0.64 | 0.27 | 0.07 |
| UNK 93/59 | Pyroxenite | 3.82 | 140.90 | 14.48 | 1110.00 | 89.18 | 4014.00 | 118.10 | 1569.00 | 39.16 | 66.83 | 4.91 | 0.24 | 2.24 | 70.47 | 5.18 | 43.51 | 1.14 | 3.87 | 0.32 | 0.33 |
| UNK 93/61 | Peridotite | 11.82 | 59.87 | 23.24 | 1692.00 | 124.00 | 3333.00 | 124.10 | 2053.00 | 43.24 | 64.12 | 5.29 | 0.55 | 1.01 | 64.14 | 5.26 | 15.03 | 0.51 | 5.34 | 0.25 | 0.70 |
| UNK 93/64 | Peridotite | 1.59 | 16.12 | 14.15 | 355.30 | 49.24 | 3938.00 | 137.00 | 2896.00 | 0.91 | 47.83 | 2.35 | 1.20 | 0.24 | 0.81 | 1.79 | 4.49 | 0.19 | 3.49 | 0.14 | 0.11 |
| UNK 93/65 | Peridotite | 6.84 | 276.80 | 27.55 | 5379.00 | 238.00 | 132.30 | 85.51 | 521.80 | 10.79 | 71.38 | 10.57 | 0.69 | 0.11 | 0.63 | 4.49 | 52.39 | 1.87 | 0.72 | 0.28 | 0.03 |
| UNK 93/67 | Pyroxenite | 4.34 | 185.50 | 36.58 | 2105.00 | 166.50 | 2857.00 | 91.21 | 821.50 | 2.75 | 73.75 | 9.33 | 0.28 | 2.95 | 49.00 | 10.98 | 25.64 | 0.90 | 22.98 | 0.30 | 0.60 |
| UNK 93/69 | Pyroxenite | 1.31 | 30.46 | 17.92 | 1733.00 | 92.14 | 3389.00 | 135.90 | 1799.00 | 76.16 | 100.90 | 5.30 | 0.42 | 0.22 | 42.80 | 5.69 | 8.01 | 0.05 | 0.26 | 0.59 | 0.01 |
| UNK 93/73 | Peridotite | 6.94 | 39.53 | 21.13 | 789.90 | 83.35 | 4317.00 | 115.70 | 2047.00 | 7.53 | 52.09 | 4.21 | 1.54 | 0.35 | 69.14 | 4.26 | 5.66 | 0.11 | 20.00 | 0.22 | 0.09 |
| UNK 93/75 | Peridotite | 10.29 | 209.10 | 51.59 | 6653.00 | 434.20 | 450.70 | 91.53 | 192.30 | 11.32 | 103.80 | 18.82 | 0.52 | 0.08 | 0.53 | 5.97 | 19.52 | 0.79 | 4.84 | 0.25 | 0.04 |
| UNK 93/76 | Quartzite | 9.63 | 32.55 | 12.31 | 368.90 | 38.35 | 1274.00 | 42.14 | 323.40 | 3.72 | 19.76 | 1.61 | 0.17 | 1.42 | 11.68 | 3.40 | 6.01 | 0.26 | 6.82 | 0.27 | 0.06 |
| UNK 93/78 | Peridotite | 6.11 | 47.47 | 14.63 | 1570.00 | 59.63 | 2590.00 | 89.18 | 1676.00 | 5.71 | 40.90 | 2.99 | 0.76 | 0.33 | 39.14 | 1.99 | 8.34 | 0.53 | 1.90 | 0.29 | 0.11 |
| UNK 93/80 | Pyroxenite | 1.40 | 61.03 | 19.93 | 1365.00 | 109.90 | 3006.00 | 116.30 | 1697.00 | 14.70 | 64.13 | 5.83 | 1.91 | 0.81 | 109.10 | 5.59 | 12.16 | 0.43 | 0.93 | 0.21 | 0.27 |
| UNK 93/84 | Pyroxenite | 0.68 | 10.45 | 20.38 | 1696.00 | 109.00 | 1467.00 | 93.77 | 1516.00 | 5.50 | 78.77 | 4.37 | 0.15 | 1.15 | 6.53 | 6.64 | 4.27 | 0.04 | 1.19 | 0.21 | 0.16 |
| UNK 93/85 | Gabbro | 16.41 | 8.71 | 52.30 | 1303.00 | 224.10 | 1003.00 | 46.05 | 256.80 | 2.64 | 24.92 | 11.73 | 0.25 | 15.59 | 72.51 | 4.91 | 3.72 | 0.05 | 29.52 | 0.37 | 0.70 |
| UNK 93/86 | Peridotite | 3.22 | 38.93 | 34.86 | 1046.00 | 122.20 | 3774.00 | 113.20 | 1436.00 | 5.64 | 79.62 | 9.59 | 0.28 | 0.89 | 63.18 | 6.09 | 6.12 | 0.07 | 8.30 | 0.14 | 0.25 |
| UNK 93/88 | Pyroxenite | 8.06 | 13.59 | 56.59 | 1686.00 | 329.10 | 1632.00 | 57.53 | 390.40 | 2.54 | 38.12 | 10.30 | 0.16 | 6.86 | 65.44 | 6.79 | 5.05 | 0.09 | 31.62 | 0.19 | 0.36 |
| UNK 93/90 | Peridotite | 0.54 | 23.90 | 29.73 | 1195.00 | 141.00 | 2572.00 | 65.68 | 1027.00 | 2.73 | 74.78 | 7.59 | 0.21 | 0.15 | 5.50 | 4.97 | 3.84 | 0.11 | 1.07 | 0.20 | 0.01 |
| UNK 93/93 | Peridotite | 4.55 | 34.96 | 14.83 | 1133.00 | 77.44 | 2981.00 | 124.50 | 2403.00 | 15.78 | 52.58 | 3.83 | 0.38 | 0.20 | 16.61 | 2.43 | 4.37 | 0.06 | 4.85 | 0.19 | 0.08 |
| UNK 93/94 | Peridotite | 2.54 | 35.91 | 11.62 | 1356.00 | 71.90 | 2152.00 | 119.90 | 2566.00 | 11.54 | 46.29 | 2.86 | 0.47 | 0.29 | 8.68 | 2.78 | 9.60 | 0.24 | 0.45 | 0.18 | 0.05 |
| UNK 93/96 | Peridotite | 1.56 | 18.93 | 21.92 | 219.70 | 105.80 | 3833.00 | 107.40 | 1549.00 | 3.48 | 48.55 | 5.07 | 0.23 | 2.16 | 16.38 | 0.29 | 0.24 | 0.02 | 1.83 | 0.12 | 0.87 |

## Table E3.3: Trace elements (ppm) for the UNK 93 surface samples by ICP-MS (Li-Cs).

| Sample # | Lithology | Li | P | Sc | Ti | V | Cr | Co | Ni | Cu | Zn | Ga | As | Rb | Sr | Y | Zr | Nb | Ba | Sn | Cs |
|---|---|---|---|---|---|---|---|---|---|---|---|---|---|---|---|---|---|---|---|---|---|
| UNK 93/98 | Gabbro | 5.52 | 14.59 | 35.30 | 868.60 | 163.70 | 222.70 | 72.91 | 91.99 | 74.12 | 51.08 | 14.36 | 0.36 | 0.80 | 185.70 | 3.36 | 2.52 | 0.03 | 39.95 | 0.19 | 0.07 |
| UNK 93/100 | Peridotite | 2.32 | 18.62 | 11.54 | 649.80 | 67.62 | 2646.00 | 106.40 | 2004.00 | 1.75 | 54.29 | 4.16 | 0.39 | 0.12 | 51.45 | 1.50 | 1.44 | 0.02 | 0.47 | 0.19 | 0.01 |
| UNK 93/101 | Gabbro | 3.46 | 17.30 | 34.97 | 931.80 | 174.20 | 171.70 | 52.51 | 109.00 | 66.82 | 42.06 | 9.52 | 0.33 | 0.54 | 157.90 | 3.03 | 3.05 | 0.12 | 26.66 | 0.48 | 0.06 |

## Table E3.3: Trace elements (ppm) for the UNK 93 surface samples by ICP-MS (La-U).

| Sample # | Lithology | La | Ce | Pr | Nd | Sm | Eu | Gd | Tb | Dy | Ho | Er | Tm | Yb | Lu | Hf | Ta | W | Pb | Th | U |
|---|---|---|---|---|---|---|---|---|---|---|---|---|---|---|---|---|---|---|---|---|---|
| UNK 93/1 | Peridotite | 0.33 | 0.75 | 0.15 | 0.84 | 0.32 | 0.10 | 0.45 | 0.09 | 0.61 | 0.13 | 0.35 | 0.05 | 0.32 | 0.04 | 0.19 | 0.01 | 0.03 | 0.80 | 0.04 | 0.01 |
| UNK 93/2A | Pyroxenite | 0.51 | 0.91 | 0.17 | 0.78 | 0.22 | 0.06 | 0.25 | 0.04 | 0.31 | 0.06 | 0.20 | 0.03 | 0.22 | 0.03 | 0.25 | 0.03 | 1.53 | 1.29 | 0.06 | 0.02 |
| UNK 93/4 | Peridotite | 0.03 | 0.06 | 0.00 | 0.04 | 0.02 | 0.01 | 0.05 | 0.01 | 0.12 | 0.03 | 0.11 | 0.02 | 0.14 | 0.02 | 0.03 | ND | 0.07 | 0.80 | ND | 0.08 |
| UNK 93/5A | Pyroxenite | 0.12 | 0.23 | 0.03 | 0.15 | 0.04 | 0.01 | 0.06 | 0.01 | 0.11 | 0.03 | 0.10 | 0.01 | 0.14 | 0.02 | 0.05 | ND | 0.16 | 0.71 | 0.04 | 0.01 |
| UNK 93/7 | Peridotite | 4.24 | 9.38 | 1.61 | 8.24 | 5.30 | 0.49 | 8.84 | 2.02 | 13.48 | 2.61 | 6.36 | 0.95 | 5.40 | 0.75 | 6.30 | 3.24 | 0.11 | 3.52 | 9.84 | 24.21 |
| UNK 93/9 | Peridotite | 0.36 | 0.62 | 0.08 | 0.35 | 0.10 | 0.09 | 0.10 | 0.01 | 0.11 | 0.02 | 0.06 | ND | 0.06 | 0.01 | 0.08 | 0.01 | 0.03 | 1.13 | 0.04 | 0.04 |
| UNK 93/13 | Peridotite | 0.08 | 0.15 | 0.01 | 0.06 | 0.01 | ND | 0.02 | ND | 0.05 | 0.01 | 0.06 | 0.01 | 0.11 | 0.02 | 0.04 | ND | 0.02 | 0.51 | 0.02 | 0.01 |
| UNK 93/15 | Peridotite | 0.11 | 0.20 | 0.02 | 0.12 | 0.03 | 0.01 | 0.05 | 0.01 | 0.08 | 0.02 | 0.07 | 0.01 | 0.10 | 0.02 | 0.05 | ND | 0.03 | 0.77 | 0.04 | 0.01 |
| UNK 93/16 | Peridotite | 0.31 | 0.35 | 0.02 | 0.08 | 0.00 | ND | 0.01 | ND | ND | ND | 0.01 | ND | 0.03 | ND | 0.01 | ND | 0.01 | 0.79 | 0.01 | 0.01 |
| UNK 93/18 | Pyroxenite | 0.49 | 0.88 | 0.12 | 0.50 | 0.12 | 0.06 | 0.15 | 0.02 | 0.21 | 0.04 | 0.15 | 0.02 | 0.18 | 0.03 | 0.10 | 0.01 | 0.05 | 1.02 | 0.11 | 0.04 |
| UNK 93/20A | Peridotite | 0.26 | 0.34 | 0.02 | 0.10 | 0.01 | 0.01 | 0.02 | ND | 0.05 | 0.01 | 0.05 | 0.01 | 0.08 | 0.01 | 0.02 | ND | 0.01 | 0.66 | ND | ND |
| UNK 93/23 | Gabbro | 0.39 | 0.90 | 0.14 | 0.76 | 0.30 | 0.23 | 0.36 | 0.07 | 0.51 | 0.11 | 0.30 | 0.04 | 0.31 | 0.04 | 0.10 | ND | 0.01 | 0.65 | 0.03 | 0.01 |
| UNK 93/24 | Gabbro | 0.07 | 0.16 | 0.03 | 0.26 | 0.16 | 0.17 | 0.27 | 0.06 | 0.50 | 0.11 | 0.35 | 0.05 | 0.39 | 0.06 | 0.05 | ND | 0.01 | 0.71 | ND | ND |
| UNK 93/29 | Pyroxenite | 0.06 | 0.09 | 0.01 | 0.06 | 0.04 | 0.09 | 0.04 | 0.01 | 0.05 | 0.01 | 0.05 | 0.01 | 0.09 | 0.01 | 0.02 | ND | 0.17 | 2.49 | 0.01 | 0.01 |
| UNK 93/32 | Peridotite | 0.04 | 0.04 | ND | 0.03 | 0.02 | ND | 0.05 | 0.02 | 0.24 | 0.08 | 0.33 | 0.07 | 0.59 | 0.11 | 0.14 | ND | 0.03 | 0.75 | ND | ND |
| UNK 93/34 | Peridotite | 0.03 | 0.03 | ND | 0.01 | 0.02 | ND | 0.05 | 0.02 | 0.18 | 0.04 | 0.16 | 0.03 | 0.21 | 0.03 | 0.07 | ND | 0.04 | 0.62 | ND | ND |
| UNK 93/37 | Pyroxenite | 0.39 | 1.24 | 0.26 | 1.61 | 0.67 | 0.22 | 0.84 | 0.17 | 1.15 | 0.24 | 0.66 | 0.10 | 0.63 | 0.09 | 0.21 | 0.01 | 0.04 | 0.63 | 0.04 | 0.01 |
| UNK 93/39 | Pyroxenite | 0.66 | 1.99 | 0.39 | 2.28 | 0.82 | 0.24 | 0.99 | 0.19 | 1.26 | 0.26 | 0.70 | 0.11 | 0.69 | 0.10 | 0.42 | 0.01 | 0.05 | 0.72 | 0.07 | 0.02 |

## Table E3.3: Trace elements (ppm) for the UNK 93 surface samples by ICP-MS (La-U).

| Sample # | Lithology | La | Ce | Pr | Nd | Sm | Eu | Gd | Tb | Dy | Ho | Er | Tm | Yb | Lu | Hf | Ta | W | Pb | Th | U |
|---|---|---|---|---|---|---|---|---|---|---|---|---|---|---|---|---|---|---|---|---|---|
| UNK 93/39 | Pyroxenite | 0.66 | 1.99 | 0.39 | 2.28 | 0.82 | 0.24 | 0.99 | 0.19 | 1.26 | 0.26 | 0.70 | 0.11 | 0.69 | 0.10 | 0.42 | 0.01 | 0.05 | 0.72 | 0.07 | 0.02 |
| UNK 93/41 | Pyroxenite | 0.41 | 0.58 | 0.09 | 0.42 | 0.15 | 0.04 | 0.23 | 0.05 | 0.39 | 0.10 | 0.30 | 0.05 | 0.37 | 0.06 | 0.17 | 0.01 | 0.03 | 0.78 | 0.05 | 0.02 |
| UNK 93/42 | Pyroxenite | 0.25 | 0.46 | 0.06 | 0.30 | 0.11 | 0.03 | 0.16 | 0.03 | 0.29 | 0.07 | 0.23 | 0.04 | 0.33 | 0.05 | 0.11 | 0.01 | 0.04 | 0.49 | 0.05 | 0.02 |
| UNK 93/46 | Peridotite | 0.59 | 1.61 | 0.30 | 1.60 | 0.52 | 0.15 | 0.64 | 0.12 | 0.77 | 0.16 | 0.45 | 0.06 | 0.42 | 0.06 | 0.19 | 0.01 | 0.03 | 0.54 | 0.06 | 0.02 |
| UNK 93/47 | Peridotite | 0.54 | 1.58 | 0.30 | 1.56 | 0.51 | 0.15 | 0.61 | 0.11 | 0.75 | 0.15 | 0.43 | 0.06 | 0.41 | 0.06 | 0.15 | ND | 0.04 | 0.63 | 0.04 | 0.01 |
| UNK 93/50 | Pyroxenite | 0.47 | 1.13 | 0.20 | 1.09 | 0.39 | 0.14 | 0.52 | 0.10 | 0.71 | 0.15 | 0.43 | 0.07 | 0.46 | 0.07 | 0.23 | 0.01 | 0.02 | 0.67 | 0.06 | 0.01 |
| UNK 93/52 | Pyroxenite | 0.58 | 1.82 | 0.37 | 2.09 | 0.77 | 0.20 | 0.96 | 0.19 | 1.26 | 0.26 | 0.71 | 0.11 | 0.69 | 0.10 | 0.34 | 0.01 | 0.03 | 0.43 | 0.07 | 0.02 |
| UNK 93/53 | Pyroxenite | 0.31 | 1.01 | 0.23 | 1.47 | 0.69 | 0.21 | 0.97 | 0.20 | 1.35 | 0.28 | 0.77 | 0.11 | 0.74 | 0.11 | 0.30 | ND | 0.03 | 0.42 | 0.04 | 0.01 |
| UNK 93/54 | Gabbro | 0.95 | 1.53 | 0.24 | 1.13 | 0.35 | 0.29 | 0.41 | 0.07 | 0.48 | 0.10 | 0.27 | 0.04 | 0.26 | 0.04 | 0.19 | 0.01 | 0.04 | 1.10 | 0.12 | 0.03 |
| UNK 93/56 | Pyroxenite | 1.01 | 2.42 | 0.41 | 2.23 | 0.82 | 0.37 | 1.05 | 0.20 | 1.38 | 0.30 | 0.82 | 0.13 | 0.85 | 0.13 | 0.42 | 0.01 | 0.02 | 0.85 | 0.12 | 0.04 |
| UNK 93/58 | Peridotite | 0.13 | 0.40 | 0.09 | 0.58 | 0.27 | 0.10 | 0.41 | 0.08 | 0.63 | 0.14 | 0.39 | 0.06 | 0.39 | 0.06 | 0.16 | ND | 0.03 | 0.92 | 0.01 | ND |
| UNK 93/59 | Pyroxenite | 2.45 | 6.05 | 0.82 | 3.54 | 0.84 | 0.18 | 0.89 | 0.13 | 0.75 | 0.14 | 0.38 | 0.05 | 0.34 | 0.05 | 0.81 | 0.24 | 0.80 | 1.73 | 0.90 | 0.14 |
| UNK 93/61 | Peridotite | 0.40 | 1.10 | 0.18 | 1.00 | 0.37 | 0.10 | 0.50 | 0.10 | 0.70 | 0.15 | 0.43 | 0.07 | 0.46 | 0.07 | 0.42 | 0.03 | 0.21 | 2.25 | 0.07 | 0.01 |
| UNK 93/64 | Peridotite | 0.24 | 0.55 | 0.09 | 0.48 | 0.16 | 0.04 | 0.20 | 0.03 | 0.23 | 0.05 | 0.14 | 0.02 | 0.16 | 0.03 | 0.10 | 0.02 | 0.79 | 0.74 | 0.06 | 0.03 |
| UNK 93/65 | Peridotite | 0.12 | 0.16 | 0.03 | 0.17 | 0.08 | 0.02 | 0.17 | 0.05 | 0.48 | 0.14 | 0.48 | 0.10 | 0.78 | 0.15 | 1.74 | 0.15 | 0.07 | 0.54 | ND | ND |
| UNK 93/67 | Pyroxenite | 0.87 | 2.34 | 0.39 | 1.95 | 0.68 | 0.16 | 0.92 | 0.18 | 1.31 | 0.30 | 0.87 | 0.14 | 0.97 | 0.15 | 0.68 | 0.07 | 0.77 | 2.56 | 0.23 | 0.06 |
| UNK 93/69 | Pyroxenite | 0.45 | 1.36 | 0.23 | 1.31 | 0.48 | 0.15 | 0.62 | 0.12 | 0.79 | 0.17 | 0.45 | 0.07 | 0.44 | 0.07 | 0.31 | ND | 0.06 | 0.63 | 0.03 | 0.01 |
| UNK 93/73 | Peridotite | 0.19 | 0.44 | 0.08 | 0.41 | 0.20 | 0.12 | 0.29 | 0.06 | 0.49 | 0.12 | 0.35 | 0.06 | 0.42 | 0.07 | 0.18 | ND | 0.68 | 2.83 | 0.01 | ND |
| UNK 93/75 | Peridotite | 0.04 | 0.11 | 0.02 | 0.10 | 0.07 | 0.02 | 0.17 | 0.05 | 0.55 | 0.17 | 0.62 | 0.13 | 1.02 | 0.18 | 0.67 | 0.06 | 0.06 | 0.47 | ND | ND |
| UNK 93/76 | Quartzite | 0.66 | 1.20 | 0.15 | 0.62 | 0.18 | 0.06 | 0.26 | 0.05 | 0.38 | 0.09 | 0.28 | 0.05 | 0.34 | 0.06 | 0.17 | 0.01 | 0.13 | 1.21 | 0.23 | 0.07 |
| UNK 93/78 | Peridotite | 0.10 | 0.24 | 0.03 | 0.18 | 0.07 | 0.04 | 0.12 | 0.03 | 0.23 | 0.05 | 0.17 | 0.03 | 0.21 | 0.03 | 0.29 | 0.04 | 0.23 | 3.32 | 0.05 | 0.01 |
| UNK 93/80 | Pyroxenite | 1.35 | 2.82 | 0.39 | 1.74 | 0.51 | 0.18 | 0.69 | 0.12 | 0.80 | 0.16 | 0.42 | 0.06 | 0.39 | 0.06 | 0.36 | 0.03 | 0.63 | 1.31 | 0.27 | 0.06 |
| UNK 93/84 | Pyroxenite | 0.14 | 0.63 | 0.15 | 1.01 | 0.47 | 0.22 | 0.66 | 0.13 | 0.92 | 0.20 | 0.54 | 0.09 | 0.57 | 0.08 | 0.23 | ND | 0.02 | 0.30 | 0.01 | ND |
| UNK 93/85 | Gabbro | 0.15 | 0.49 | 0.10 | 0.71 | 0.38 | 0.17 | 0.52 | 0.10 | 0.72 | 0.16 | 0.41 | 0.06 | 0.40 | 0.06 | 0.20 | ND | 0.13 | 0.74 | 0.04 | 0.01 |

## Table E3.3: Trace elements (ppm) for the UNK 93 surface samples by ICP-MS (La-U).

| Sample # | Lithology | La | Ce | Pr | Nd | Sm | Eu | Gd | Tb | Dy | Ho | Er | Tm | Yb | Lu | Hf | Ta | W | Pb | Th | U |
|---|---|---|---|---|---|---|---|---|---|---|---|---|---|---|---|---|---|---|---|---|---|
| UNK 93/84 | Pyroxenite | 0.14 | 0.63 | 0.15 | 1.01 | 0.47 | 0.22 | 0.66 | 0.13 | 0.92 | 0.20 | 0.54 | 0.09 | 0.57 | 0.08 | 0.23 | ND | 0.02 | 0.30 | 0.01 | ND |
| UNK 93/85 | Gabbro | 0.15 | 0.49 | 0.10 | 0.71 | 0.38 | 0.17 | 0.52 | 0.10 | 0.72 | 0.16 | 0.41 | 0.06 | 0.40 | 0.06 | 0.20 | ND | 0.13 | 0.74 | 0.04 | 0.01 |
| UNK 93/86 | Peridotite | 0.77 | 1.11 | 0.18 | 0.99 | 0.38 | 0.17 | 0.56 | 0.11 | 0.81 | 0.18 | 0.52 | 0.09 | 0.56 | 0.08 | 0.27 | 0.01 | 0.02 | 0.47 | 0.08 | 0.02 |
| UNK 93/88 | Pyroxenite | 0.29 | 0.97 | 0.20 | 1.26 | 0.57 | 0.23 | 0.75 | 0.15 | 1.03 | 0.22 | 0.56 | 0.09 | 0.55 | 0.08 | 0.28 | 0.01 | 0.20 | 0.80 | 0.09 | 0.02 |
| UNK 93/90 | Peridotite | 0.12 | 0.23 | 0.05 | 0.36 | 0.19 | 0.10 | 0.34 | 0.08 | 0.62 | 0.15 | 0.42 | 0.07 | 0.47 | 0.07 | 0.17 | 0.01 | 0.02 | 0.57 | ND | ND |
| UNK 93/93 | Peridotite | 0.11 | 0.27 | 0.04 | 0.24 | 0.10 | 0.07 | 0.17 | 0.04 | 0.31 | 0.07 | 0.22 | 0.04 | 0.26 | 0.04 | 0.18 | 0.00 | 0.10 | 0.72 | ND | ND |
| UNK 93/94 | Peridotite | 0.34 | 0.78 | 0.11 | 0.57 | 0.19 | 0.07 | 0.27 | 0.05 | 0.37 | 0.08 | 0.24 | 0.04 | 0.25 | 0.04 | 0.27 | 0.02 | 0.22 | 1.00 | 0.02 | 0.01 |
| UNK 93/96 | Peridotite | 0.05 | 0.04 | 0.00 | 0.02 | 0.00 | 0.01 | 0.01 | 0.00 | 0.02 | 0.01 | 0.04 | 0.01 | 0.09 | 0.02 | 0.01 | ND | 0.01 | 0.53 | 0.01 | ND |
| UNK 93/98 | Gabbro | 0.50 | 1.18 | 0.16 | 0.80 | 0.30 | 0.22 | 0.35 | 0.07 | 0.49 | 0.11 | 0.30 | 0.05 | 0.34 | 0.05 | 0.11 | ND | 0.01 | 1.28 | 0.02 | 0.01 |
| UNK 93/100 | Peridotite | 0.08 | 0.07 | 0.01 | 0.08 | 0.04 | 0.05 | 0.08 | 0.02 | 0.16 | 0.04 | 0.13 | 0.02 | 0.17 | 0.03 | 0.06 | ND | 0.05 | 0.78 | 0.01 | ND |
| UNK 93/101 | Gabbro | 0.43 | 0.71 | 0.14 | 0.67 | 0.25 | 0.19 | 0.30 | 0.06 | 0.42 | 0.09 | 0.27 | 0.04 | 0.30 | 0.05 | 0.12 | 0.01 | 0.04 | 0.99 | 0.04 | 0.01 |

## Table E4.1: Whole rock major element oxide (wt%) analyses for the BC xenoliths by XRF.

| Sample # | Lithology | $SiO_2$ | $Al_2O_3$ | $Fe_2O_3$ | FeO | MnO | MgO | CaO | $Na_2O$ | $K_2O$ | $TiO_2$ | $P_2O_5$ | $Cr_2O_3$ | NiO | Total |
|---|---|---|---|---|---|---|---|---|---|---|---|---|---|---|---|
| BC 10/90 5 | Harzburgite | 47.29 | 4.82 | 1.17 | 9.45 | 0.19 | 31.27 | 4.95 | 0.24 | 0.02 | 0.22 | 0.02 | 0.35 | 0.24 | 100.20 |
| BC 10/90 6 | Harzburgite | 47.23 | 5.82 | 1.17 | 9.51 | 0.17 | 30.99 | 3.81 | 0.39 | 0.06 | 0.23 | 0.02 | 0.46 | 0.23 | 100.10 |
| BC 10/90 7 | Lherzolite | 43.74 | 3.69 | 1.04 | 8.42 | 0.16 | 36.64 | 5.06 | 0.21 | 0.01 | 0.21 | 0.02 | 0.36 | 0.30 | 99.86 |
| BC 10/90 23 | Lherzolite | 44.42 | 6.12 | 0.94 | 7.65 | 0.14 | 32.19 | 7.62 | 0.11 | 0.01 | 0.11 | 0.02 | 0.57 | 0.23 | 100.10 |
| BC 10/90 26 | Pyroxenite | 55.06 | 3.22 | 0.84 | 6.77 | 0.10 | 31.56 | 1.27 | 0.16 | 0.01 | 0.10 | 0.01 | 0.38 | 0.20 | 99.68 |
| BC 10/90 56 | Gabbro | 46.42 | 13.87 | 1.89 | 15.31 | 0.28 | 6.30 | 12.01 | 1.37 | 0.52 | 1.51 | 0.12 | 0.04 | 0.01 | 99.65 |
| BC 10/90 113 | Greenstone | 32.49 | 21.54 | 1.19 | 9.62 | 0.10 | 33.68 | 0.16 | 0.15 | 0.02 | 0.66 | 0.05 | 0.03 | 0.02 | 99.71 |
| BC 8/91 104 | Webstrite | 52.04 | 2.04 | 0.93 | 7.55 | 0.19 | 23.42 | 13.07 | 0.29 | 0.02 | 0.15 | 0.02 | 0.49 | 0.10 | 100.30 |
| BC 8/91 105 | Webstrite | 52.50 | 1.97 | 0.83 | 6.74 | 0.19 | 21.24 | 15.91 | 0.20 | 0.04 | 0.15 | 0.02 | 0.47 | 0.07 | 100.30 |

## Table E4.2: Whole rock trace element (ppm) analyses for the BC xenoliths by XRF.

| Sample # | Lithology | %S | %Sul | Nb | Y | Rb | Zr | Sr | Ba | K | P | Cu | Ni | Zn |
|---|---|---|---|---|---|---|---|---|---|---|---|---|---|---|
| BC 10/90 5 | Harzburgite | ND | 0.1 | ND | 8.0 | 0.7 | 10.0 | 27.7 | ND | 187.0 | 41.0 | ND | 1874.0 | 65.5 |
| BC 10/90 6 | Harzburgite | 0.1 | 0.2 | 0.4 | 7.2 | 2.0 | 9.4 | 31.2 | 2.0 | 570.0 | 62.0 | ND | 1780.5 | 62.8 |
| BC 10/90 7 | Lherzolite | 0.1 | 0.3 | ND | 6.9 | ND | 6.7 | 24.8 | 5.0 | 94.0 | 33.0 | ND | 2266.1 | 52.6 |
| BC 10/90 23 | Lherzolite | 0.1 | 0.3 | ND | 5.9 | ND | 4.8 | 30.9 | ND | 81.0 | 46.0 | 12.7 | 1786.3 | 34.4 |
| BC 10/90 26 | Pyroxenite | 0.3 | 0.1 | ND | 3.8 | ND | 6.3 | 3.6 | 9.0 | 93.0 | 19.0 | ND | 1586.6 | 99.9 |
| BC 10/90 56 | Gabbro | 0.3 | 0.8 | 1.1 | 28.6 | 21.2 | 33.2 | 122.4 | 57.7 | 3568.0 | 772.0 | 95.9 | 60.2 | 108.9 |
| BC 10/90 113 | Greenstone | ND | ND | 0.3 | 17.2 | 0.9 | 20.6 | 0.1 | 6.5 | 122.0 | 121.0 | ND | 158.3 | 46.1 |
| BC 8/91 104 | Webstrite | 0.1 | 0.1 | ND | 5.8 | 2.0 | 6.6 | 10.8 | 4.0 | 224.0 | 38.0 | 0.9 | 739.6 | 47.7 |
| BC 8/91 105 | Webstrite | 0.1 | 0.2 | ND | 7.0 | 0.8 | 5.1 | 11.9 | 16.2 | 380.0 | 23.0 | ND | 549.3 | 41.3 |

# APPENDIX F:-MICROPROBE ANALYSES RESULTS

## Table F1.1 Orthopyroxene analyses

| | BC10/90/5 OPX27 | BC10/90/5 OPX3 | BC10/90/5 OPX2 | BC10/90/5 OPX41 | BC10/90/5 OPX19 | BC10/90/5 OPX16 | BC10/90/5 OPX17 | BC10/90/5 OPX14 | BC10/90/5 OPX18 | BC10/90/6 OPX54 | BC10/90/6 OPX36 | BC10/90/6 OPX14 | BC10/90/6 OPX57 |
|---|---|---|---|---|---|---|---|---|---|---|---|---|---|
| $SiO_2$ | 55.65 | 55.56 | 54.88 | 54.99 | 54.70 | 54.63 | 54.78 | 55.02 | 54.73 | 55.23 | 55.71 | 55.39 | 54.98 |
| $TiO_2$ | 0.35 | 0.35 | 0.38 | 0.33 | 0.31 | 0.31 | 0.35 | 0.34 | 0.38 | 0.35 | 0.50 | 0.48 | 0.50 |
| $Al_2O_3$ | 2.03 | 2.03 | 2.01 | 1.99 | 1.97 | 1.88 | 1.86 | 1.86 | 1.84 | 2.24 | 2.19 | 2.16 | 2.14 |
| $Cr_2O_3$ | 0.43 | 0.59 | 0.35 | 0.35 | 0.39 | 0.43 | 0.55 | 0.54 | 0.50 | 0.42 | 0.43 | 0.44 | 0.46 |
| FeO | 10.50 | 9.84 | 10.02 | 10.24 | 10.31 | 10.33 | 10.10 | 9.96 | 10.20 | 9.74 | 9.98 | 9.78 | 9.81 |
| MnO | 0.30 | 0.15 | 0.14 | 0.25 | 0.19 | 0.28 | 0.22 | 0.28 | 0.23 | 0.12 | 0.22 | 0.24 | 0.20 |
| MgO | 31.62 | 31.36 | 30.85 | 30.98 | 30.85 | 31.27 | 31.23 | 31.03 | 31.61 | 30.96 | 30.97 | 30.86 | 31.20 |
| CaO | 1.42 | 1.61 | 1.47 | 1.44 | 1.72 | 1.34 | 1.40 | 1.38 | 1.02 | 1.34 | 1.37 | 1.27 | 1.20 |
| $Na_2O$ | 0.00 | 0.02 | 0.01 | 0.03 | 0.01 | 0.00 | 0.00 | 0.00 | 0.01 | 0.00 | 0.00 | 0.00 | 0.02 |
| $K_2O$ | 0.02 | 0.00 | 0.00 | 0.00 | 0.00 | 0.00 | 0.00 | 0.01 | 0.00 | 0.01 | 0.00 | 0.01 | 0.00 |
| TOTAL | 102.31 | 101.50 | 100.12 | 100.58 | 100.44 | 100.46 | 100.51 | 100.42 | 100.52 | 100.41 | 101.37 | 100.63 | 100.50 |
| | | | | | | | | | | | | | |
| Si | 1.91 | 1.92 | 1.93 | 1.92 | 1.92 | 1.91 | 1.92 | 1.93 | 1.91 | 1.93 | 1.93 | 1.94 | 1.92 |
| Ti | 0.01 | 0.01 | 0.01 | 0.01 | 0.01 | 0.01 | 0.01 | 0.01 | 0.01 | 0.01 | 0.01 | 0.01 | 0.01 |
| Al | 0.08 | 0.08 | 0.08 | 0.08 | 0.08 | 0.08 | 0.08 | 0.08 | 0.08 | 0.09 | 0.09 | 0.09 | 0.09 |
| Cr | 0.01 | 0.02 | 0.01 | 0.01 | 0.01 | 0.01 | 0.02 | 0.01 | 0.01 | 0.01 | 0.01 | 0.01 | 0.01 |
| Fe(ii) | 0.30 | 0.28 | 0.29 | 0.30 | 0.30 | 0.30 | 0.30 | 0.29 | 0.30 | 0.28 | 0.29 | 0.29 | 0.29 |
| Mn | 0.01 | 0.00 | 0.00 | 0.01 | 0.01 | 0.01 | 0.01 | 0.01 | 0.01 | 0.00 | 0.01 | 0.01 | 0.01 |
| Mg | 1.62 | 1.62 | 1.62 | 1.61 | 1.61 | 1.63 | 1.63 | 1.62 | 1.65 | 1.61 | 1.60 | 1.61 | 1.63 |
| Ca | 0.05 | 0.06 | 0.06 | 0.05 | 0.06 | 0.05 | 0.05 | 0.05 | 0.04 | 0.05 | 0.05 | 0.05 | 0.05 |
| | | | | | | | | | | | | | |
| Wo | 2.63 | 3.03 | 2.81 | 2.72 | 3.26 | 2.52 | 2.66 | 2.62 | 1.92 | 2.58 | 2.61 | 2.45 | 2.29 |
| En | 81.77 | 82.25 | 82.04 | 81.71 | 81.27 | 81.97 | 82.17 | 82.20 | 82.80 | 82.66 | 82.19 | 82.53 | 82.79 |
| Fs | 15.60 | 14.66 | 15.11 | 15.47 | 15.44 | 15.52 | 15.17 | 15.19 | 15.24 | 14.76 | 15.19 | 15.03 | 14.85 |
| Mg# | 0.84 | 0.85 | 0.85 | 0.84 | 0.84 | 0.84 | 0.85 | 0.85 | 0.85 | 0.85 | 0.85 | 0.85 | 0.85 |

**Table F1.1 Continued.**

| | BC10/90/6 OPX37 | BC10/90/6 OPX24 | BC10/90/6 OPX38 | BC10/90/6 OPX31 | BC10/90/6 OPX21 | BC10/90/6 OPX25 | BC10/90/6 OPX30 | BC10/90/6 OPX28 | BC10/90/6 OPX40 | BC10/90/6 OPX65 | BC10/90/6 OPX27 | BC10/90/6 OPX8 | BC10/90/6 OPX11 |
|---|---|---|---|---|---|---|---|---|---|---|---|---|---|
| $SiO_2$ | 55.20 | 55.09 | 55.41 | 56.21 | 55.03 | 55.72 | 55.96 | 55.58 | 55.70 | 55.66 | 55.45 | 55.10 | 55.58 |
| $TiO_2$ | 0.49 | 0.43 | 0.51 | 0.43 | 0.44 | 0.39 | 0.31 | 0.37 | 0.36 | 0.44 | 0.41 | 0.48 | 0.35 |
| $Al_2O_3$ | 2.08 | 2.03 | 2.03 | 2.01 | 2.00 | 1.98 | 1.92 | 1.90 | 1.89 | 1.88 | 1.88 | 1.88 | 1.88 |
| $Cr_2O_3$ | 0.45 | 0.59 | 0.42 | 0.41 | 0.56 | 0.47 | 0.52 | 0.47 | 0.55 | 0.61 | 0.51 | 0.49 | 0.50 |
| FeO | 10.20 | 9.83 | 9.90 | 9.54 | 10.05 | 9.79 | 9.72 | 9.71 | 9.80 | 9.62 | 9.72 | 9.70 | 10.04 |
| MnO | 0.14 | 0.20 | 0.22 | 0.24 | 0.22 | 0.19 | 0.17 | 0.19 | 0.19 | 0.16 | 0.11 | 0.20 | 0.18 |
| MgO | 30.56 | 30.71 | 30.87 | 31.15 | 30.66 | 30.53 | 30.65 | 30.55 | 31.11 | 30.81 | 30.94 | 30.97 | 30.45 |
| CaO | 1.33 | 1.64 | 1.19 | 1.58 | 1.48 | 1.54 | 1.64 | 1.69 | 1.14 | 1.60 | 1.68 | 1.13 | 1.55 |
| $Na_2O$ | 0.00 | 0.03 | 0.01 | 0.01 | 0.02 | 0.03 | 0.02 | 0.04 | 0.01 | 0.03 | 0.02 | 0.00 | 0.04 |
| $K_2O$ | 0.01 | 0.02 | 0.01 | 0.00 | 0.00 | 0.01 | 0.01 | 0.00 | 0.00 | 0.00 | 0.00 | 0.00 | 0.01 |
| TOTAL | 100.44 | 100.56 | 100.58 | 101.59 | 100.45 | 100.66 | 100.90 | 100.52 | 100.76 | 100.81 | 100.71 | 99.94 | 100.57 |
| | | | | | | | | | | | | | |
| Si | 1.94 | 1.93 | 1.94 | 1.95 | 1.93 | 1.95 | 1.95 | 1.95 | 1.94 | 1.94 | 1.94 | 1.94 | 1.95 |
| Ti | 0.01 | 0.01 | 0.01 | 0.01 | 0.01 | 0.01 | 0.01 | 0.01 | 0.01 | 0.01 | 0.01 | 0.01 | 0.01 |
| Al | 0.09 | 0.08 | 0.08 | 0.08 | 0.08 | 0.08 | 0.08 | 0.08 | 0.08 | 0.08 | 0.08 | 0.08 | 0.08 |
| Cr | 0.01 | 0.02 | 0.01 | 0.01 | 0.02 | 0.01 | 0.01 | 0.01 | 0.02 | 0.02 | 0.01 | 0.01 | 0.01 |
| Fe(ii) | 0.30 | 0.29 | 0.29 | 0.28 | 0.29 | 0.29 | 0.28 | 0.28 | 0.29 | 0.28 | 0.28 | 0.29 | 0.29 |
| Mn | 0.00 | 0.01 | 0.01 | 0.01 | 0.01 | 0.01 | 0.01 | 0.01 | 0.01 | 0.00 | 0.00 | 0.01 | 0.01 |
| Mg | 1.60 | 1.60 | 1.61 | 1.61 | 1.60 | 1.59 | 1.59 | 1.60 | 1.62 | 1.60 | 1.61 | 1.62 | 1.59 |
| Ca | 0.05 | 0.06 | 0.04 | 0.06 | 0.06 | 0.06 | 0.06 | 0.06 | 0.04 | 0.06 | 0.06 | 0.04 | 0.06 |
| | | | | | | | | | | | | | |
| Wo | 2.56 | 3.13 | 2.29 | 3.01 | 2.83 | 2.97 | 3.15 | 3.25 | 2.17 | 3.06 | 3.20 | 2.18 | 2.99 |
| En | 81.90 | 81.81 | 82.49 | 82.43 | 81.77 | 81.89 | 81.93 | 81.75 | 82.86 | 82.20 | 82.11 | 82.97 | 81.53 |
| Fs | 15.53 | 14.97 | 15.17 | 14.53 | 15.34 | 15.03 | 14.85 | 14.86 | 14.94 | 14.65 | 14.61 | 14.86 | 15.35 |
| Mg# | 0.84 | 0.85 | 0.85 | 0.85 | 0.84 | 0.85 | 0.85 | 0.85 | 0.85 | 0.85 | 0.85 | 0.85 | 0.84 |

**Table F1.1 Continued.**

| | BC10/90/6 OPX55 | BC10/90/6 OPX1 | BC10/90/6 OPX20 | BC10/90/6 OPX12 | BC10/90/6 OPX51 | BC10/90/6 OPX19 | BC10/90/6 OPX29 | BC10/90/6 OPX26 | BC10/90/6 OPX10 | BC10/90/6 OPX63 | BC10/90/6 OPX2 | BC10/90/6 OPX48 | BC10/90/6 OPX13 |
|---|---|---|---|---|---|---|---|---|---|---|---|---|---|
| $SiO_2$ | 55.77 | 55.51 | 55.68 | 55.31 | 55.51 | 55.56 | 56.05 | 55.37 | 54.89 | 56.29 | 55.96 | 56.53 | 55.60 |
| $TiO_2$ | 0.41 | 0.38 | 0.45 | 0.36 | 0.39 | 0.40 | 0.43 | 0.36 | 0.37 | 0.39 | 0.38 | 0.36 | 0.43 |
| $Al_2O_3$ | 1.86 | 1.83 | 1.82 | 1.79 | 1.76 | 1.75 | 1.72 | 1.70 | 1.70 | 1.69 | 1.69 | 1.69 | 1.69 |
| $Cr_2O_3$ | 0.37 | 0.53 | 0.43 | 0.52 | 0.44 | 0.52 | 0.45 | 0.52 | 0.46 | 0.40 | 0.45 | 0.44 | 0.47 |
| FeO | 9.64 | 9.95 | 9.69 | 9.64 | 9.79 | 9.83 | 10.01 | 9.48 | 9.57 | 9.67 | 9.71 | 9.79 | 9.61 |
| MnO | 0.18 | 0.18 | 0.18 | 0.16 | 0.27 | 0.26 | 0.16 | 0.22 | 0.27 | 0.17 | 0.21 | 0.18 | 0.21 |
| MgO | 30.81 | 30.87 | 31.04 | 30.66 | 31.46 | 30.92 | 31.66 | 30.72 | 30.38 | 31.53 | 31.56 | 31.54 | 31.34 |
| CaO | 1.32 | 1.17 | 1.11 | 1.40 | 1.10 | 1.31 | 1.02 | 1.60 | 1.59 | 0.98 | 0.92 | 0.89 | 1.37 |
| $Na_2O$ | 0.01 | 0.01 | 0.01 | 0.02 | 0.02 | 0.03 | 0.00 | 0.01 | 0.00 | 0.02 | 0.04 | 0.00 | 0.00 |
| $K_2O$ | 0.01 | 0.00 | 0.00 | 0.00 | 0.01 | 0.00 | 0.01 | 0.00 | 0.01 | 0.00 | 0.00 | 0.00 | 0.00 |
| TOTAL | 100.37 | 100.42 | 100.40 | 99.85 | 100.76 | 100.57 | 101.51 | 99.99 | 99.23 | 101.15 | 100.92 | 101.42 | 100.70 |
| | | | | | | | | | | | | | |
| Si | 1.95 | 1.95 | 1.95 | 1.95 | 1.93 | 1.94 | 1.94 | 1.95 | 1.95 | 1.95 | 1.95 | 1.96 | 1.94 |
| Ti | 0.01 | 0.01 | 0.01 | 0.01 | 0.01 | 0.01 | 0.01 | 0.01 | 0.01 | 0.01 | 0.01 | 0.01 | 0.01 |
| Al | 0.08 | 0.08 | 0.08 | 0.07 | 0.07 | 0.07 | 0.07 | 0.07 | 0.07 | 0.07 | 0.07 | 0.07 | 0.07 |
| Cr | 0.01 | 0.01 | 0.01 | 0.01 | 0.01 | 0.01 | 0.01 | 0.01 | 0.01 | 0.01 | 0.01 | 0.01 | 0.01 |
| Fe(ii) | 0.28 | 0.29 | 0.28 | 0.28 | 0.29 | 0.29 | 0.29 | 0.28 | 0.28 | 0.28 | 0.28 | 0.28 | 0.28 |
| Mn | 0.01 | 0.01 | 0.01 | 0.00 | 0.01 | 0.01 | 0.00 | 0.01 | 0.01 | 0.01 | 0.01 | 0.01 | 0.01 |
| Mg | 1.61 | 1.61 | 1.62 | 1.61 | 1.63 | 1.61 | 1.63 | 1.61 | 1.61 | 1.63 | 1.64 | 1.63 | 1.63 |
| Ca | 0.05 | 0.04 | 0.04 | 0.05 | 0.04 | 0.05 | 0.04 | 0.06 | 0.06 | 0.04 | 0.03 | 0.03 | 0.05 |
| | | | | | | | | | | | | | |
| Wo | 2.54 | 2.25 | 2.13 | 2.71 | 2.08 | 2.50 | 1.93 | 3.09 | 3.08 | 1.86 | 1.74 | 1.70 | 2.59 |
| En | 82.63 | 82.54 | 83.03 | 82.45 | 82.98 | 82.32 | 83.12 | 82.29 | 82.01 | 83.44 | 83.42 | 83.48 | 82.85 |
| Fs | 14.80 | 15.19 | 14.82 | 14.79 | 14.87 | 15.07 | 14.96 | 14.58 | 14.90 | 14.63 | 14.71 | 14.82 | 14.55 |
| Mg# | 0.85 | 0.85 | 0.85 | 0.85 | 0.85 | 0.85 | 0.85 | 0.85 | 0.85 | 0.85 | 0.85 | 0.85 | 0.85 |

## Table F1.1 Continued.

| | BC10/90/6 OPX64 | BC10/90/6 OPX44 | USM65 OPX12 | USM65 OPX58 | USM65 OPX3 | USM65 OPX81 | USM65 OPX14 | USM65 OPX13 | USM65 OPX15 | USM65 OPX4 | USM65 OPX19 | USM65 OPX20 | USM65 OPX18 |
|---|---|---|---|---|---|---|---|---|---|---|---|---|---|
| $SiO_2$ | 55.39 | 39.86 | 54.93 | 53.95 | 54.24 | 54.50 | 54.90 | 54.98 | 55.16 | 54.68 | 54.44 | 54.72 | 54.76 |
| $TiO_2$ | 0.37 | 0.01 | 0.28 | 0.34 | 0.32 | 0.29 | 0.27 | 0.37 | 0.26 | 0.32 | 0.35 | 0.29 | 0.37 |
| $Al_2O_3$ | 1.63 | 0.02 | 3.57 | 3.32 | 3.24 | 3.21 | 3.21 | 3.16 | 3.13 | 3.12 | 3.08 | 3.07 | 3.06 |
| $Cr_2O_3$ | 0.36 | 0.01 | 0.59 | 0.54 | 0.59 | 0.50 | 0.52 | 0.67 | 0.49 | 0.53 | 0.77 | 0.59 | 0.57 |
| FeO | 9.59 | 14.74 | 10.37 | 10.30 | 10.58 | 10.21 | 9.98 | 10.41 | 9.90 | 10.15 | 10.41 | 10.22 | 10.07 |
| MnO | 0.11 | 0.19 | 0.15 | 0.13 | 0.14 | 0.16 | 0.17 | 0.21 | 0.20 | 0.15 | 0.11 | 0.25 | 0.19 |
| MgO | 31.20 | 44.51 | 30.02 | 30.26 | 29.78 | 30.19 | 30.26 | 30.20 | 30.31 | 30.35 | 30.01 | 30.45 | 30.25 |
| CaO | 1.12 | 0.09 | 1.00 | 0.92 | 0.84 | 0.88 | 0.92 | 0.77 | 0.91 | 0.73 | 0.66 | 0.53 | 0.72 |
| $Na_2O$ | 0.01 | 0.02 | 0.01 | 0.01 | 0.02 | 0.00 | 0.03 | 0.01 | 0.03 | 0.03 | 0.01 | 0.00 | 0.00 |
| $K_2O$ | 0.00 | 0.01 | 0.00 | 0.00 | 0.00 | 0.00 | 0.00 | 0.03 | 0.00 | 0.00 | 0.00 | 0.00 | 0.00 |
| TOTAL | 99.79 | 99.47 | 100.92 | 99.77 | 99.74 | 99.94 | 100.26 | 100.82 | 100.40 | 100.07 | 99.85 | 100.13 | 99.98 |
| | | | | | | | | | | | | | |
| Si | 1.95 | 1.34 | 1.92 | 1.90 | 1.92 | 1.92 | 1.93 | 1.92 | 1.93 | 1.92 | 1.92 | 1.92 | 1.93 |
| Ti | 0.01 | 0.00 | 0.01 | 0.01 | 0.01 | 0.01 | 0.01 | 0.01 | 0.01 | 0.01 | 0.01 | 0.01 | 0.01 |
| Al | 0.07 | 0.00 | 0.15 | 0.14 | 0.14 | 0.13 | 0.13 | 0.13 | 0.13 | 0.13 | 0.13 | 0.13 | 0.13 |
| Cr | 0.01 | 0.00 | 0.02 | 0.02 | 0.02 | 0.01 | 0.01 | 0.02 | 0.01 | 0.01 | 0.02 | 0.02 | 0.02 |
| Fe(ii) | 0.28 | 0.41 | 0.30 | 0.30 | 0.31 | 0.30 | 0.29 | 0.30 | 0.29 | 0.30 | 0.31 | 0.30 | 0.30 |
| Mn | 0.00 | 0.01 | 0.00 | 0.00 | 0.00 | 0.00 | 0.01 | 0.01 | 0.01 | 0.00 | 0.00 | 0.01 | 0.01 |
| Mg | 1.64 | 2.23 | 1.56 | 1.59 | 1.57 | 1.59 | 1.58 | 1.58 | 1.58 | 1.59 | 1.58 | 1.60 | 1.59 |
| Ca | 0.04 | 0.00 | 0.04 | 0.03 | 0.03 | 0.03 | 0.03 | 0.03 | 0.03 | 0.03 | 0.02 | 0.02 | 0.03 |
| | | | | | | | | | | | | | |
| Wo | 2.15 | 0.13 | 1.96 | 1.80 | 1.65 | 1.73 | 1.80 | 1.80 | 1.78 | 1.44 | 1.30 | 1.03 | 1.41 |
| En | 83.29 | 85.48 | 81.87 | 82.28 | 81.75 | 82.38 | 82.53 | 82.53 | 82.63 | 82.70 | 82.44 | 82.96 | 82.81 |
| Fs | 14.52 | 14.35 | 16.12 | 15.88 | 16.51 | 15.88 | 15.55 | 15.55 | 15.48 | 15.75 | 16.24 | 16.01 | 15.78 |
| Mg# | 0.85 | 0.84 | 0.84 | 0.84 | 0.83 | 0.84 | 0.84 | 0.84 | 0.85 | 0.84 | 0.84 | 0.84 | 0.84 |

**Table F1.1 Continued.**

| | USM65 OPX35 | USM65 OPX46 | USM65 OPX16 | USM65 OPX44 | USM65 OPX38 | USM65 OPX2 | USM65 OPX11 | USM65 OPX85 | USM65 OPX84 | USM65 OPX82 | USM65 OPX45 | USM8 OPX42 | USM8 OPX |
|---|---|---|---|---|---|---|---|---|---|---|---|---|---|
| $SiO_2$ | 54.50 | 54.92 | 54.57 | 54.71 | 54.95 | 54.53 | 54.55 | 54.77 | 54.93 | 54.78 | 55.20 | 54.14 | 54.19 |
| $TiO_2$ | 0.30 | 0.31 | 0.30 | 0.27 | 0.32 | 0.29 | 0.28 | 0.21 | 0.29 | 0.38 | 0.34 | 0.27 | 0.32 |
| $Al_2O_3$ | 3.02 | 3.00 | 2.94 | 2.94 | 2.92 | 2.91 | 2.91 | 2.90 | 2.86 | 2.82 | 2.43 | 4.44 | 4.35 |
| $Cr_2O_3$ | 0.58 | 0.67 | 0.44 | 0.62 | 0.50 | 0.48 | 0.63 | 0.52 | 0.52 | 0.53 | 0.43 | 0.44 | 0.40 |
| FeO | 9.57 | 10.30 | 10.18 | 10.38 | 9.78 | 10.03 | 10.08 | 10.19 | 10.06 | 10.06 | 9.97 | 9.31 | 9.53 |
| MnO | 0.21 | 0.17 | 0.21 | 0.21 | 0.29 | 0.22 | 0.27 | 0.17 | 0.24 | 0.22 | 0.21 | 0.20 | 0.20 |
| MgO | 30.67 | 30.41 | 30.38 | 30.63 | 30.36 | 30.37 | 30.49 | 30.82 | 30.55 | 30.52 | 31.00 | 30.64 | 30.98 |
| CaO | 0.71 | 0.72 | 0.72 | 0.61 | 0.64 | 0.62 | 0.71 | 0.79 | 0.73 | 0.69 | 0.52 | 0.72 | 0.62 |
| $Na_2O$ | 0.00 | 0.01 | 0.01 | 0.00 | 0.00 | 0.01 | 0.00 | 0.00 | 0.01 | 0.01 | 0.01 | 0.00 | 0.02 |
| $K_2O$ | 0.00 | 0.02 | 0.01 | 0.00 | 0.01 | 0.00 | 0.00 | 0.01 | 0.02 | 0.00 | 0.01 | 0.00 | 0.01 |
| TOTAL | 99.57 | 100.53 | 99.77 | 100.38 | 99.76 | 99.46 | 99.92 | 100.39 | 100.20 | 100.01 | 100.12 | 100.15 | 100.61 |
| | | | | | | | | | | | | | |
| Si | 1.92 | 1.92 | 1.92 | 1.92 | 1.94 | 54.53 | 1.92 | 1.92 | 1.93 | 1.93 | 1.94 | 1.89 | 1.89 |
| Ti | 0.01 | 0.01 | 0.01 | 0.01 | 0.01 | 0.29 | 0.01 | 0.01 | 0.01 | 0.01 | 0.01 | 0.01 | 0.01 |
| Al | 0.13 | 0.12 | 0.12 | 0.12 | 0.12 | 2.91 | 0.12 | 0.12 | 0.12 | 0.12 | 0.10 | 0.18 | 0.18 |
| Cr | 0.02 | 0.02 | 0.01 | 0.02 | 0.01 | 0.48 | 0.02 | 0.01 | 0.01 | 0.01 | 0.01 | 0.01 | 0.01 |
| Fe(ii) | 0.28 | 0.30 | 0.30 | 0.30 | 0.29 | 10.03 | 0.30 | 0.30 | 0.30 | 0.30 | 0.29 | 0.27 | 0.28 |
| Mn | 0.01 | 0.01 | 0.01 | 0.01 | 0.01 | 0.22 | 0.01 | 0.01 | 0.01 | 0.01 | 0.01 | 0.01 | 0.01 |
| Mg | 1.61 | 1.59 | 1.60 | 1.60 | 1.60 | 30.37 | 1.60 | 1.61 | 1.60 | 1.60 | 1.62 | 1.60 | 1.61 |
| Ca | 0.03 | 0.03 | 0.03 | 0.02 | 0.02 | 0.62 | 0.03 | 0.03 | 0.03 | 0.03 | 0.02 | 0.03 | 0.02 |
| | | | | | | | | | | | | | |
| Wo | 1.38 | 1.41 | 1.40 | 1.19 | 1.25 | 1.21 | 1.40 | 1.53 | 1.42 | 1.34 | 1.01 | 1.42 | 1.21 |
| En | 83.63 | 82.58 | 82.69 | 82.75 | 83.23 | 83.04 | 82.83 | 82.86 | 82.88 | 82.93 | 83.57 | 83.97 | 83.96 |
| Fs | 14.97 | 15.97 | 15.87 | 16.05 | 15.52 | 15.73 | 15.78 | 15.60 | 15.68 | 15.69 | 15.41 | 14.61 | 14.77 |
| Mg# | 0.85 | 0.84 | 0.84 | 0.84 | 0.85 | 0.84 | 0.84 | 0.84 | 0.84 | 0.84 | 0.85 | 0.85 | 0.85 |

## Table F1.1 Continued.

| | USM8 OPX 10 | USM8 OPX5 | USM8 OPX2 | USM8 OPX3 | USM8 OPX39 | USM8 OPX6 | USM8 OPX8 | USM8 OPX44 | USM8 OPX10 | USM8 OPX12 | USM8 OPX11 | USM8 OPX36 | USM8 OPX24 |
|---|---|---|---|---|---|---|---|---|---|---|---|---|---|
| $SiO_2$ | 54.80 | 53.81 | 54.13 | 54.46 | 54.24 | 54.18 | 53.89 | 54.75 | 55.29 | 54.60 | 54.83 | 55.18 | 54.46 |
| $TiO_2$ | 0.25 | 0.34 | 0.36 | 0.29 | 0.30 | 0.30 | 0.33 | 0.33 | 0.32 | 0.28 | 0.38 | 0.27 | 0.31 |
| $Al_2O_3$ | 4.34 | 4.19 | 4.11 | 3.85 | 3.73 | 3.69 | 3.69 | 3.43 | 3.16 | 3.15 | 2.96 | 2.94 | 2.82 |
| $Cr_2O_3$ | 0.42 | 0.48 | 0.48 | 0.52 | 0.47 | 0.57 | 0.56 | 0.38 | 0.32 | 0.50 | 0.44 | 0.36 | 0.44 |
| FeO | 9.51 | 9.53 | 9.44 | 9.08 | 9.58 | 9.90 | 9.48 | 9.35 | 9.22 | 9.56 | 9.30 | 9.10 | 9.46 |
| MnO | 0.12 | 0.21 | 0.26 | 0.24 | 0.17 | 0.25 | 0.21 | 0.27 | 0.23 | 0.17 | 0.24 | 0.21 | 0.15 |
| MgO | 30.90 | 30.82 | 31.19 | 30.82 | 31.29 | 31.15 | 31.08 | 31.53 | 31.44 | 31.39 | 31.73 | 31.68 | 31.36 |
| CaO | 0.77 | 0.73 | 0.58 | 0.63 | 0.78 | 0.62 | 0.53 | 0.56 | 0.91 | 0.70 | 0.72 | 0.73 | 0.78 |
| $Na_2O$ | 0.03 | 0.01 | 0.00 | 0.00 | 0.02 | 0.02 | 0.00 | 0.00 | 0.04 | 0.01 | 0.03 | 0.00 | 0.00 |
| $K_2O$ | 0.00 | 0.03 | 0.03 | 0.00 | 0.01 | 0.00 | 0.00 | 0.02 | 0.00 | 0.00 | 0.00 | 0.00 | 0.00 |
| TOTAL | 101.13 | 100.15 | 100.59 | 99.89 | 100.58 | 100.67 | 99.77 | 100.63 | 100.93 | 100.35 | 100.63 | 100.45 | 99.77 |
| | | | | | | | | | | | | | |
| Si | 1.90 | 1.88 | 1.88 | 1.91 | 1.89 | 1.89 | 1.89 | 1.90 | 1.92 | 1.91 | 1.91 | 1.92 | 1.91 |
| Ti | 0.01 | 0.01 | 0.01 | 0.01 | 0.01 | 0.01 | 0.01 | 0.01 | 0.01 | 0.01 | 0.01 | 0.01 | 0.01 |
| Al | 0.18 | 0.17 | 0.17 | 0.16 | 0.15 | 0.15 | 0.15 | 0.14 | 0.13 | 0.13 | 0.12 | 0.12 | 0.12 |
| Cr | 0.01 | 0.01 | 0.01 | 0.01 | 0.01 | 0.02 | 0.02 | 0.01 | 0.01 | 0.01 | 0.01 | 0.01 | 0.01 |
| Fe(ii) | 0.28 | 0.28 | 0.27 | 0.27 | 0.28 | 0.29 | 0.28 | 0.27 | 0.27 | 0.28 | 0.27 | 0.26 | 0.28 |
| Mn | 0.00 | 0.01 | 0.01 | 0.01 | 0.00 | 0.01 | 0.01 | 0.01 | 0.01 | 0.00 | 0.01 | 0.01 | 0.00 |
| Mg | 1.60 | 1.61 | 1.62 | 1.61 | 1.62 | 1.62 | 1.63 | 1.63 | 1.63 | 1.63 | 1.64 | 1.64 | 1.64 |
| Ca | 0.03 | 0.03 | 0.02 | 0.02 | 0.03 | 0.02 | 0.02 | 0.02 | 0.03 | 0.03 | 0.03 | 0.03 | 0.03 |
| | | | | | | | | | | | | | |
| Wo | 1.49 | 1.42 | 1.13 | 1.23 | 1.51 | 1.19 | 1.03 | 1.07 | 1.75 | 1.34 | 1.38 | 1.40 | 1.49 |
| En | 83.77 | 83.73 | 84.21 | 84.43 | 83.84 | 83.52 | 84.27 | 84.49 | 83.96 | 84.05 | 84.33 | 84.67 | 84.09 |
| Fs | 14.63 | 14.80 | 14.66 | 14.33 | 14.60 | 15.21 | 14.70 | 14.44 | 14.15 | 14.57 | 14.18 | 13.93 | 14.42 |
| Mg# | 0.85 | 0.85 | 0.85 | 0.86 | 0.85 | 0.85 | 0.85 | 0.86 | 0.86 | 0.85 | 0.86 | 0.86 | 0.86 |

## Table F1.1 Continued.

| | USM8 OPX | USM8 OPX21 | USM8 OPX26 | USM8 OPX19 | USM8 OPX23 | USM8 OPX33 | USM66 OPX5 | USM66 OPX16 | USM66 OPX25 | USM66 OPX16 | USM66 OPX50 | USM66 OPX40 | USM66 OPX35 |
|---|---|---|---|---|---|---|---|---|---|---|---|---|---|
| $SiO_2$ | 55.33 | 54.75 | 55.70 | 55.30 | 55.51 | 55.00 | 53.00 | 52.40 | 53.52 | 54.17 | 54.17 | 53.99 | 53.94 |
| $TiO_2$ | 0.33 | 0.36 | 0.33 | 0.26 | 0.31 | 0.34 | 0.21 | 0.20 | 0.25 | 0.23 | 0.24 | 0.19 | 0.20 |
| $Al_2O_3$ | 2.77 | 2.74 | 2.70 | 2.59 | 2.58 | 2.33 | 1.43 | 1.42 | 1.89 | 1.86 | 1.61 | 1.60 | 1.50 |
| $Cr_2O_3$ | 0.40 | 0.46 | 0.45 | 0.45 | 0.44 | 0.43 | 0.30 | 0.22 | 0.39 | 0.37 | 0.26 | 0.40 | 0.31 |
| FeO | 9.03 | 9.41 | 9.30 | 8.97 | 9.31 | 8.82 | 16.18 | 15.90 | 14.84 | 14.97 | 15.74 | 15.53 | 15.78 |
| MnO | 0.21 | 0.26 | 0.31 | 0.14 | 0.19 | 0.22 | 0.46 | 0.51 | 0.53 | 0.46 | 0.51 | 0.48 | 0.46 |
| MgO | 31.18 | 31.68 | 31.67 | 31.34 | 31.61 | 31.67 | 26.87 | 26.46 | 23.38 | 24.70 | 26.68 | 26.45 | 26.37 |
| CaO | 0.96 | 0.87 | 1.11 | 0.94 | 0.90 | 0.90 | 1.12 | 1.40 | 4.74 | 3.16 | 1.12 | 1.27 | 1.62 |
| $Na_2O$ | 0.02 | 0.00 | 0.03 | 0.02 | 0.00 | 0.00 | 0.00 | 0.03 | 0.08 | 0.06 | 0.02 | 0.00 | 0.00 |
| $K_2O$ | 0.00 | 0.02 | 0.02 | 0.00 | 0.00 | 0.01 | 0.00 | 0.02 | 0.00 | 0.00 | 0.00 | 0.00 | 0.01 |
| TOTAL | 100.22 | 100.56 | 101.62 | 100.02 | 100.87 | 99.72 | 99.58 | 98.57 | 99.62 | 99.98 | 100.34 | 99.92 | 100.19 |
| | | | | | | | | | | | | | |
| Si | 1.93 | 1.91 | 1.92 | 1.94 | 1.93 | 1.93 | 1.92 | 1.92 | 1.96 | 1.97 | 1.95 | 1.95 | 1.95 |
| Ti | 0.01 | 0.01 | 0.01 | 0.01 | 0.01 | 0.01 | 0.01 | 0.01 | 0.01 | 0.01 | 0.01 | 0.01 | 0.01 |
| Al | 0.11 | 0.11 | 0.11 | 0.11 | 0.11 | 0.10 | 0.06 | 0.06 | 0.08 | 0.08 | 0.07 | 0.07 | 0.06 |
| Cr | 0.01 | 0.01 | 0.01 | 0.01 | 0.01 | 0.01 | 0.01 | 0.01 | 0.01 | 0.01 | 0.01 | 0.01 | 0.01 |
| Fe(ii) | 0.26 | 0.27 | 0.27 | 0.26 | 0.27 | 0.26 | 0.49 | 0.49 | 0.45 | 0.46 | 0.47 | 0.47 | 0.48 |
| Mn | 0.01 | 0.01 | 0.01 | 0.00 | 0.01 | 0.01 | 0.01 | 0.02 | 0.02 | 0.01 | 0.02 | 0.01 | 0.01 |
| Mg | 1.62 | 1.64 | 1.63 | 1.64 | 1.64 | 1.66 | 1.45 | 1.45 | 1.28 | 1.34 | 1.43 | 1.43 | 1.42 |
| Ca | 0.04 | 0.03 | 0.04 | 0.04 | 0.03 | 0.03 | 0.04 | 0.05 | 0.19 | 0.12 | 0.04 | 0.05 | 0.06 |
| | | | | | | | | | | | | | |
| Wo | 1.86 | 1.65 | 2.11 | 1.82 | 1.73 | 1.73 | 2.17 | 2.75 | 9.59 | 6.35 | 2.19 | 2.52 | 3.18 |
| En | 84.10 | 83.99 | 83.58 | 84.36 | 84.10 | 84.72 | 72.70 | 72.19 | 65.81 | 69.12 | 72.85 | 72.77 | 71.99 |
| Fs | 13.98 | 14.34 | 14.20 | 13.76 | 14.17 | 13.54 | 25.12 | 24.96 | 24.32 | 24.30 | 24.87 | 24.71 | 24.83 |
| Mg# | 0.86 | 0.86 | 0.86 | 0.86 | 0.86 | 0.86 | 0.75 | 0.75 | 0.74 | 0.75 | 0.75 | 0.75 | 0.75 |

## Table F1.1 Continued.

| | USM66 OPX37 | USM66 OPX34 | USM66 OPX33 | USM66 OPX55 |
|---|---|---|---|---|
| $SiO_2$ | 53.68 | 54.40 | 54.42 | 53.85 |
| $TiO_2$ | 0.19 | 0.15 | 0.14 | 0.18 |
| $Al_2O_3$ | 1.44 | 1.43 | 1.38 | 1.33 |
| $Cr_2O_3$ | 0.30 | 0.24 | 0.15 | 0.41 |
| FeO | 15.74 | 15.68 | 15.77 | 17.12 |
| MnO | 0.55 | 0.53 | 0.47 | 0.57 |
| MgO | 27.03 | 26.70 | 26.79 | 25.92 |
| CaO | 1.13 | 1.26 | 1.27 | 0.83 |
| $Na_2O$ | 0.01 | 0.02 | 0.01 | 0.00 |
| $K_2O$ | 0.00 | 0.00 | 0.01 | 0.02 |
| TOTAL | 100.07 | 100.40 | 100.41 | 100.23 |
| | | | | |
| Si | 1.94 | 1.96 | 1.96 | 1.95 |
| Ti | 0.01 | 0.00 | 0.00 | 0.00 |
| Al | 0.06 | 0.06 | 0.06 | 0.06 |
| Cr | 0.01 | 0.01 | 0.00 | 0.01 |
| Fe(ii) | 0.47 | 0.47 | 0.47 | 0.52 |
| Mn | 0.02 | 0.02 | 0.01 | 0.02 |
| Mg | 1.45 | 1.43 | 1.44 | 1.40 |
| Ca | 0.04 | 0.05 | 0.05 | 0.03 |
| | | | | |
| Wo | 2.20 | 2.47 | 2.47 | 1.64 |
| En | 73.13 | 72.71 | 72.77 | 71.15 |
| Fs | 24.62 | 24.76 | 24.72 | 27.21 |
| Mg# | 0.75 | 0.75 | 0.75 | 0.73 |

## Table F1.2 Olivine analyses

| | BC10/90/5 OL1 | BC10/90/5 OL8 | BC10/90/5 OL11 | BC10/90/5 OL13 | BC10/90/5 OL20 | BC10/90/5 OL29 | BC10/90/5 OL33 | BC10/90/5 OL44 | BC10/90/6 OL4 | BC10/90/6 OL5 | BC10/90/6 OL6 | BC10/90/6 OL7 | BC10/90/6 OL16 |
|---|---|---|---|---|---|---|---|---|---|---|---|---|---|
| $SiO_2$ | 39.29 | 38.61 | 39.12 | 38.89 | 38.36 | 39.13 | 39.15 | 39.16 | 39.55 | 39.38 | 39.51 | 39.79 | 39.73 |
| TiO2 | 0.00 | 0.02 | 0.00 | 0.01 | 0.03 | 0.02 | 0.04 | 0.03 | 0.05 | 0.04 | 0.03 | 0.05 | 0.00 |
| FeO | 15.36 | 14.96 | 14.89 | 15.12 | 15.34 | 15.27 | 14.43 | 15.11 | 15.37 | 15.59 | 15.73 | 15.37 | 15.55 |
| MnO | 0.22 | 0.18 | 0.22 | 0.21 | 0.22 | 0.28 | 0.22 | 0.18 | 0.15 | 0.16 | 0.16 | 0.15 | 0.17 |
| MgO | 44.70 | 44.60 | 44.69 | 44.72 | 44.70 | 44.78 | 44.89 | 44.82 | 44.42 | 44.65 | 44.58 | 45.10 | 44.46 |
| NiO | 0.50 | 0.44 | 0.48 | 0.45 | 0.49 | 0.51 | 0.54 | 0.53 | 0.45 | 0.57 | 0.55 | 0.46 | 0.55 |
| CaO | 0.04 | 0.04 | 0.05 | 0.03 | 0.02 | 0.04 | 0.05 | 0.04 | 0.04 | 0.03 | 0.04 | 0.04 | 0.04 |
| TOTAL | 100.11 | 98.84 | 99.45 | 99.43 | 99.17 | 100.03 | 99.32 | 99.86 | 100.02 | 100.42 | 100.59 | 100.95 | 100.50 |
| | | | | | | | | | | | | | |
| Si | 0.99 | 0.99 | 0.99 | 0.99 | 0.98 | 0.99 | 0.99 | 0.99 | 1.00 | 0.99 | 0.99 | 0.99 | 1.00 |
| Ti | 0.00 | 0.00 | 0.00 | 0.00 | 0.00 | 0.00 | 0.00 | 0.00 | 0.00 | 0.00 | 0.00 | 0.00 | 0.00 |
| Fe(ii) | 0.32 | 0.32 | 0.32 | 0.32 | 0.33 | 0.32 | 0.31 | 0.32 | 0.32 | 0.33 | 0.33 | 0.32 | 0.33 |
| Mn | 0.00 | 0.00 | 0.00 | 0.00 | 0.00 | 0.01 | 0.00 | 0.00 | 0.00 | 0.00 | 0.00 | 0.00 | 0.00 |
| Mg | 1.68 | 1.70 | 1.69 | 1.69 | 1.70 | 1.69 | 1.69 | 1.69 | 1.67 | 1.67 | 1.67 | 1.68 | 1.66 |
| Ni | 0.01 | 0.01 | 0.01 | 0.01 | 0.01 | 0.01 | 0.01 | 0.01 | 0.01 | 0.01 | 0.01 | 0.01 | 0.01 |
| | | | | | | | | | | | | | |
| Fo | 83.65 | 84 | 84.05 | 83.87 | 83.66 | 83.7 | 84.52 | 83.93 | 83.61 | 83.48 | 83.34 | 83.82 | 83.45 |
| Fa | 16.12 | 15.8 | 15.71 | 15.91 | 16.11 | 16 | 15.24 | 15.97 | 16.23 | 16.35 | 16.49 | 16.02 | 16.37 |
| | **BC10/90/6 OL17** | **BC10/90/6 OL18** | **BC10/90/6 OL21** | **BC10/90/6 OL22** | **BC10/90/6 OL35** | **BC10/90/6 OL42** | **BC10/90/6 OL43** | **BC10/90/6 OL46** | **BC10/90/6 OL49** | **BC10/90/6 OL50** | **BC10/90/6 OL53** | **BC10/90/6 OL54** | **BC10/90/6 OL54** |
| $SiO_2$ | 39.60 | 39.48 | 39.57 | 39.14 | 39.79 | 39.43 | 39.19 | 39.58 | 54.28 | 39.48 | 39.87 | 39.76 | 39.80 |
| TiO2 | 0.04 | 0.03 | 0.02 | 0.02 | 0.03 | 0.02 | 0.02 | 0.02 | 0.59 | 0.00 | 0.00 | 0.04 | 0.05 |
| FeO | 15.32 | 15.74 | 15.66 | 15.55 | 15.05 | 15.25 | 15.37 | 14.98 | 10.41 | 15.07 | 15.37 | 15.20 | 15.22 |
| MnO | 0.17 | 0.23 | 0.22 | 0.21 | 0.23 | 0.20 | 0.19 | 0.17 | 0.19 | 0.14 | 0.19 | 0.11 | 0.15 |
| MgO | 44.59 | 44.62 | 44.86 | 44.21 | 44.99 | 44.63 | 44.15 | 44.67 | 30.78 | 44.71 | 44.93 | 44.89 | 44.69 |
| NiO | 0.54 | 0.49 | 0.59 | 0.51 | 0.47 | 0.54 | 0.45 | 0.51 | 0.13 | 0.55 | 0.52 | 0.51 | 0.53 |
| CaO | 0.06 | 0.03 | 0.05 | 0.06 | 0.03 | 0.04 | 0.04 | 0.06 | 1.31 | 0.06 | 0.09 | 0.04 | 0.03 |
| TOTAL | 100.32 | 100.63 | 100.96 | 99.69 | 100.60 | 100.12 | 99.42 | 99.99 | 97.69 | 100.03 | 100.97 | 100.56 | 100.47 |
| | | | | | | | | | | | | | |
| Si | 1.00 | 0.99 | 0.99 | 0.99 | 1.00 | 0.99 | 0.99 | 1.00 | 1.32 | 0.99 | 1.00 | 1.00 | 1.00 |
| Ti | 0.00 | 0.00 | 0.00 | 0.00 | 0.00 | 0.00 | 0.00 | 0.00 | 0.01 | 0.00 | 0.00 | 0.00 | 0.00 |
| Fe(ii) | 0.32 | 0.33 | 0.33 | 0.33 | 0.31 | 0.32 | 0.33 | 0.32 | 0.21 | 0.32 | 0.32 | 0.32 | 0.32 |
| Mn | 0.00 | 0.00 | 0.00 | 0.00 | 0.00 | 0.00 | 0.00 | 0.00 | 0.00 | 0.00 | 0.00 | 0.00 | 0.00 |
| Mg | 1.67 | 1.67 | 1.67 | 1.67 | 1.68 | 1.68 | 1.67 | 1.68 | 1.12 | 1.68 | 1.67 | 1.68 | 1.67 |
| Ni | 0.01 | 0.01 | 0.01 | 0.01 | 0.01 | 0.01 | 0.01 | 0.01 | 0.00 | 0.01 | 0.01 | 0.01 | 0.01 |
| | | | | | | | | | | | | | |
| Fo | 83.69 | 83.28 | 83.44 | 83.33 | 83.99 | 83.72 | 83.49 | 84.01 | 83.81 | 83.97 | 83.73 | 83.94 | 83.83 |
| Fa | 16.13 | 16.48 | 16.33 | 16.44 | 15.76 | 16.05 | 16.3 | 15.8 | 15.89 | 15.88 | 16.07 | 15.94 | 16.02 |

## Table F1.2 Continued.

| | BC10/90/6 OL59 | BC10/90/6 OL60 | BC10/90/6 OL62 | USM65 OL5 | USM65 OL6 | USM65 OL8 | USM65 OL21 | USM65 OL28 | USM65 OL30 | USM65 OL31 | USM65 OL33 | USM65 OL39 | USM65 OL40 |
|---|---|---|---|---|---|---|---|---|---|---|---|---|---|
| $SiO_2$ | 39.58 | 39.65 | 39.37 | 39.25 | 39.35 | 39.38 | 39.51 | 39.53 | 39.16 | 39.36 | 39.32 | 39.43 | 39.93 |
| TiO2 | 0.01 | 0.05 | 0.02 | 0.04 | 0.01 | 0.05 | 0.01 | 0.02 | 0.01 | 0.05 | 0.01 | 0.04 | 0.02 |
| FeO | 15.18 | 15.40 | 15.06 | 15.88 | 16.23 | 16.12 | 16.23 | 16.17 | 16.06 | 16.03 | 15.68 | 16.07 | 16.20 |
| MnO | 0.21 | 0.21 | 0.13 | 0.26 | 0.22 | 0.19 | 0.22 | 0.22 | 0.21 | 0.20 | 0.21 | 0.16 | 0.22 |
| MgO | 44.87 | 44.79 | 44.42 | 43.65 | 43.58 | 43.81 | 43.71 | 43.73 | 43.38 | 43.74 | 43.69 | 43.41 | 43.34 |
| NiO | 0.46 | 0.53 | 0.53 | 0.59 | 0.57 | 0.60 | 0.65 | 0.61 | 0.53 | 0.53 | 0.63 | 0.58 | 0.62 |
| CaO | 0.04 | 0.01 | 0.07 | 0.03 | 0.02 | 0.05 | 0.04 | 0.03 | 0.02 | 0.04 | 0.04 | 0.04 | 0.03 |
| TOTAL | 100.34 | 100.64 | 99.61 | 99.70 | 99.98 | 100.20 | 100.36 | 100.32 | 99.36 | 99.95 | 99.58 | 99.72 | 100.36 |
| | | | | | | | | | | | | | |
| Si | 0.99 | 0.99 | 1.00 | 1.00 | 1.00 | 1.00 | 1.00 | 1.00 | 1.00 | 1.00 | 1.00 | 1.00 | 1.01 |
| Ti | 0.00 | 0.00 | 0.00 | 0.00 | 0.00 | 0.00 | 0.00 | 0.00 | 0.00 | 0.00 | 0.00 | 0.00 | 0.00 |
| Fe(ii) | 0.32 | 0.32 | 0.32 | 0.34 | 0.34 | 0.34 | 0.34 | 0.34 | 0.34 | 0.34 | 0.33 | 0.34 | 0.34 |
| Mn | 0.00 | 0.00 | 0.00 | 0.01 | 0.00 | 0.00 | 0.00 | 0.00 | 0.00 | 0.00 | 0.00 | 0.00 | 0.00 |
| Mg | 1.68 | 1.67 | 1.68 | 1.65 | 1.65 | 1.65 | 1.64 | 1.65 | 1.65 | 1.65 | 1.65 | 1.64 | 1.63 |
| Ni | 0.01 | 0.01 | 0.01 | 0.01 | 0.01 | 0.01 | 0.01 | 0.01 | 0.01 | 0.01 | 0.01 | 0.01 | 0.01 |
| | | | | | | | | | | | | | |
| Fo | 83.87 | 83.65 | 83.9 | 82.81 | 82.52 | 82.72 | 82.57 | 82.62 | 82.62 | 82.77 | 83.06 | 82.66 | 82.47 |
| Fa | 15.91 | 16.13 | 15.65 | 16.9 | 17.24 | 17.07 | 17.2 | 17.14 | 17.15 | 17.01 | 16.72 | 17.17 | 17.29 |
| | **USM65 OL42** | **USM65 OL55** | **USM65 OL56** | **USM65 OL62** | **USM65 OL70** | **USM66 OL22** | **USM66 OL15** | **USM66 OL21** | **USM66 OL25** | **USM66 OL20** | **USM66 OL15** | **USM66 OL23** | **USM66 OL5** |
| $SiO_2$ | 53.91 | 39.41 | 39.56 | 39.38 | 39.35 | 37.03 | 36.35 | 36.72 | 36.57 | 36.58 | 38.11 | 38.21 | 37.50 |
| TiO2 | 0.28 | 0.01 | 0.01 | 0.00 | 0.03 | 0.00 | 0.00 | 0.00 | 0.02 | 0.01 | 0.00 | 0.02 | 0.00 |
| FeO | 10.67 | 15.89 | 15.41 | 15.84 | 15.82 | 25.75 | 26.39 | 26.35 | 26.45 | 25.96 | 26.08 | 26.49 | 26.34 |
| MnO | 0.23 | 0.29 | 0.21 | 0.25 | 0.23 | 0.49 | 0.60 | 0.55 | 0.53 | 0.49 | 0.58 | 0.65 | 0.49 |
| MgO | 30.26 | 43.92 | 43.55 | 43.71 | 43.77 | 35.54 | 35.78 | 35.95 | 35.68 | 35.73 | 35.51 | 35.83 | 35.41 |
| NiO | 0.11 | 0.55 | 0.63 | 0.54 | 0.54 | 0.00 | 0.00 | 0.00 | 0.00 | 0.00 | 0.00 | 0.00 | 0.00 |
| CaO | 0.71 | 0.06 | 0.04 | 0.03 | 0.02 | 0.25 | 0.01 | 0.02 | 0.02 | 0.03 | 0.04 | 0.02 | 0.02 |
| TOTAL | 96.18 | 100.13 | 99.41 | 99.75 | 99.77 | 99.11 | 99.16 | 99.68 | 99.31 | 98.84 | 100.35 | 101.34 | 99.79 |
| | | | | | | | | | | | | | |
| Si | 1.33 | 1.00 | 1.00 | 1.00 | 1.00 | 0.99 | 0.98 | 0.98 | 0.98 | 0.98 | 1.01 | 1.00 | 1.00 |
| Ti | 0.01 | 0.00 | 0.00 | 0.00 | 0.00 | 0.00 | 0.00 | 0.00 | 0.00 | 0.00 | 0.00 | 0.00 | 0.00 |
| Fe(ii) | 0.22 | 0.34 | 0.33 | 0.34 | 0.34 | 0.58 | 0.59 | 0.59 | 0.59 | 0.58 | 0.58 | 0.58 | 0.59 |
| Mn | 0.00 | 0.01 | 0.00 | 0.01 | 0.00 | 0.01 | 0.01 | 0.01 | 0.01 | 0.01 | 0.01 | 0.01 | 0.01 |
| Mg | 1.11 | 1.65 | 1.65 | 1.65 | 1.65 | 1.42 | 1.44 | 1.43 | 1.43 | 1.43 | 1.40 | 1.40 | 1.41 |
| Ni | 0.00 | 0.01 | 0.01 | 0.01 | 0.01 | 0.00 | 0.00 | 0.00 | 0.00 | 0.00 | 0.00 | 0.00 | 0.00 |
| | | | | | | | | | | | | | |
| Fo | 83.18 | 82.87 | 83.26 | 82.88 | 82.94 | 70.71 | 70.27 | 70.43 | 70.21 | 70.66 | 70.36 | 70.17 | 70.18 |
| Fa | 16.45 | 16.82 | 16.52 | 16.85 | 16.81 | 28.73 | 29.06 | 28.96 | 29.19 | 28.79 | 28.98 | 29.1 | 29.27 |

## Table F1.2 Continued.

| | **USM66 OL12** | **USM66 OL20** | **USM66 OL17** | **USM66 OL8** | **USM66 OL18** | **USM66 OL52** | **USM66 OL44** | **USM66 OL9** | **USM66 OL7** | **USM66 OL19** | **USM66 OL19** | **USM66 OL13** | **USM66 OL5** |
|---|---|---|---|---|---|---|---|---|---|---|---|---|---|
| $SiO_2$ | 38.00 | 38.03 | 37.81 | 37.85 | 38.04 | 37.77 | 37.46 | 37.85 | 37.87 | 37.63 | 38.09 | 38.25 | 37.93 |
| TiO2 | 0.03 | 0.03 | 0.08 | 0.00 | 0.05 | 0.04 | 0.01 | 0.01 | 0.01 | 0.00 | 0.06 | 0.04 | 0.00 |
| FeO | 26.23 | 26.07 | 25.92 | 26.07 | 26.23 | 25.60 | 24.83 | 25.34 | 26.68 | 26.13 | 26.21 | 25.53 | 26.54 |
| MnO | 0.51 | 0.54 | 0.52 | 0.49 | 0.63 | 0.59 | 0.58 | 0.53 | 0.43 | 0.58 | 0.70 | 0.49 | 0.56 |
| MgO | 35.37 | 35.69 | 35.41 | 35.41 | 35.42 | 35.19 | 35.82 | 35.24 | 35.09 | 35.91 | 35.21 | 35.18 | 35.54 |
| NiO | 0.00 | 0.00 | 0.00 | 0.00 | 0.00 | 0.00 | 0.00 | 0.00 | 0.00 | 0.00 | 0.00 | 0.00 | 0.23 |
| CaO | 0.01 | 0.08 | 0.03 | 0.02 | 0.02 | 0.03 | 0.04 | 0.04 | 0.04 | 0.03 | 0.03 | 0.04 | 0.02 |
| TOTAL | 100.22 | 100.45 | 99.79 | 99.86 | 100.43 | 99.23 | 98.80 | 99.07 | 100.17 | 100.30 | 100.30 | 99.52 | 100.83 |
| | | | | | | | | | | | | | |
| Si | 1.01 | 1.00 | 1.00 | 1.00 | 1.00 | 1.01 | 1.00 | 1.01 | 1.00 | 1.00 | 1.01 | 1.01 | 1.00 |
| Ti | 0.00 | 0.00 | 0.00 | 0.00 | 0.00 | 0.00 | 0.00 | 0.00 | 0.00 | 0.00 | 0.00 | 0.00 | 0.00 |
| Fe(ii) | 0.58 | 0.58 | 0.58 | 0.58 | 0.58 | 0.57 | 0.55 | 0.57 | 0.59 | 0.58 | 0.58 | 0.57 | 0.59 |
| Mn | 0.01 | 0.01 | 0.01 | 0.01 | 0.01 | 0.01 | 0.01 | 0.01 | 0.01 | 0.01 | 0.02 | 0.01 | 0.01 |
| Mg | 1.39 | 1.40 | 1.40 | 1.40 | 1.39 | 1.40 | 1.43 | 1.40 | 1.39 | 1.42 | 1.39 | 1.39 | 1.40 |
| Ni | 0.00 | 0.00 | 0.00 | 0.00 | 0.00 | 0.00 | 0.00 | 0.00 | 0.00 | 0.00 | 0.00 | 0.00 | 0.00 |
| | | | | | | | | | | | | | |
| Fo | 70.22 | 70.51 | 70.48 | 70.38 | 70.15 | 70.54 | 71.53 | 70.83 | 69.76 | 70.55 | 69.99 | 70.68 | 70.04 |
| Fa | 29.21 | 28.88 | 28.93 | 29.06 | 29.14 | 28.79 | 27.81 | 28.57 | 29.75 | 28.79 | 29.22 | 28.77 | 29.33 |
| | USM66 OL7 | USM66 OL8 | USM66 OL9 | USM66 OL12 | USM66 OL15 | USM66 OL17 | USM66 OL19 | USM66 OL20 | USM66 OL23 | USM66 OL44 | USM66 OL52 | USM8 OL31 | USM8 OL7 |
| $SiO_2$ | 37.85 | 37.93 | 37.59 | 37.96 | 37.86 | 37.86 | 37.92 | 38.10 | 37.97 | 37.93 | 38.08 | 56.05 | 39.95 |
| TiO2 | 0.02 | 0.02 | 0.00 | 0.00 | 0.01 | 0.04 | 0.00 | 0.00 | 0.02 | 0.00 | 0.04 | 0.22 | 0.05 |
| FeO | 26.20 | 26.01 | 25.72 | 26.12 | 26.61 | 26.34 | 26.32 | 26.26 | 25.95 | 25.46 | 26.03 | 8.84 | 13.56 |
| MnO | 0.54 | 0.60 | 0.57 | 0.61 | 0.53 | 0.61 | 0.55 | 0.50 | 0.58 | 0.59 | 0.56 | 0.23 | 0.20 |
| MgO | 35.36 | 35.66 | 35.65 | 35.69 | 35.44 | 35.68 | 35.44 | 35.69 | 35.54 | 35.78 | 35.32 | 31.91 | 46.00 |
| NiO | 0.23 | 0.20 | 0.22 | 0.24 | 0.21 | 0.27 | 0.22 | 0.18 | 0.23 | 0.18 | 0.20 | 0.00 | 0.00 |
| CaO | 0.05 | 0.03 | 0.05 | 0.03 | 0.04 | 0.04 | 0.03 | 0.04 | 0.05 | 0.04 | 0.04 | 0.91 | 0.07 |
| TOTAL | 100.25 | 100.46 | 99.79 | 100.64 | 100.69 | 100.85 | 100.49 | 100.77 | 100.34 | 99.98 | 100.26 | 100.53 | 99.81 |
| | | | | | | | | | | | | | |
| Si | 1.00 | 1.00 | 1.00 | 1.00 | 1.00 | 1.00 | 1.00 | 1.00 | 1.00 | 1.00 | 1.01 | 1.31 | 1.00 |
| Ti | 0.00 | 0.00 | 0.00 | 0.00 | 0.00 | 0.00 | 0.00 | 0.00 | 0.00 | 0.00 | 0.00 | 0.00 | 0.00 |
| Fe(ii) | 0.58 | 0.57 | 0.57 | 0.58 | 0.59 | 0.58 | 0.58 | 0.58 | 0.57 | 0.56 | 0.58 | 0.17 | 0.28 |
| Mn | 0.01 | 0.01 | 0.01 | 0.01 | 0.01 | 0.01 | 0.01 | 0.01 | 0.01 | 0.01 | 0.01 | 0.00 | 0.00 |
| Mg | 1.40 | 1.40 | 1.41 | 1.40 | 1.40 | 1.40 | 1.40 | 1.40 | 1.40 | 1.41 | 1.39 | 1.11 | 1.71 |
| Ni | 0.00 | 0.00 | 0.00 | 0.01 | 0.00 | 0.01 | 0.00 | 0.00 | 0.00 | 0.00 | 0.00 | 0.00 | 0.00 |
| | | | | | | | | | | | | | |
| Fo | 70.21 | 70.79 | 70.73 | 70.42 | 69.95 | 70.23 | 70.15 | 70.39 | 70.48 | 71 | 70.31 | 86.25 | 85.63 |
| Fa | 29.18 | 28.83 | 28.63 | 28.9 | 29.46 | 29.08 | 29.22 | 29.04 | 28.86 | 28.34 | 29.06 | 13.4 | 14.16 |

**Table F1.2 Continued.**

| | USM8 OL5 | USM8 OL9 | USM8 OL13 | USM8 OL14 | USM8 OL15 | USM8 OL | USM8 OL20 | USM8 OL22 | USM8 OL31 | USM8 OL32 | USM8 OL35 | USM8 OL40 | USM8 OL43 | USM8 OL44 |
|---|---|---|---|---|---|---|---|---|---|---|---|---|---|---|
| $SiO_2$ | 39.24 | 39.74 | 39.41 | 39.24 | 39.55 | 39.52 | 39.64 | 39.25 | 39.45 | 39.16 | 39.62 | 39.79 | 39.64 | 39.15 |
| TiO2 | 0.03 | 0.00 | 0.00 | 0.00 | 0.03 | 0.02 | 0.01 | 0.03 | 0.03 | 0.02 | 0.02 | 0.04 | 0.00 | 0.02 |
| FeO | 13.11 | 12.97 | 12.67 | 12.67 | 13.36 | 13.12 | 13.04 | 12.83 | 13.09 | 13.59 | 13.35 | 12.93 | 13.73 | 13.26 |
| MnO | 0.28 | 0.20 | 0.20 | 0.18 | 0.21 | 0.19 | 0.25 | 0.19 | 0.23 | 0.26 | 0.27 | 0.16 | 0.16 | 0.21 |
| MgO | 45.88 | 46.11 | 46.06 | 46.01 | 45.99 | 45.91 | 45.83 | 46.01 | 46.64 | 46.22 | 46.53 | 46.41 | 46.02 | 46.00 |
| NiO | 0.62 | 0.60 | 0.57 | 0.56 | 0.51 | 0.47 | 0.54 | 0.61 | 0.63 | 0.48 | 0.48 | 0.57 | 0.59 | 0.56 |
| CaO | 0.02 | 0.03 | 0.02 | 0.04 | 0.01 | 0.03 | 0.04 | 0.03 | 0.04 | 0.01 | 0.02 | 0.02 | 0.02 | 0.06 |
| TOTAL | 99.17 | 99.64 | 98.94 | 98.71 | 99.65 | 99.26 | 99.35 | 98.94 | 100.11 | 99.74 | 100.29 | 99.92 | 100.17 | 99.25 |
| | | | | | | | | | | | | | | |
| Si | 0.99 | 1.00 | 0.99 | 0.99 | 0.99 | 0.99 | 1.00 | 0.99 | 0.99 | 0.98 | 0.99 | 0.99 | 0.99 | 0.99 |
| Ti | 0.00 | 0.00 | 0.00 | 0.00 | 0.00 | 0.00 | 0.00 | 0.00 | 0.00 | 0.00 | 0.00 | 0.00 | 0.00 | 0.00 |
| Fe(ii) | 0.28 | 0.27 | 0.27 | 0.27 | 0.28 | 0.28 | 0.27 | 0.27 | 0.27 | 0.29 | 0.28 | 0.27 | 0.29 | 0.28 |
| Mn | 0.01 | 0.00 | 0.00 | 0.00 | 0.00 | 0.00 | 0.01 | 0.00 | 0.00 | 0.01 | 0.01 | 0.00 | 0.00 | 0.00 |
| Mg | 1.73 | 1.72 | 1.73 | 1.73 | 1.72 | 1.72 | 1.72 | 1.73 | 1.74 | 1.73 | 1.73 | 1.73 | 1.72 | 1.73 |
| Ni | 0.01 | 0.01 | 0.01 | 0.01 | 0.01 | 0.01 | 0.01 | 0.01 | 0.01 | 0.01 | 0.01 | 0.01 | 0.01 | 0.01 |
| | | | | | | | | | | | | | | |
| Fo | 85.94 | 86.19 | 86.45 | 86.45 | 85.81 | 86.1 | 86.01 | 86.3 | 86.18 | 85.61 | 85.89 | 86.33 | 85.52 | 85.89 |
| Fa | 13.77 | 13.6 | 13.33 | 13.36 | 13.98 | 13.79 | 13.72 | 13.5 | 13.27 | 14.12 | 13.83 | 13.49 | 14.31 | 13.89 |

## Table F1.3 Clinopyroxene analyses

| | BC10/90/5 CPX25 | BC10/90/5 CPX5 | BC10/90/5 CPX10 | BC10/90/5 CPX7 | BC10/90/5 CPX28 | BC10/90/5 CPX46 | BC10/90/5 CPX6 | BC10/90/5 CPX11 | USM66 CPX11 | USM66 CPX28 | USM66 CPX14 | USM66 CPX51 | USM66 CPX42 |
|---|---|---|---|---|---|---|---|---|---|---|---|---|---|
| $SiO_2$ | 52.24 | 51.40 | 51.79 | 52.25 | 51.93 | 52.02 | 51.93 | 52.16 | 51.07 | 51.81 | 52.10 | 52.06 | 52.22 |
| $TiO_2$ | 0.66 | 0.72 | 0.52 | 0.73 | 0.55 | 0.75 | 0.64 | 0.65 | 0.41 | 0.42 | 0.48 | 0.49 | 0.44 |
| $Al_2O_3$ | 3.21 | 3.16 | 3.09 | 3.09 | 3.07 | 3.00 | 2.96 | 2.95 | 3.27 | 2.80 | 2.75 | 2.58 | 2.57 |
| $Cr_2O_3$ | 0.75 | 0.72 | 0.82 | 0.74 | 0.71 | 0.75 | 0.63 | 0.61 | 0.54 | 0.77 | 0.52 | 0.76 | 0.77 |
| FeO | 5.18 | 4.98 | 5.57 | 5.14 | 5.40 | 4.91 | 4.83 | 4.95 | 9.04 | 6.93 | 7.31 | 7.22 | 7.13 |
| MnO | 0.19 | 0.13 | 0.19 | 0.15 | 0.17 | 0.13 | 0.21 | 0.15 | 0.35 | 0.41 | 0.36 | 0.25 | 0.30 |
| MgO | 16.36 | 16.96 | 17.12 | 17.03 | 17.24 | 16.41 | 16.90 | 17.06 | 16.43 | 14.75 | 14.84 | 14.61 | 14.60 |
| CaO | 21.31 | 20.92 | 20.63 | 21.27 | 20.27 | 21.94 | 21.49 | 21.02 | 18.00 | 21.23 | 21.59 | 21.55 | 21.63 |
| $Na_2O$ | 0.11 | 0.16 | 0.14 | 0.19 | 0.15 | 0.15 | 0.15 | 0.17 | 0.32 | 0.30 | 0.30 | 0.28 | 0.38 |
| $K_2O$ | 0.00 | 0.00 | 0.02 | 0.02 | 0.01 | 0.00 | 0.00 | 0.02 | 0.00 | 0.01 | 0.00 | 0.00 | 0.00 |
| ZnO | 0.04 | 0.00 | 0.00 | 0.01 | 0.00 | 0.12 | 0.02 | 0.00 | 0.06 | 0.05 | 0.00 | 0.00 | 0.04 |
| TOTAL | 100.05 | 99.16 | 99.89 | 100.62 | 99.51 | 100.16 | 99.75 | 99.74 | 99.48 | 99.48 | 100.25 | 99.79 | 100.07 |
| | | | | | | | | | | | | | |
| Si | 1.92 | 1.89 | 1.90 | 1.90 | 1.91 | 1.91 | 1.90 | 1.91 | 1.89 | 1.93 | 1.92 | 1.93 | 1.93 |
| Ti | 0.02 | 0.02 | 0.01 | 0.02 | 0.02 | 0.02 | 0.02 | 0.02 | 0.01 | 0.01 | 0.01 | 0.01 | 0.01 |
| Al | 0.14 | 0.14 | 0.13 | 0.13 | 0.13 | 0.13 | 0.13 | 0.13 | 0.14 | 0.12 | 0.12 | 0.11 | 0.11 |
| Cr | 0.02 | 0.02 | 0.02 | 0.02 | 0.02 | 0.02 | 0.02 | 0.02 | 0.02 | 0.02 | 0.02 | 0.02 | 0.02 |
| Fe(ii) | 0.16 | 0.15 | 0.17 | 0.16 | 0.17 | 0.15 | 0.15 | 0.15 | 0.28 | 0.22 | 0.23 | 0.22 | 0.22 |
| Mn | 0.01 | 0.00 | 0.01 | 0.00 | 0.01 | 0.00 | 0.01 | 0.00 | 0.01 | 0.01 | 0.01 | 0.01 | 0.01 |
| Mg | 0.89 | 0.93 | 0.93 | 0.92 | 0.94 | 0.90 | 0.92 | 0.93 | 0.91 | 0.82 | 0.82 | 0.81 | 0.81 |
| Ca | 0.84 | 0.83 | 0.81 | 0.83 | 0.80 | 0.86 | 0.84 | 0.82 | 0.72 | 0.85 | 0.85 | 0.86 | 0.86 |
| Na | 0.01 | 0.01 | 0.01 | 0.01 | 0.01 | 0.01 | 0.01 | 0.01 | 0.02 | 0.02 | 0.02 | 0.02 | 0.03 |
| | | | | | | | | | | | | | |
| Wo | 43.96 | 42.88 | 41.93 | 43.02 | 41.47 | 44.81 | 43.66 | 42.84 | 36.94 | 44.21 | 44.27 | 44.69 | 44.66 |
| En | 46.95 | 48.37 | 48.44 | 47.94 | 49.09 | 46.62 | 47.79 | 48.40 | 46.90 | 42.73 | 42.35 | 42.16 | 41.95 |
| Fs | 8.67 | 8.16 | 9.11 | 8.35 | 8.89 | 8.02 | 7.99 | 8.11 | 14.97 | 11.95 | 12.27 | 12.11 | 11.97 |
| Mg# | 0.85 | 0.86 | 0.85 | 0.86 | 0.85 | 0.86 | 0.86 | 0.86 | 0.76 | 0.79 | 0.78 | 0.78 | 0.79 |

**Table F1.3 Continued.**

| | USM66 CPX26 | USM66 CPX6 | USM66 CPX1 | USM66 CPX10 | USM66 CPX4 | USM66 CPX41 | USM66 CPX47 | USM66 CPX2 | USM66 CPX1 | USM66 CPX23 | USM66 CPX13 | USM66 CPX11 | USM66 CPX |
|---|---|---|---|---|---|---|---|---|---|---|---|---|---|
| $SiO_2$ | 51.83 | 52.35 | 52.22 | 51.72 | 52.09 | 51.57 | 52.01 | 52.54 | 50.59 | 50.60 | 50.10 | 50.76 | 50.89 |
| $TiO_2$ | 0.38 | 0.47 | 0.37 | 0.42 | 0.39 | 0.35 | 0.42 | 0.39 | 0.50 | 0.41 | 0.42 | 0.45 | 0.38 |
| $Al_2O_3$ | 2.55 | 2.51 | 2.51 | 2.42 | 2.42 | 2.38 | 2.32 | 2.23 | 2.79 | 2.66 | 2.63 | 2.61 | 2.36 |
| $Cr_2O_3$ | 0.70 | 0.73 | 0.55 | 0.57 | 0.69 | 0.90 | 0.56 | 0.53 | 0.67 | 0.83 | 0.70 | 0.61 | 0.59 |
| FeO | 7.50 | 7.36 | 7.78 | 7.50 | 6.91 | 6.58 | 8.03 | 7.26 | 7.46 | 7.60 | 7.91 | 7.97 | 7.37 |
| MnO | 0.39 | 0.30 | 0.31 | 0.32 | 0.30 | 0.26 | 0.24 | 0.34 | 0.36 | 0.25 | 0.25 | 0.35 | 0.36 |
| MgO | 14.77 | 15.14 | 15.63 | 15.51 | 14.78 | 14.74 | 16.49 | 15.15 | 14.98 | 15.04 | 15.70 | 15.74 | 15.20 |
| CaO | 21.54 | 21.00 | 19.97 | 20.58 | 21.45 | 21.99 | 19.86 | 21.04 | 20.80 | 20.42 | 19.71 | 19.83 | 20.54 |
| $Na_2O$ | 0.31 | 0.33 | 0.33 | 0.32 | 0.34 | 0.33 | 0.30 | 0.31 | 0.29 | 0.35 | 0.30 | 0.30 | 0.31 |
| $K_2O$ | 0.00 | 0.02 | 0.03 | 0.02 | 0.03 | 0.00 | 0.00 | 0.00 | 0.00 | 0.01 | 0.01 | 0.00 | 0.00 |
| ZnO | 0.15 | 0.00 | 0.06 | 0.00 | 0.00 | 0.09 | 0.08 | 0.00 | 0.00 | 0.00 | 0.00 | 0.00 | 0.00 |
| TOTAL | 100.12 | 100.22 | 99.75 | 99.39 | 99.39 | 99.19 | 100.29 | 99.80 | 98.44 | 98.19 | 97.72 | 98.63 | 98.00 |
| | | | | | | | | | | | | | |
| Si | 1.92 | 1.93 | 1.93 | 1.92 | 1.94 | 1.92 | 1.91 | 1.95 | 1.90 | 1.90 | 1.89 | 1.90 | 1.92 |
| Ti | 0.01 | 0.01 | 0.01 | 0.01 | 0.01 | 0.01 | 0.01 | 0.01 | 0.01 | 0.01 | 0.01 | 0.01 | 0.01 |
| Al | 0.11 | 0.11 | 0.11 | 0.11 | 0.11 | 0.10 | 0.10 | 0.10 | 0.12 | 0.12 | 0.12 | 0.11 | 0.10 |
| Cr | 0.02 | 0.02 | 0.02 | 0.02 | 0.02 | 0.03 | 0.02 | 0.02 | 0.02 | 0.02 | 0.02 | 0.02 | 0.02 |
| Fe(ii) | 0.23 | 0.23 | 0.24 | 0.23 | 0.22 | 0.21 | 0.25 | 0.23 | 0.23 | 0.24 | 0.25 | 0.25 | 0.23 |
| Mn | 0.01 | 0.01 | 0.01 | 0.01 | 0.01 | 0.01 | 0.01 | 0.01 | 0.01 | 0.01 | 0.01 | 0.01 | 0.01 |
| Mg | 0.82 | 0.83 | 0.86 | 0.86 | 0.82 | 0.82 | 0.90 | 0.84 | 0.84 | 0.84 | 0.88 | 0.88 | 0.85 |
| Ca | 0.85 | 0.83 | 0.79 | 0.82 | 0.85 | 0.88 | 0.78 | 0.84 | 0.84 | 0.82 | 0.80 | 0.79 | 0.83 |
| Na | 0.02 | 0.02 | 0.02 | 0.02 | 0.02 | 0.02 | 0.02 | 0.02 | 0.02 | 0.03 | 0.02 | 0.02 | 0.02 |
| | | | | | | | | | | | | | |
| Wo | 44.13 | 43.17 | 41.07 | 42.14 | 44.44 | 45.40 | 39.90 | 43.27 | 43.10 | 42.45 | 40.70 | 40.68 | 42.56 |
| En | 42.12 | 43.31 | 44.73 | 44.19 | 42.61 | 42.36 | 46.11 | 43.34 | 43.19 | 43.51 | 45.12 | 44.93 | 43.83 |
| Fs | 12.59 | 12.29 | 12.98 | 12.48 | 11.68 | 11.00 | 12.92 | 12.22 | 12.61 | 12.70 | 13.07 | 13.26 | 12.46 |
| Mg# | 0.78 | 0.79 | 0.78 | 0.79 | 0.79 | 0.80 | 0.79 | 0.79 | 0.78 | 0.78 | 0.78 | 0.78 | 0.79 |

**Table F1.3 Continued.**

| | USM66 CPX3 | USM60 17EX IN CPX | USM60 16EX IN CPX | USM60 10EX IN CPX | USM60 12EX IN CPX | USM60 8CPX HOST | USM60 21 EXIN CPX | USM60 4EX IN CPX | USM60 3EX IN CPX | USM60 CPX20 | USM60 CPX18 |
|---|---|---|---|---|---|---|---|---|---|---|---|
| $SiO_2$ | 50.90 | 28.90 | 31.84 | 33.49 | 36.38 | 36.79 | 45.20 | 46.77 | 48.35 | 48.99 | 49.92 |
| $TiO_2$ | 0.49 | 0.00 | 0.09 | 0.15 | 0.15 | 0.21 | 0.39 | 0.63 | 0.60 | 0.53 | 0.90 |
| $Al_2O_3$ | 2.30 | 16.94 | 14.69 | 13.73 | 12.16 | 10.42 | 6.03 | 3.96 | 3.27 | 2.83 | 2.19 |
| $Cr_2O_3$ | 0.55 | 0.06 | 0.02 | 0.04 | 0.00 | 0.05 | 0.00 | 0.09 | 0.06 | 0.11 | 0.05 |
| FeO | 7.20 | 25.75 | 23.28 | 23.04 | 21.29 | 20.34 | 15.60 | 14.27 | 13.04 | 13.08 | 12.61 |
| MnO | 0.34 | 0.48 | 0.47 | 0.36 | 0.37 | 0.44 | 0.36 | 0.41 | 0.37 | 0.44 | 0.34 |
| MgO | 15.05 | 13.96 | 13.56 | 13.54 | 13.08 | 12.97 | 12.71 | 11.82 | 11.76 | 11.63 | 11.65 |
| CaO | 21.25 | 2.06 | 4.86 | 6.10 | 8.06 | 8.99 | 15.94 | 18.59 | 19.87 | 20.27 | 21.31 |
| $Na_2O$ | 0.35 | 0.03 | 0.09 | 0.07 | 0.07 | 0.08 | 0.16 | 0.21 | 0.25 | 0.15 | 0.25 |
| $K_2O$ | 0.00 | 0.01 | 0.02 | 0.00 | 0.01 | 0.00 | 0.00 | 0.02 | 0.00 | 0.00 | 0.00 |
| ZnO | 0.00 | 0.00 | 0.01 | 0.00 | 0.00 | 0.00 | 0.01 | 0.00 | 0.00 | 0.00 | 0.02 |
| TOTAL | 98.43 | 88.19 | 88.92 | 90.52 | 91.57 | 90.27 | 96.40 | 96.79 | 97.57 | 98.04 | 99.23 |
| | | | | | | | | | | | |
| Si | 1.91 | 1.92 | 1.34 | 1.39 | 1.50 | 1.54 | 1.77 | 1.83 | 1.87 | 1.89 | 1.91 |
| Ti | 0.01 | 0.02 | 0.00 | 0.00 | 0.00 | 0.01 | 0.01 | 0.02 | 0.02 | 0.02 | 0.03 |
| Al | 0.10 | 0.08 | 0.73 | 0.67 | 0.59 | 0.51 | 0.28 | 0.18 | 0.15 | 0.13 | 0.10 |
| Cr | 0.02 | 0.00 | 0.00 | 0.00 | 0.00 | 0.00 | 0.00 | 0.00 | 0.00 | 0.00 | 0.00 |
| Fe(ii) | 0.23 | 0.37 | 0.82 | 0.80 | 0.73 | 0.71 | 0.51 | 0.47 | 0.42 | 0.42 | 0.40 |
| Mn | 0.01 | 0.02 | 0.02 | 0.01 | 0.01 | 0.02 | 0.01 | 0.01 | 0.01 | 0.01 | 0.01 |
| Mg | 0.84 | 0.65 | 0.85 | 0.84 | 0.80 | 0.81 | 0.74 | 0.69 | 0.68 | 0.67 | 0.66 |
| Ca | 0.85 | 0.92 | 0.22 | 0.27 | 0.36 | 0.40 | 0.67 | 0.78 | 0.82 | 0.84 | 0.87 |
| Na | 0.03 | 0.02 | 0.01 | 0.01 | 0.01 | 0.01 | 0.01 | 0.02 | 0.02 | 0.01 | 0.02 |
| | | | | | | | | | | | |
| Wo | 43.64 | 5.04 | 11.70 | 14.35 | 18.87 | 20.98 | 34.50 | 39.76 | 42.20 | 42.92 | 44.36 |
| En | 43.01 | 47.54 | 45.42 | 44.29 | 42.60 | 42.10 | 38.28 | 35.17 | 34.76 | 34.25 | 33.75 |
| Fs | 12.04 | 47.26 | 42.51 | 41.05 | 38.22 | 36.59 | 26.58 | 24.25 | 22.08 | 22.24 | 20.95 |
| Mg# | 0.79 | 0.49 | 0.51 | 0.51 | 0.52 | 0.53 | 0.59 | 0.60 | 0.62 | 0.61 | 0.62 |

## Table F1.3 Continued.

| | USM60 CPX HOST | USM60 CPX9 HOST | USM60 CPX22 | USM60 CPX7 | USM60 CPX1 | USM60 CPX13 |
|---|---|---|---|---|---|---|
| $SiO_2$ | 51.06 | 50.65 | 51.28 | 51.26 | 50.95 | 50.17 |
| $TiO_2$ | 0.65 | 0.75 | 0.73 | 0.81 | 0.76 | 0.75 |
| $Al_2O_3$ | 2.12 | 2.02 | 1.96 | 1.89 | 1.89 | 1.83 |
| $Cr_2O_3$ | 0.09 | 0.05 | 0.12 | 0.05 | 0.12 | 0.04 |
| FeO | 11.77 | 11.38 | 11.53 | 12.03 | 11.48 | 11.59 |
| MnO | 0.39 | 0.35 | 0.44 | 0.32 | 0.37 | 0.50 |
| MgO | 11.92 | 11.53 | 12.05 | 11.66 | 11.52 | 11.37 |
| CaO | 21.24 | 22.23 | 21.88 | 22.09 | 22.57 | 22.37 |
| $Na_2O$ | 0.23 | 0.24 | 0.16 | 0.18 | 0.18 | 0.25 |
| $K_2O$ | 0.01 | 0.00 | 0.00 | 0.00 | 0.00 | 0.01 |
| ZnO | 0.00 | 0.14 | 0.04 | 0.02 | 0.00 | 0.00 |
| TOTAL | 99.48 | 99.33 | 100.17 | 100.30 | 99.85 | 98.88 |
| | | | | | | |
| Si | 1.94 | 1.93 | 1.94 | 1.94 | 1.93 | 1.92 |
| Ti | 0.02 | 0.02 | 0.02 | 0.02 | 0.02 | 0.02 |
| Al | 0.10 | 0.09 | 0.09 | 0.08 | 0.08 | 0.08 |
| Cr | 0.00 | 0.00 | 0.00 | 0.00 | 0.00 | 0.00 |
| Fe(ii) | 0.37 | 0.36 | 0.36 | 0.38 | 0.36 | 0.37 |
| Mn | 0.01 | 0.01 | 0.01 | 0.01 | 0.01 | 0.02 |
| Mg | 0.68 | 0.66 | 0.68 | 0.66 | 0.65 | 0.65 |
| Ca | 0.86 | 0.91 | 0.88 | 0.89 | 0.92 | 0.92 |
| Na | 0.02 | 0.02 | 0.01 | 0.01 | 0.01 | 0.02 |
| | | | | | | |
| Wo | 44.50 | 46.46 | 45.32 | 45.76 | 46.85 | 46.56 |
| En | 34.74 | 33.54 | 34.72 | 33.61 | 33.27 | 32.93 |
| Fs | 19.90 | 19.11 | 19.34 | 19.95 | 19.19 | 19.58 |
| Mg# | 0.64 | 0.64 | 0.65 | 0.63 | 0.64 | 0.64 |

## Table F1.4 Feldspar analyses

| | BC10/90/5 PLAG9 | BC10/90/5 PLAG21 | BC10/90/5 PLAG30 | BC10/90/5 PLAG34 | BC10/90/5 PLAG15 | BC10/90/5 PLAG26 | BC10/90/5 PLAG42 | BC10/90/6 PLAG39 | BC10/90/6 PLAG47 | BC10/90/6 PLAG2 NEAR 2 | BC10/90/6 PLAG41 | BC10/90/6 PLAG45 | BC10/90/6 PLAG52 |
|---|---|---|---|---|---|---|---|---|---|---|---|---|---|
| $SiO_2$ | 44.78 | 44.53 | 44.48 | 44.71 | 43.88 | 44.93 | 42.44 | 47.19 | 46.89 | 47.69 | 47.80 | 46.77 | 47.12 |
| $Al_2O_3$ | 35.00 | 34.83 | 34.57 | 34.26 | 34.23 | 34.11 | 32.90 | 33.47 | 33.45 | 33.45 | 33.24 | 33.23 | 33.22 |
| FeO | 0.38 | 0.52 | 0.29 | 0.40 | 0.33 | 0.43 | 0.41 | 0.42 | 0.23 | 0.37 | 0.42 | 0.33 | 0.40 |
| CaO | 19.03 | 18.99 | 18.87 | 18.88 | 18.75 | 18.33 | 20.69 | 17.46 | 17.46 | 17.26 | 17.04 | 17.27 | 17.41 |
| $Na_2O$ | 0.73 | 0.74 | 0.64 | 0.72 | 0.69 | 0.83 | 0.60 | 1.59 | 1.60 | 1.56 | 1.73 | 1.46 | 1.62 |
| $K_2O$ | 0.08 | 0.10 | 0.10 | 0.16 | 0.06 | 0.16 | 0.12 | 0.23 | 0.28 | 0.56 | 0.36 | 0.33 | 0.20 |
| TOTAL | 99.99 | 99.71 | 98.97 | 99.13 | 97.93 | 98.79 | 97.16 | 100.36 | 99.91 | 100.89 | 100.59 | 99.39 | 99.97 |
| | | | | | | | | | | | | | |
| Si | 8.29 | 8.28 | 8.31 | 8.35 | 8.29 | 8.40 | 8.17 | 8.66 | 8.65 | 8.71 | 8.75 | 8.67 | 8.68 |
| Al | 7.63 | 7.63 | 7.61 | 7.54 | 7.62 | 7.52 | 7.47 | 7.24 | 7.27 | 7.20 | 7.17 | 7.26 | 7.21 |
| Fe(ii) | 0.06 | 0.08 | 0.05 | 0.06 | 0.05 | 0.07 | 0.07 | 0.07 | 0.04 | 0.06 | 0.06 | 0.05 | 0.06 |
| Ca | 3.77 | 3.78 | 3.78 | 3.78 | 3.80 | 3.67 | 4.27 | 3.43 | 3.45 | 3.38 | 3.34 | 3.43 | 3.44 |
| Na | 0.26 | 0.27 | 0.23 | 0.26 | 0.25 | 0.30 | 0.23 | 0.57 | 0.57 | 0.55 | 0.61 | 0.53 | 0.58 |
| K | 0.02 | 0.02 | 0.02 | 0.04 | 0.01 | 0.04 | 0.03 | 0.05 | 0.07 | 0.13 | 0.08 | 0.08 | 0.05 |
| | | | | | | | | | | | | | |
| An | 93.09 | 92.88 | 93.61 | 92.65 | 93.44 | 91.55 | 94.39 | 84.70 | 84.38 | 83.18 | 82.71 | 85.01 | 84.58 |
| Ab | 6.43 | 6.55 | 5.77 | 6.43 | 6.22 | 7.49 | 4.98 | 13.97 | 14.03 | 13.59 | 15.20 | 13.03 | 14.29 |
| Or | 0.48 | 0.58 | 0.62 | 0.92 | 0.34 | 0.96 | 0.63 | 1.32 | 1.59 | 3.23 | 2.09 | 1.96 | 1.13 |

| | BC10/90/6 PLAG58 | BC10/90/6 PLAG23 | BC10/90/6 PLAG34 | BC10/90/6 PLAG15 | BC10/90/6 PLAG9 | USM8 PLAG30 | USM8 PLAG37 | USM8 PLAG27 | USM8 PLAG45 | USM8 PLAG4 | USM8 PLAG29 | USM8 PLAG 41 | USM8 PLAG34 |
|---|---|---|---|---|---|---|---|---|---|---|---|---|---|
| $SiO_2$ | 47.61 | 47.59 | 46.93 | 46.75 | 46.30 | 43.85 | 44.26 | 44.19 | 44.36 | 44.21 | 43.86 | 44.16 | 43.99 |
| $Al_2O_3$ | 33.14 | 33.12 | 32.95 | 32.74 | 32.07 | 35.41 | 35.38 | 35.28 | 35.21 | 35.02 | 34.96 | 34.94 | 34.86 |
| FeO | 0.34 | 0.32 | 0.44 | 0.88 | 0.62 | 0.34 | 0.37 | 0.50 | 0.30 | 0.42 | 0.48 | 0.38 | 0.49 |
| CaO | 17.01 | 17.25 | 17.18 | 17.02 | 16.26 | 19.96 | 19.94 | 19.46 | 19.38 | 19.57 | 19.70 | 19.40 | 19.66 |
| $Na_2O$ | 1.68 | 1.81 | 1.75 | 1.69 | 1.53 | 0.24 | 0.36 | 0.41 | 0.50 | 0.48 | 0.46 | 0.53 | 0.37 |
| K2O | 0.28 | 0.35 | 0.23 | 0.27 | 0.43 | 0.04 | 0.03 | 0.07 | 0.10 | 0.05 | 0.11 | 0.09 | 0.05 |
| TOTAL | 100.06 | 100.43 | 99.49 | 99.36 | 97.22 | 99.84 | 100.35 | 99.90 | 99.84 | 99.76 | 99.57 | 99.49 | 99.43 |
| | | | | | | | | | | | | | |
| Si | 8.75 | 8.73 | 8.69 | 8.69 | 8.77 | 8.15 | 8.18 | 8.20 | 8.23 | 8.22 | 8.18 | 8.23 | 8.21 |
| Al | 7.18 | 7.16 | 7.19 | 7.17 | 7.16 | 7.75 | 7.71 | 7.71 | 7.70 | 7.67 | 7.68 | 7.67 | 7.67 |
| Fe(ii) | 0.05 | 0.05 | 0.07 | 0.14 | 0.10 | 0.05 | 0.06 | 0.08 | 0.05 | 0.07 | 0.08 | 0.06 | 0.08 |
| Ca | 3.35 | 3.39 | 3.41 | 3.39 | 3.30 | 3.97 | 3.95 | 3.87 | 3.85 | 3.90 | 3.94 | 3.87 | 3.93 |
| Na | 0.60 | 0.64 | 0.63 | 0.61 | 0.56 | 0.09 | 0.13 | 0.15 | 0.18 | 0.17 | 0.17 | 0.19 | 0.13 |
| K | 0.07 | 0.08 | 0.05 | 0.07 | 0.11 | 0.01 | 0.01 | 0.02 | 0.02 | 0.01 | 0.03 | 0.02 | 0.01 |
| | | | | | | | | | | | | | |
| An | 83.43 | 82.37 | 83.28 | 83.39 | 83.15 | 97.65 | 96.64 | 95.90 | 95.02 | 95.47 | 95.31 | 94.82 | 96.39 |
| Ab | 14.91 | 15.64 | 15.38 | 15.00 | 14.20 | 2.11 | 3.17 | 3.68 | 4.40 | 4.21 | 4.05 | 4.67 | 3.30 |
| Or | 1.66 | 1.99 | 1.34 | 1.60 | 2.65 | 0.24 | 0.19 | 0.42 | 0.58 | 0.31 | 0.65 | 0.50 | 0.31 |

## Table F1.4 Continued.

| | **USM66 PLAG3** | **USM66 PLAG38** | **USM66 PLAG46** | **USM66 PLAG32** | **USM66 PLAG15** | **USM66 PLAG27** | **USM65 PLAG4** | **USM65 PLAG57** | **USM65 PLAG32** | **USM65 PLAG77** | **USM65 PLAG49** | **USM65 PLAG10** | **USM65 PLAG17** |
|---|---|---|---|---|---|---|---|---|---|---|---|---|---|
| $SiO_2$ | 48.92 | 48.97 | 47.53 | 48.44 | 49.04 | 47.98 | 46.28 | 45.65 | 46.20 | 46.13 | 46.66 | 46.44 | 46.50 |
| $Al_2O_3$ | 32.49 | 32.13 | 31.94 | 31.90 | 31.85 | 31.19 | 34.24 | 34.08 | 33.90 | 33.83 | 33.81 | 33.79 | 33.78 |
| FeO | 0.37 | 0.42 | 1.37 | 0.26 | 0.34 | 1.76 | 0.69 | 0.46 | 0.29 | 0.39 | 0.29 | 0.26 | 0.41 |
| CaO | 16.13 | 16.16 | 15.70 | 16.10 | 16.24 | 14.84 | 18.08 | 18.15 | 18.21 | 18.02 | 17.86 | 17.67 | 17.82 |
| $Na_2O$ | 2.46 | 2.54 | 2.36 | 2.36 | 2.53 | 2.22 | 1.47 | 1.32 | 1.33 | 1.36 | 1.47 | 1.47 | 1.63 |
| K2O | 0.11 | 0.19 | 0.12 | 0.14 | 0.13 | 0.15 | 0.09 | 0.04 | 0.01 | 0.03 | 0.07 | 0.08 | 0.05 |
| TOTAL | 100.49 | 100.41 | 99.02 | 99.21 | 100.13 | 98.15 | 100.85 | 99.69 | 99.93 | 99.78 | 100.16 | 99.73 | 100.18 |
| | | | | | | | | | | | | | |
| Si | 8.93 | 8.95 | 8.85 | 8.95 | 8.99 | 8.99 | 8.49 | 8.46 | 8.53 | 8.53 | 8.58 | 8.58 | 8.56 |
| Al | 6.99 | 6.93 | 7.01 | 6.95 | 6.88 | 6.89 | 7.40 | 7.44 | 7.37 | 7.37 | 7.33 | 7.36 | 7.33 |
| Fe(ii) | 0.06 | 0.06 | 0.21 | 0.04 | 0.05 | 0.28 | 0.11 | 0.07 | 0.04 | 0.06 | 0.04 | 0.04 | 0.06 |
| Ca | 3.15 | 3.17 | 3.13 | 3.19 | 3.19 | 2.98 | 3.55 | 3.60 | 3.60 | 3.57 | 3.52 | 3.50 | 3.52 |
| Na | 0.87 | 0.90 | 0.85 | 0.85 | 0.90 | 0.81 | 0.52 | 0.47 | 0.48 | 0.49 | 0.52 | 0.53 | 0.58 |
| K | 0.03 | 0.04 | 0.03 | 0.03 | 0.03 | 0.04 | 0.02 | 0.01 | 0.00 | 0.01 | 0.02 | 0.02 | 0.01 |
| | | | | | | | | | | | | | |
| An | 77.83 | 77.05 | 78.06 | 78.37 | 77.43 | 77.90 | 86.70 | 88.19 | 88.27 | 87.82 | 86.67 | 86.48 | 85.56 |
| Ab | 21.52 | 21.89 | 21.21 | 20.82 | 21.80 | 21.13 | 12.78 | 11.56 | 11.66 | 11.98 | 12.91 | 13.04 | 14.13 |
| Or | 0.65 | 1.06 | 0.73 | 0.81 | 0.77 | 0.96 | 0.52 | 0.24 | 0.07 | 0.20 | 0.42 | 0.48 | 0.31 |
| | **USM65 PLAG29** | **USM65 PLAG43** | **USM65 PLAG9** | **USM65 PLAG64** | **USM65 PLAG47** | **USM65 PLAG1** | **USM65 PLAG83** | **USM60 PLAG 11** | **USM60 PALG 14** | **USM60 PLAG 23** | **USM60 PLAG 19** | **USM60 PLAG 2** | **USM60 PLAG 15** |
| $SiO_2$ | 46.59 | 46.26 | 46.49 | 46.37 | 46.53 | 46.53 | 45.99 | 48.40 | 48.77 | 48.71 | 48.60 | 49.44 | 46.39 |
| $Al_2O_3$ | 33.63 | 33.62 | 33.59 | 33.53 | 33.33 | 33.12 | 33.11 | 31.98 | 31.51 | 31.47 | 31.46 | 31.20 | 29.73 |
| FeO | 0.35 | 0.39 | 0.36 | 0.67 | 0.34 | 0.28 | 0.46 | 0.58 | 0.52 | 0.60 | 0.60 | 0.76 | 0.49 |
| CaO | 17.97 | 18.03 | 17.64 | 18.22 | 17.67 | 17.74 | 17.12 | 16.01 | 15.55 | 15.73 | 15.97 | 15.34 | 18.84 |
| $Na_2O$ | 1.54 | 1.23 | 1.53 | 1.39 | 1.63 | 1.55 | 1.46 | 2.52 | 2.70 | 2.57 | 2.61 | 2.74 | 1.57 |
| K2O | 0.08 | 0.04 | 0.07 | 0.12 | 0.02 | 0.06 | 0.09 | 0.09 | 0.07 | 0.10 | 0.08 | 0.12 | 0.39 |
| TOTAL | 100.15 | 99.58 | 99.67 | 100.30 | 99.52 | 99.28 | 98.22 | 99.57 | 99.13 | 99.18 | 99.32 | 99.61 | 97.41 |
| | | | | | | | | | | | | | |
| Si | 8.58 | 8.57 | 8.60 | 8.55 | 8.62 | 8.64 | 8.62 | 8.93 | 9.02 | 9.01 | 8.99 | 9.10 | 8.85 |
| Al | 7.30 | 7.34 | 7.32 | 7.29 | 7.27 | 7.24 | 7.31 | 6.95 | 6.87 | 6.86 | 6.86 | 6.77 | 6.68 |
| Fe(ii) | 0.05 | 0.06 | 0.05 | 0.10 | 0.05 | 0.04 | 0.07 | 0.09 | 0.08 | 0.09 | 0.09 | 0.12 | 0.08 |
| Ca | 3.55 | 3.58 | 3.49 | 3.60 | 3.51 | 3.53 | 3.44 | 3.16 | 3.08 | 3.12 | 3.16 | 3.03 | 3.85 |
| Na | 0.55 | 0.44 | 0.55 | 0.50 | 0.59 | 0.56 | 0.53 | 0.90 | 0.97 | 0.92 | 0.94 | 0.98 | 0.58 |
| K | 0.02 | 0.01 | 0.02 | 0.03 | 0.00 | 0.01 | 0.02 | 0.02 | 0.02 | 0.02 | 0.02 | 0.03 | 0.09 |
| | | | | | | | | | | | | | |
| An | 86.14 | 88.78 | 86.09 | 87.27 | 85.59 | 86.04 | 86.20 | 77.40 | 75.75 | 76.74 | 76.81 | 75.03 | 85.07 |
| Ab | 13.40 | 11.00 | 13.52 | 12.07 | 14.30 | 13.61 | 13.26 | 22.06 | 23.83 | 22.71 | 22.75 | 24.29 | 12.84 |
| Or | 0.46 | 0.23 | 0.39 | 0.66 | 0.11 | 0.35 | 0.53 | 0.54 | 0.43 | 0.55 | 0.43 | 0.69 | 2.09 |

## Table F1.4 Continued.

| | USM60 PLAG 18 | USM66 PLAG 19 | USM66 PLAG 24 | USM66 PLAG 2 | USM66 PLAG 7 | USM66 PLAG 9 |
|---|---|---|---|---|---|---|
| $SiO_2$ | 56.61 | 47.43 | 47.09 | 47.14 | 47.33 | 47.09 |
| $Al_2O_3$ | 26.21 | 32.40 | 32.40 | 32.25 | 31.94 | 31.62 |
| FeO | 0.30 | 0.48 | 0.30 | 0.32 | 0.31 | 0.63 |
| CaO | 9.33 | 16.41 | 16.01 | 16.05 | 15.97 | 15.58 |
| $Na_2O$ | 6.08 | 2.36 | 2.43 | 2.32 | 2.48 | 2.53 |
| K2O | 0.09 | 0.11 | 0.09 | 0.14 | 0.10 | 0.09 |
| TOTAL | 98.61 | 99.19 | 98.32 | 98.22 | 98.13 | 97.54 |
| | | | | | | |
| Si | 10.31 | 8.80 | 8.80 | 8.82 | 8.86 | 8.87 |
| Al | 5.62 | 7.08 | 7.13 | 7.11 | 7.05 | 7.02 |
| Fe(ii) | 0.05 | 0.07 | 0.05 | 0.05 | 0.05 | 0.10 |
| Ca | 1.82 | 3.26 | 3.20 | 3.22 | 3.20 | 3.15 |
| Na | 2.15 | 0.85 | 0.88 | 0.84 | 0.90 | 0.93 |
| K | 0.02 | 0.03 | 0.02 | 0.03 | 0.02 | 0.02 |
| | | | | | | |
| An | 45.64 | 78.87 | 78.01 | 78.58 | 77.64 | 76.88 |
| Ab | 53.85 | 20.49 | 21.45 | 20.57 | 21.79 | 22.62 |
| Or | 0.51 | 0.64 | 0.55 | 0.84 | 0.57 | 0.50 |

## Table F1.5 Spinel analyses

| | USM65 SPIN76 | USM65 SPIN34 | USM65 SPIN24 | USM65 SPIN69 | USM65 SPIN80 | USM65 SPIN67 | USM65 SPIN74 | USM65 SPIN68 | USM65 SPIN75 | USM65 SPIN71 | USM65 SPIN72 | USM65 SPIN79 | USM65 SPIN73 |
|---|---|---|---|---|---|---|---|---|---|---|---|---|---|
| $SiO_2$ | 0.05 | 0.05 | 0.04 | 0.01 | 0.03 | 0.04 | 0.04 | 0.03 | 0.06 | 0.02 | 0.04 | 0.01 | 0.01 |
| $TiO_2$ | 0.73 | 1.26 | 1.23 | 1.47 | 1.39 | 1.12 | 1.33 | 1.15 | 1.01 | 1.37 | 1.41 | 1.19 | 1.17 |
| $Al_2O_3$ | 37.15 | 26.86 | 26.36 | 25.89 | 25.81 | 25.35 | 25.34 | 25.33 | 25.25 | 25.15 | 24.62 | 24.51 | 24.07 |
| $Cr_2O_3$ | 20.77 | 28.10 | 27.63 | 26.60 | 26.48 | 26.40 | 26.78 | 26.71 | 26.56 | 26.46 | 27.30 | 27.15 | 27.62 |
| FeO | 24.95 | 31.04 | 32.68 | 34.16 | 35.15 | 34.87 | 34.56 | 34.68 | 34.10 | 35.45 | 35.33 | 37.36 | 35.07 |
| MnO | 0.15 | 0.22 | 0.19 | 0.26 | 0.24 | 0.26 | 0.24 | 0.24 | 0.19 | 0.20 | 0.22 | 0.29 | 0.30 |
| MgO | 11.98 | 7.36 | 7.24 | 7.02 | 6.94 | 6.82 | 6.84 | 6.46 | 6.67 | 6.77 | 6.88 | 6.26 | 6.17 |
| CaO | 0.18 | 0.32 | 0.38 | 0.01 | 0.03 | 0.02 | 0.02 | 0.04 | 0.04 | 0.00 | 0.00 | 0.01 | 0.01 |
| ZnO | 0.42 | 0.34 | 0.38 | 0.41 | 0.49 | 0.55 | 0.57 | 0.64 | 0.47 | 0.72 | 0.68 | 0.44 | 0.44 |
| TOTAL | 96.38 | 95.55 | 96.14 | 95.82 | 96.57 | 95.42 | 95.72 | 95.29 | 94.36 | 96.15 | 96.48 | 97.23 | 94.85 |
| | | | | | | | | | | | | | |
| Si | 0.01 | 0.01 | 0.01 | 0.00 | 0.01 | 0.01 | 0.01 | 0.01 | 0.02 | 0.01 | 0.01 | 0.00 | 0.00 |
| Ti | 0.13 | 0.25 | 0.24 | 0.29 | 0.27 | 0.22 | 0.26 | 0.23 | 0.20 | 0.27 | 0.28 | 0.23 | 0.23 |
| Al | 10.49 | 8.21 | 8.03 | 7.94 | 7.87 | 7.83 | 7.81 | 7.85 | 7.88 | 7.73 | 7.55 | 7.50 | 7.55 |
| Cr | 3.93 | 5.76 | 5.65 | 5.47 | 5.42 | 5.47 | 5.53 | 5.56 | 5.56 | 5.45 | 5.62 | 5.57 | 5.81 |
| V | 0.00 | 0.00 | 0.00 | 0.00 | 0.00 | 0.00 | 0.00 | 0.00 | 0.00 | 0.00 | 0.00 | 0.00 | 0.00 |
| Fe(iii) | 1.28 | 1.52 | 1.82 | 2.01 | 2.16 | 2.24 | 2.12 | 2.12 | 2.12 | 2.27 | 2.26 | 2.45 | 2.17 |
| Fe(ii) | 3.72 | 5.21 | 5.24 | 5.43 | 5.45 | 5.40 | 5.44 | 5.51 | 5.44 | 5.46 | 5.44 | 5.66 | 5.63 |
| Mn | 0.03 | 0.05 | 0.04 | 0.06 | 0.05 | 0.06 | 0.05 | 0.05 | 0.04 | 0.04 | 0.05 | 0.06 | 0.07 |
| Mg | 4.28 | 2.84 | 2.79 | 2.72 | 2.68 | 2.66 | 2.66 | 2.53 | 2.64 | 2.63 | 2.67 | 2.43 | 2.45 |
| Ca | 0.05 | 0.09 | 0.11 | 0.00 | 0.01 | 0.01 | 0.01 | 0.01 | 0.01 | 0.00 | 0.00 | 0.00 | 0.00 |
| Zn | 0.07 | 0.07 | 0.07 | 0.08 | 0.09 | 0.11 | 0.11 | 0.12 | 0.09 | 0.14 | 0.13 | 0.08 | 0.09 |
| | | | | | | | | | | | | | |
| $Fe^{2+}/(Mg+Fe^{2+})$ | 0.54 | 0.70 | 0.72 | 0.73 | 0.74 | 0.74 | 0.74 | 0.75 | 0.74 | 0.75 | 0.74 | 0.77 | 0.76 |
| Cr/Cr+Al | 0.27 | 0.41 | 0.41 | 0.41 | 0.41 | 0.41 | 0.41 | 0.41 | 0.41 | 0.41 | 0.43 | 0.43 | 0.43 |

## Table F1.5 Continued.

| | USM65 SPIN65 | USM65 SPIN36 | USM65 SPIN37 | USM65 SPIN38 | USM65 SPIN41 | USM65 SPIN66 | USM65 SPIN60 | USM65 SPIN54 | USM65 SPIN63 | USM65 SPIN25 | USM65 SPIN51 | USM65 SPIN26 | USM65 SPIN27 |
|---|---|---|---|---|---|---|---|---|---|---|---|---|---|
| $SiO_2$ | 0.01 | 0.03 | 0.03 | 0.02 | 0.05 | 0.09 | 0.05 | 0.07 | 0.03 | 0.04 | 0.07 | 0.08 | 0.02 |
| $TiO_2$ | 1.56 | 1.33 | 1.55 | 1.66 | 1.61 | 1.56 | 1.66 | 1.70 | 1.86 | 1.61 | 1.91 | 1.77 | 1.63 |
| $Al_2O_3$ | 23.93 | 23.08 | 23.01 | 22.73 | 22.39 | 21.55 | 21.46 | 21.41 | 21.14 | 20.55 | 20.47 | 20.20 | 20.09 |
| $Cr_2O_3$ | 27.21 | 27.52 | 27.35 | 27.82 | 28.38 | 28.73 | 28.79 | 29.10 | 28.36 | 29.14 | 28.96 | 29.42 | 29.06 |
| FeO | 36.24 | 36.80 | 36.55 | 36.34 | 36.70 | 37.84 | 37.98 | 37.13 | 36.58 | 37.17 | 37.27 | 37.43 | 38.24 |
| MnO | 0.10 | 0.14 | 0.21 | 0.16 | 0.24 | 0.31 | 0.22 | 0.25 | 0.27 | 0.22 | 0.25 | 0.39 | 0.36 |
| MgO | 6.30 | 5.92 | 5.85 | 5.94 | 5.78 | 5.37 | 5.53 | 5.56 | 5.39 | 5.55 | 5.31 | 5.36 | 5.17 |
| CaO | 0.01 | 0.00 | 0.02 | 0.00 | 0.02 | 0.03 | 0.02 | 0.00 | 0.02 | 0.02 | 0.05 | 0.00 | 0.01 |
| ZnO | 0.49 | 0.59 | 0.65 | 0.59 | 0.61 | 0.63 | 0.82 | 0.66 | 0.76 | 0.64 | 0.73 | 0.82 | 0.98 |
| TOTAL | 95.84 | 95.41 | 95.22 | 95.26 | 95.78 | 96.11 | 96.52 | 95.87 | 94.41 | 94.94 | 95.02 | 95.48 | 95.56 |
| | | | | | | | | | | | | | |
| Si | 0.00 | 0.01 | 0.01 | 0.01 | 0.01 | 0.02 | 0.01 | 0.02 | 0.01 | 0.01 | 0.02 | 0.02 | 0.00 |
| Ti | 0.31 | 0.27 | 0.31 | 0.33 | 0.32 | 0.31 | 0.33 | 0.34 | 0.38 | 0.33 | 0.39 | 0.36 | 0.33 |
| Al | 7.43 | 7.24 | 7.24 | 7.15 | 7.03 | 6.79 | 6.73 | 6.76 | 6.78 | 6.56 | 6.55 | 6.44 | 6.41 |
| Cr | 5.67 | 5.79 | 5.77 | 5.87 | 5.98 | 6.07 | 6.06 | 6.16 | 6.10 | 6.25 | 6.22 | 6.29 | 6.22 |
| V | 0.00 | 0.00 | 0.00 | 0.00 | 0.00 | 0.00 | 0.00 | 0.00 | 0.00 | 0.00 | 0.00 | 0.00 | 0.00 |
| Fe(iii) | 2.27 | 2.42 | 2.35 | 2.30 | 2.32 | 2.47 | 2.52 | 2.36 | 2.35 | 2.51 | 2.42 | 2.50 | 2.69 |
| Fe(ii) | 5.72 | 5.78 | 5.81 | 5.82 | 5.86 | 5.99 | 5.93 | 5.95 | 5.98 | 5.91 | 6.05 | 5.97 | 5.97 |
| Mn | 0.02 | 0.03 | 0.05 | 0.04 | 0.05 | 0.07 | 0.05 | 0.06 | 0.06 | 0.05 | 0.06 | 0.09 | 0.08 |
| Mg | 2.48 | 2.35 | 2.33 | 2.37 | 2.29 | 2.14 | 2.20 | 2.22 | 2.19 | 2.24 | 2.15 | 2.16 | 2.09 |
| Ca | 0.00 | 0.00 | 0.01 | 0.00 | 0.01 | 0.01 | 0.01 | 0.00 | 0.01 | 0.01 | 0.01 | 0.00 | 0.00 |
| Zn | 0.09 | 0.12 | 0.13 | 0.12 | 0.12 | 0.12 | 0.16 | 0.13 | 0.15 | 0.13 | 0.15 | 0.16 | 0.20 |
| | | | | | | | | | | | | | |
| $Fe^{2+}/(Mg+Fe^{2+})$ | 0.76 | 0.78 | 0.78 | 0.77 | 0.78 | 0.80 | 0.79 | 0.79 | 0.79 | 0.79 | 0.80 | 0.80 | 0.81 |
| Cr/Cr+Al | 0.43 | 0.44 | 0.44 | 0.45 | 0.46 | 0.47 | 0.47 | 0.48 | 0.47 | 0.49 | 0.49 | 0.49 | 0.49 |

## Table F1.5 Continued.

| | USM65 SPIN53 | USM65 SPIN61 | USM65 SPIN59 | USM65 SPIN22 | USM65 SPIN23 | USM65 SPIN52 | USM65 SPIN50 | BC10/90/5 SPIN22 | BC10/90/5 SPIN45 | BC10/90/5 SPIN37 | BC10/90/5 SPIN39 | BC10/90/5 SPIN31 | BC10/90/5 SPIN38 |
|---|---|---|---|---|---|---|---|---|---|---|---|---|---|
| $SiO_2$ | 0.06 | 0.01 | 0.04 | 0.05 | 0.08 | 0.09 | 0.46 | 0.04 | 0.02 | 0.03 | 0.04 | 0.00 | 0.01 |
| $TiO_2$ | 1.89 | 1.45 | 1.85 | 1.76 | 1.73 | 1.88 | 1.62 | 2.12 | 2.10 | 1.95 | 2.09 | 1.56 | 3.07 |
| $Al_2O_3$ | 20.04 | 19.82 | 19.76 | 19.58 | 19.35 | 19.07 | 18.03 | 14.91 | 14.67 | 14.60 | 14.44 | 14.19 | 14.18 |
| $Cr_2O_3$ | 29.18 | 28.86 | 29.40 | 29.33 | 29.23 | 29.47 | 25.92 | 30.65 | 30.35 | 30.47 | 30.51 | 30.64 | 31.43 |
| FeO | 38.33 | 38.69 | 37.35 | 38.09 | 38.34 | 37.76 | 31.37 | 43.01 | 44.74 | 44.61 | 44.01 | 45.66 | 42.47 |
| MnO | 0.16 | 0.27 | 0.32 | 0.26 | 0.28 | 0.23 | 0.22 | 0.30 | 0.33 | 0.28 | 0.26 | 0.34 | 0.26 |
| MgO | 5.04 | 4.77 | 5.02 | 4.98 | 4.87 | 4.74 | 5.14 | 5.17 | 4.60 | 4.51 | 4.56 | 4.20 | 5.52 |
| CaO | 0.00 | 0.05 | 0.00 | 0.03 | 0.01 | 0.03 | 5.68 | 0.20 | 0.03 | 0.02 | 0.01 | 0.05 | 0.07 |
| ZnO | 0.68 | 0.81 | 0.77 | 0.65 | 0.57 | 0.63 | 0.55 | 0.18 | 0.09 | 0.14 | 0.42 | 0.17 | 0.25 |
| TOTAL | 95.37 | 94.71 | 94.51 | 94.74 | 94.45 | 93.92 | 88.98 | 96.57 | 96.93 | 96.61 | 96.34 | 96.82 | 97.25 |
| | | | | | | | | | | | | | |
| Si | 0.02 | 0.00 | 0.01 | 0.01 | 0.02 | 0.02 | 0.13 | 0.01 | 0.01 | 0.01 | 0.01 | 0.00 | 0.00 |
| Ti | 0.39 | 0.30 | 0.38 | 0.36 | 0.36 | 0.39 | 0.35 | 0.44 | 0.43 | 0.40 | 0.43 | 0.32 | 0.63 |
| Al | 6.41 | 6.40 | 6.39 | 6.32 | 6.27 | 6.23 | 6.07 | 4.81 | 4.74 | 4.74 | 4.70 | 4.61 | 4.55 |
| Cr | 6.27 | 6.25 | 6.37 | 6.35 | 6.36 | 6.46 | 5.86 | 6.63 | 6.58 | 6.63 | 6.66 | 6.68 | 6.77 |
| V | 0.00 | 0.00 | 0.00 | 0.00 | 0.00 | 0.00 | 0.00 | 0.00 | 0.00 | 0.00 | 0.00 | 0.00 | 0.00 |
| Fe(iii) | 2.52 | 2.75 | 2.45 | 2.58 | 2.61 | 2.48 | 3.11 | 3.67 | 3.80 | 3.81 | 3.74 | 4.06 | 3.42 |
| Fe(ii) | 6.19 | 6.11 | 6.11 | 6.14 | 6.20 | 6.27 | 4.38 | 6.17 | 6.45 | 6.46 | 6.42 | 6.47 | 6.26 |
| Mn | 0.04 | 0.06 | 0.08 | 0.06 | 0.07 | 0.05 | 0.05 | 0.07 | 0.08 | 0.07 | 0.06 | 0.08 | 0.06 |
| Mg | 2.04 | 1.95 | 2.05 | 2.03 | 2.00 | 1.96 | 2.19 | 2.11 | 1.88 | 1.85 | 1.88 | 1.73 | 2.24 |
| Ca | 0.00 | 0.01 | 0.00 | 0.01 | 0.00 | 0.01 | 1.74 | 0.06 | 0.01 | 0.01 | 0.00 | 0.01 | 0.02 |
| Zn | 0.14 | 0.16 | 0.16 | 0.13 | 0.12 | 0.13 | 0.12 | 0.04 | 0.02 | 0.03 | 0.09 | 0.04 | 0.05 |
| | | | | | | | | | | | | | |
| $Fe^{2+}/(Mg+Fe^{2+})$ | 0.81 | 0.82 | 0.81 | 0.81 | 0.82 | 0.82 | 0.77 | 0.82 | 0.84 | 0.85 | 0.84 | 0.86 | 0.81 |
| Cr/Cr+Al | 0.49 | 0.49 | 0.50 | 0.50 | 0.50 | 0.51 | 0.49 | 0.58 | 0.58 | 0.58 | 0.59 | 0.59 | 0.60 |

**Table F1.5 Continued.**

| | BC10/90/6 SPIN66 | BC10/90/6 SPIN32 | BC10/90/6 SPIN33 | USM8 SPIN17 | USM8 SPIN25 | USM8 SPIN49. | USM8 SPIN48 | USM8 SPIN18 | USM8 SPIN46 | USM8 SPIN38 | USM8 SPIN51 | USM8 SPIN50 | USM8 SPIN47 |
|---|---|---|---|---|---|---|---|---|---|---|---|---|---|
| $SiO_2$ | 0.04 | 0.00 | 0.05 | 0.06 | 0.05 | 0.05 | 0.04 | 0.03 | 0.05 | 0.00 | 0.05 | 0.06 | 0.01 |
| $TiO_2$ | 1.30 | 1.29 | 3.68 | 1.12 | 1.92 | 2.05 | 2.24 | 0.89 | 0.90 | 0.99 | 1.86 | 1.87 | 1.23 |
| $Al_2O_3$ | 18.85 | 18.66 | 14.08 | 14.00 | 13.52 | 12.88 | 12.62 | 12.35 | 12.33 | 19.65 | 15.44 | 15.33 | 14.31 |
| $Cr_2O_3$ | 34.49 | 35.26 | 35.42 | 27.01 | 27.67 | 29.63 | 28.49 | 25.85 | 24.91 | 24.12 | 28.61 | 30.47 | 27.47 |
| FeO | 35.50 | 35.72 | 34.93 | 50.15 | 47.51 | 46.07 | 47.55 | 54.13 | 54.69 | 44.46 | 43.63 | 42.66 | 47.82 |
| MnO | 0.34 | 0.34 | 0.22 | 0.37 | 0.38 | 0.28 | 0.32 | 0.25 | 0.44 | 0.23 | 0.29 | 0.38 | 0.40 |
| MgO | 6.24 | 6.29 | 7.73 | 3.86 | 4.71 | 4.83 | 4.83 | 3.16 | 3.24 | 6.18 | 5.39 | 6.17 | 5.05 |
| CaO | 0.05 | 0.08 | 0.21 | 0.01 | 0.06 | 0.20 | 0.15 | 0.02 | 0.01 | 0.03 | 0.01 | 0.06 | 0.00 |
| ZnO | 0.24 | 0.24 | 0.21 | 0.22 | 0.00 | 0.23 | 0.34 | 0.14 | 0.20 | 0.24 | 0.20 | 0.20 | 0.20 |
| TOTAL | 97.05 | 97.86 | 96.54 | 96.79 | 95.83 | 96.21 | 96.57 | 96.80 | 96.77 | 95.91 | 95.47 | 97.21 | 96.49 |
| | | | | | | | | | | | | | |
| Si | 0.01 | 0.00 | 0.01 | 0.02 | 0.01 | 0.01 | 0.01 | 0.01 | 0.01 | 0.00 | 0.01 | 0.01 | 0.00 |
| Ti | 0.26 | 0.26 | 0.75 | 0.23 | 0.40 | 0.43 | 0.47 | 0.19 | 0.19 | 0.20 | 0.39 | 0.38 | 0.25 |
| Al | 5.92 | 5.82 | 4.49 | 4.56 | 4.42 | 4.21 | 4.11 | 4.06 | 4.05 | 6.19 | 5.01 | 4.87 | 4.62 |
| Cr | 7.27 | 7.38 | 7.57 | 5.90 | 6.07 | 6.50 | 6.23 | 5.70 | 5.49 | 5.10 | 6.23 | 6.49 | 5.96 |
| V | 0.00 | 0.00 | 0.00 | 0.00 | 0.00 | 0.00 | 0.00 | 0.00 | 0.00 | 0.00 | 0.00 | 0.00 | 0.00 |
| Fe(iii) | 2.27 | 2.28 | 2.41 | 5.05 | 4.67 | 4.41 | 4.70 | 5.85 | 6.05 | 4.31 | 3.97 | 3.85 | 4.91 |
| Fe(ii) | 5.65 | 5.63 | 5.49 | 6.53 | 6.36 | 6.27 | 6.30 | 6.79 | 6.71 | 5.63 | 6.08 | 5.77 | 6.06 |
| Mn | 0.08 | 0.08 | 0.05 | 0.09 | 0.09 | 0.07 | 0.07 | 0.06 | 0.10 | 0.05 | 0.07 | 0.09 | 0.09 |
| Mg | 2.48 | 2.48 | 3.12 | 1.59 | 1.95 | 2.00 | 1.99 | 1.31 | 1.35 | 2.46 | 2.21 | 2.48 | 2.07 |
| Ca | 0.02 | 0.02 | 0.06 | 0.00 | 0.02 | 0.06 | 0.04 | 0.01 | 0.00 | 0.01 | 0.00 | 0.02 | 0.00 |
| Zn | 0.05 | 0.05 | 0.04 | 0.04 | 0.00 | 0.05 | 0.07 | 0.03 | 0.04 | 0.05 | 0.04 | 0.04 | 0.04 |
| | | | | | | | | | | | | | |
| $Fe^{2+}/(Mg+Fe^{2+})$ | 0.76 | 0.76 | 0.72 | 0.88 | 0.85 | 0.84 | 0.85 | 0.91 | 0.90 | 0.80 | 0.82 | 0.79 | 0.84 |
| Cr/Cr+Al | 0.55 | 0.56 | 0.63 | 0.56 | 0.58 | 0.61 | 0.60 | 0.58 | 0.58 | 0.45 | 0.55 | 0.57 | 0.56 |

**Table F1.5 Continued.**

| | USM66 SPIN36 | USM66 SPIN39 | USM66 SPIN31 | USM66 SPIN43 | USM66 SPIN21 | USM66 SPIN45 | USM66 SPIN22 | USM66 SPIN53 | USM66 SPIN48 | USM66 SPIN24 | USM66 SPIN30 | USM66 SPIN29 | USM66 SPIN54 |
|---|---|---|---|---|---|---|---|---|---|---|---|---|---|
| $SiO_2$ | 0.07 | 0.03 | 0.07 | 0.07 | 0.05 | 0.05 | 0.07 | 0.03 | 1.64 | 0.17 | 0.01 | 0.04 | 0.05 |
| $TiO_2$ | 4.76 | 4.95 | 4.44 | 4.31 | 4.62 | 4.61 | 4.01 | 3.76 | 3.96 | 5.09 | 2.87 | 3.03 | 2.73 |
| $Al_2O_3$ | 8.61 | 7.35 | 7.20 | 6.66 | 6.44 | 6.41 | 6.34 | 6.21 | 5.94 | 5.63 | 4.15 | 4.07 | 3.57 |
| $Cr_2O_3$ | 21.27 | 21.74 | 22.20 | 19.65 | 23.14 | 22.58 | 18.06 | 19.03 | 15.38 | 17.35 | 13.25 | 13.41 | 11.03 |
| FeO | 56.57 | 59.08 | 59.53 | 62.09 | 57.28 | 59.76 | 63.52 | 64.24 | 62.64 | 64.91 | 71.96 | 72.48 | 75.05 |
| MnO | 1.18 | 2.79 | 0.99 | 0.80 | 0.47 | 0.59 | 0.81 | 0.43 | 0.70 | 0.96 | 0.57 | 0.73 | 0.61 |
| MgO | 1.43 | 0.27 | 0.98 | 1.04 | 1.19 | 1.21 | 0.68 | 1.00 | 2.28 | 0.62 | 0.42 | 0.11 | 0.39 |
| CaO | 0.39 | 0.04 | 0.00 | 0.11 | 0.00 | 0.12 | 0.02 | 0.01 | 0.54 | 0.02 | 0.06 | 0.00 | 0.03 |
| ZnO | 0.23 | 0.43 | 0.55 | 0.30 | 0.53 | 0.35 | 0.55 | 0.37 | 0.12 | 0.38 | 0.31 | 0.27 | 0.10 |
| TOTAL | 94.51 | 96.67 | 95.96 | 95.01 | 93.71 | 95.68 | 94.07 | 95.07 | 93.19 | 95.12 | 93.59 | 94.13 | 93.57 |
| | | | | | | | | | | | | | |
| Si | 0.02 | 0.01 | 0.02 | 0.02 | 0.01 | 0.01 | 0.02 | 0.01 | 0.49 | 0.05 | 0.00 | 0.01 | 0.02 |
| Ti | 1.05 | 1.09 | 0.98 | 0.96 | 1.04 | 1.02 | 0.90 | 0.84 | 0.89 | 1.14 | 0.66 | 0.69 | 0.62 |
| Al | 2.98 | 2.53 | 2.49 | 2.32 | 2.28 | 2.22 | 2.24 | 2.17 | 2.08 | 1.97 | 1.48 | 1.45 | 1.28 |
| Cr | 4.94 | 5.02 | 5.14 | 4.59 | 5.50 | 5.25 | 4.28 | 4.45 | 3.61 | 4.08 | 3.18 | 3.21 | 2.65 |
| V | 0.00 | 0.00 | 0.00 | 0.00 | 0.00 | 0.00 | 0.00 | 0.00 | 0.00 | 0.00 | 0.00 | 0.00 | 0.00 |
| Fe(iii) | 5.92 | 6.25 | 6.38 | 7.13 | 6.11 | 6.46 | 7.63 | 7.69 | 7.57 | 7.56 | 10.02 | 9.94 | 10.79 |
| Fe(ii) | 7.98 | 8.19 | 8.20 | 8.22 | 8.29 | 8.24 | 8.28 | 8.21 | 7.99 | 8.59 | 8.23 | 8.40 | 8.27 |
| Mn | 0.29 | 0.69 | 0.25 | 0.20 | 0.12 | 0.15 | 0.21 | 0.11 | 0.18 | 0.24 | 0.15 | 0.19 | 0.16 |
| Mg | 0.63 | 0.12 | 0.43 | 0.46 | 0.53 | 0.53 | 0.31 | 0.44 | 1.01 | 0.27 | 0.19 | 0.05 | 0.18 |
| Ca | 0.12 | 0.01 | 0.00 | 0.03 | 0.00 | 0.04 | 0.01 | 0.00 | 0.17 | 0.01 | 0.02 | 0.00 | 0.01 |
| Zn | 0.05 | 0.09 | 0.12 | 0.06 | 0.12 | 0.08 | 0.12 | 0.08 | 0.03 | 0.08 | 0.07 | 0.06 | 0.02 |
| | | | | | | | | | | | | | |
| $Fe^{2+}/(Mg+Fe^{2+})$ | 0.96 | 0.99 | 0.97 | 0.97 | 0.96 | 0.97 | 0.98 | 0.97 | 0.94 | 0.98 | 0.99 | 1.00 | 0.99 |
| Cr/Cr+Al | 0.62 | 0.67 | 0.67 | 0.66 | 0.71 | 0.70 | 0.66 | 0.67 | 0.63 | 0.67 | 0.68 | 0.69 | 0.67 |

## Table F1.5 Continued.

| | USM66 SPIN49 | USM66 SPIN56 | BC10/90/5 SPIN40 | BC10/90/5 SPIN32 | BC10/90/5 SPIN24 | BC10/90/5 SPIN43 | BC10/90/5 SPIN23 | BC10/90/5 SPIN36 | BC10/90/5 SPIN35 |
|---|---|---|---|---|---|---|---|---|---|
| $SiO_2$ | 0.05 | 0.04 | 0.03 | 0.04 | 0.04 | 0.03 | 0.05 | 0.02 | 0.06 |
| $TiO_2$ | 2.43 | 2.40 | 3.05 | 3.04 | 3.35 | 2.04 | 3.07 | 2.96 | 2.73 |
| $Al_2O_3$ | 3.52 | 2.51 | 13.83 | 13.81 | 13.78 | 13.51 | 13.24 | 13.17 | 12.77 |
| $Cr_2O_3$ | 13.61 | 10.28 | 31.34 | 30.99 | 30.80 | 29.85 | 29.67 | 30.35 | 29.96 |
| FeO | 73.54 | 77.32 | 44.17 | 44.14 | 43.54 | 46.31 | 44.76 | 45.57 | 46.02 |
| MnO | 0.26 | 0.59 | 0.30 | 0.41 | 0.32 | 0.36 | 0.34 | 0.34 | 0.37 |
| MgO | 0.22 | 0.16 | 5.00 | 4.98 | 5.13 | 4.12 | 4.73 | 4.53 | 4.52 |
| CaO | 0.00 | 0.11 | 0.05 | 0.06 | 0.09 | 0.12 | 0.05 | 0.09 | 0.06 |
| ZnO | 0.28 | 0.13 | 0.26 | 0.17 | 0.14 | 0.22 | 0.25 | 0.22 | 0.30 |
| TOTAL | 93.92 | 93.42 | 98.02 | 97.64 | 97.18 | 96.57 | 96.16 | 97.27 | 96.80 |
| | | | | | | | | | |
| Si | 0.02 | 0.01 | 0.01 | 0.01 | 0.01 | 0.01 | 0.01 | 0.01 | 0.02 |
| Ti | 0.56 | 0.55 | 0.62 | 0.62 | 0.69 | 0.43 | 0.64 | 0.61 | 0.57 |
| Al | 1.26 | 0.91 | 4.43 | 4.44 | 4.45 | 4.41 | 4.33 | 4.27 | 4.17 |
| Cr | 3.27 | 2.48 | 6.74 | 6.68 | 6.67 | 6.54 | 6.51 | 6.61 | 6.56 |
| V | 0.00 | 0.00 | 0.00 | 0.00 | 0.00 | 0.00 | 0.00 | 0.00 | 0.00 |
| Fe(iii) | 10.33 | 11.48 | 3.57 | 3.61 | 3.49 | 4.18 | 3.84 | 3.88 | 4.10 |
| Fe(ii) | 8.34 | 8.27 | 6.47 | 6.46 | 6.48 | 6.56 | 6.55 | 6.61 | 6.55 |
| Mn | 0.07 | 0.15 | 0.07 | 0.10 | 0.07 | 0.08 | 0.08 | 0.08 | 0.09 |
| Mg | 0.10 | 0.07 | 2.03 | 2.02 | 2.09 | 1.70 | 1.96 | 1.86 | 1.87 |
| Ca | 0.00 | 0.03 | 0.01 | 0.02 | 0.03 | 0.04 | 0.02 | 0.03 | 0.02 |
| Zn | 0.06 | 0.03 | 0.05 | 0.03 | 0.03 | 0.05 | 0.05 | 0.05 | 0.06 |
| | | | | | | | | | |
| $Fe^{2+}/(Mg+Fe^{2+})$ | 0.99 | 1.00 | 0.83 | 0.83 | 0.83 | 0.86 | 0.84 | 0.85 | 0.85 |
| Cr/Cr+Al | 0.72 | 0.73 | 0.60 | 0.60 | 0.60 | 0.60 | 0.60 | 0.61 | 0.61 |